ATLAS PROJECT	Finite Element Analysis and the ATLAS Liquid Argon Calorimeter Signal Feedthrough Assembly		
ATLAS Project Document No.: **ATL-AE-EA-0005**	Institute Document No.:	Created: 20 Nov 2001	Page: **1 of 169**
		Modified:	Rev. No.:

LAr Signal Feedthroughs

Finite Element Analysis and the ATLAS Liquid Argon Calorimeter Signal Feedthrough Assembly

Abstract

The design of the ATLAS liquid argon calorimeter signal feedthrough assembly has gone through detailed finite element analyses (FEA) to ensure the integrity of the assembly under the expected pressure loads. Results of the FEA have been useful in determining many parameters of the feedthrough assembly design. This document is a compilation of FEA analyses performed up to Dec 1998.

Prepared by:	Checked by:	Approved by:
T. Hodges M. Lefebvre U. of Victoria/TRIUMF		for information

History of Changes

Rev. No.	Date	Pages	Description of changes

Contents

List of Figures

List of Tables

1 Introduction

The design of the ATLAS liquid argon calorimeter signal feedthrough assembly has gone through detailed finite element analyses (FEA) to ensure the integrity of the assembly under the pressure differences we expect. Results of the FEA have been useful in determining many parameters of the feedthrough assembly design.

Finite element analyses of the component parts of the feedthrough assembly are being carried out using the ANSYS code [1]. Deformation and stress created in the feedthrough by the application of mechanical and pressure loads and from cooling part of the feedthrough to liquid argon temperature have been studied, as well as the temperature of the vacuum cables under various operating currents.

[1] ANSYS v5.3 Swanson Analysis Systems Inc.,Houston,PA,USA

2 Cold Flange Study (Release of 96/12/04)

The cold flange was originally designed with a thickness of 1.5 inches (38 mm). The model has then been modified by reducing the flange thickness to 1.4 inches (36 mm) to enable cutting from 1.5 inch stock. The pin carriers were reduced in depth to 0.9 inches by reducing the "skirt" part of the carrier between the weld lip and the region where the socket begins. The resulting finite element model of half a cold flange is shown in Figure 1. In this model, the pin carriers are mounted on different sides of the flange.

Under an applied load of 5 bars and compared to the 1.5 inch model, the maximum deflection in the direction of the applied pressure increases from 79.3 mm to 90.5 mm. The (Von Mises) stress in the corner where the pins carrier meets the flange increases from 122 MPa to 136 MPa. Deflection and stress for the 1.4 inch cold flange are shown in Figure 2 and Figure 3 respectively. Note that the yield and ultimate stress values for the flange and pin carrier material (AISI 304L stainless steel) are 172 MPa and 483 MPa respectively.

Figure 4 shows that the high stress region is very localized and does not extend to the region where the pins are sealed to the stainless carrier; the stress in this region remains low (< 13 MPa) as required.

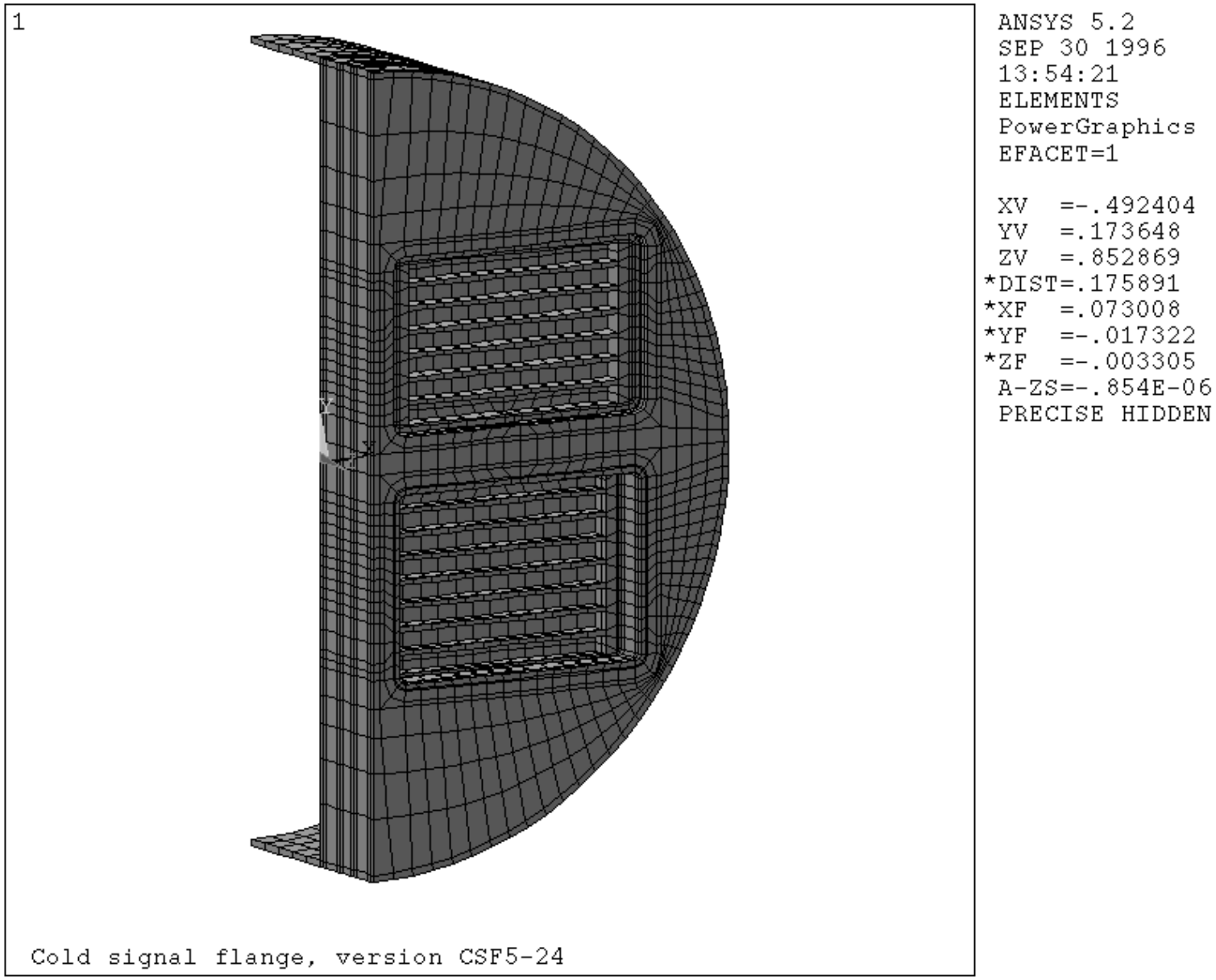

Figure 1: Finite element analysis model of half a cold flange. Dimensions in metres.

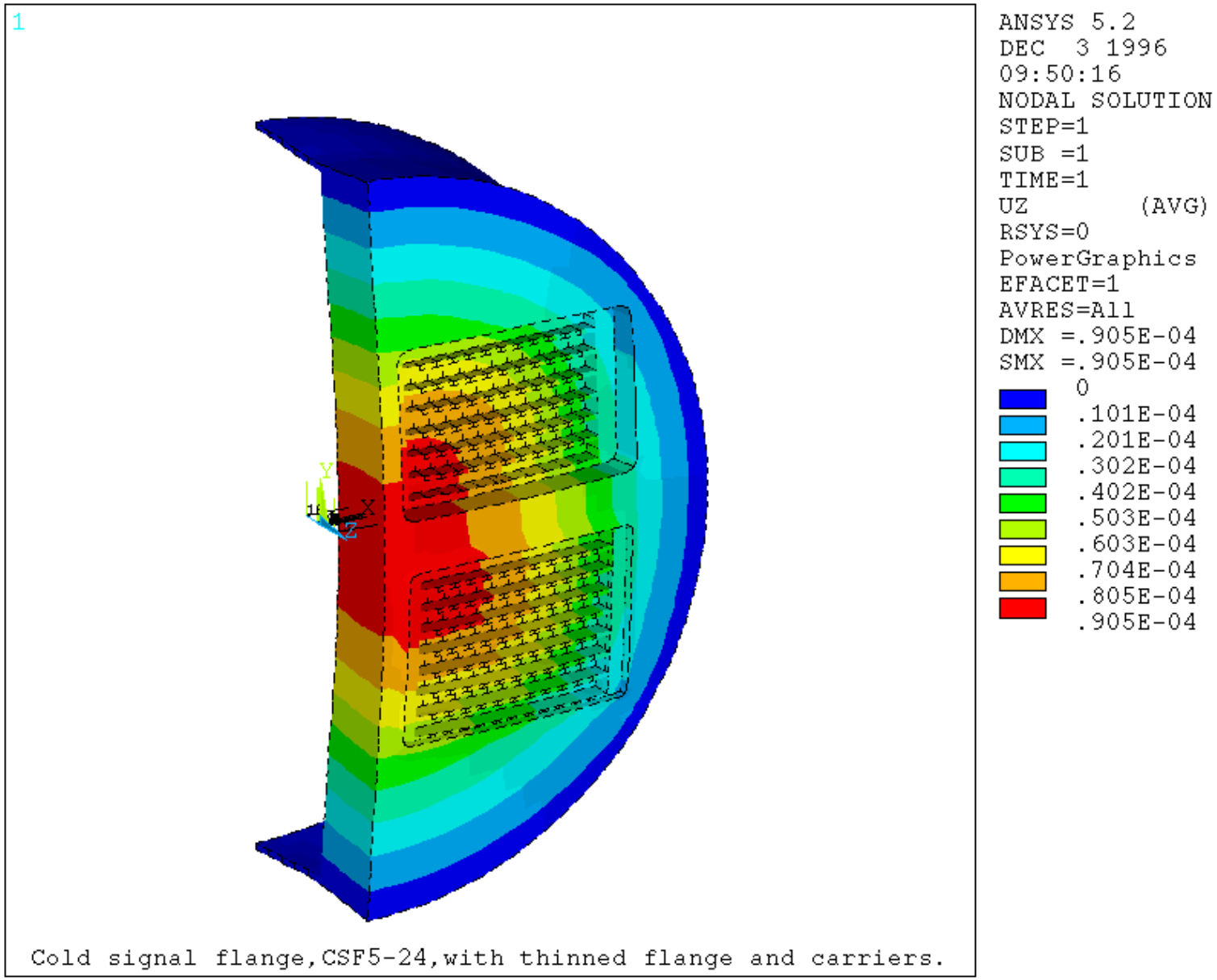

Figure 2: Finite element analysis of the cold flange showing the deflection in metres under an applied load of 5 bars. Note the maximum deflection of 90.5 μm.

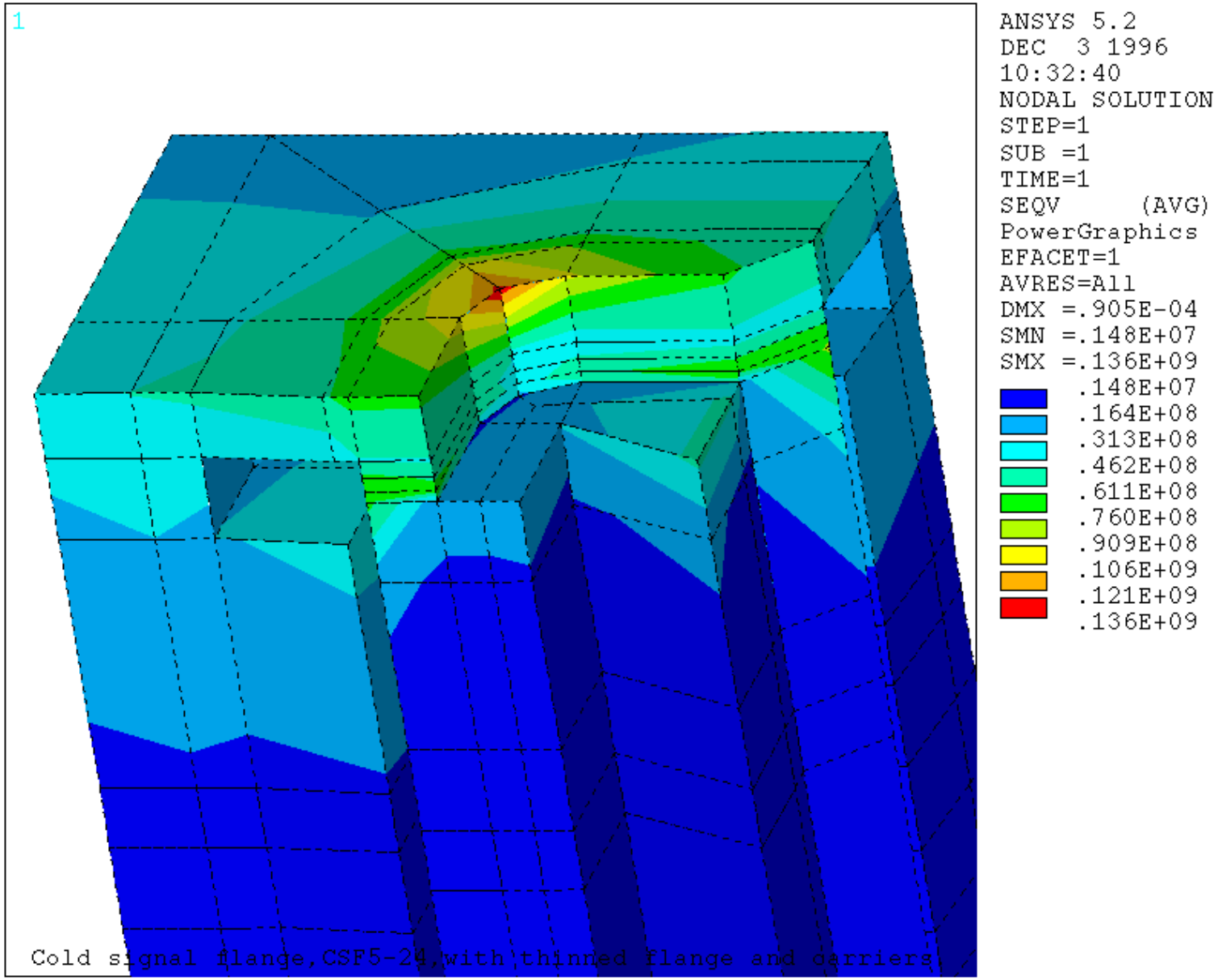

Figure 3: Finite element analysis of the cold flange showing (Von Mises) stress in Pascals under an applied load of 5 bars. Note the maximum stress of 136 MPa in the corner where the pin carrier meets the flange.

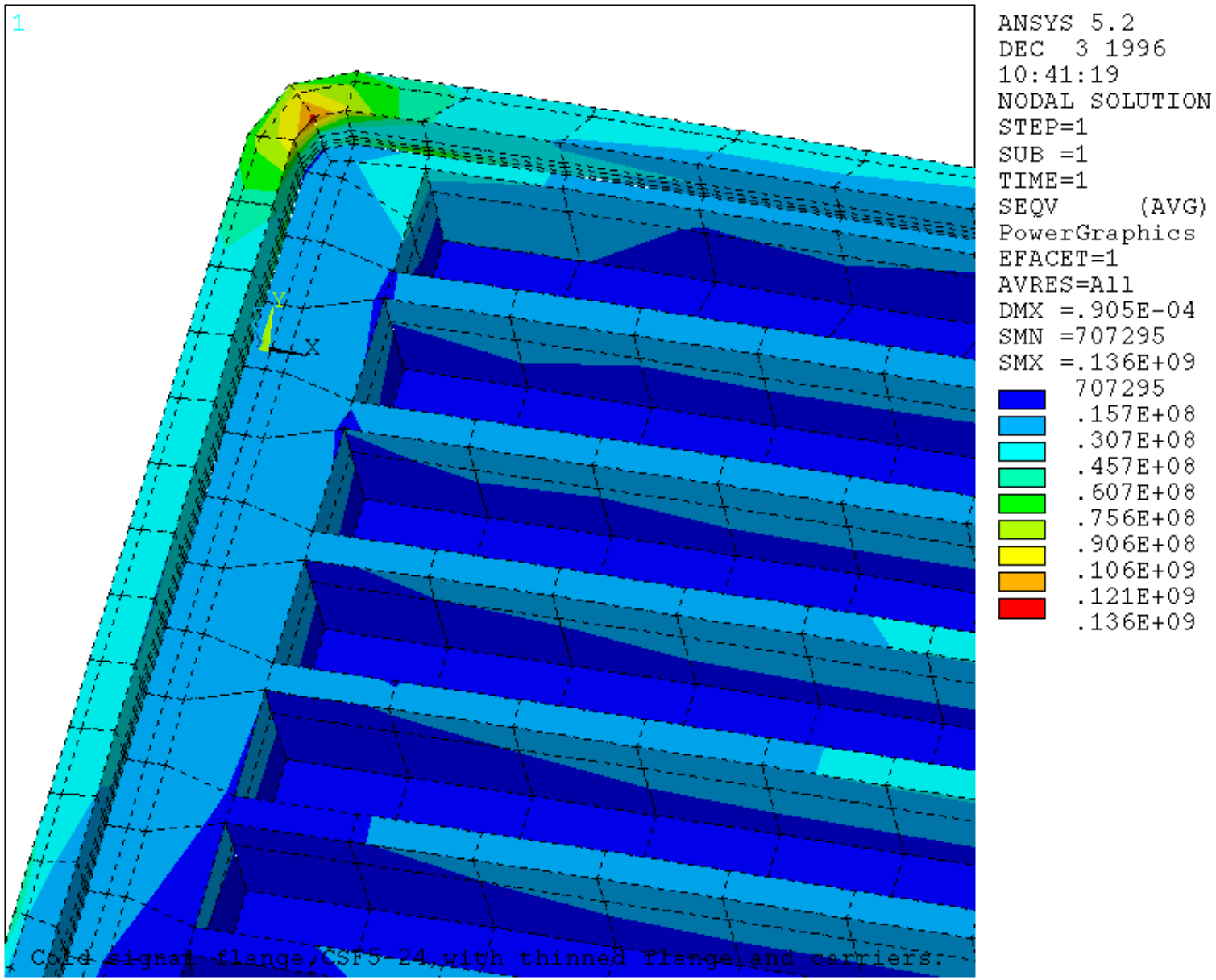

Figure 4: Finite element analysis of the cold flange showing (Von Mises) stress in Pascals under an applied load of 5 bars. Note that the high stress region is very localised.

3 Cold Flange Study (Release of 96/12/10)

The manufacturing of 15 connector pin carriers has been considered by Ceramaseal. The finite element analysis model for the cold flange was modified accordingly, replacing the 7 and 8 connector pin carriers with a single 15 connector pin carrier. One small difference between the present model and the earlier ones is the omission of the small section of cylindrical "skirt" attached to the outer edge of the flange (this would have an insignificant effect on the results). The finite element model of half a cold flange is shown in Figure 5.

The results are a little surprising at first glance: the bending of the flange under the pressure load of 5 bars increases only slightly from 90.5 mm to 95 mm (see Figure 6). On reflection, this is understandable, since the removal of the thick horizontal section between the 7 and 8 connector pin carriers is replaced in part by the 15 pin carrier thick sections and the cut-out section of the flange is reduced in size and is centered. The other surprise is that the stress in the corners of the pin carrier is reduced from 136 MPa to 102 MPa (see Figure 7) . The reason is that the high stress region of the 7 and 8 pin carriers was located at the corners close to the centre of the flange. In the 15 connector version, these corners do not exist, and the high stress region is in the corners near the centerline of the flange but much farther from the centre. The model does not include the extra material at the ends of the 15 connector carrier, as suggested by Ceramaseal, but this is not expected to produce a significant change in the results.

Note that the yield and ultimate stress values for the flange and pin carrier material (AISI 304L stainless steel) are $\sim$230 MPa and 483 MPa respectively.

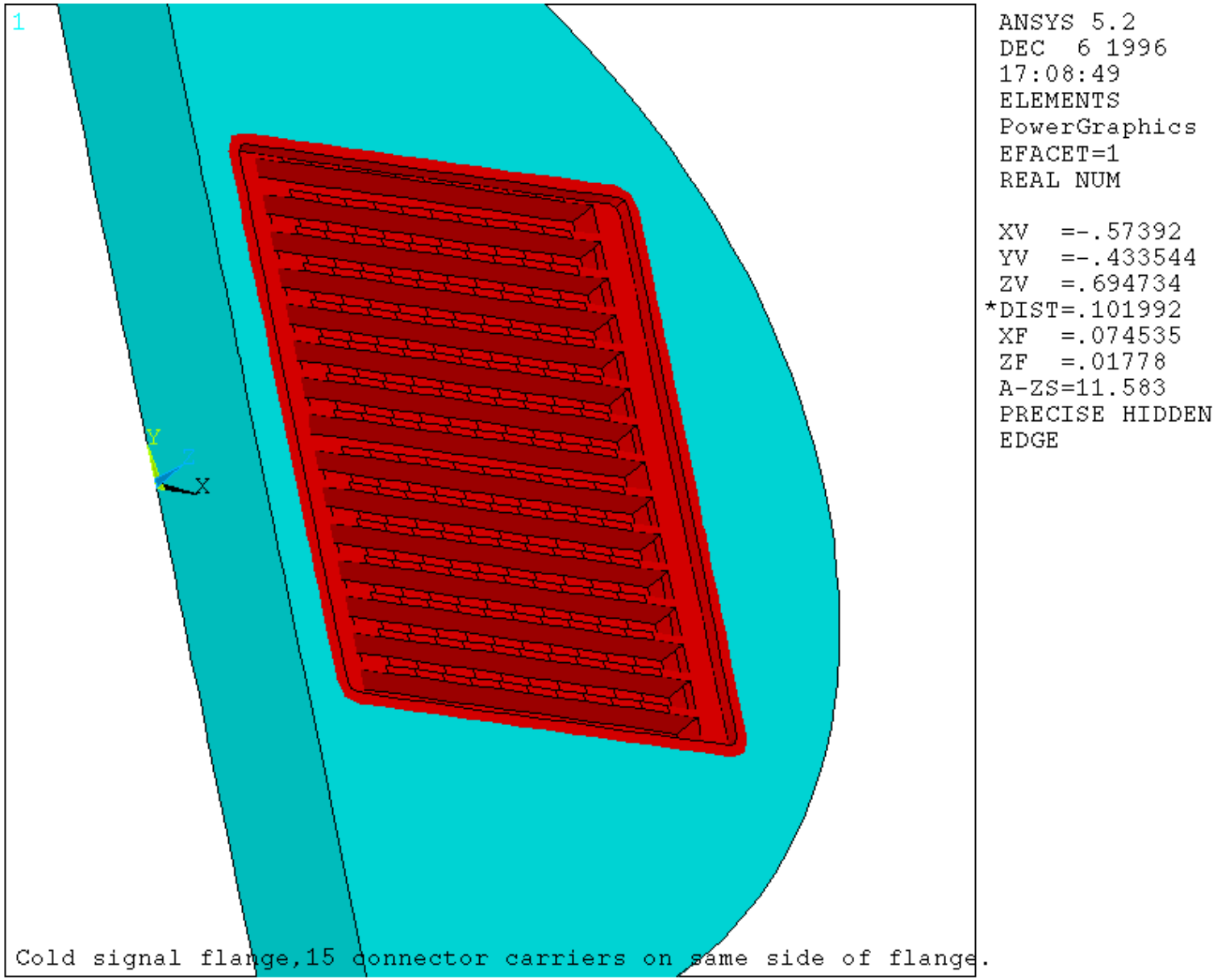

Figure 5: Finite element analysis model of half a cold flange for 15 connector pin carriers. Dimensions in metres.

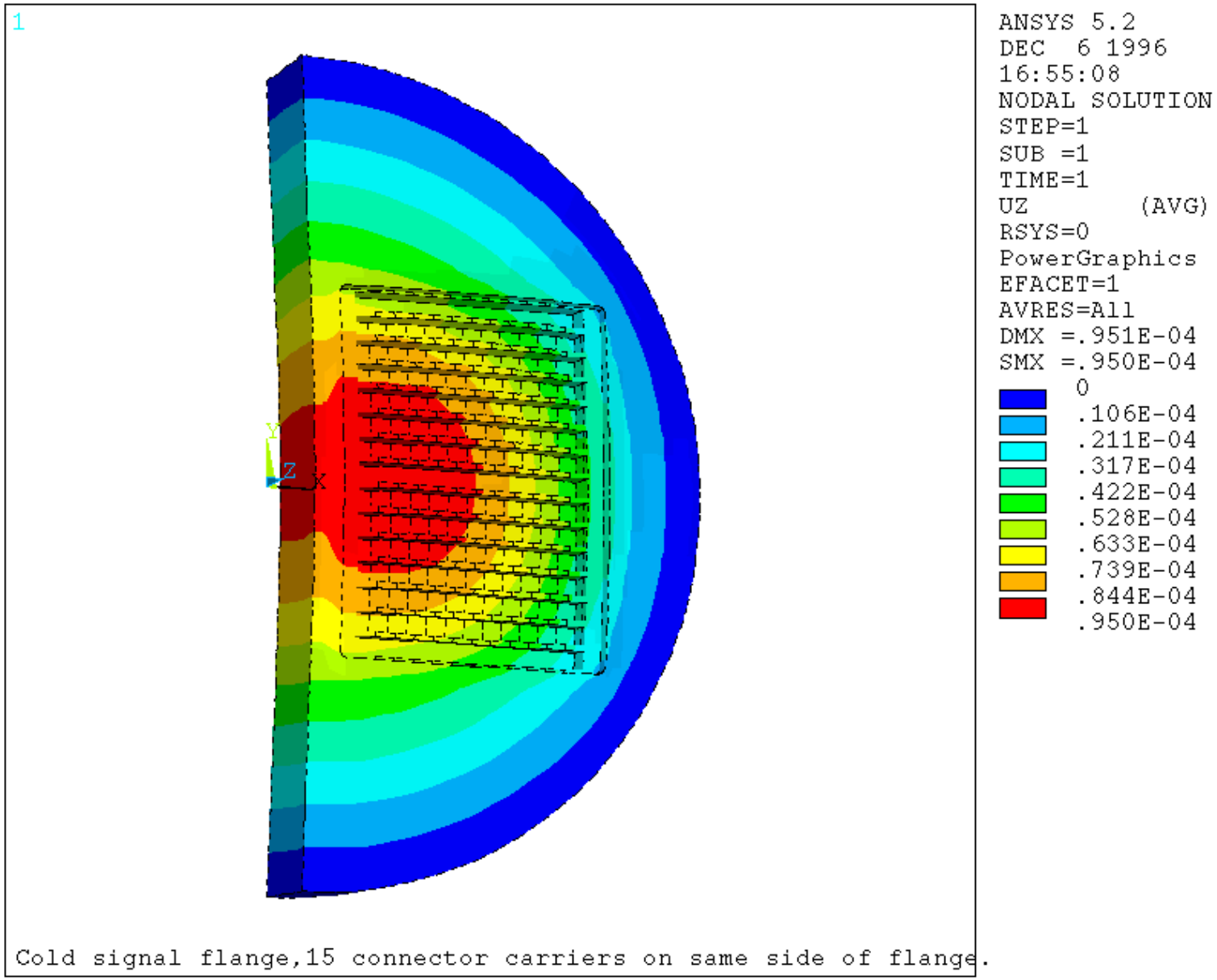

Figure 6: Finite element analysis of the cold flange for 15 connector pin carriers showing the deflection in metres under an applied load of 5 bars. Note the maximum deflection of 95 μm.

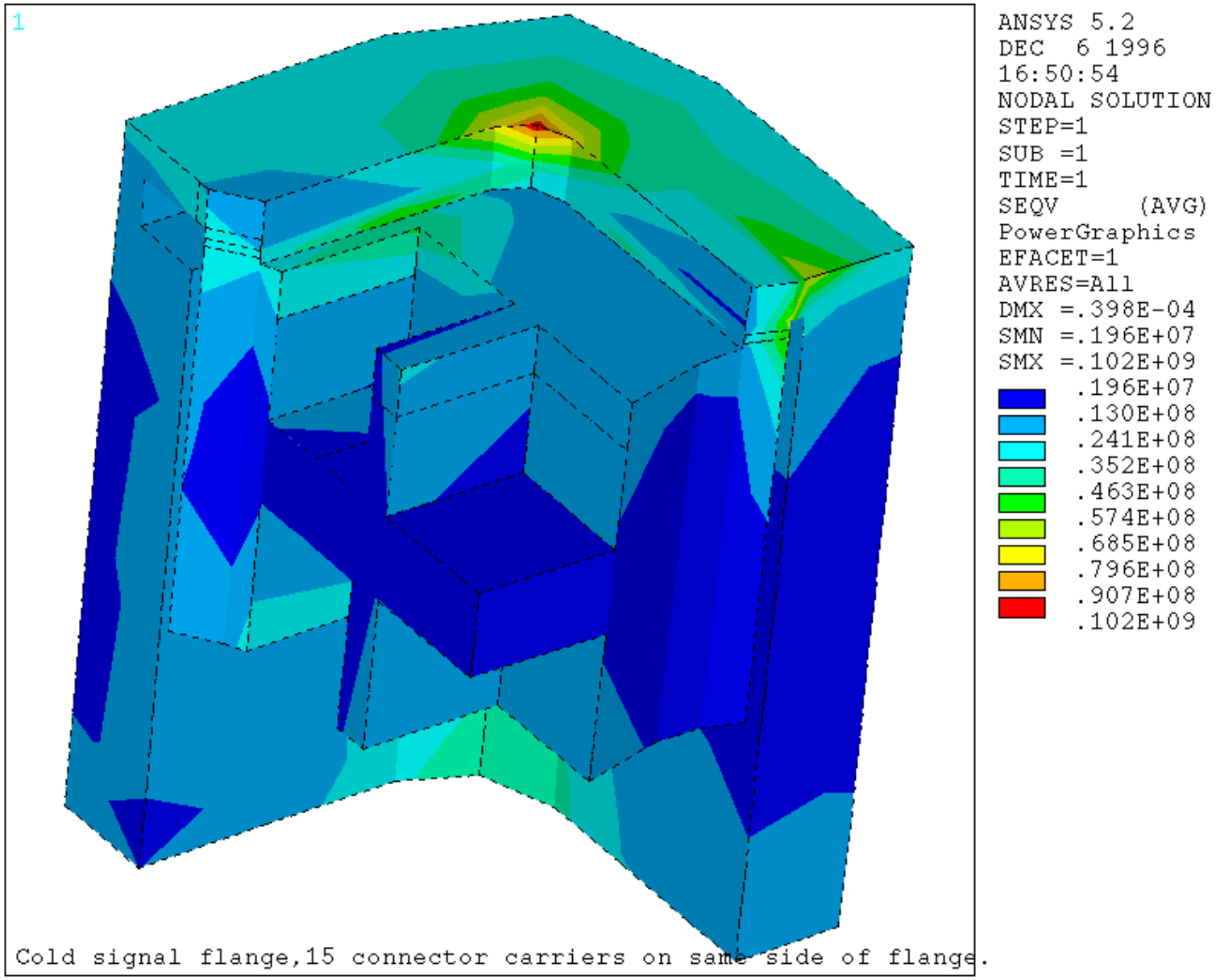

Figure 7: Finite element analysis of the cold flange for 15 connector pin carriers under an applied load of 5 bars. Details of (Von Mises) stress in Pascals at corner of pin carrier. Note the very localised maximum stress of 102 MPa.

4 Cold Flange Study (Release of 97/02/07)

The cold flange described in drawing GBL 20011-600004-5 is modelled for finite element analysis. As for previous analyses, half the flange is modelled using the symmetry plane of the flange. The pin carriers are considered joined to the flange over a 1 mm wide strip around the lip of the pin carrier weld flange (simulating the weld). Details of the model are shown on Figure 8, Figure 9 and Figure 10. A pressure of 5 bars is applied to the flange face and to the pin carriers on the surface where the welding was done. The flange is supported at the outer edge.

This analysis addresses the question of whether the pin carrier web can be safely reduced to 1.5 mm thick, and what is the required cold flange thickness.

Reducing the pin carrier web thickness has little effect on the flange deflection or on the maximum stress levels (which occur at the inner surface of the corners of the pin carrier weld flange). In the region of the web penetrated by the signal pins, there is a general reduction in stress level. There is, however, a very small (5%) increase in the localized maximum stress.

Reduction of the flange thickness causes increased deflection and an increase in the maximum stress level in the pin carrier corners. Varying the flange thickness has a somewhat more complex effect on the pin carrier in the region of the web penetrated by the signal pins. A thicker flange produces lower general stress levels in the web but increases the maximum stress in localized areas. As the flange thickness is reduced, the general stress levels rise slowly and the maximum (localized) stress falls, and then begins to rise again.

Deflection and stress for a 36 mm (1.4 inch) cold flange with a 1.5 mm thick pin carrier web are shown in Figure 11, Figure 12 and Figure 13. Results for various flange thickness are shown in Table 1.

Note that the yield and ultimate stress values for the flange and pin carrier material (AISI 304L stainless steel) are 172 MPa and 483 MPa respectively.

flange thickness (mm)	flange web thickness (mm)	pressure (bars)	deflection (mm)	pin carrier corner stress (MPa)	maximum web stress in pin region (MPa)	general web stress in pin region (MPa)
32	3.3	5	0.110	138	13	4–10
32	1.5	5	0.110	138	15	3–6
36	1.5	5	0.081	111	18	2–6
30.5	1.5	5	0.126	151	14	4–6
29	1.5	5	0.144	166	16	4–9

Table 1: Deflection and stress for cold flange.

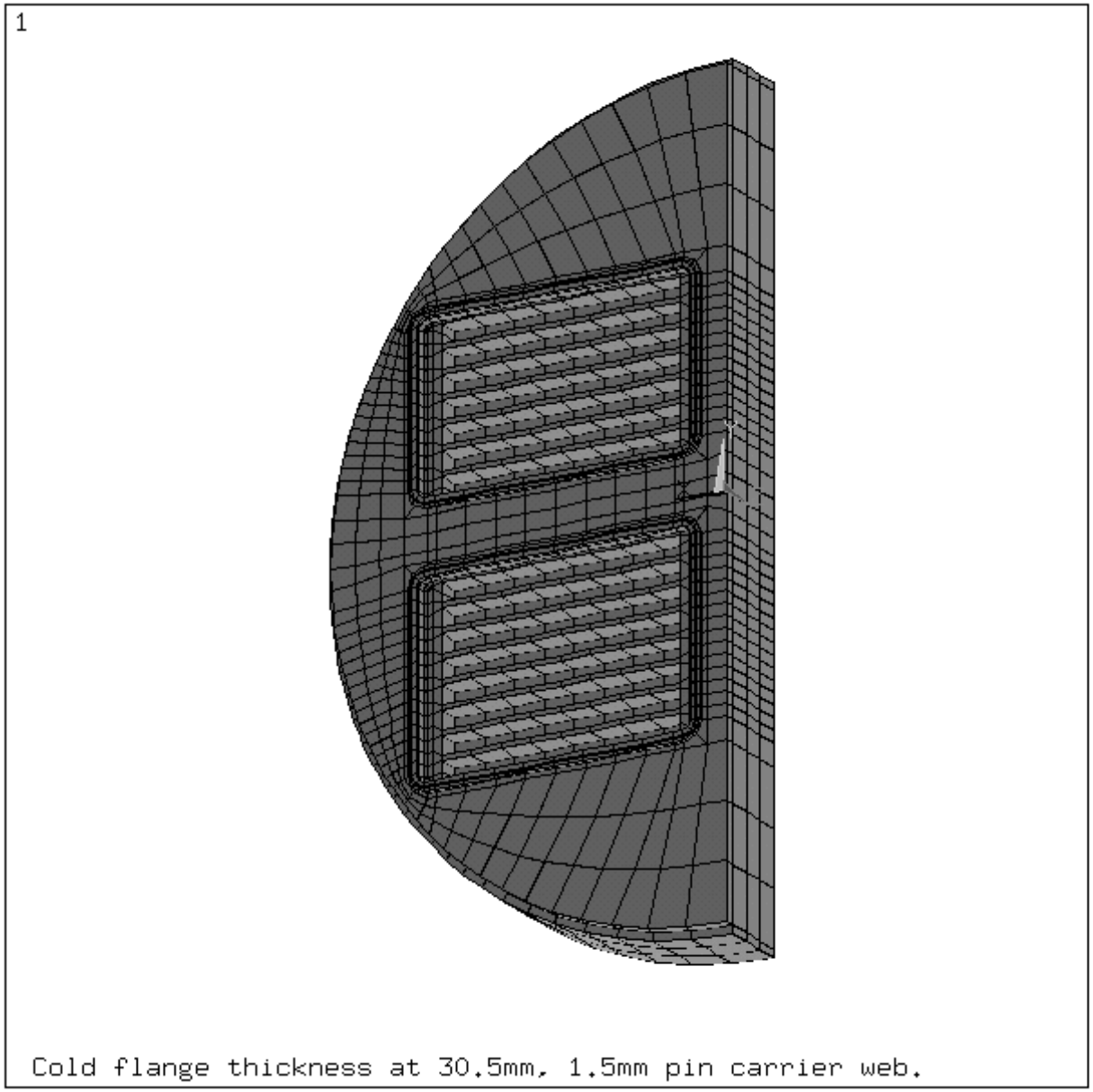

Figure 8: Finite element analysis model of half a cold flange. Dimensions in metres.

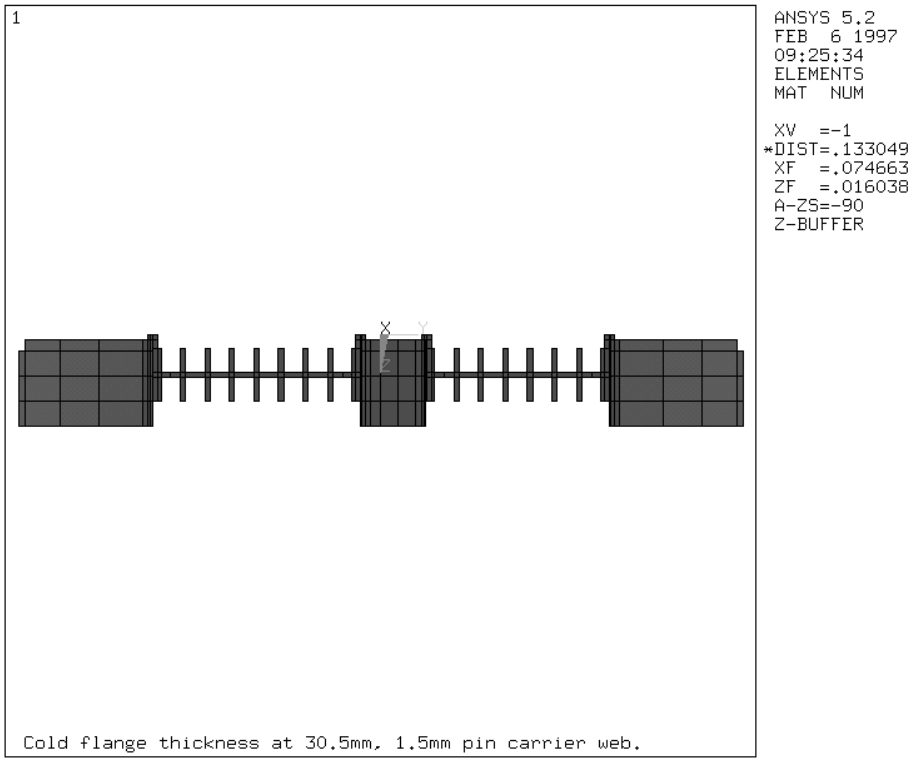

Figure 9: Detail of the finite element analysis model of the cold flange. Section through the flange and pin carrier. Dimensions in metres.

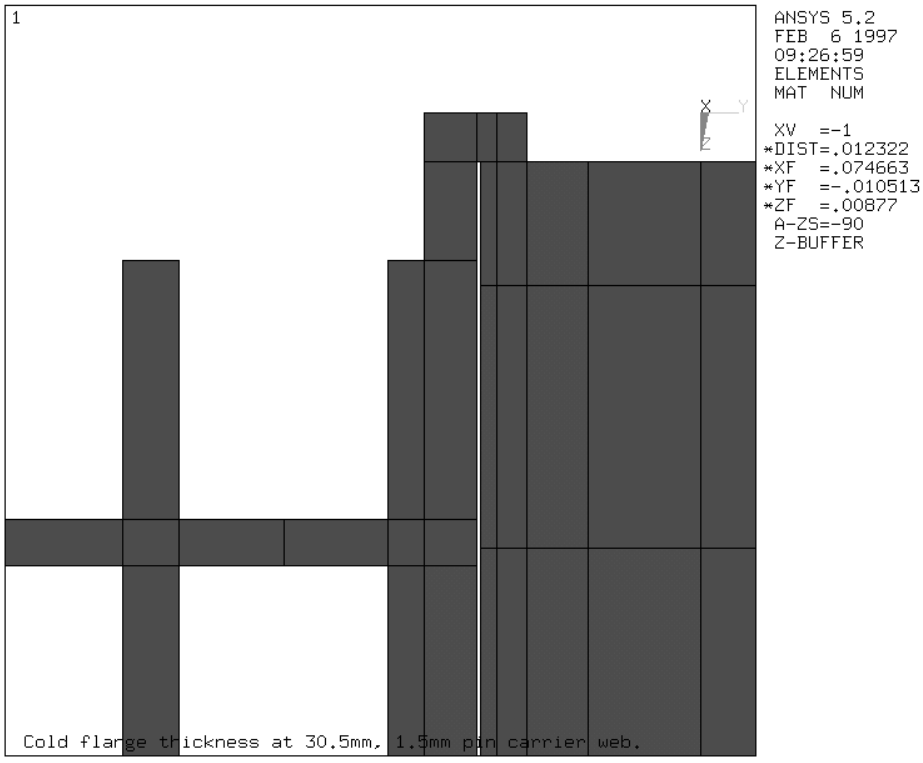

Figure 10: Detail of the finite element analysis model of the cold flange. Enlarged section showing the flange and pin carrier joint. Dimensions in metres.

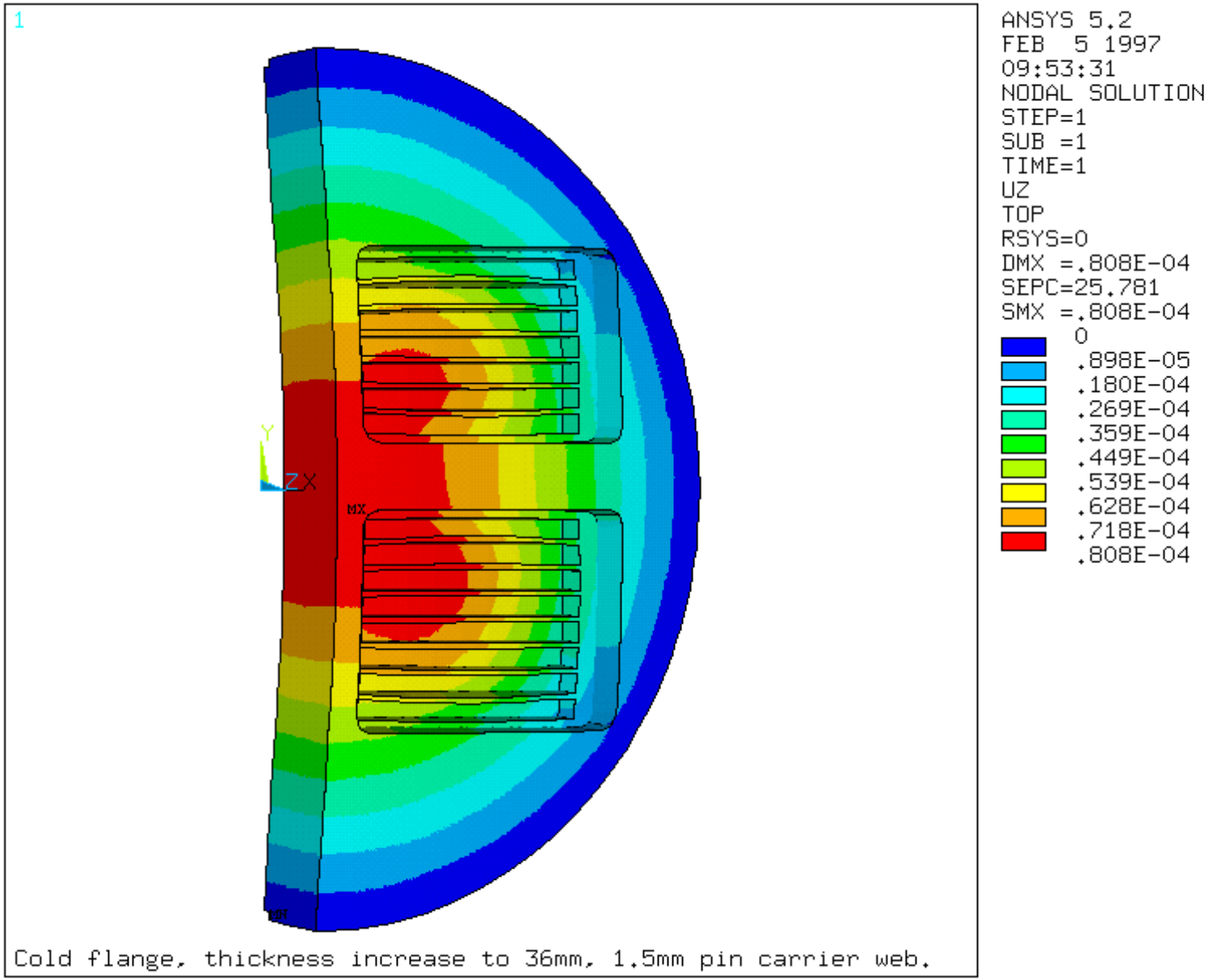

Figure 11: Finite element analysis of a cold flange with thickness 36 mm (1.4 inches) and web thickness 1.5 mm showing deflections in metres under an applied load of 5 bars.

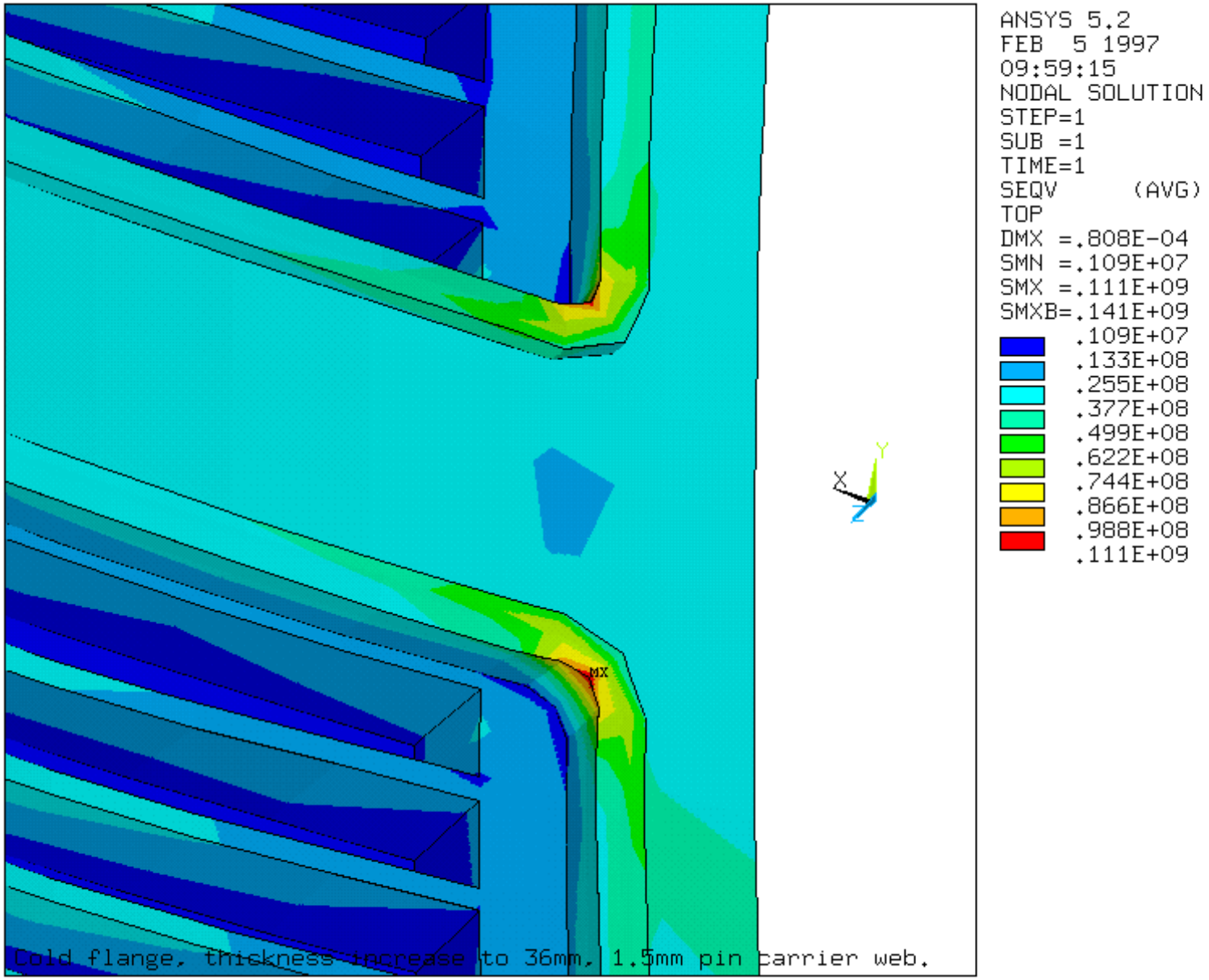

Figure 12: Finite element analysis of a cold flange with thickness 36 mm (1.4 inches) and web thickness 1.5 mm showing (Von Mises) stress in Pascals in the corners of the pin carrier under an applied load of 5 bars.

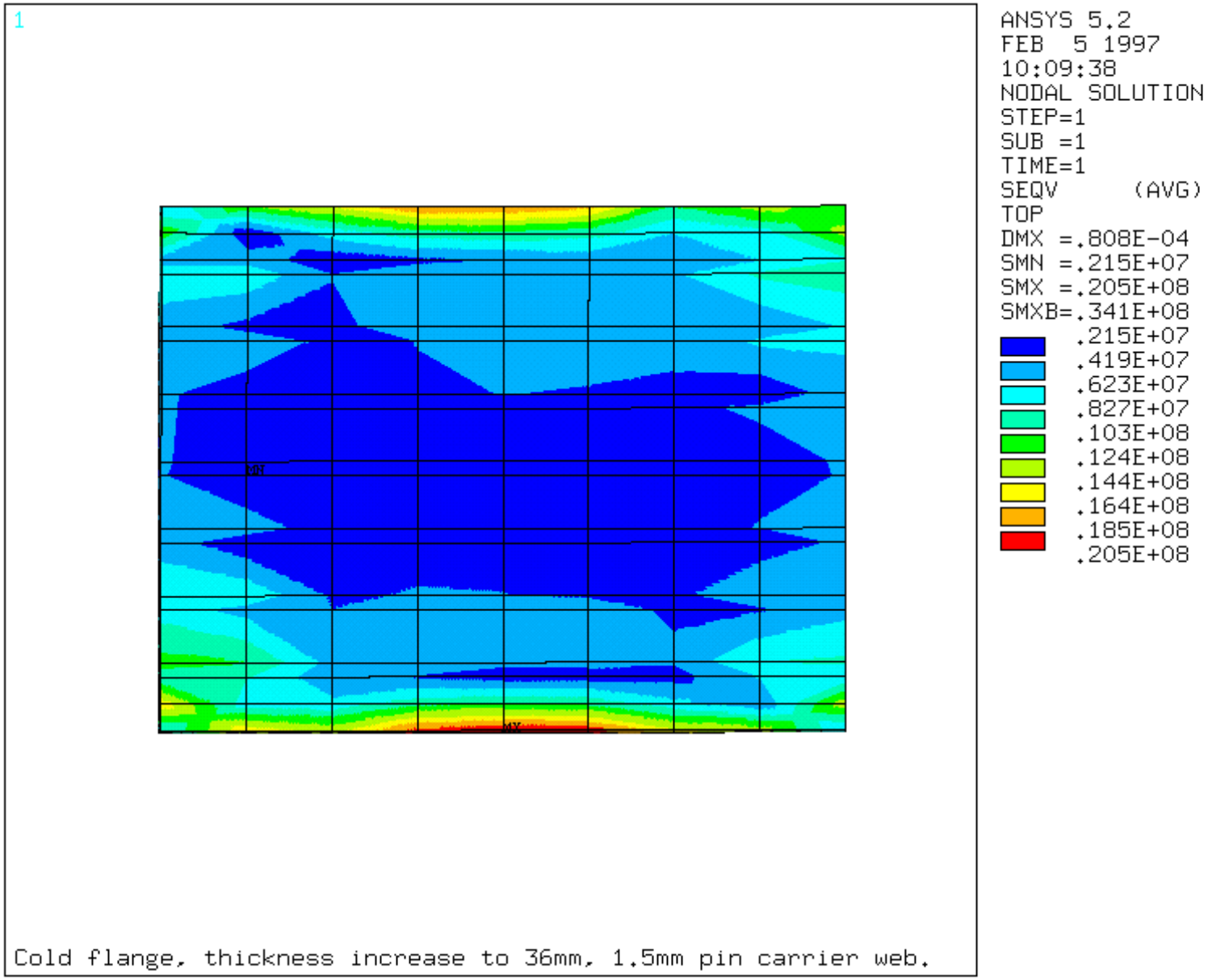

Figure 13: Finite element analysis of a cold flange with thickness 36 mm (1.4 inches) and web thickness 1.5 mm showing (Von Mises) stress in Pascals in the pin carrier web under an applied load of 5 bars.

5 Ambient Flange Study (Releases of 97/02/26 and 97/02/28)

The ambient flange described in drawing GBL 20011-600004-5 is modelled for finite element analysis. As for previous analyses, half the flange is modelled using the symmetry plane of the flange. The pin carriers are considered joined to the flange over a 1 mm wide strip around the lip of the pin carrier weld flange (simulating the weld). The pin carrier web thickness is 1.5 mm. Pressures of 1 bar and 5 bars are applied to the flange face and to the pin carriers on the surface where the pin carriers are welded to the flange. The flange is supported at the outer edge.

Results for deflection and (Von Mises) stress for an ambient flange 22.9 mm (0.9 inch) thick under an applied load of 1 bar are shown in Figure 14, Figure 15 and Figure 16. Results for 5 bars are shown in Figure 17, Figure 18 and Figure 19.

As expected, the deflection and stresses change linearly with the applied pressure while the model remains elastic. The highest stress in the flange and pin carrier occurs, as usual, in the corner of the pin carriers near the flange centre. Results are summarized in Table 2.

The way in which the flange would likely fail under pressure load can be inferred from Figure 20. The high stress region near the centre of the plate between the two 8 connector pin carriers would probably buckle: the feedthrough might already be leaking due to cracking at the pin carrier corners or at the weld.

The use of a 36 mm (1.4 inches) thick ambient flange is also considered for possible operation with service at the cold flange position. Results for deflection and stress for this thick ambient flange under an applied load of 5 bars are shown in Figure 21, Figure 22 and Figure 23, and are summarized in Table 2.

Comparing Figure 20 with Figure 24 we see that the maximum stress in the flange reduces from 136 MPa to 61 MPa. Note that the yield and ultimate stress values for the flange and pin carrier material (AISI 304L stainless steel) are $\sim$230 MPa and 483 MPa respectively.

The results are in accord with the findings for the cold flange. There is an optimum thickness for the plate in terms of pin carrier web stresses, but one must also consider the stress in the corner of the pin carriers and in the flange, especially in the regions near the plate centre. The smaller diameter ambient flange, with the same thickness as the cold flange (1.4 inches), is slightly stiffer than the cold flange. The pin carrier stresses are therefore slightly increased, while the pin carrier corner stress and flange stress are slightly reduced. Some "fine tuning" on the thickness of the flange and position of the pin carriers would make some small improvement.

flange thickness (mm)	flange web thickness (mm)	pressure (bars)	deflection (mm)	pin carrier corner stress (MPa)	maximum web stress in pin region (MPa)	general web stress in pin region (MPa)
22.9	1.5	1	0.051	46	4	0.5–2
22.9	1.5	5	0.255	229	20	2–10
36	1.5	5	0.085	101	20	3–10

Table 2: Deflection and stress for ambient flange.

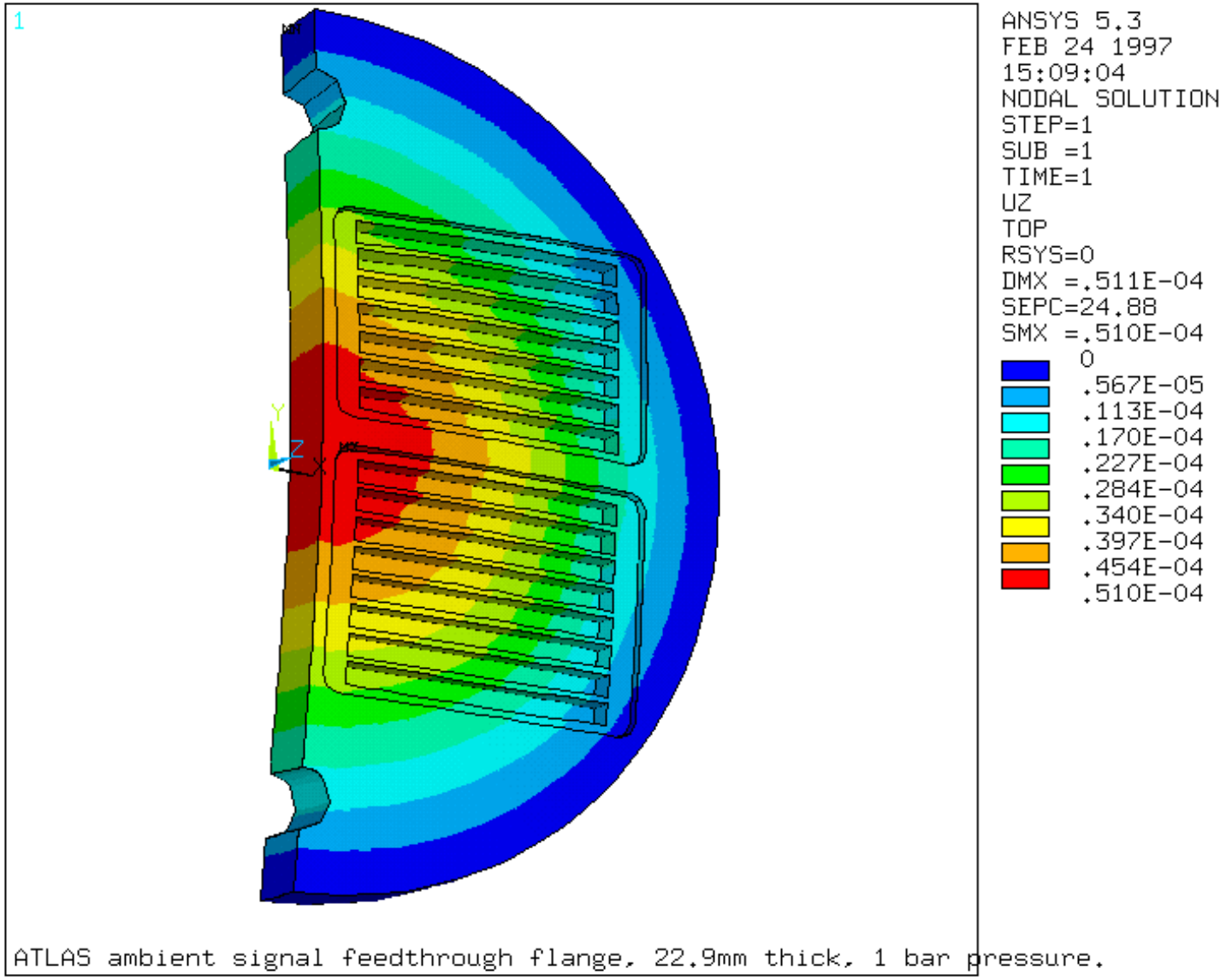

Figure 14: Finite element analysis of an ambient flange with thickness 22.9 mm (0.9 inch) and web thickness 1.5 mm showing deflections in metres under an applied load of 1 bar.

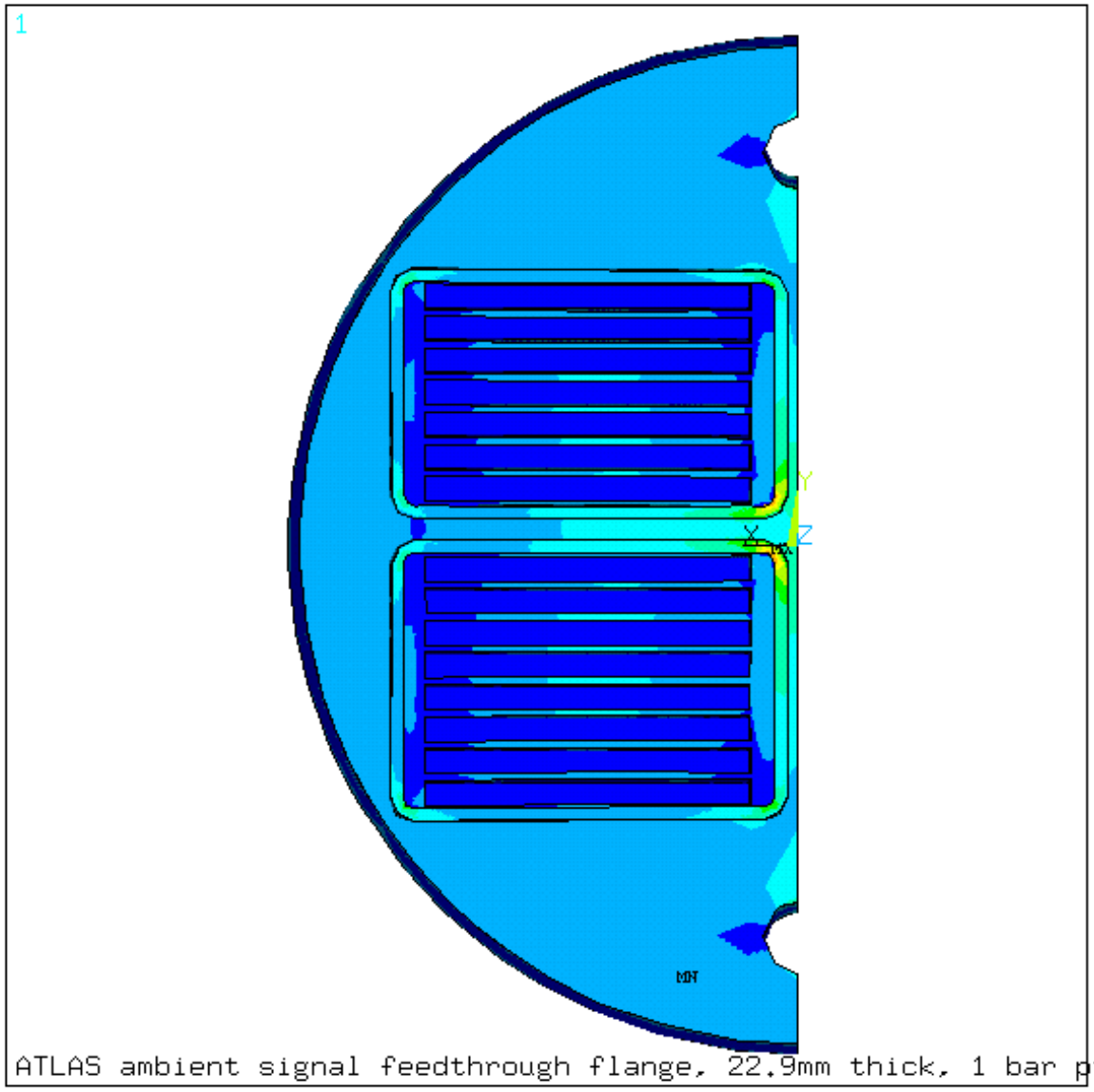

Figure 15: Finite element analysis of an ambient flange with thickness 22.9 mm (0.9 inch) and web thickness 1.5 mm showing (Von Mises) stress in Pascals in the flange and the pin carriers under an applied load of 1 bar.

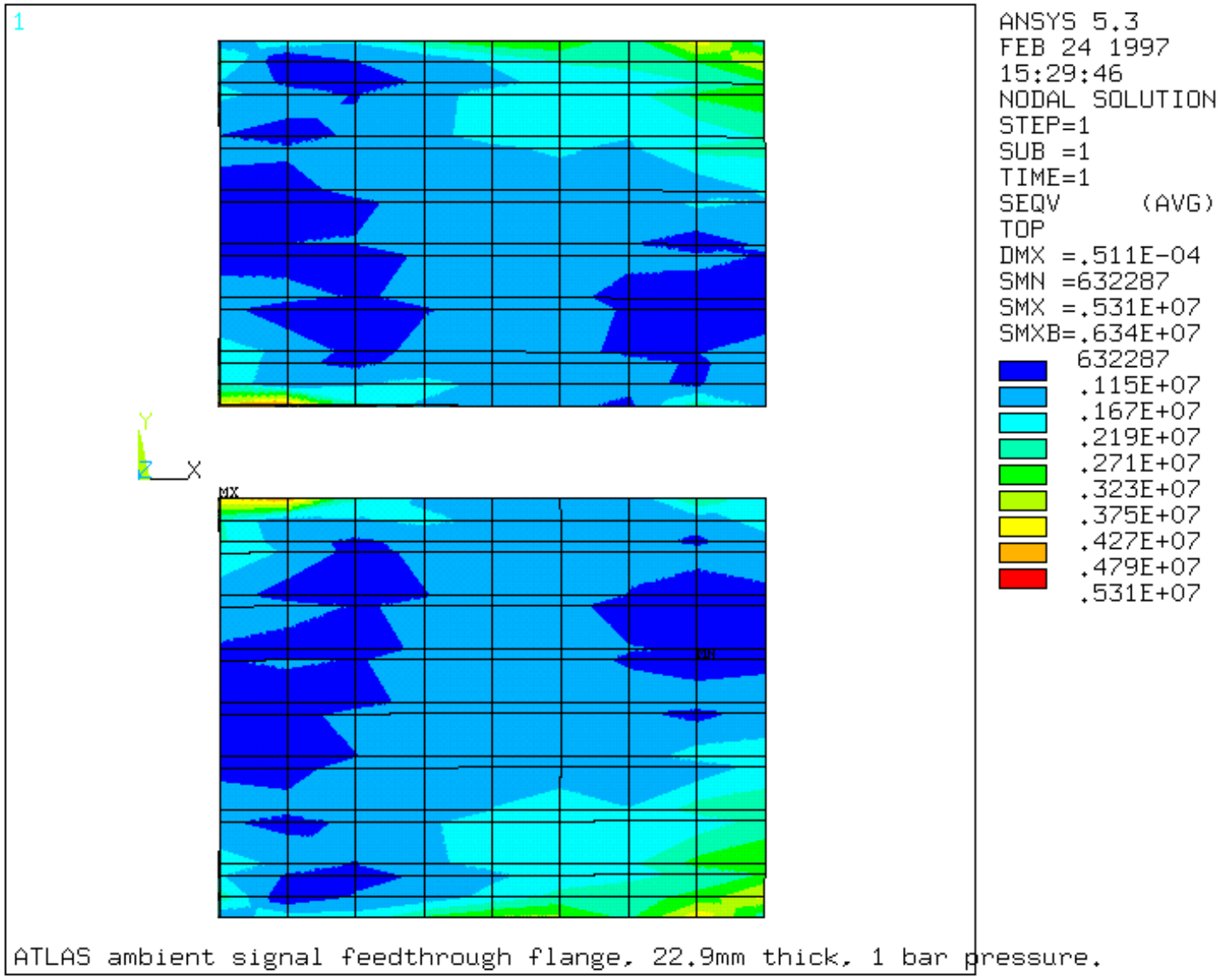

Figure 16: Finite element analysis of an ambient flange with thickness 22.9 mm (0.9 inch) and web thickness 1.5 mm showing (Von Mises) stress in Pascals in the pin carriers' web under an applied load of 1 bar.

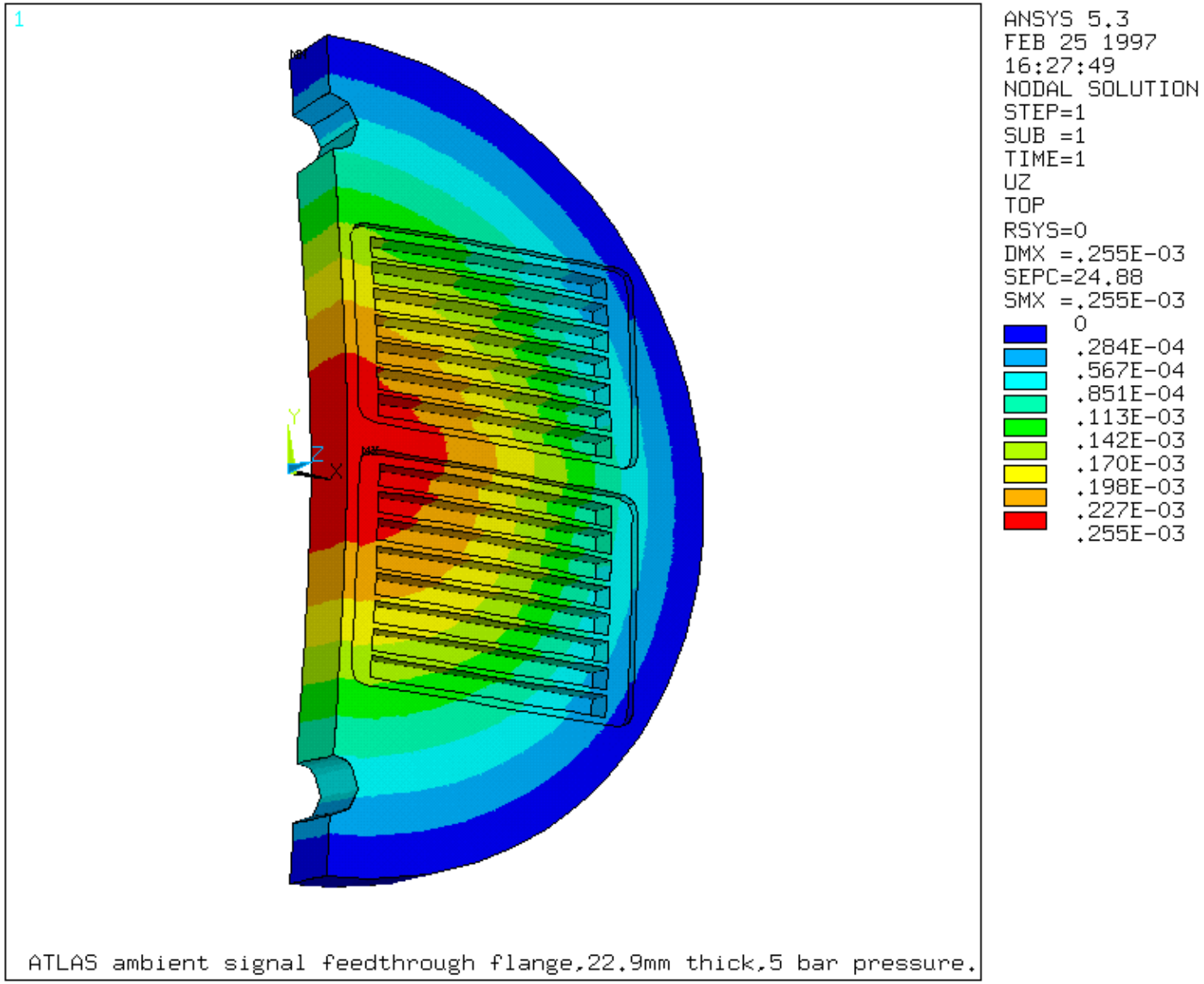

Figure 17: Finite element analysis of an ambient flange with thickness 22.9 mm (0.9 inch) and web thickness 1.5 mm showing deflections in metres under an applied load of 5 bar.

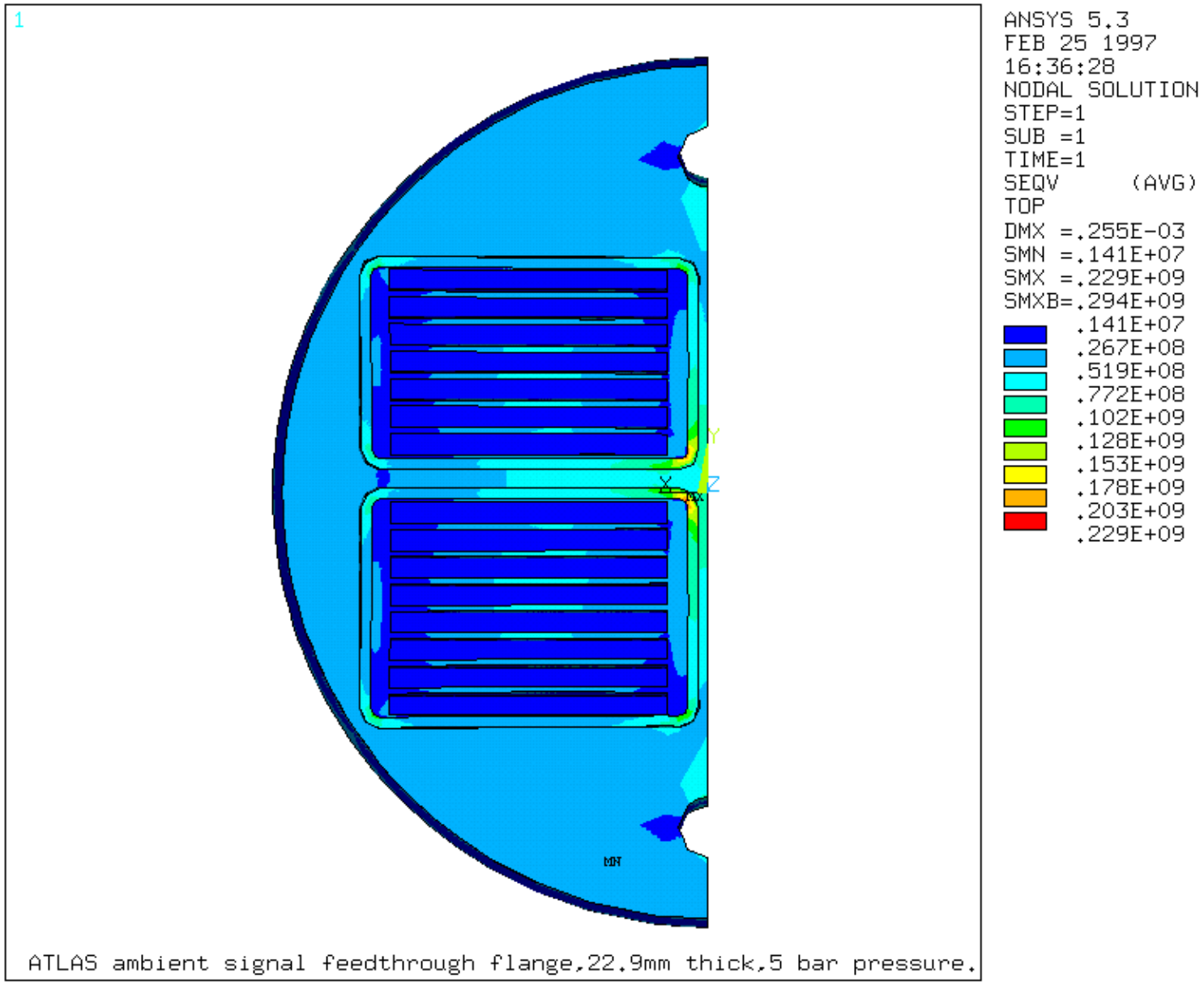

Figure 18: Finite element analysis of an ambient flange with thickness 22.9 mm (0.9 inch) and web thickness 1.5 mm showing (Von Mises) stress in Pascals in the flange and the pin carriers under an applied load of 5 bar.

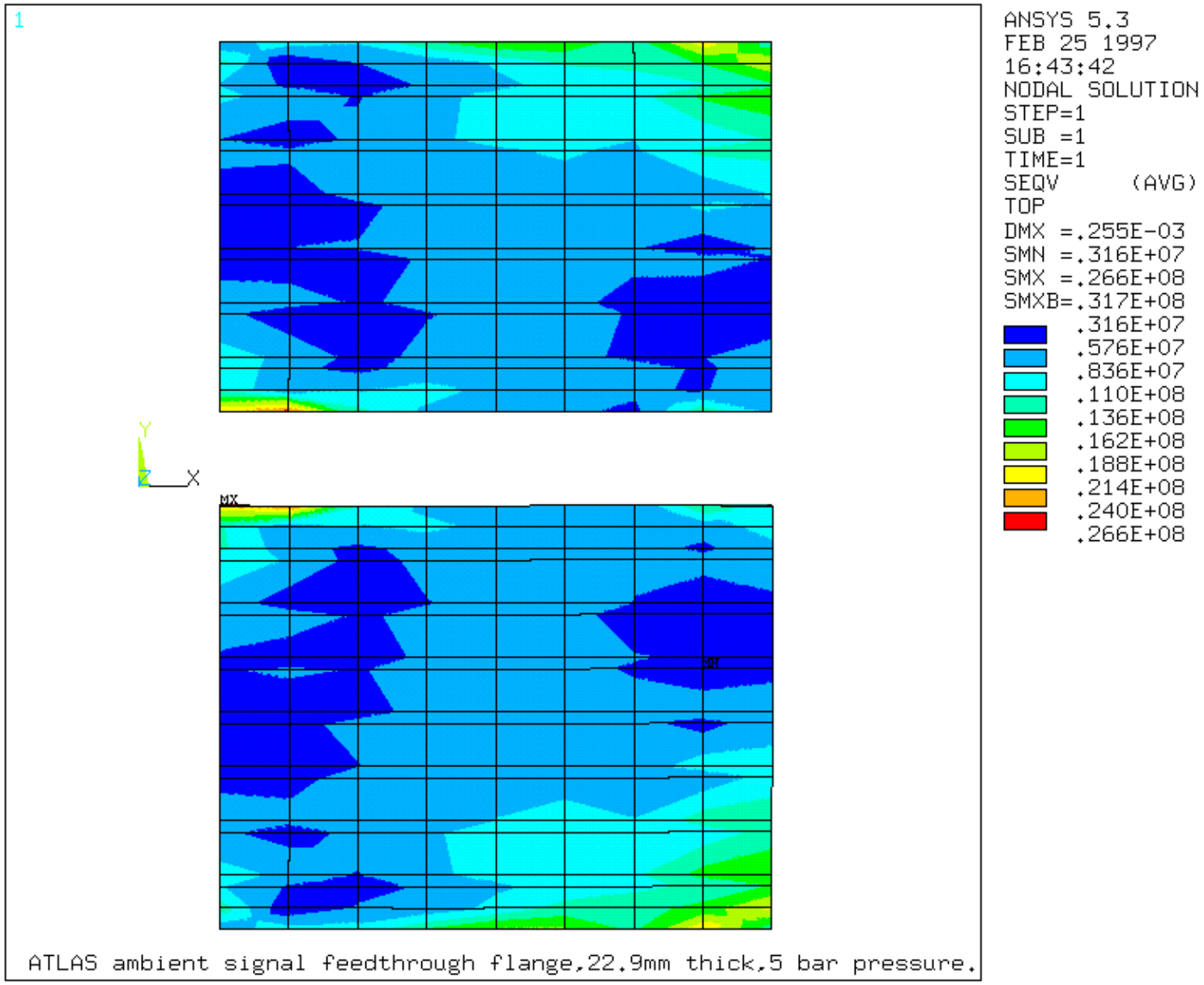

Figure 19: Finite element analysis of an ambient flange with thickness 22.9 mm (0.9 inch) and web thickness 1.5 mm showing (Von Mises) stress in Pascals in the pin carriers' web under an applied load of 5 bar.

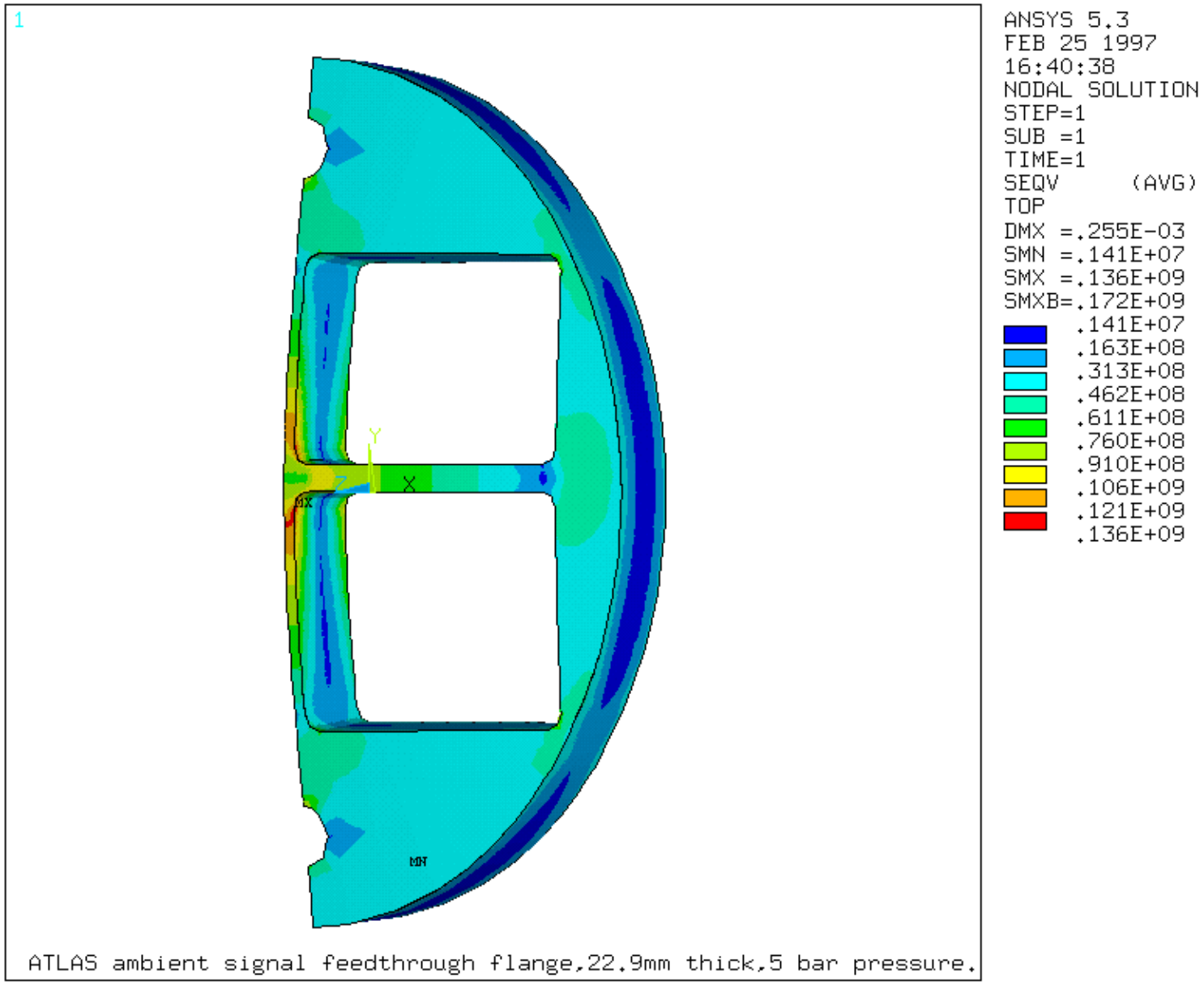

Figure 20: Finite element analysis of an ambient flange with thickness 22.9 mm (0.9 inch) and web thickness 1.5 mm showing (Von Mises) stress in Pascals in the flange alone (back view) under an applied load of 5 bar.

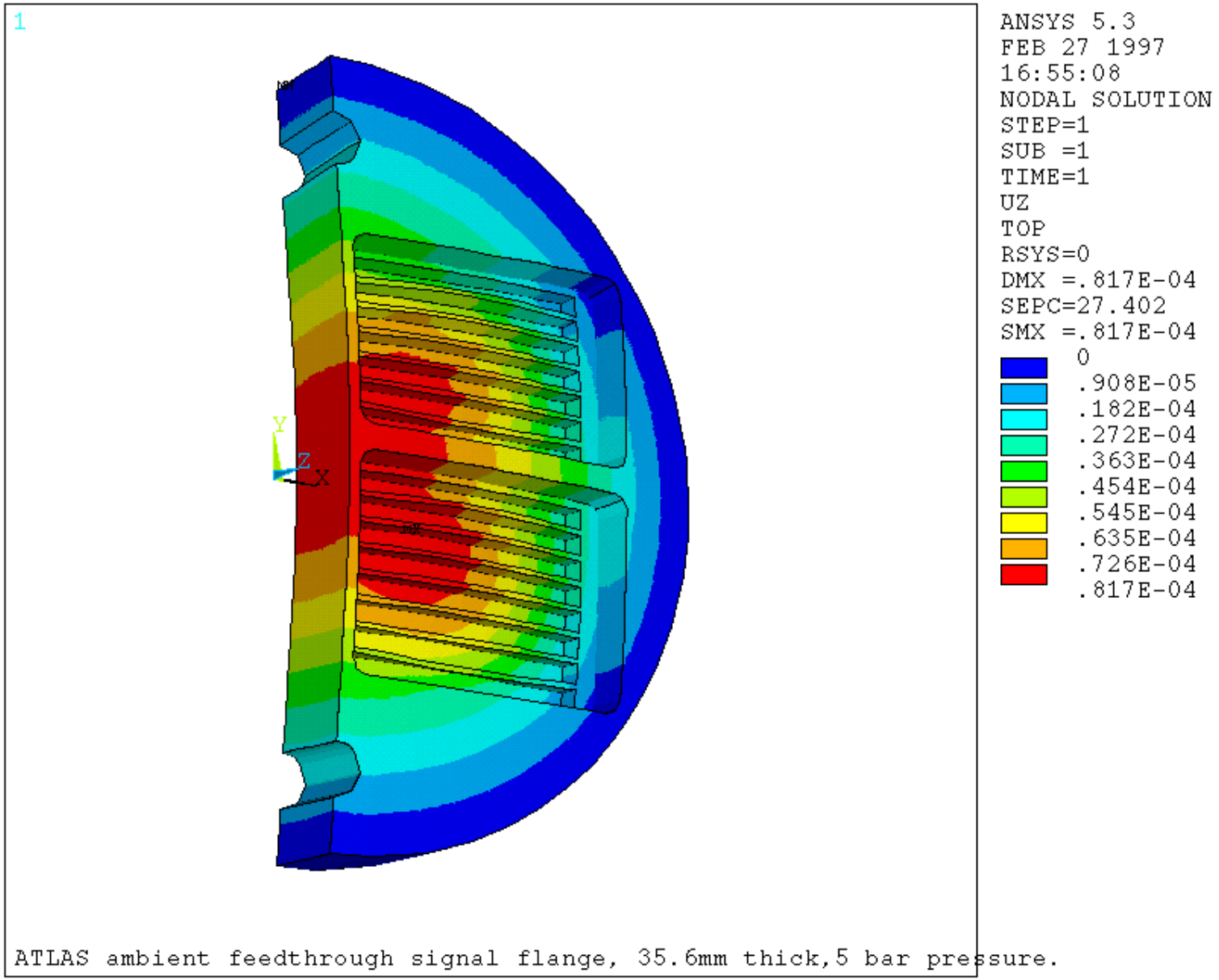

Figure 21: Finite element analysis of an ambient flange with thickness 36 mm (1.4 inches) and web thickness 1.5 mm showing deflections in metres under an applied load of 5 bar.

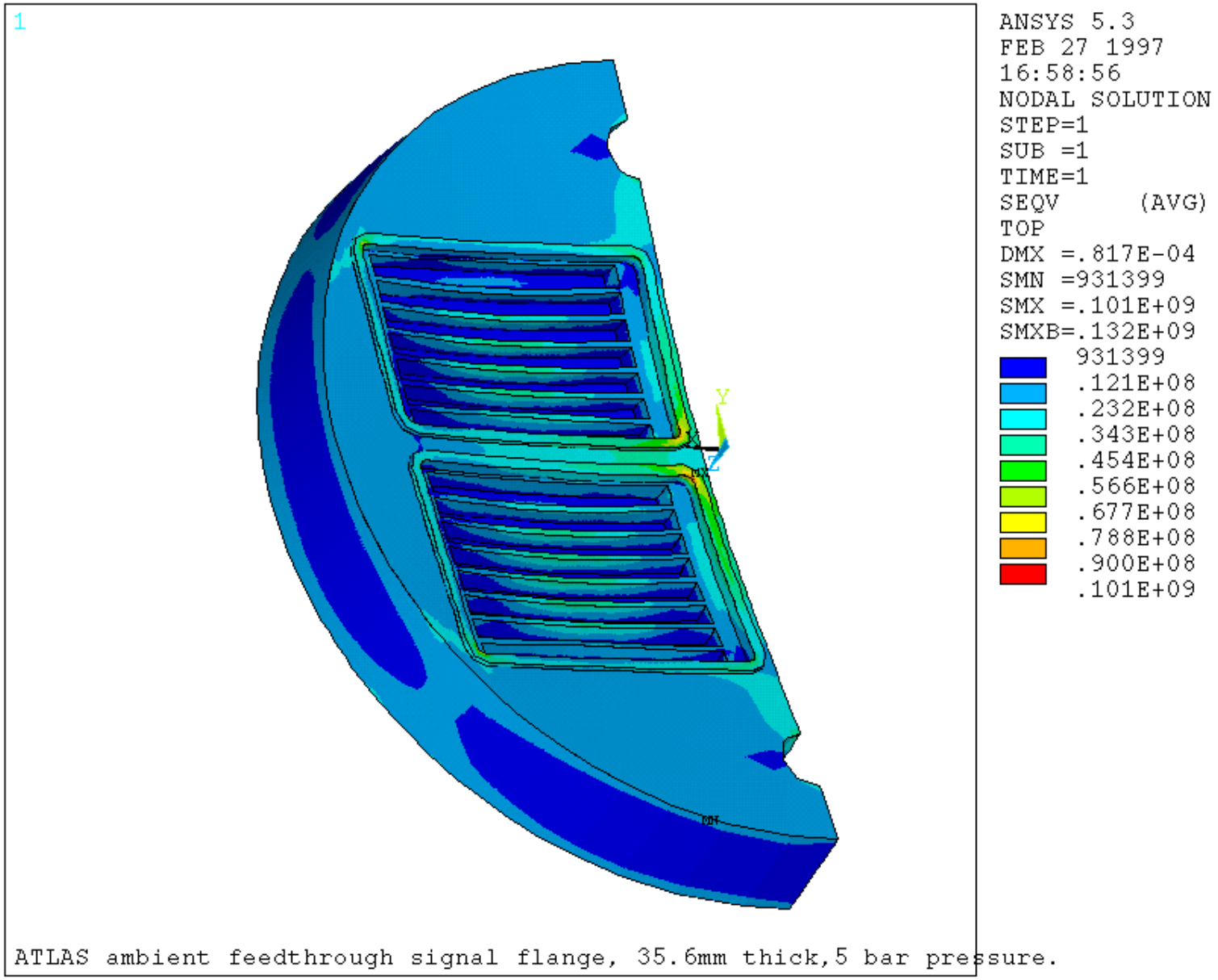

Figure 22: Finite element analysis of an ambient flange with thickness 36 mm (1.4 inches) and web thickness 1.5 mm showing (Von Mises) stress in Pascals in the flange and the pin carriers under an applied load of 5 bar.

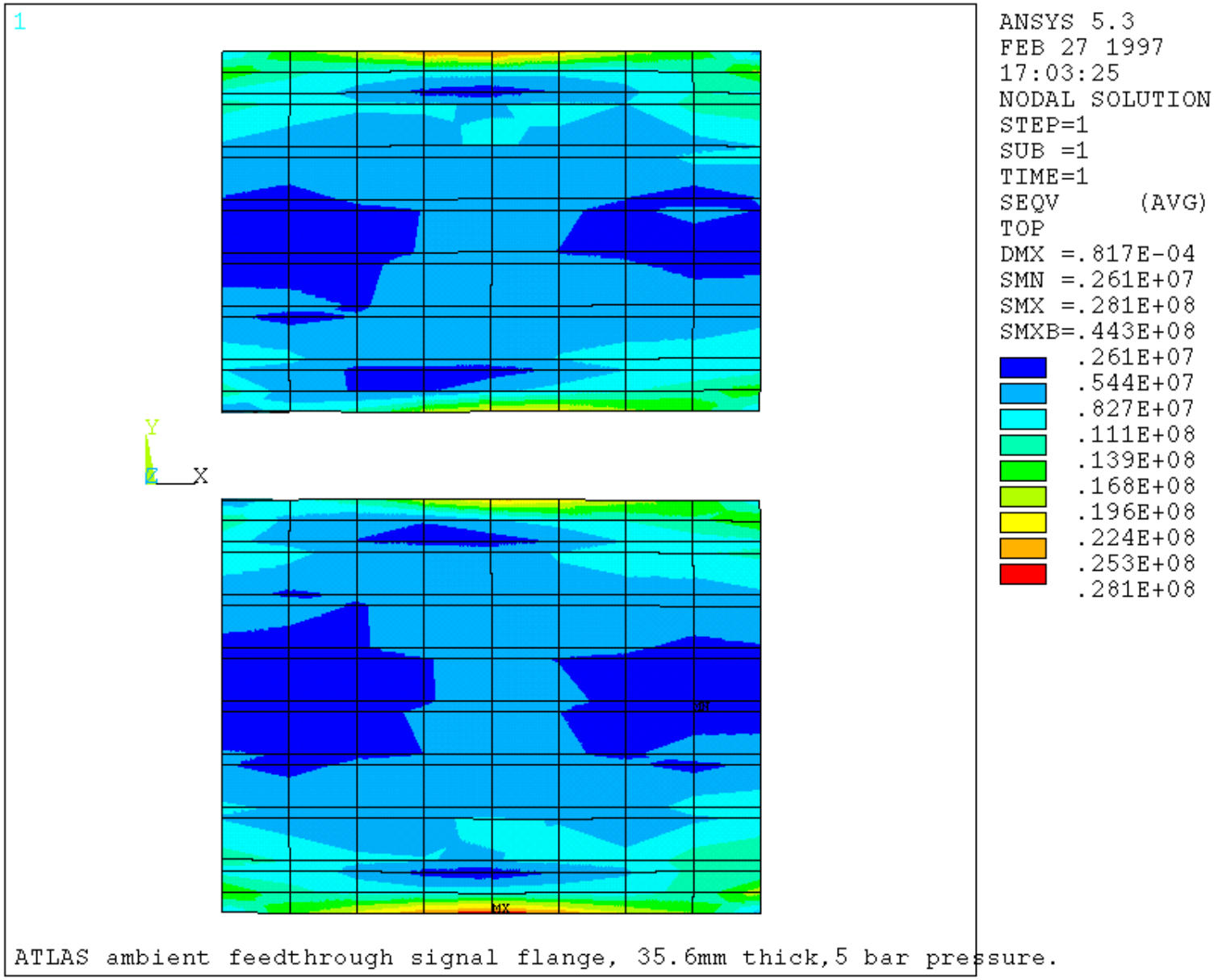

Figure 23: Finite element analysis of an ambient flange with thickness 36 mm (1.4 inches) and web thickness 1.5 mm showing (Von Mises) stress in Pascals in the pin carriers' web under an applied load of 5 bar.

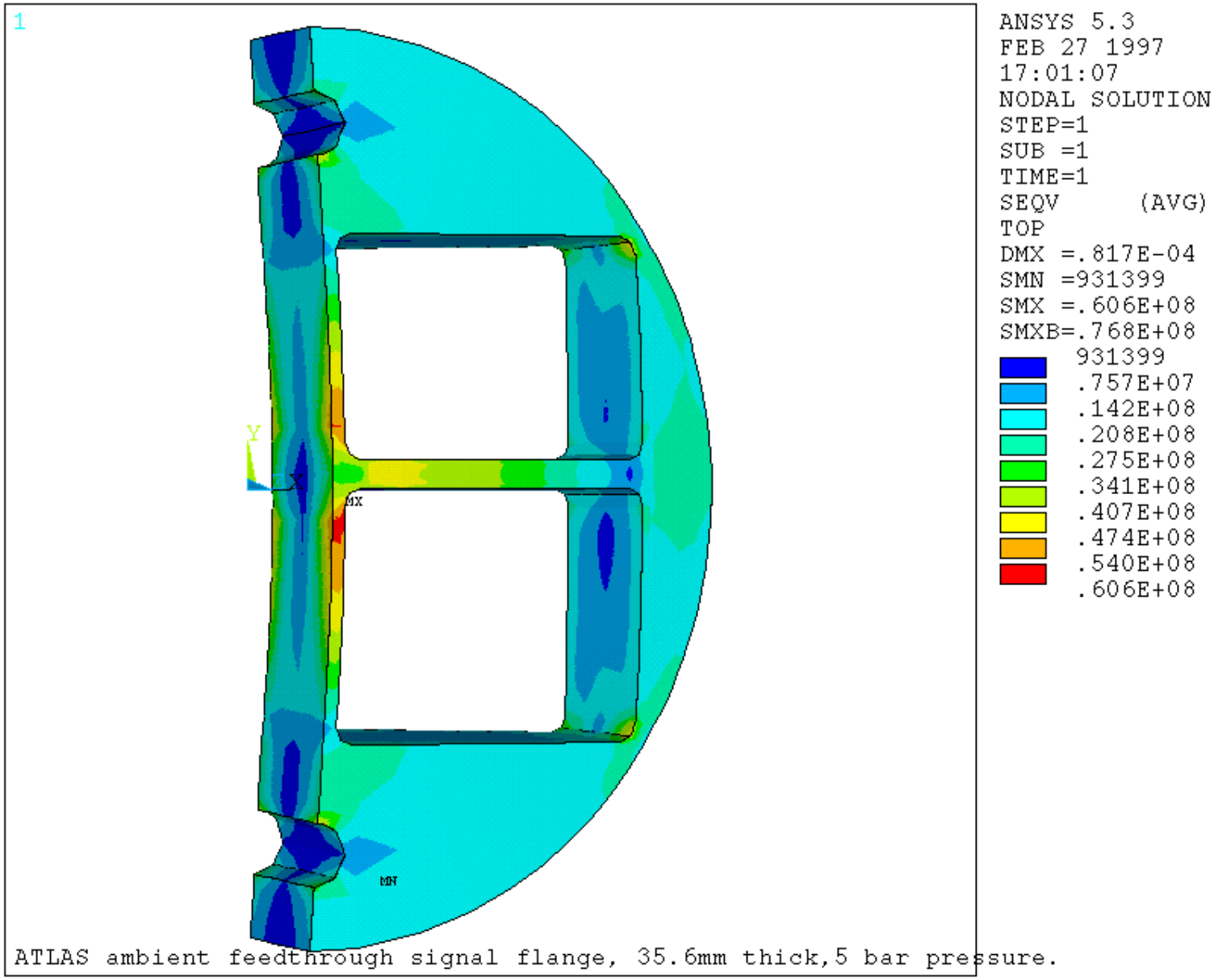

Figure 24: Finite element analysis of an ambient flange with thickness 36 mm (1.4 inches) and web thickness 1.5 mm showing (Von Mises) stress in Pascals in the flange alone (back view) under an applied load of 5 bar.

6 Ambient Flange with attached Seal Ring (Release of 97/04/29)

The ambient flange with the seal ring attached by a "weld" 1 mm thick (in radial direction) and 3 mm in depth (Z-direction, through the flange thickness) is modelled for finite element analysis. As before, half the flange was modelled using the symmetry plane of the flange. Pressure of 1 bar was applied to the flange face and pin carriers on the surface where the pin carriers are welded to the flange. The flange is supported by the seal ring which in turn was fixed in the Z-direction at the surface which would be clamped against the cryostat wall by the bolt ring. The model is shown on Figure 25.

The results for the ambient flange are quite similar to those obtained previously (see section 5). Deflection slightly increases from 51 μm to 53 μm (see Figure 26) and pin carrier corner stresses slightly reduce from 46 MPa to 43 MPa (see Figure 27). The pin carrier web stresses are little changed (see Figure 28).

The region of interest for this study is in the weld. The maximum stresses occur in the region where the corners of the pin carriers are closest to the flange perimeter. See Figure 29. The maximum stress is small, 20 MPa, and a weld of this nature should be quite adequate.

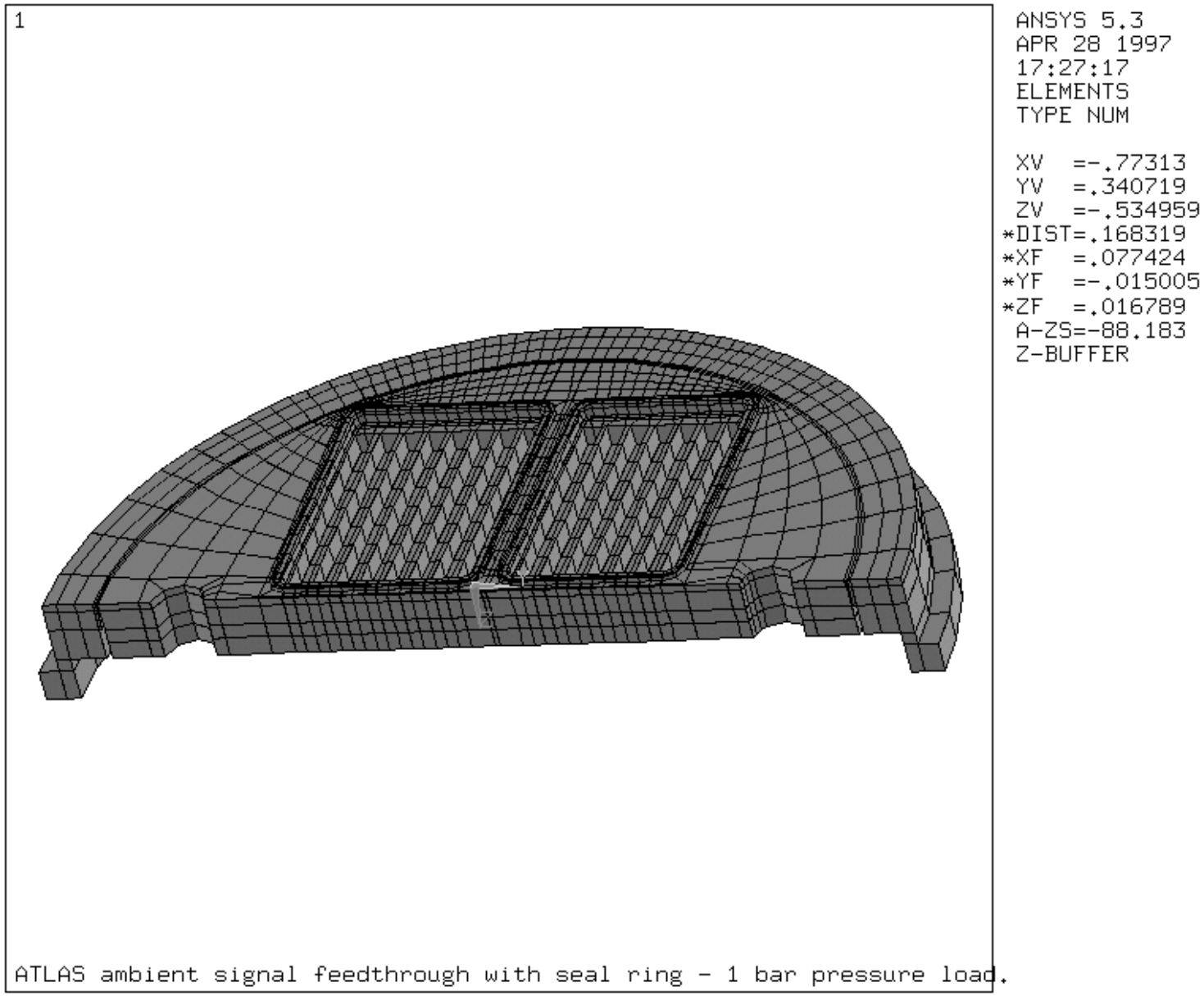

Figure 25: Finite element analysis model of half an ambient flange with the seal ring attached by a weld. Dimensions in metres.

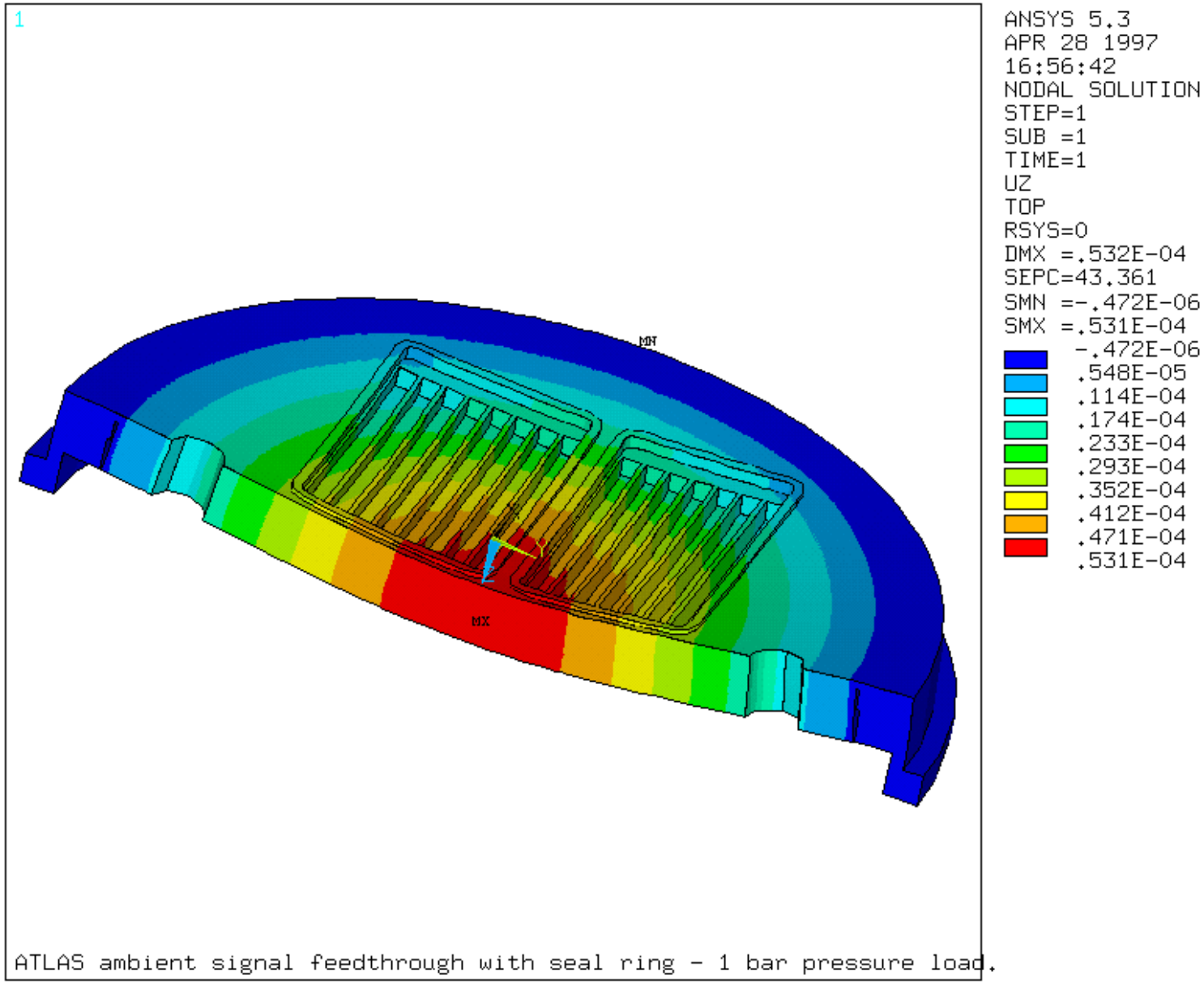

Figure 26: Finite element analysis of an ambient flange with thickness 22.9 mm (0.9 inch) and web thickness 1.5 mm with seal ring attached by a weld showing deflections in metres under an applied load of 1 bar.

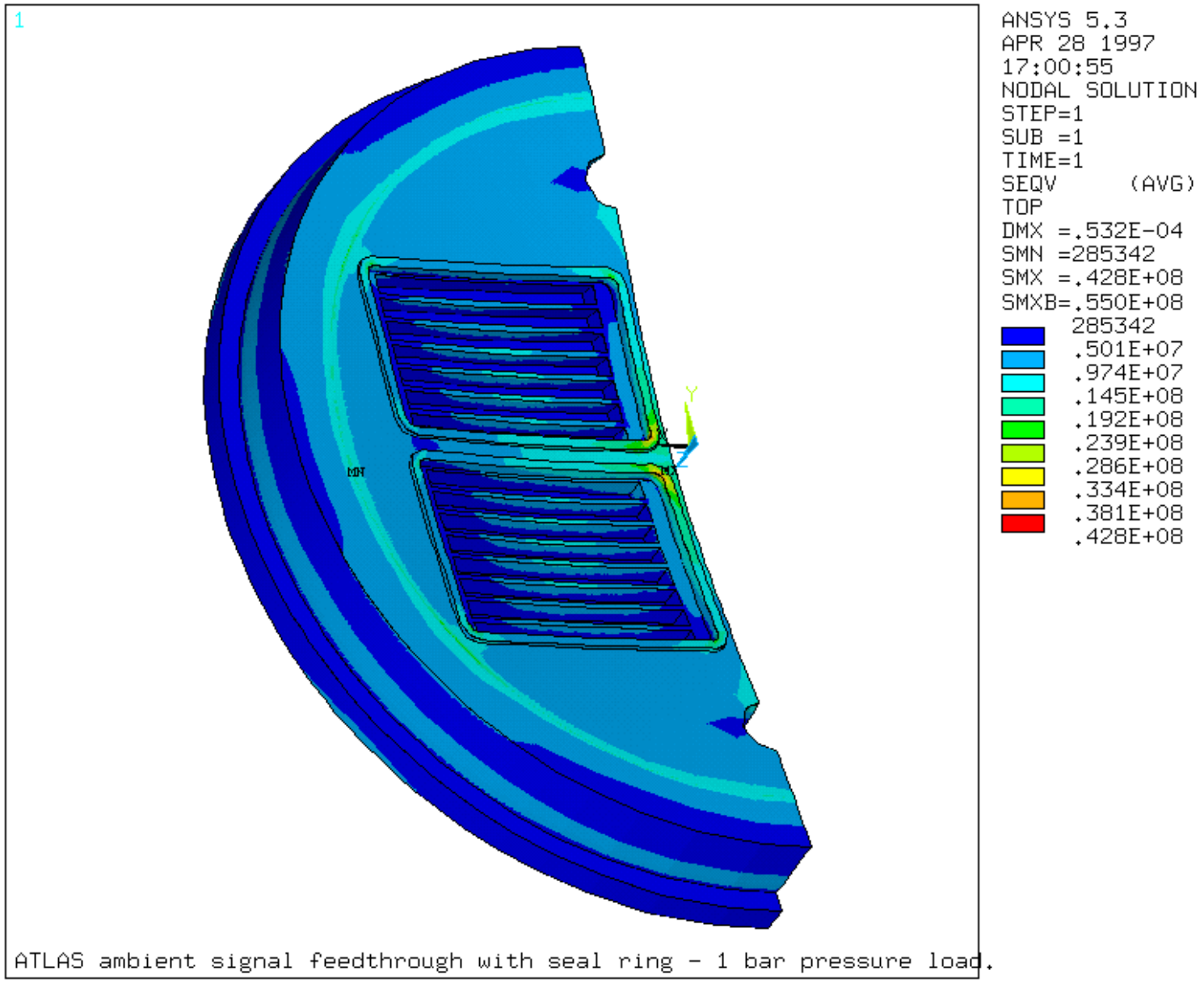

Figure 27: Finite element analysis of an ambient flange with thickness 22.9 mm (0.9 inch) and web thickness 1.5 mm with seal ring attached by a weld showing (Von Mises) stress in Pascals in the flange and the pin carriers under an applied load of 1 bar.

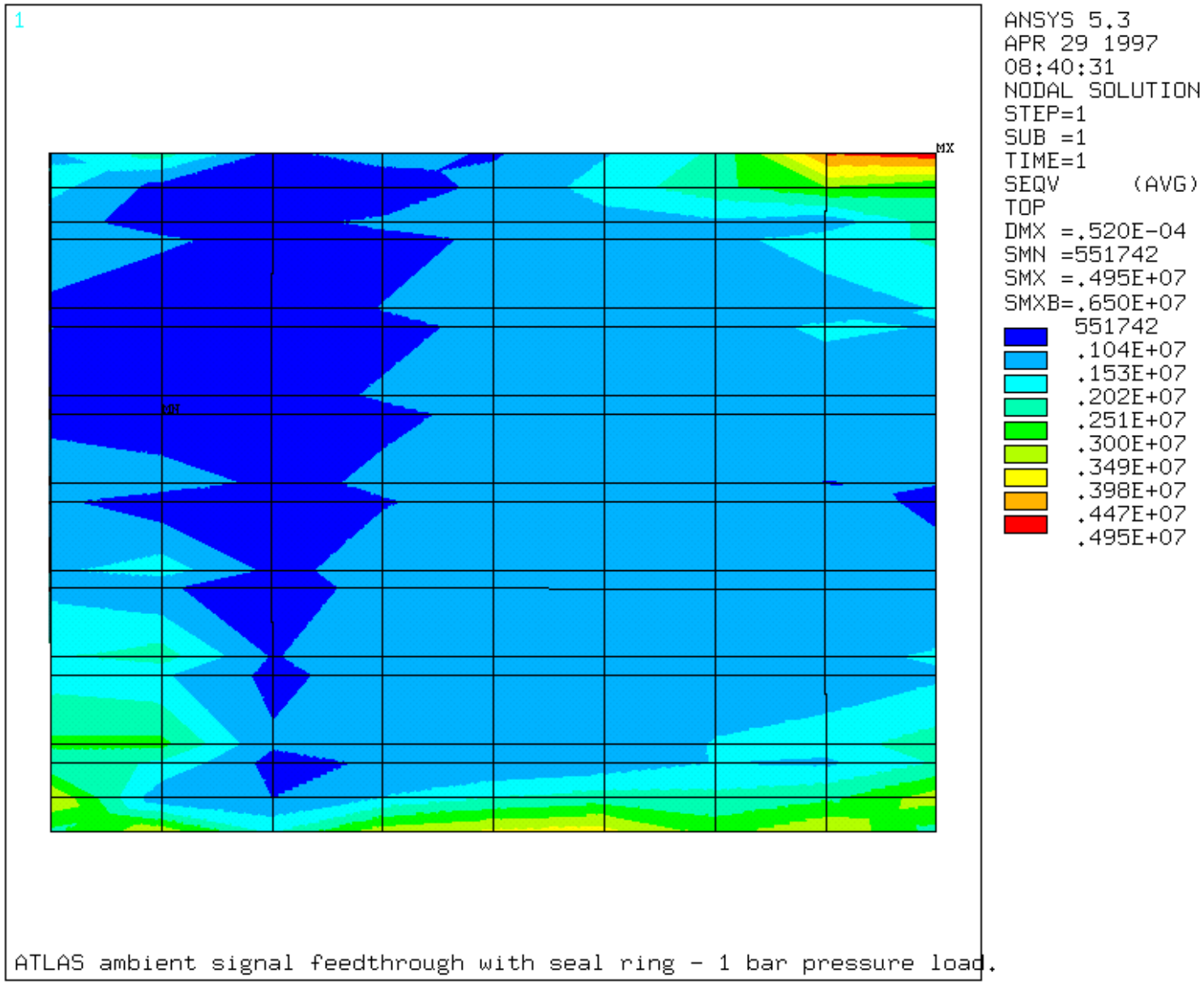

Figure 28: Finite element analysis of an ambient flange with thickness 22.9 mm (0.9 inch) and web thickness 1.5 mm with seal ring attached by a weld showing (Von Mises) stress in Pascals in the pin carriers' web under an applied load of 1 bar.

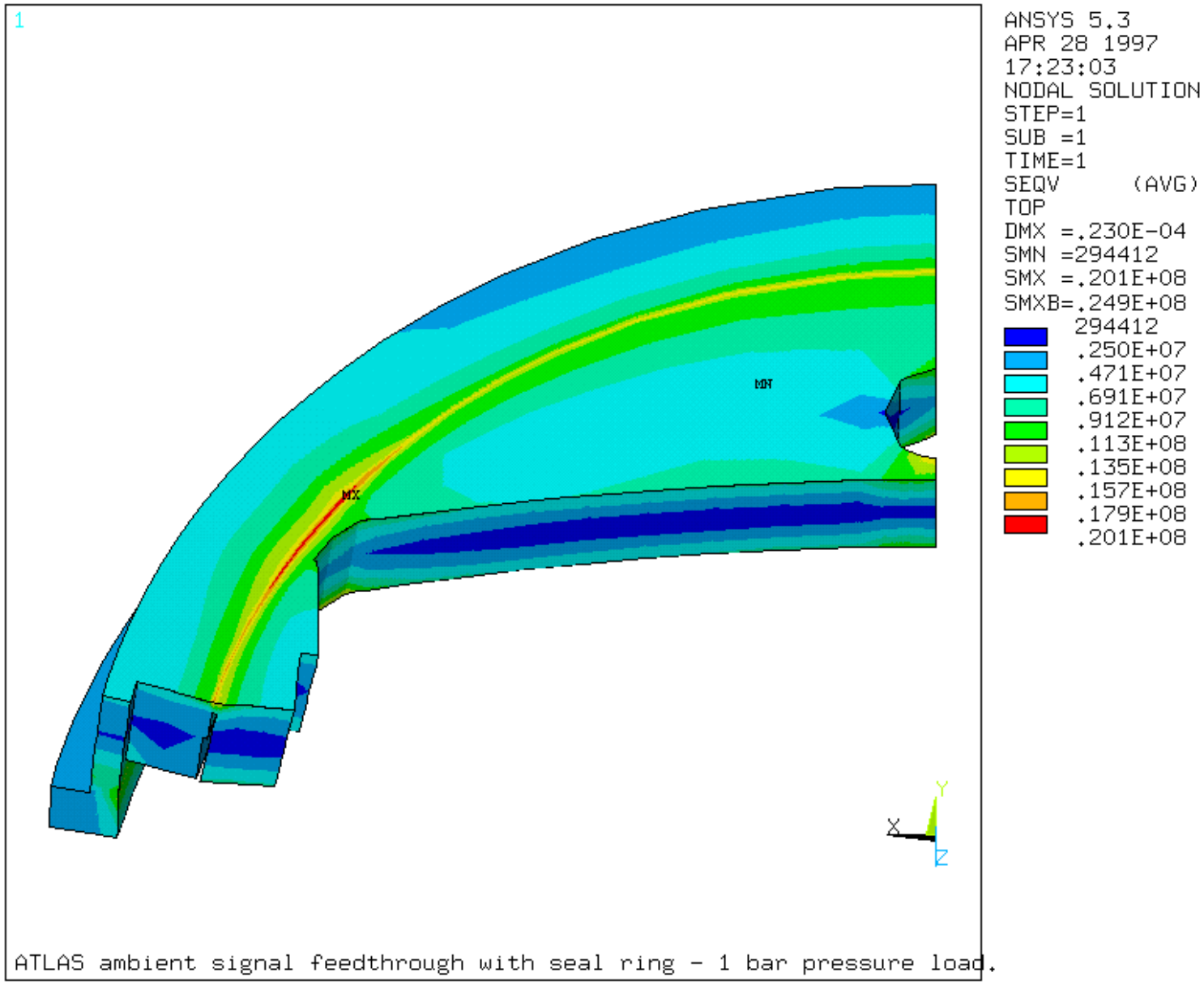

Figure 29: Finite element analysis of an ambient flange with thickness 22.9 mm (0.9 inch) and web thickness 1.5 mm with seal ring attached by a weld showing (Von Mises) stress in Pascals in the weld region under an applied load of 1 bar.

7 Feedthrough Funnel (Release of 97/05/20)

Several finite element analyses are performed on the "funnel" section of the signal feedthroughs. The large diameter cylinder end is restrained from all motion and the whole model from motion perpendicular to the symmetry plane. A force of 5387 Newtons is applied to the free end of the smaller diameter cylinder end, simulating the force on the funnel due to the internal pressure of 3.5 bar. A force of 695 Newtons can also be applied at the same location but in a lateral direction, simulating the force required to displace the bellows laterally by 15 mm, this displacement occurring due to contraction of the barrel cryostat on cooling to liquid argon temperature (this effect is not present in the endcaps).

A funnel formed as a uniform shell of 4 mm wall thickness is first studied. Results show that it would have a maximum stress of 163 MPa for 3.5 bar pressure load only (see Figure 30), and 224 MPa with the lateral force added. This is to be compared with the yield stress of 240 MPa. The stress is found to rise rapidly as the wall thickness is decreased. The stress decreases from 224 MPa to 99.8 MPa if the wall thickness is incresed from 4 mm to 6 mm (see Figure 31).

A funnel constructed from two cylinders joined by a flange is then studied, varying the thickness of the flange section and cylindrical sections of the funnel. The finite element model used is shown on Figure 32, along with pressure and lateral forces. For a 16 mm thick flange and 1.6 mm thick cylinders under a load of 3.5 bar, the maximum stress level increases from 106 MPa (see Figure 33) to 153 MPa (see Figure 34) when the lateral forces are included.

The thickness of the flange exerts the most control over the maximum stress level. For 1.6 mm thick cylinders, it falls from 153 MPa for a 16 mm thick flange (see Figure 34) to 119 MPa for a 19 mm thick flange (see Figure 35) and to 86.5 MPa for a 25 mm thick flange (see Figure 36). Increasing the lower cylinder wall thickness produces a slower reduction in stress, as seen from comparing Figure 34 with Figure 37 where doubling the cylinder wall thickness reduces the maximum stress by 15%.

The effect of locally thickening the lower cylinder wall is shown in Figures 38, 39 and 40. Compared to Figure 33, a lip of 4 mm, 8 mm and 12 mm, respectively, is added the junction between the flange and the small cylinder. The local thickening must extend down the cylinder more than 8 mm before any effect is seen. For the 12 mm lip case, the maximum stress level of 93.4 MPa (see Figure 40) decreases to 78 MPa if the small cylinder wall thickness is increased from 1.6 mm to 2.6 mm (see Figure 41). It then increases to 102 MPa if the lateral load is added (see Figure 42).

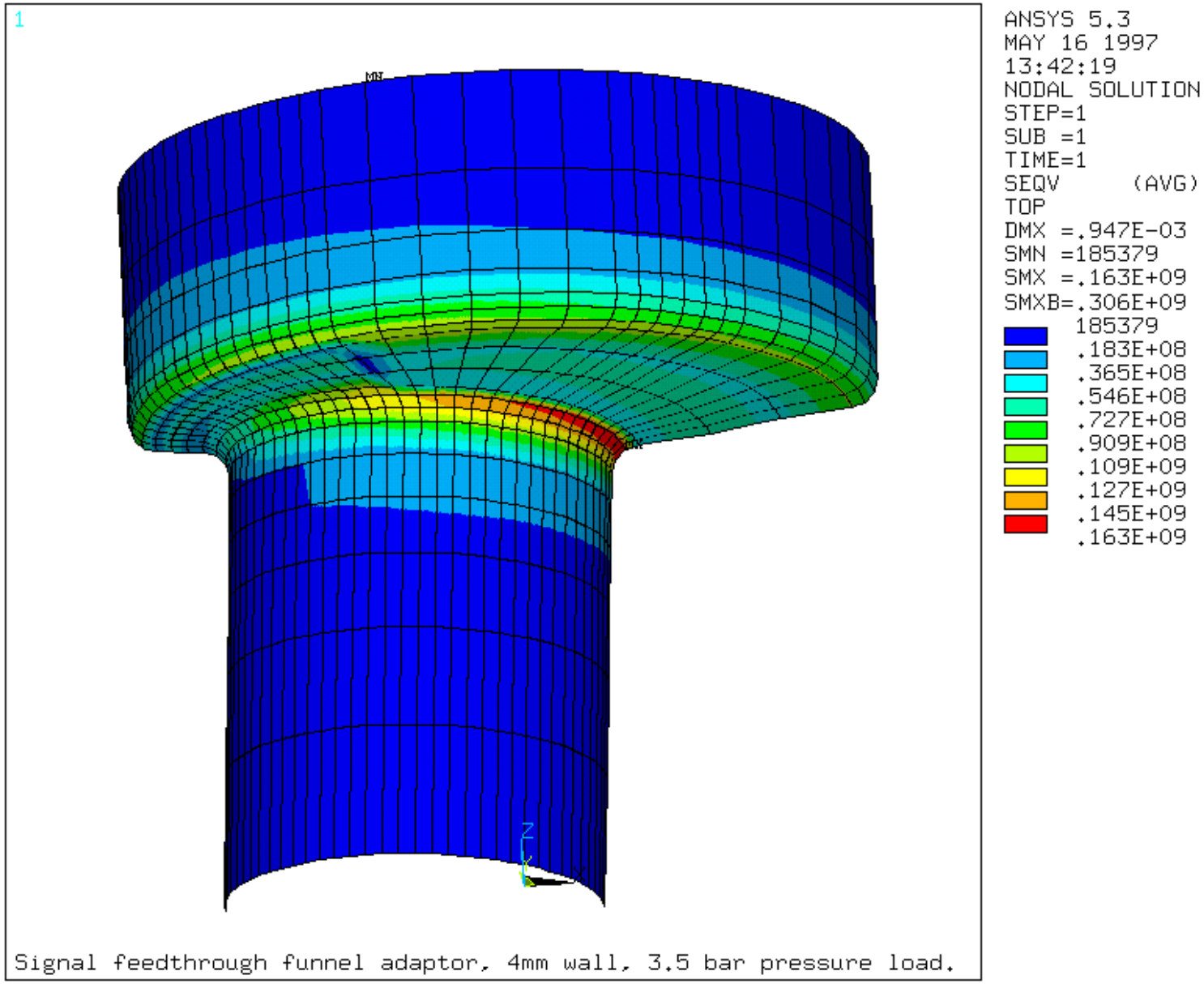

Figure 30: Finite element analysis of a uniform shell funnel with wall thickness 4 mm showing (Von Mises) stress in Pascals under an applied load of 3.5 bar.

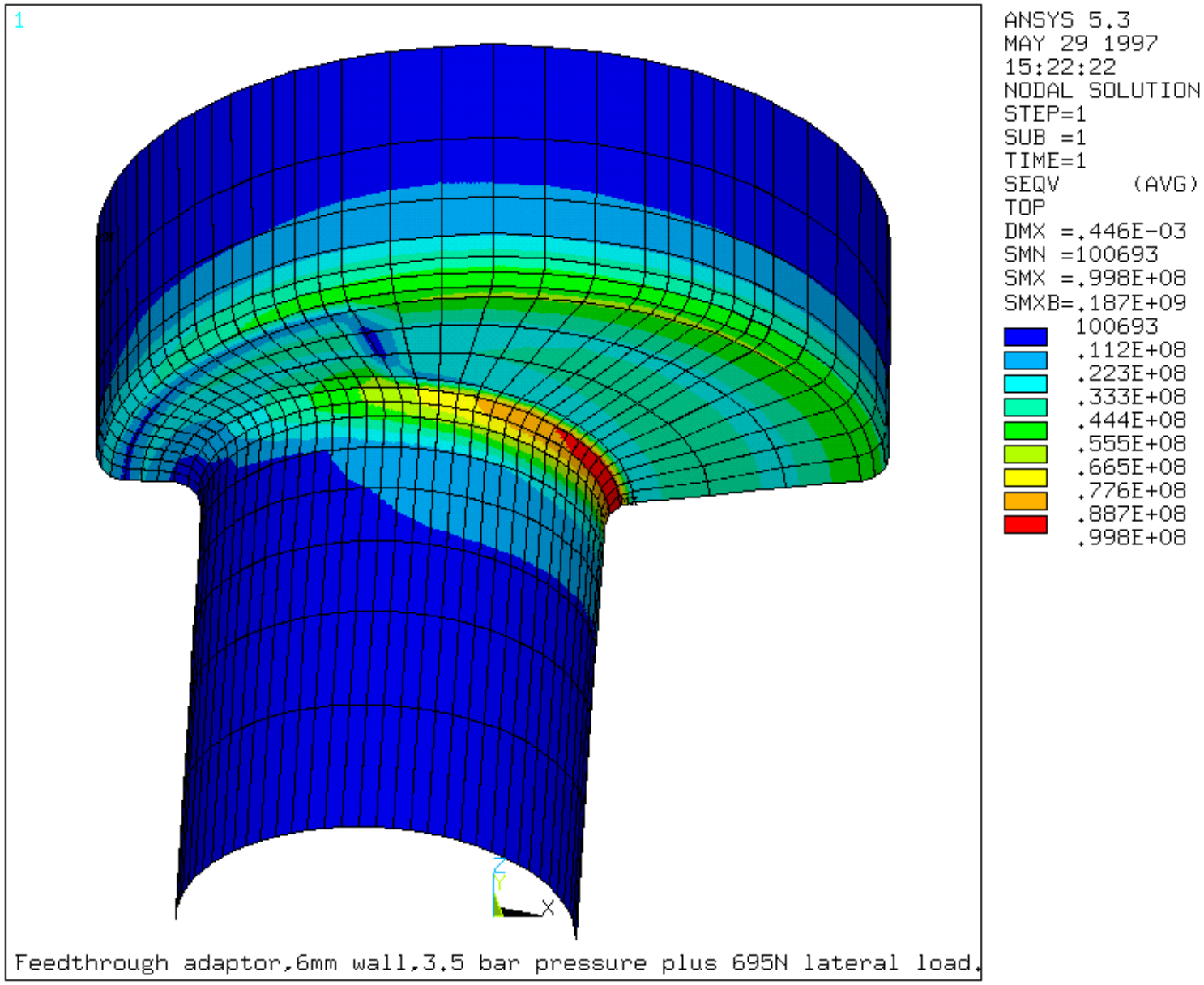

Figure 31: Finite element analysis of a uniform shell funnel with wall thickness 6 mm showing (Von Mises) stress in Pascals under an applied load of 3.5 bar, and a lateral load of 695 N (for a 15 mm displacement).

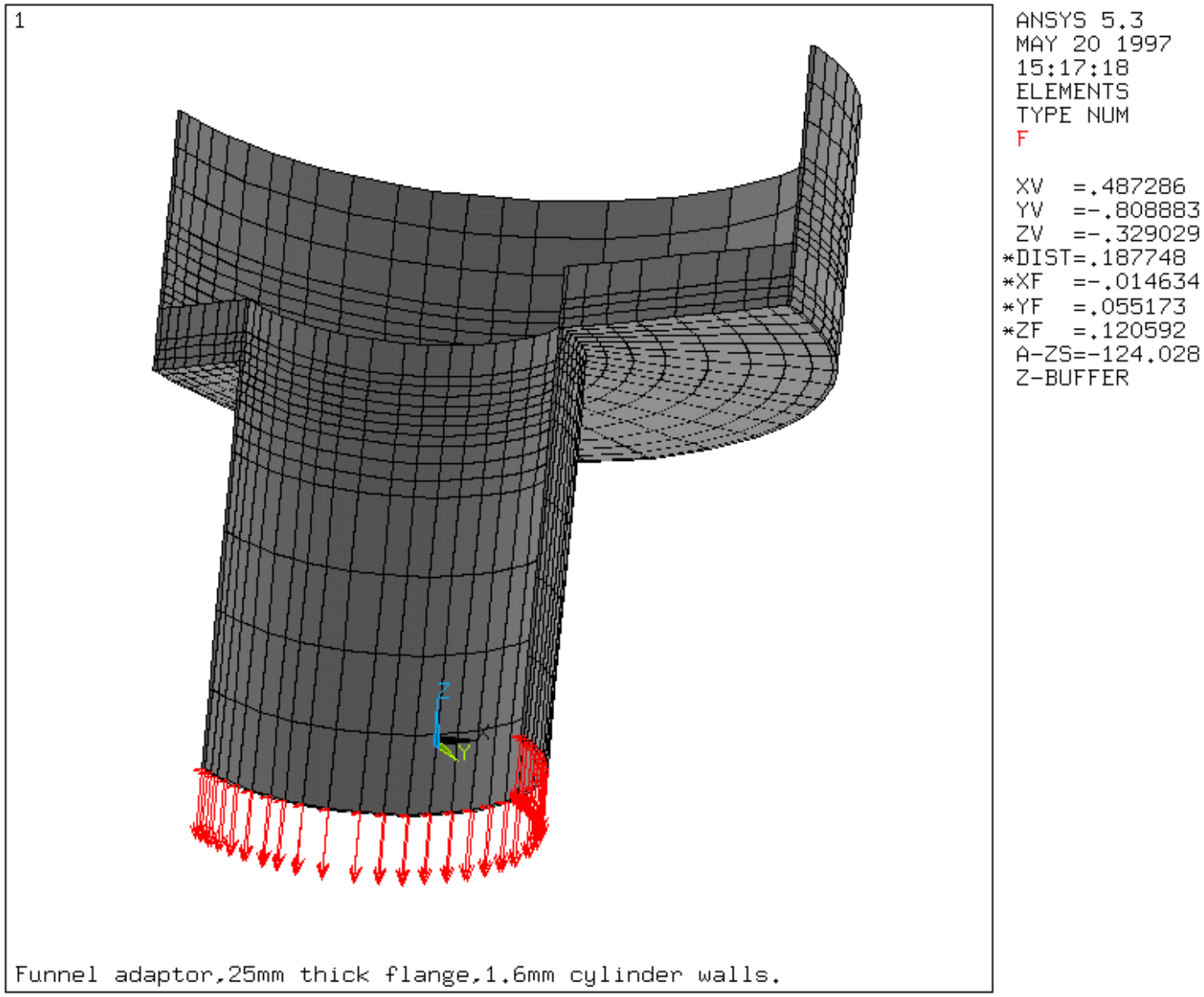

Figure 32: Finite element analysis model of a funnel made of two cylinders and a flange showing the pressure (3.5 bar or 5387 N) and lateral forces (695 N for a 15 mm displacement). Dimensions in metres.

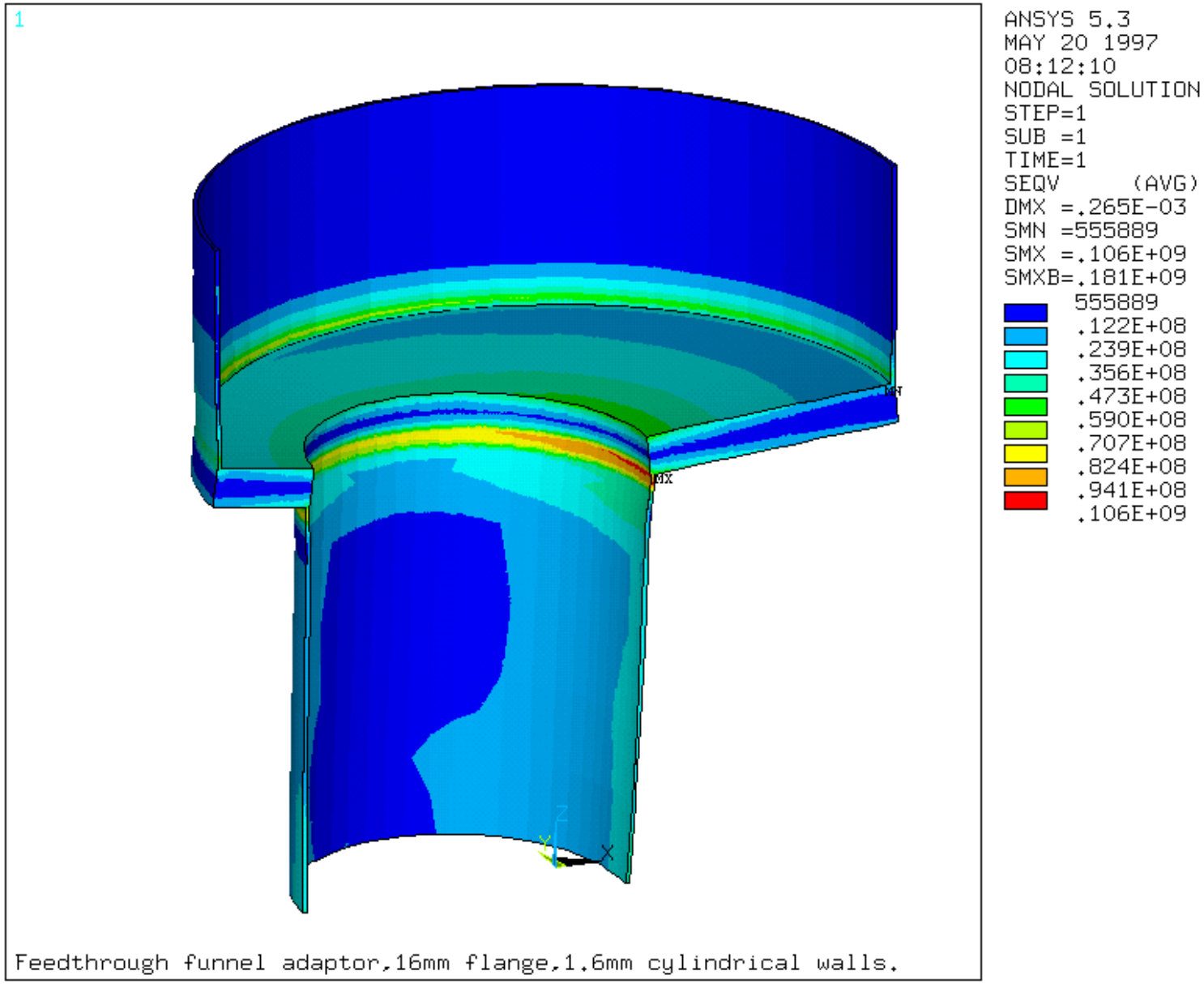

Figure 33: Finite element analysis of a funnel with a 16 mm thick flange and 1.6 mm thick cylinders showing (Von Mises) stress in Pascals under an applied load of 3.5 bar, and no lateral load.

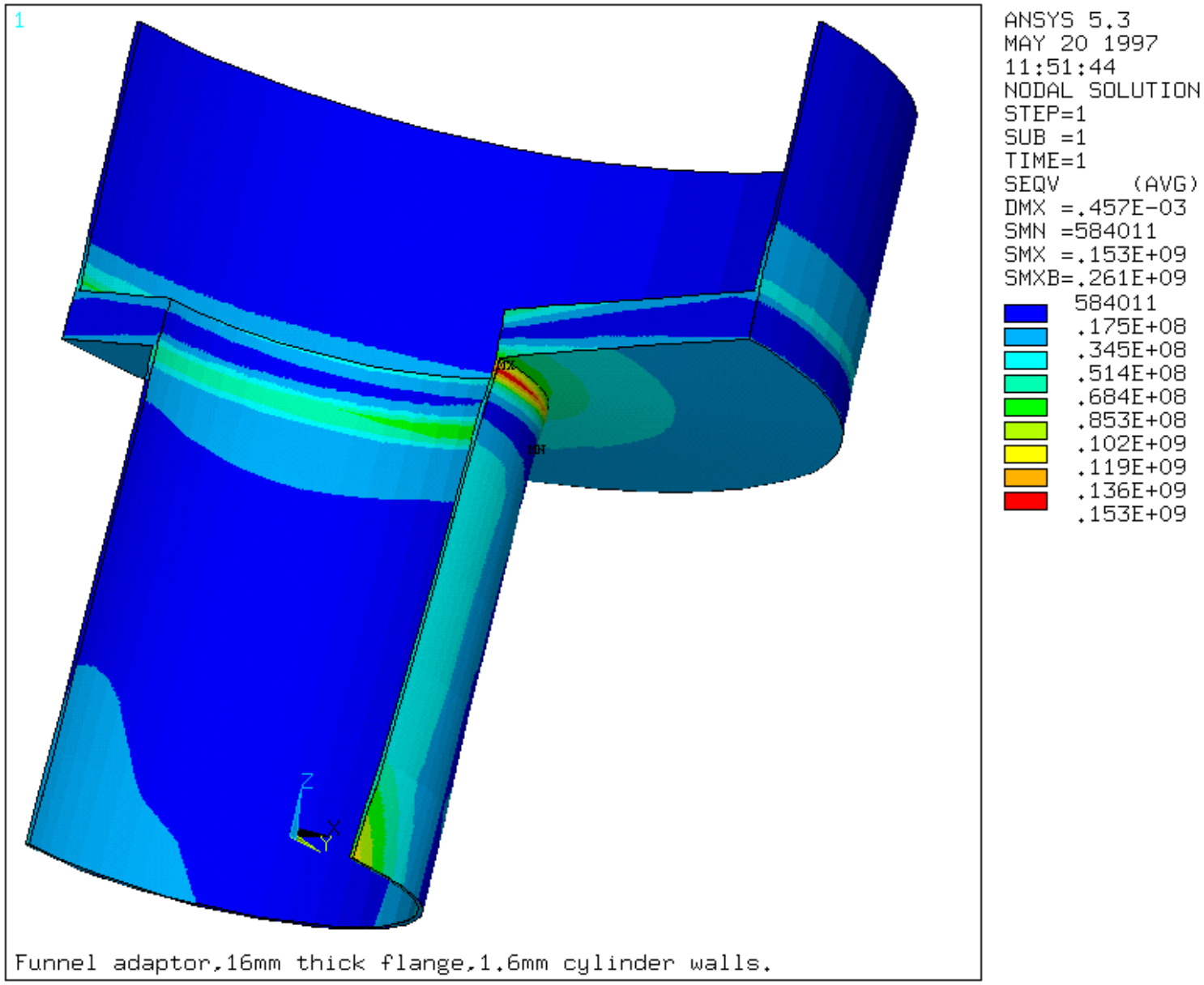

Figure 34: Finite element analysis of a funnel with a 16 mm thick flange and 1.6 mm thick cylinders showing (Von Mises) stress in Pascals under an applied load of 3.5 bar, and a lateral load of 695 N (for a 15 mm displacement).

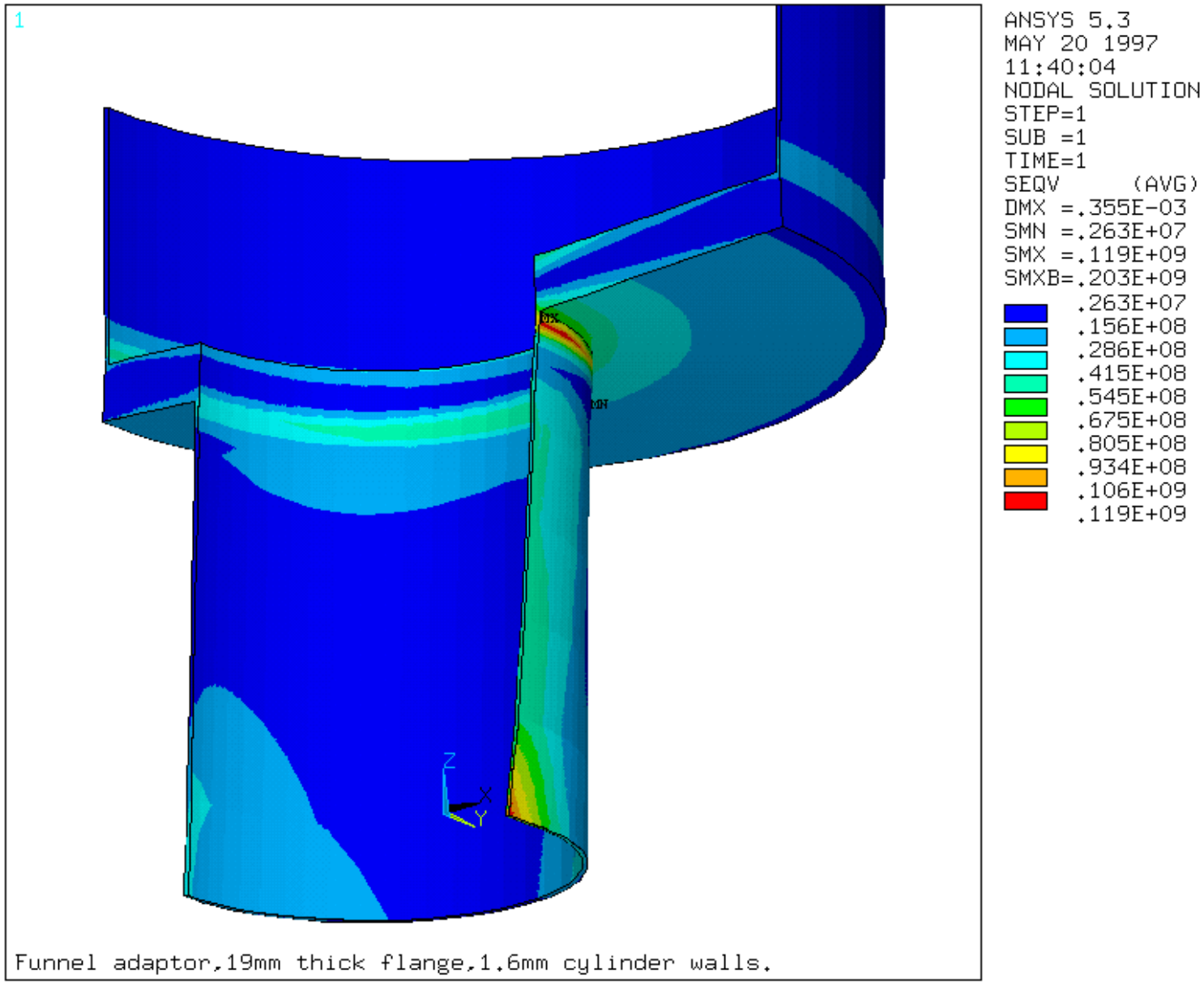

Figure 35: Finite element analysis of a funnel with a 19 mm thick flange and 1.6 mm thick cylinders showing (Von Mises) stress in Pascals under an applied load of 3.5 bar, and a lateral load of 695 N (for a 15 mm displacement).

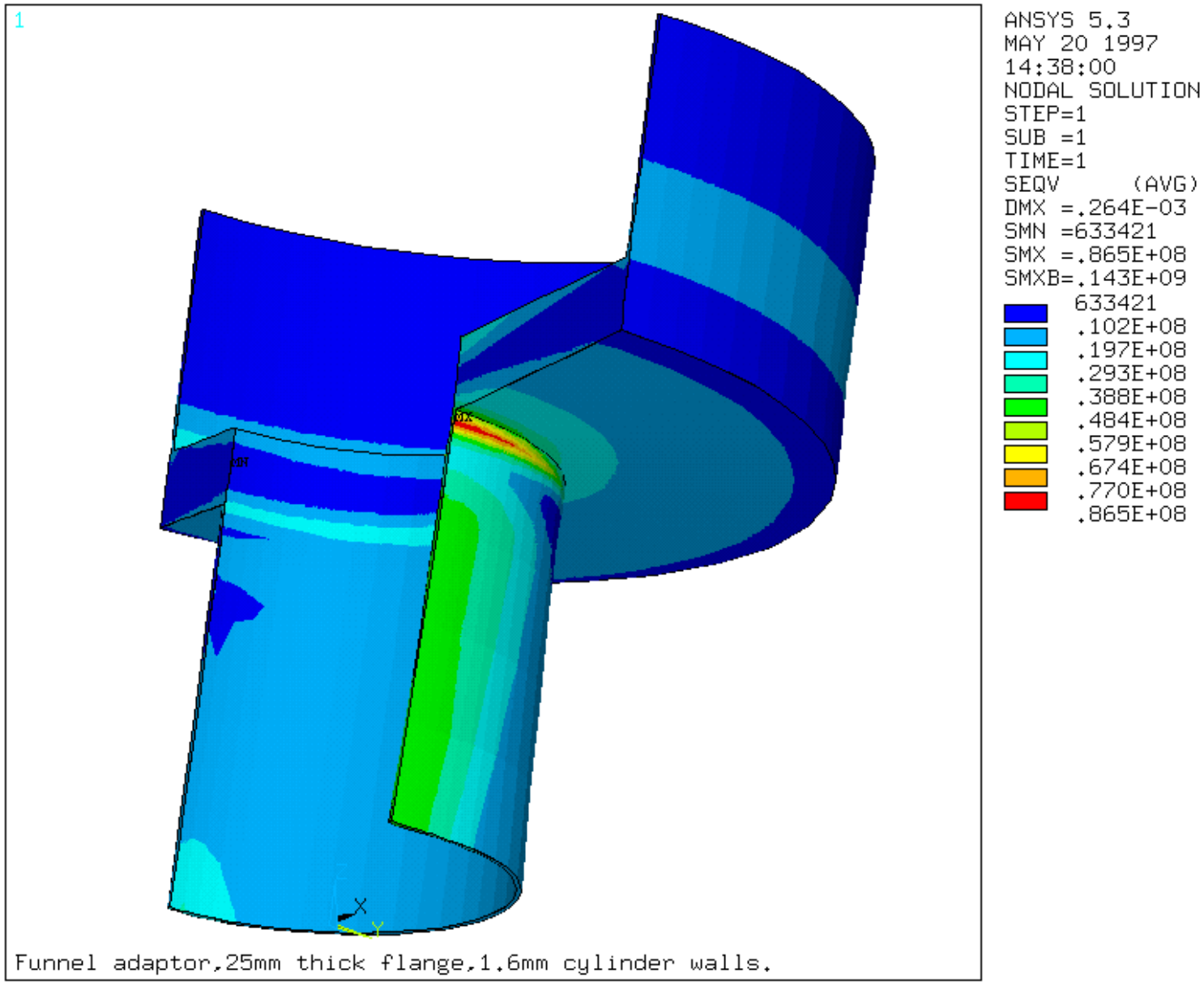

Figure 36: Finite element analysis of a funnel with a 25 mm thick flange and 1.6 mm thick cylinders showing (Von Mises) stress in Pascals under an applied load of 3.5 bar, and a lateral load of 695 N (for a 15 mm displacement).

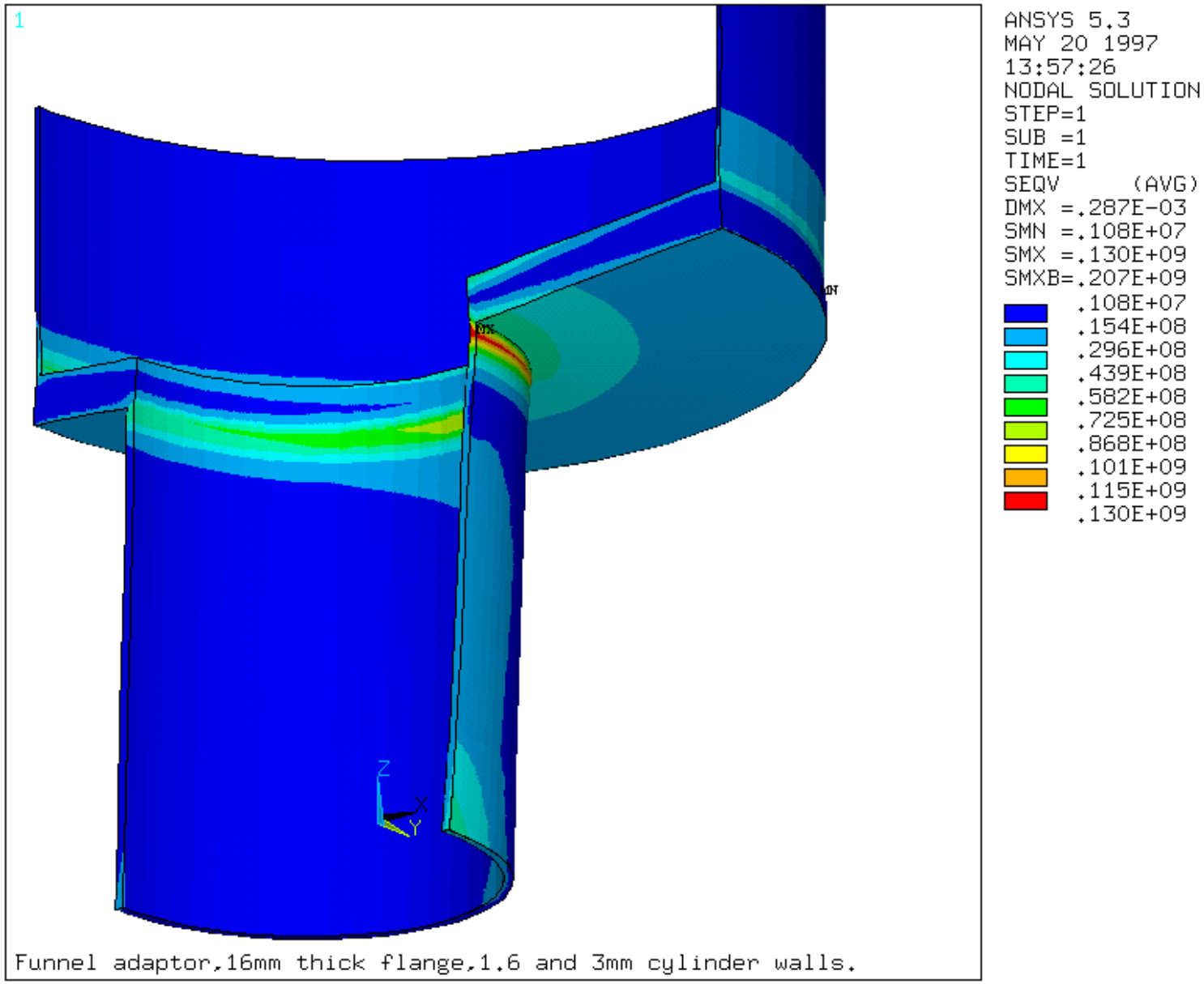

Figure 37: Finite element analysis of a funnel with a 16 mm thick flange and 3 mm thick cylinders showing (Von Mises) stress in Pascals under an applied load of 3.5 bar, and a lateral load of 695 N (for a 15 mm displacement).

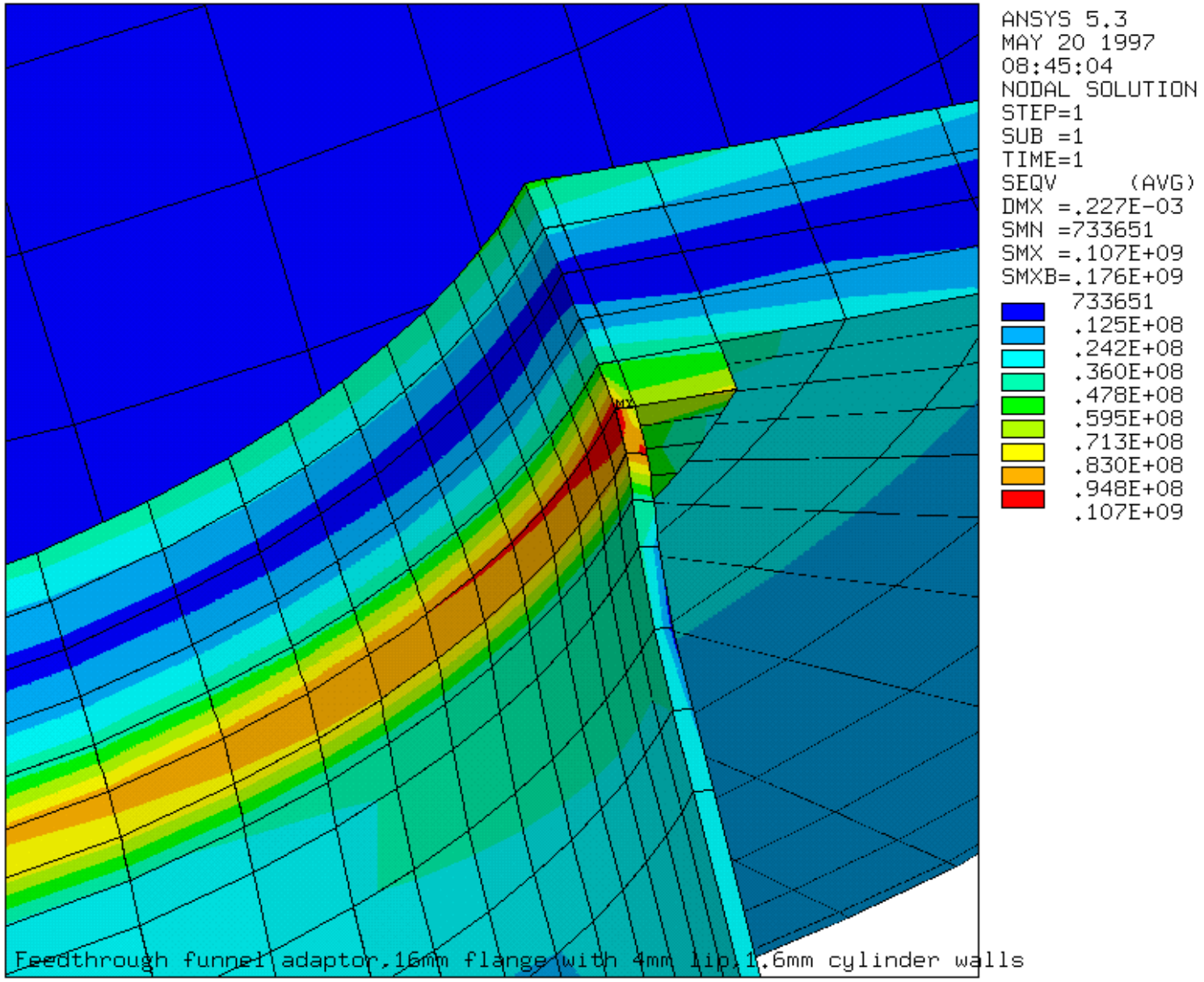

Figure 38: Finite element analysis of a funnel with a 16 mm thick flange, 1.6 mm thick cylinders and a 4 mm lip added to the junction between the flange and the small cylinder showing (Von Mises) stress in Pascals under an applied load of 3.5 bar, and no lateral load.

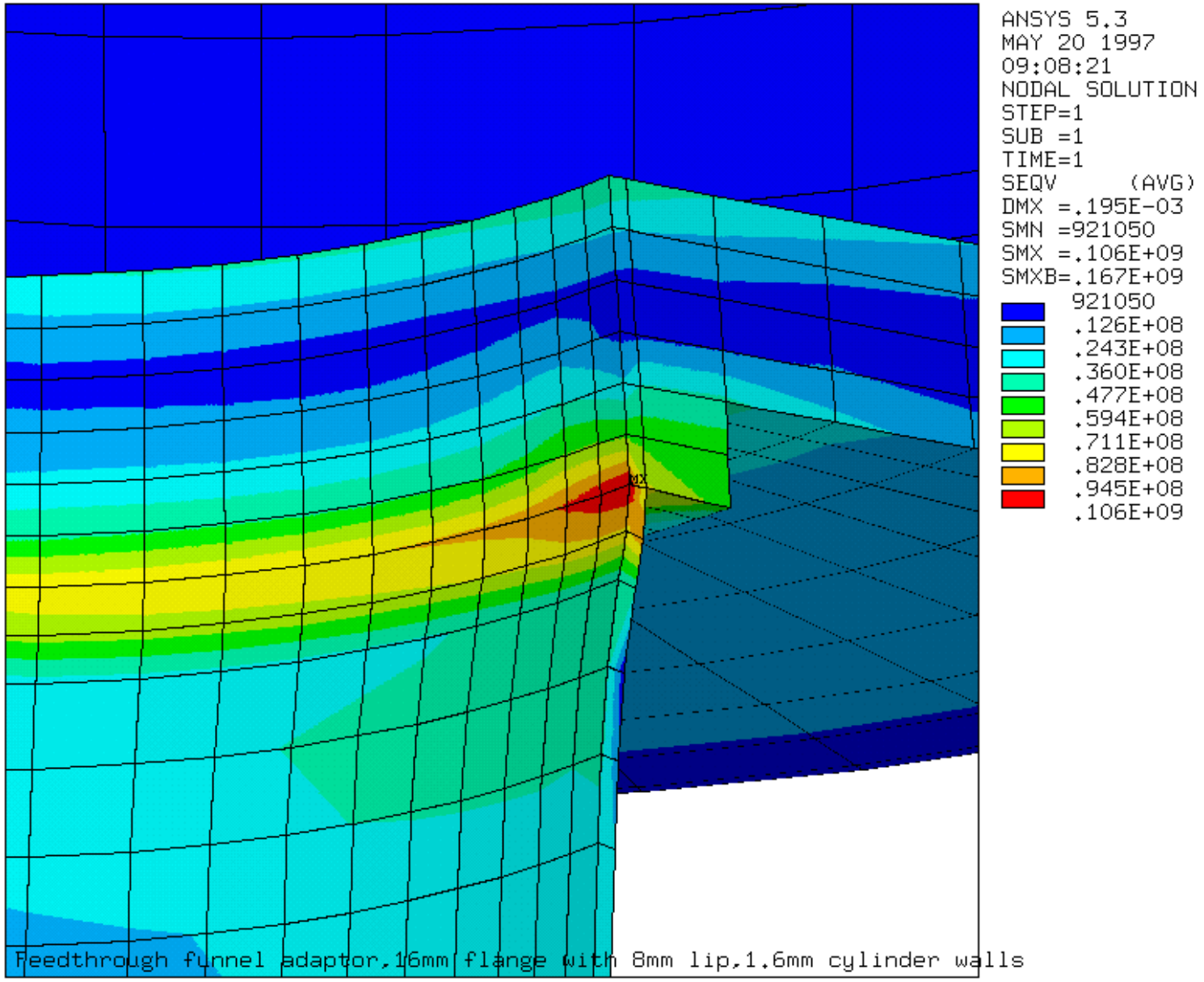

Figure 39: Finite element analysis of a funnel with a 16 mm thick flange, 1.6 mm thick cylinders and a 8 mm lip added to the junction between the flange and the small cylinder showing (Von Mises) stress in Pascals under an applied load of 3.5 bar, and no lateral load.

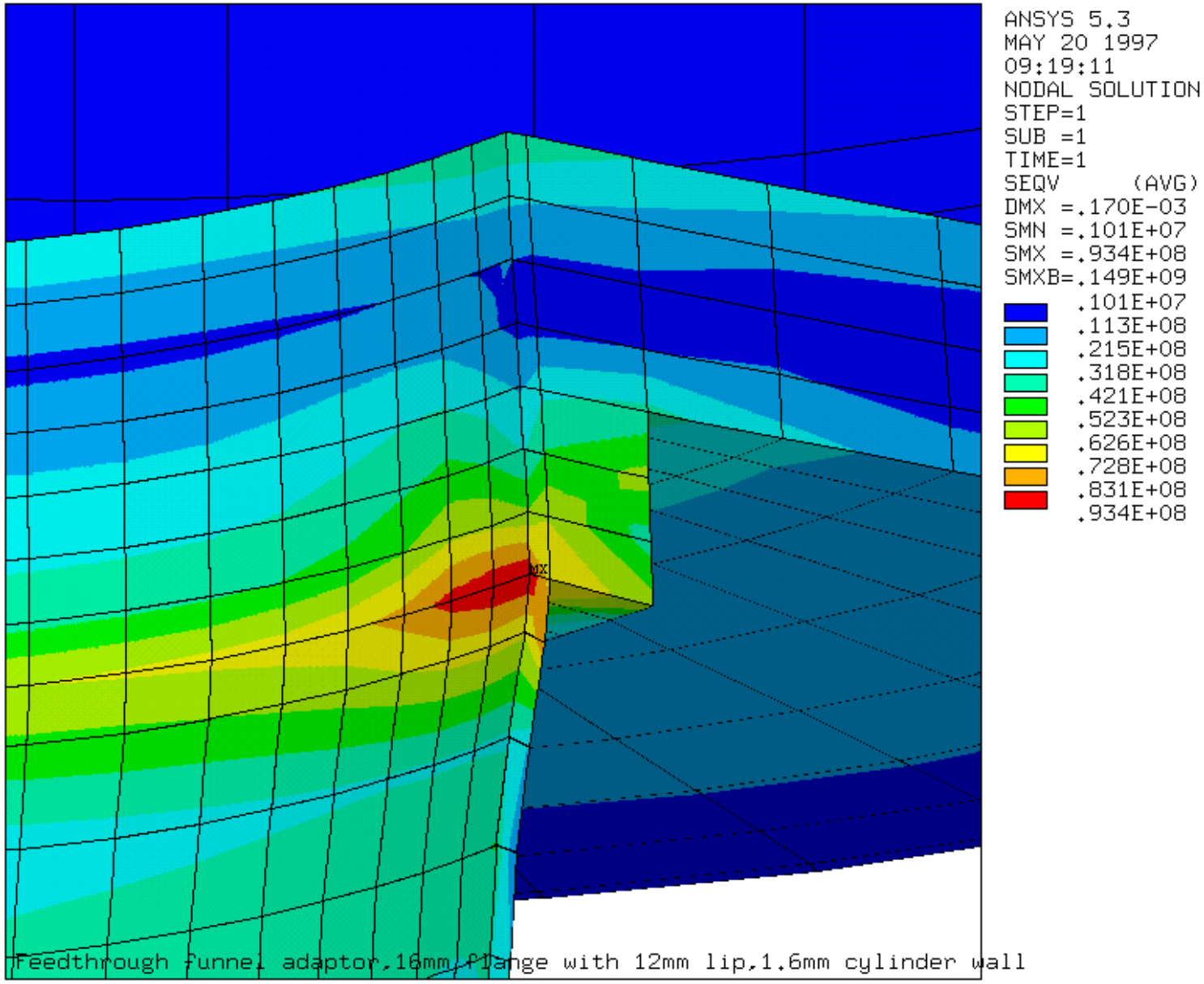

Figure 40: Finite element analysis of a funnel with a 16 mm thick flange, 1.6 mm thick cylinders and a 12 mm lip added to the junction between the flange and the small cylinder showing (Von Mises) stress in Pascals under an applied load of 3.5 bar, and no lateral load.

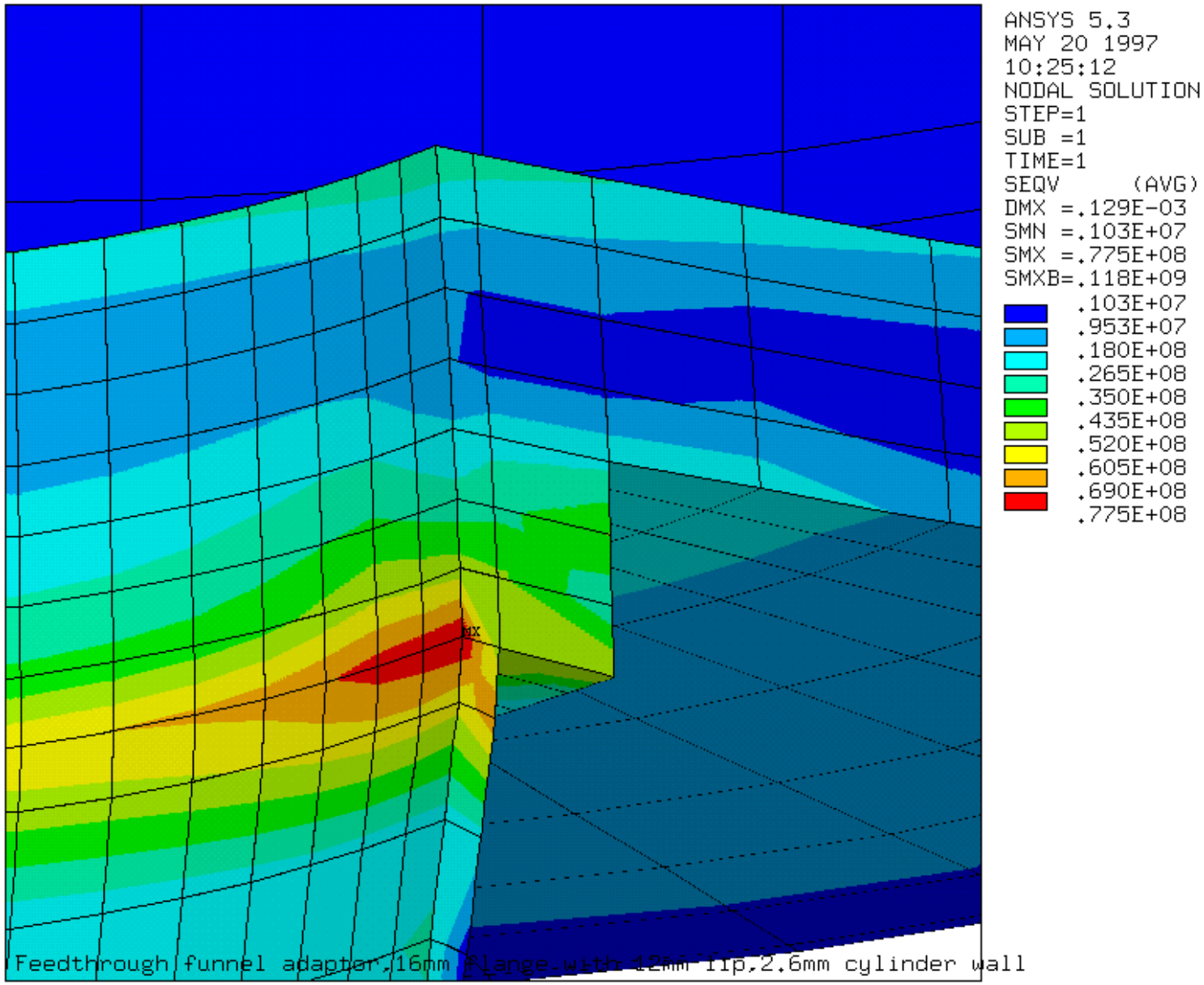

Figure 41: Finite element analysis of a funnel with a 16 mm thick flange, 1.6 mm thick large cylinder, 2.6 mm thick small cylinder and a 12 mm lip added to the junction between the flange and the small cylinder showing (Von Mises) stress in Pascals under an applied load of 3.5 bar, and no lateral load.

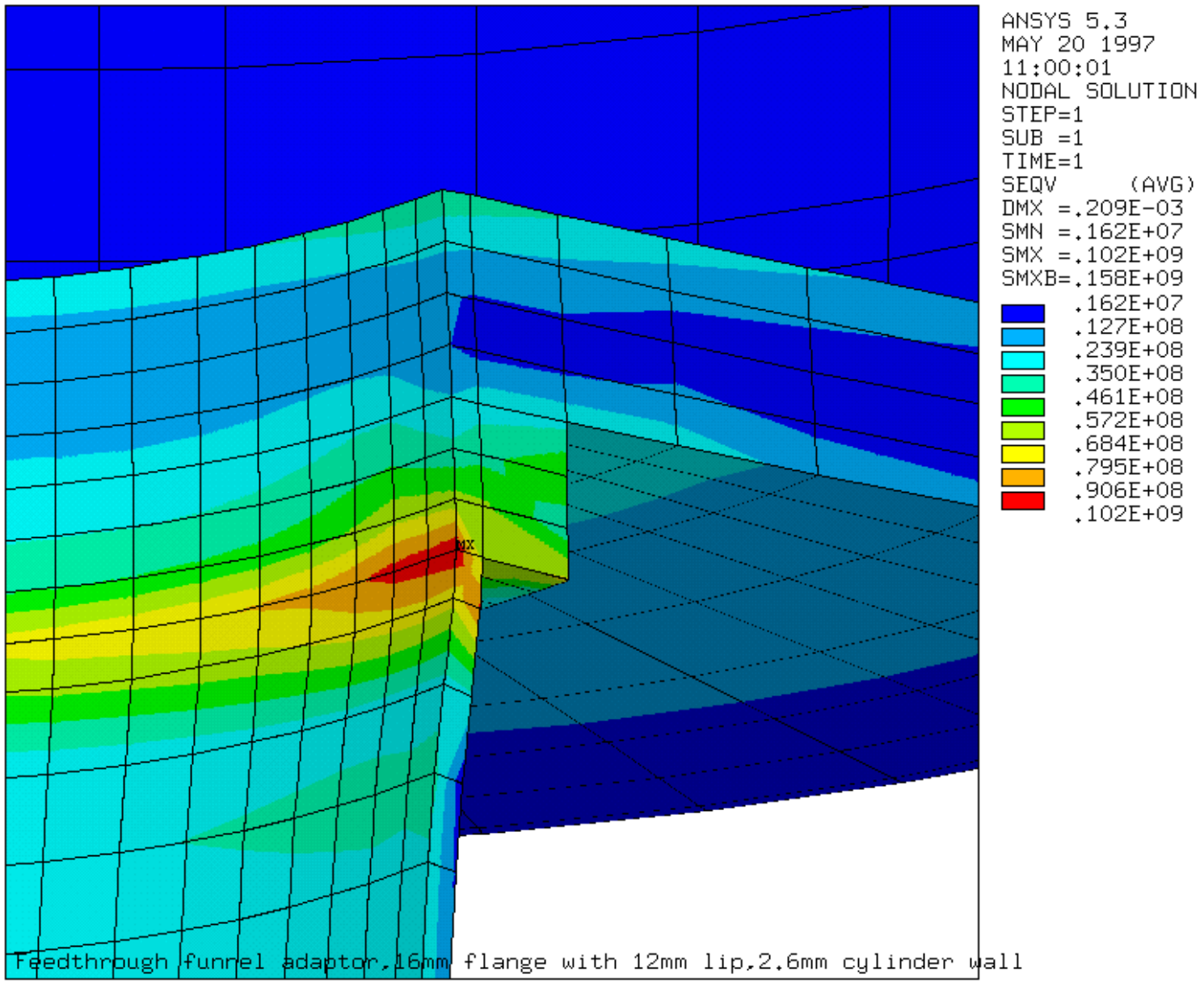

Figure 42: Finite element analysis of a funnel with a 16 mm thick flange, 1.6 mm thick large cylinder, 2.6 mm thick small cylinder and a 12 mm lip added to the junction between the flange and the small cylinder showing (Von Mises) stress in Pascals under an applied load of 3.5 bar, and a lateral load of 695 N (for a 15 mm displacement).

8 Feedthrough Funnel and Bi-metal Joint (Release of 97/06/09)

The bi-metal joint is added to the model of the feedthrough "funnel" adaptor. The open end of the aluminum section of the bi-metal joint is restrained from lateral and vertical motion and the normal symmetry constraints are applied at the symmetry plane of the model. The flange is 16 mm thick and the cylinders are 1.6 mm thick. The smaller diameter cylinder of the funnel is attached at its lower end to the adjacent tube (mauve colour in Figure 43) by a 2 mm weld section. The latter tube is attached at its upper end to the bi-metal joint (blue colour in Figure 43) by a similar 2 mm weld. A force of 5387 Newtons is applied to the open end of of the funnel larger diameter cylinder, simulating the force on the funnel due to the internal pressure of 3.5 bar. A force of 695 Newtons is also applied at the same location in a lateral direction, simulating the force required to displace the bellows laterally by 15 mm, this displacement occurring due to contraction of the barrel cryostat on cooling to liquid argon temperature (this effect is not present in the endcaps). The forces applied are shown in Figure 44.

The maximum stress occurs (as in the earlier model without the bi-metal adaptor) at the funnel plate and lower cylinder junction. The stress is lower, 114 MPa (see Figure 120) compared to the previous value of 153 MPa (see Figure 34), probably due to a more uniform distribution of the lateral force by the adaptor. The maximum stress of 50 MPa in the transition joint region occurs near the weld at the lower edge of the smaller funnel cylinder (see Figure 121). The stress in the bi-metal union is low, less than 6 MPa.

Displacemement in the x direction (left to right) are shown in Figure 45; displacements in the z direction (bottom to top) are shown in Figure 46.

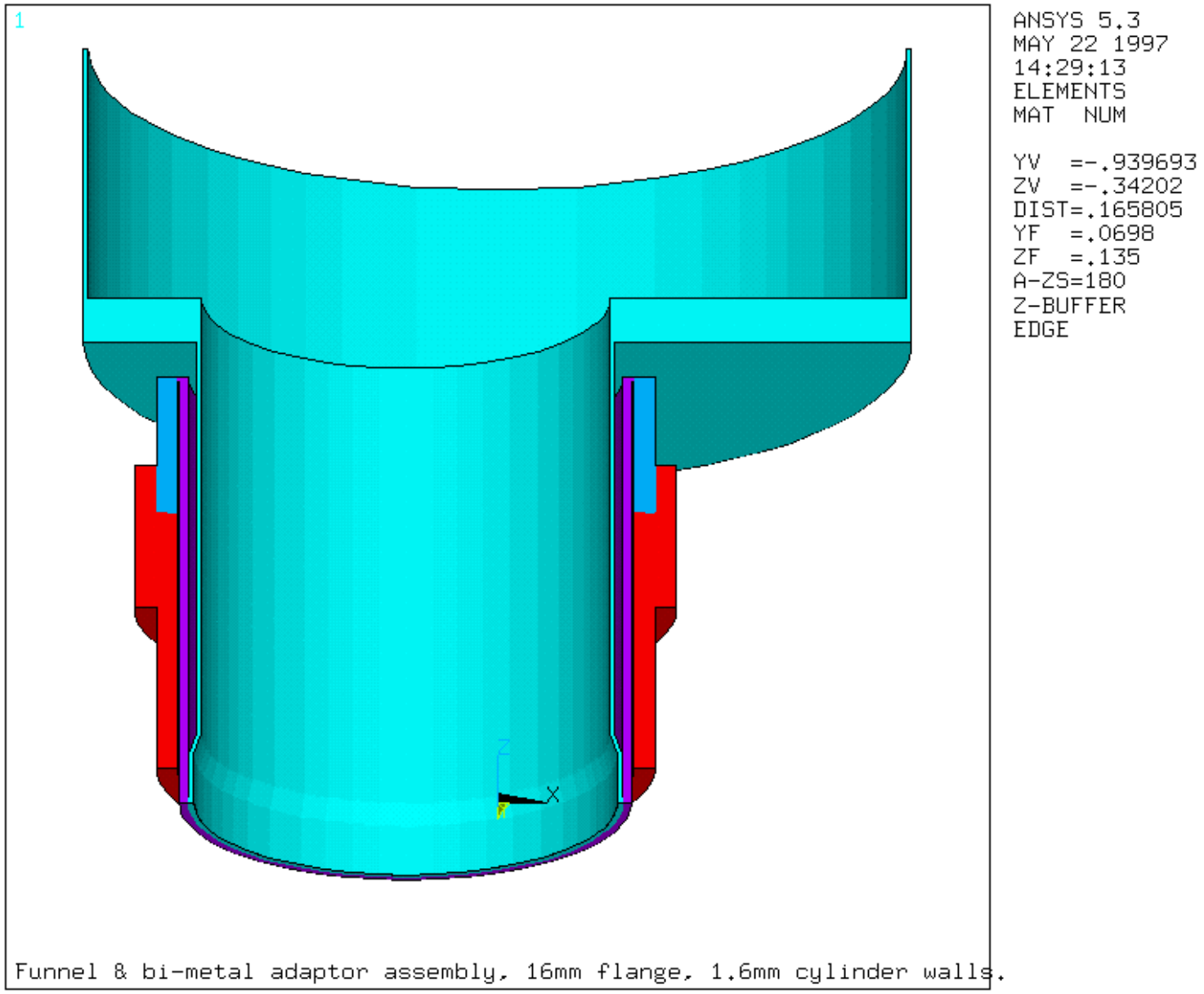

Figure 43: Finite element analysis model of a funnel made of two cylinders and a flange, connected to a bi-metal joint, showing the materials: red is aluminium and all others are stainless steel. Dimensions in metres.

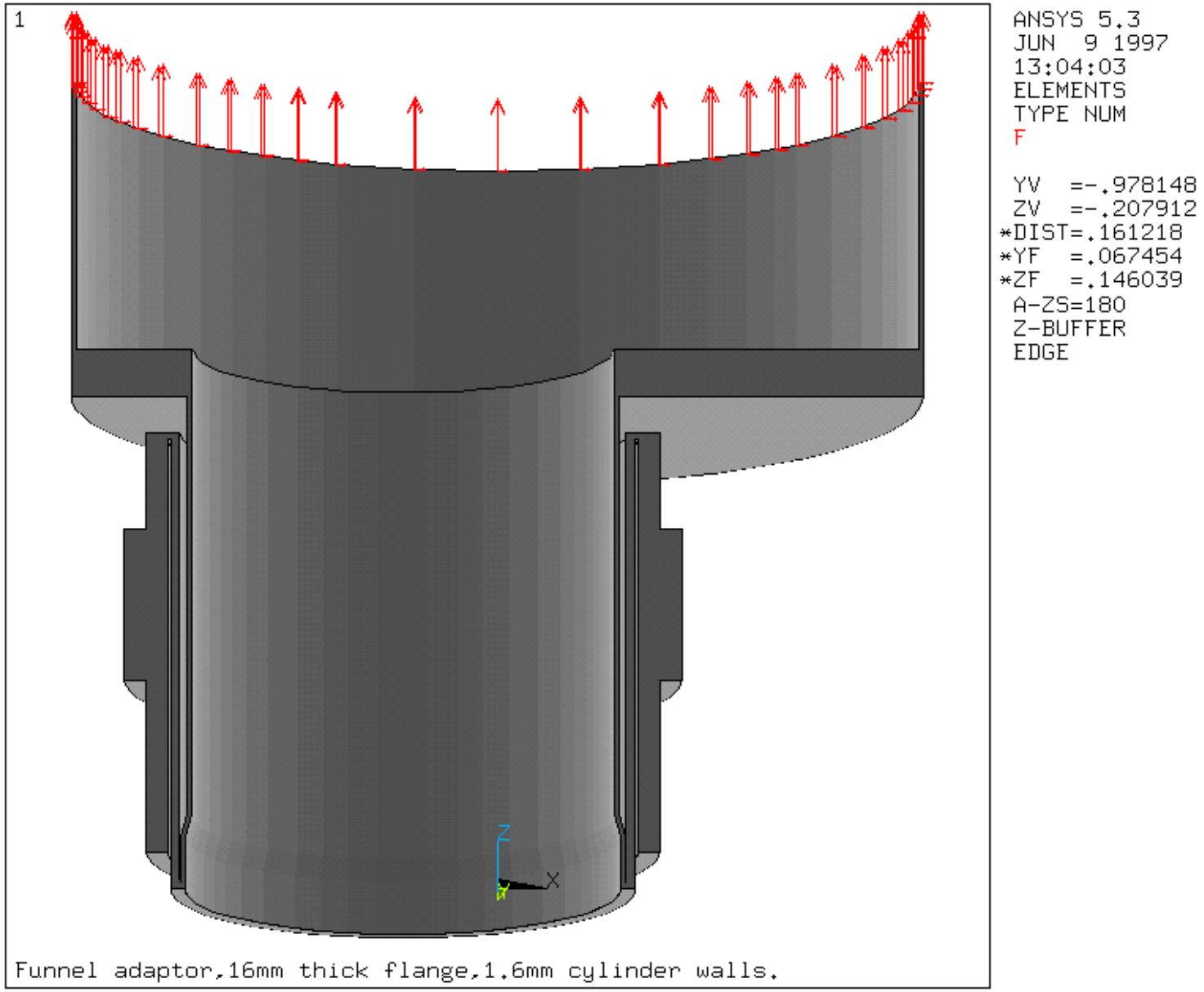

Figure 44: Finite element analysis model of a funnel made of two cylinders and a flange, connected to a bi-metal joint, showing the pressure (3.5 bar or 5387 N) and lateral forces (695 N for a 15 mm displacement). Dimensions in metres.

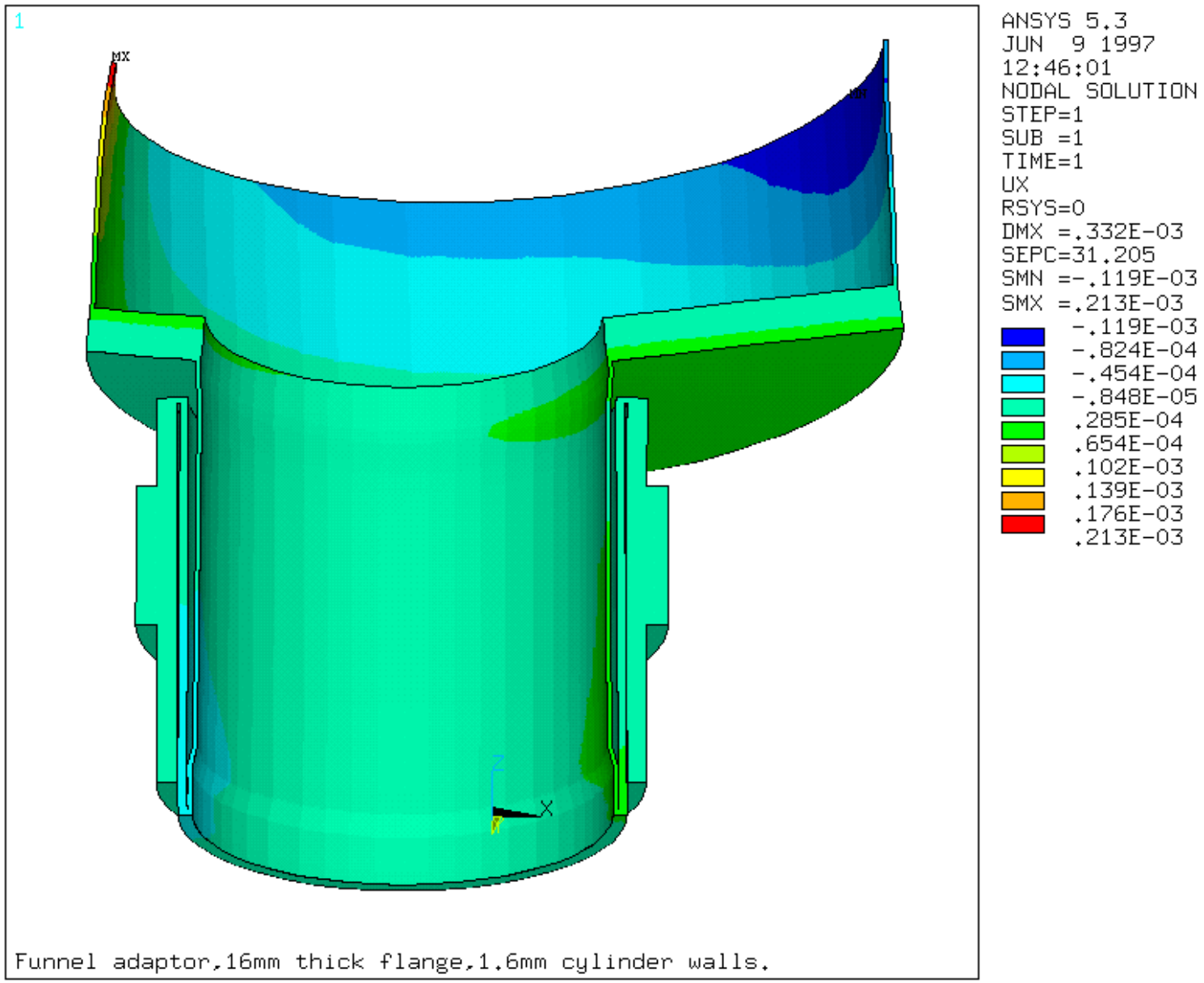

Figure 45: Finite element analysis of a funnel with a 16 mm thick flange and 1.6 mm thick cylinders, connected to a bi-metal joint, showing x displacements (left to right) in metres under an applied load of 3.5 bar, and a lateral load of 695 N (for a 15 mm displacement).

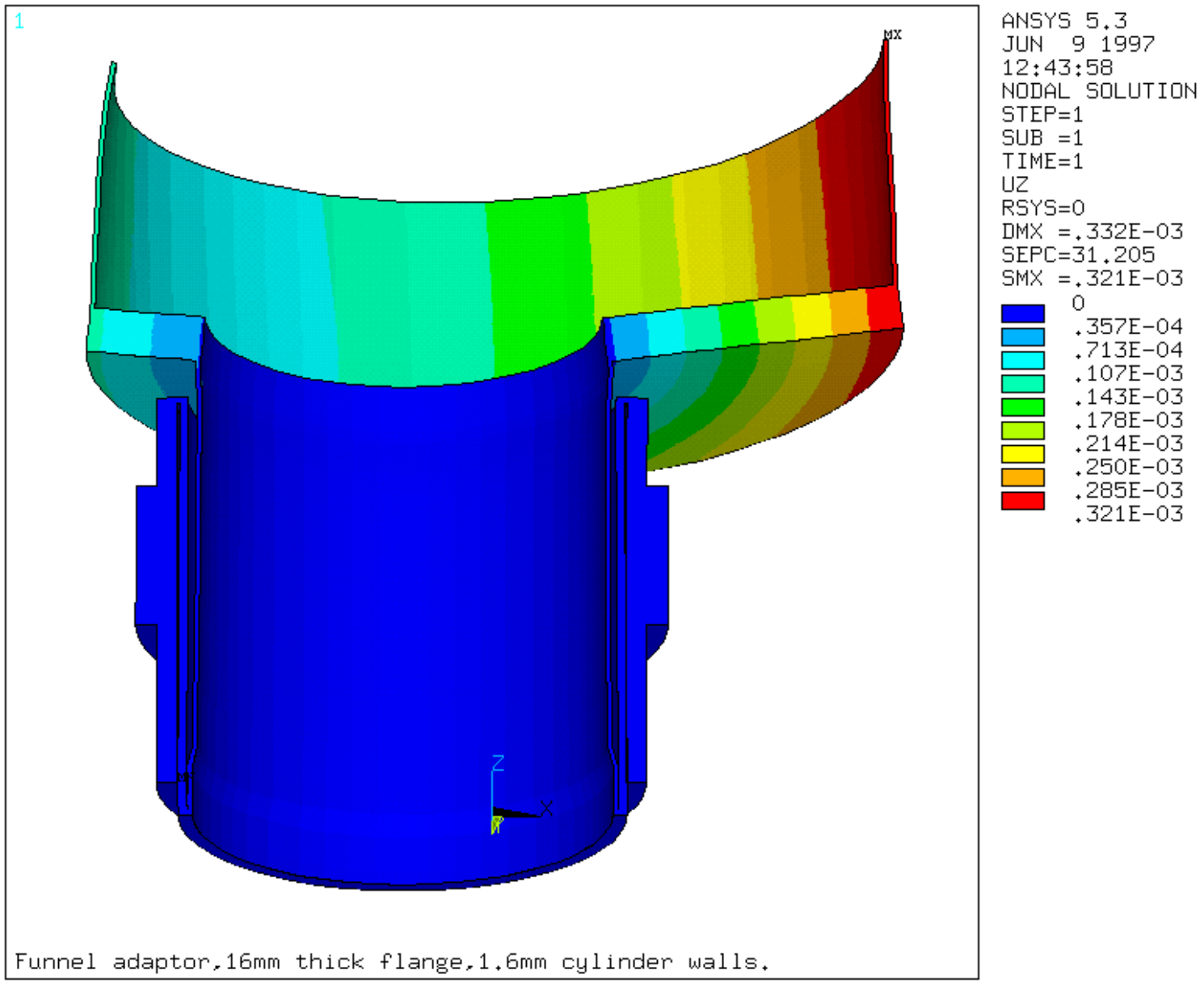

Figure 46: Finite element analysis of a funnel with a 16 mm thick flange and 1.6 mm thick cylinders, connected to a bi-metal joint, showing z displacements (bottom to top) in metres under an applied load of 3.5 bar, and a lateral load of 695 N (for a 15 mm displacement).

9 Stripline Temperatures (Release of 97/06/23)

The vacuum stripline is modelled for finite element analysis to investigate the effect the current supply to the HEC cold electronics would have on the stripline temperature. The first model is a single signal copper trace on a ground trace, separated by the kapton base material. The dimensions of the model are taken from the current design with a length of 300 mm (See Figure 47). The values used for the resistivity and thermal conductivity of the copper are temperature dependent but the kapton thermal conductivity is fixed at 3 Wm/K.

The ends of the stripline are held at 300 K and 80 K. The heat flow due to the temperature gradient alone is 1.64 mW in the signal trace alone and 4.93 mW for a signal plus ground pair of traces. The temperature of the signal stripline for several values of current is shown in Figure 48. The current flows only in the signal trace, the return current is assumed distributed widely enough to have no effect. The heat transfer from the signal trace via the kapton to the ground trace is included (the temperature difference between the signal and ground traces is very small). It appears the current in a single trace should be limited to 125–150 mA: to accommodate the required 0.5 A supply we will have to modify some of the striplines.

If we increase the width of the signal trace to match the 0.305 mm wide ground trace, it could handle 250 mA, and using two such traces for each current supply would give the required 500 mA capability. See Figure 49.

If we increase the copper signal trace thickness, as suggested by V. Radeka, (say by a factor of 2) and also retain the wide signal trace mentioned above, we could easily manage 500 mA on two traces, and, in the event of a failure of one of the traces in a pair, the whole 500 mA could be delivered on one trace. In Figure 50 the dashed curve shows the temperature of a single trace carrying the 500 mA, and the lower curve a single trace carrying 250 mA. If the trace carrying 500 mA is between two traces carrying 250 mA, the temperature profile of all three traces is modified to that shown in the centre curve.

The heat load into the liquid argon (with no current flow) will be increased by a factor of 2 for the latter option for each pin used for current supply. Generally the heat flow into the liquid argon is the sum of the heat conducted down the stripline plus the Joule heating from the current. If the temperature in the stripline is raised above the warm flange temperature however, some fraction of the heat will flow out of the warm flange.

Other possible scenarios could include leaving the entire ground plane of the stripline un-etched; and/or leaving pairs of current supply lines un-etched to form a single conductor, which could be joined to two adjacent pins in the pin carrier.

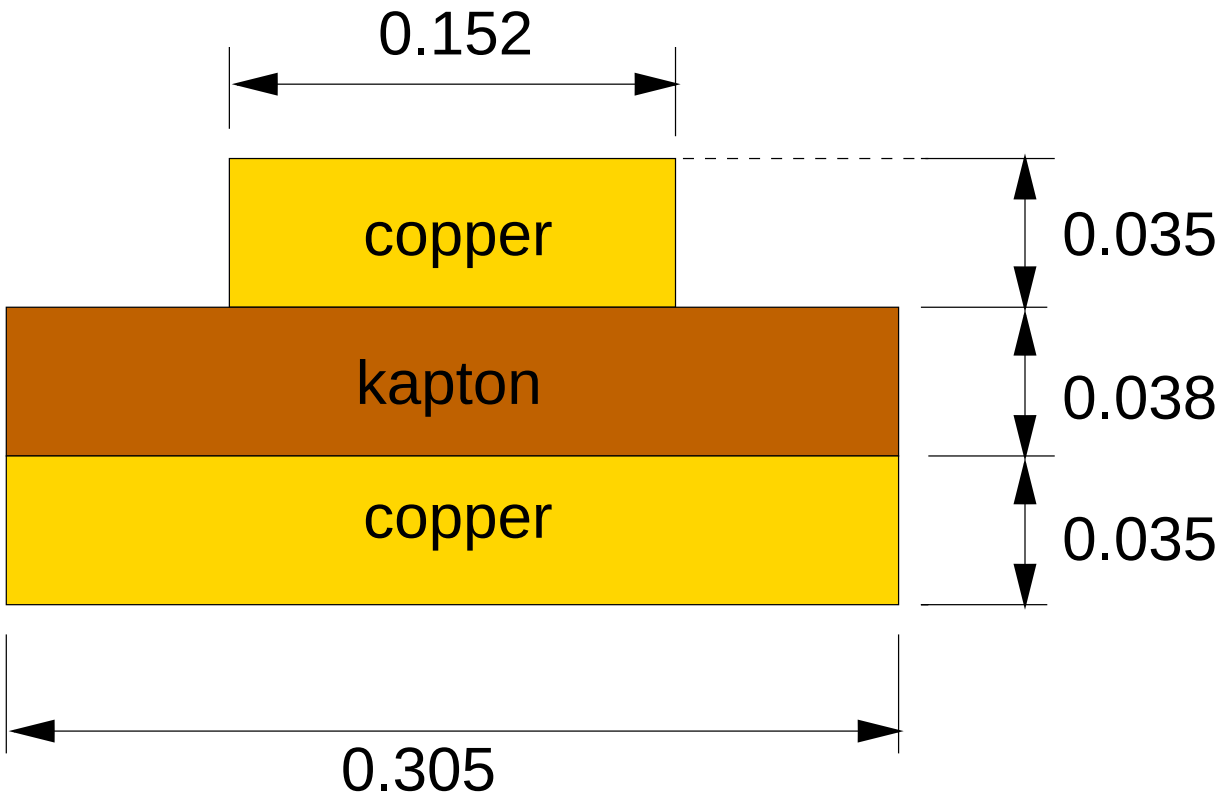

Figure 47: Finite element analysis model of one signal and return trace of the vacuum stripline. Dimensions in millimetres.

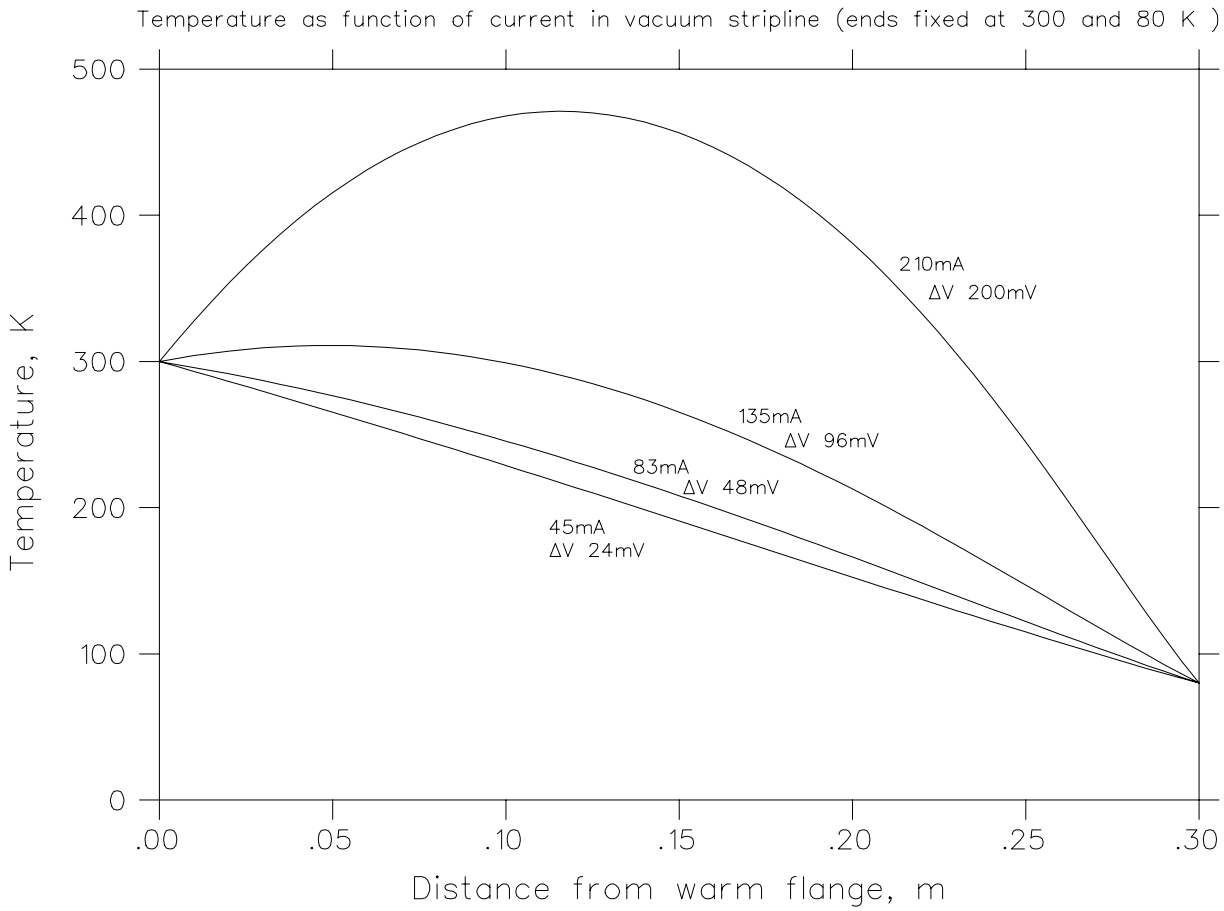

Figure 48: Temperature of vacuum stripline as a function of the distance from the ambient flange for several current values.

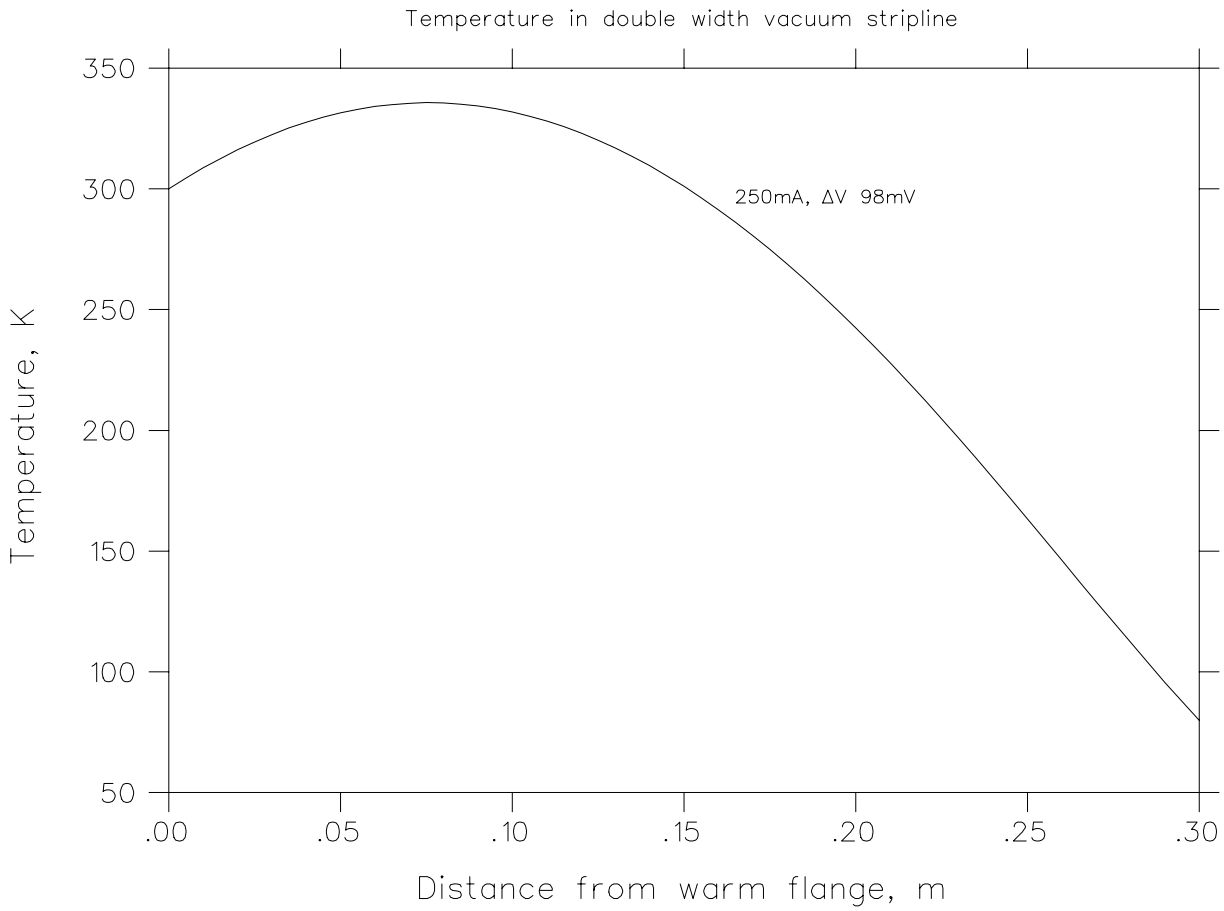

Figure 49: Temperature of vacuum stripline as a function of the distance from the ambient flange for one current value. The signal trace width is doubled to 305 μm.

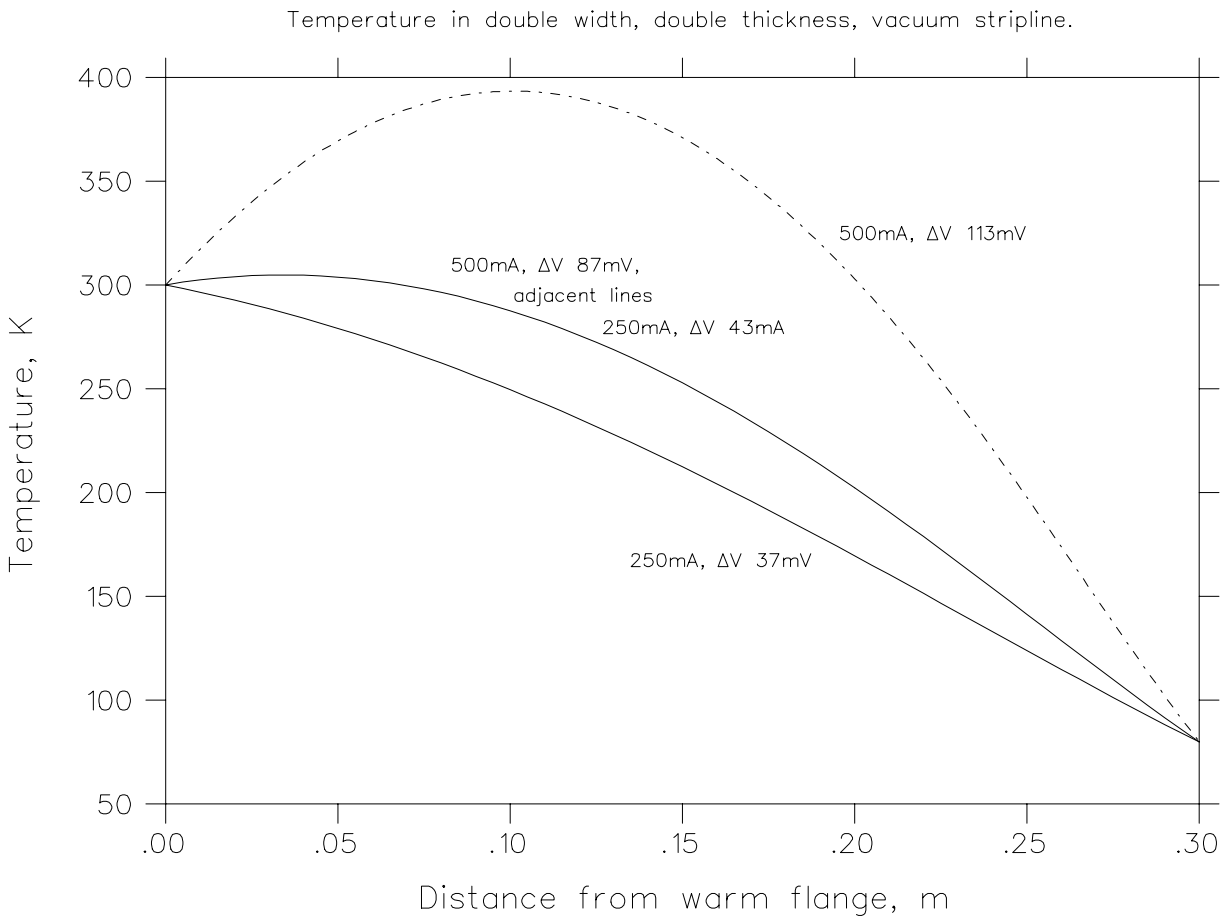

Figure 50: Temperature of vacuum stripline as a function of the distance from the ambient flange for several current values. The signal trace width is doubled to 305 μm, and the signal trace thickness is doubled to 70 μm.

10 Ambient Flange Temperature (Release of 97/07/07)

The temperature distribution in the ambient flange arising from the heat drain down the signal and ground connections to the cold flange is studied using finite element analysis. A heat drain of 5 mW per signal-plus-ground trace pair is assumed. This heat is removed uniformly over the 1.5 mm thick webs of the pin carriers. Three locations around the edge of the flange were held at 300 K to simulate the effect of three heating resistors. The result can be seen in the temperature contour plot in Figure 51. The red (300 K) regions are the locations of the resistors and the minimum temperatures, some 16 K lower, are in the central regions of the pin carriers. An extra resistor at the centre of the flange gave a small (2.4 K) improvement but would not be worth adding in practice. The temperature drop across the pin-ceramic region is found to be negligible (about 0.01 K).

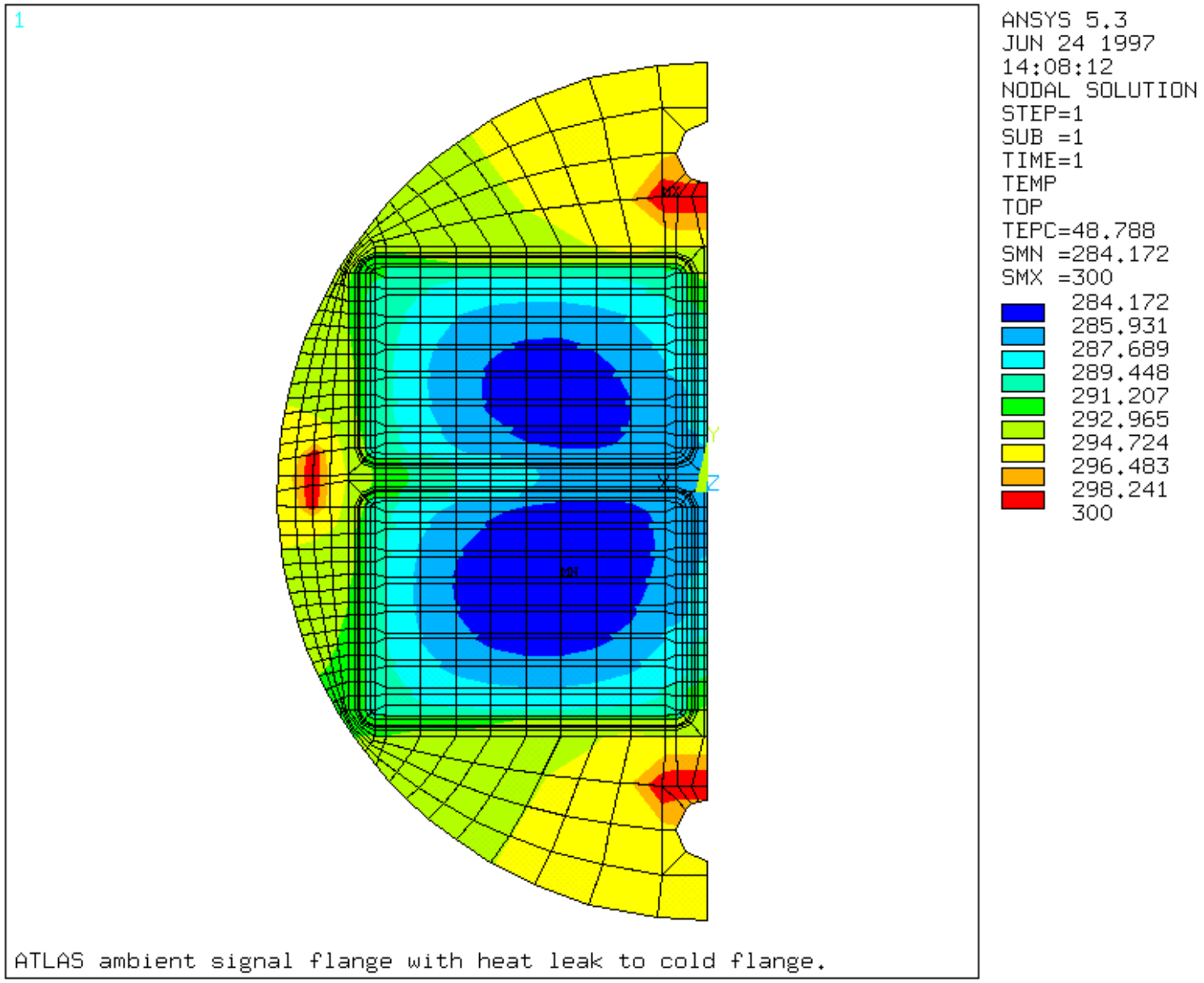

Figure 51: Finite element analysis of the temperature distribution in degrees Kelvin on the anbient flange.

11 Low Tension Current Supplies to HEC Circuit Boards via Signal Feedthroughs (Release of 97/09/02)

The "standard" signal cable, which connects each pair of 64-pin connectors in the ambient (300 K) and cold (80 K) flanges of the Barrel and Endcap signal feedthroughs, is a flexible circuit stripline. The flexible circuit is a sandwich of 38 μm thick kapton between two layers of 35 μm thick copper. Each pin in the feedthrough is connected to a copper trace 200 μm wide etched in one of the copper surfaces and is opposite a 400 μm wide ground trace on the other copper surface. Such an arrangement provides the correct impedance for the signal lines. Two pins, a supply and ground, are required for each HEC Low Tension (LT) current supply (a common ground is not suitable). The Joule heat from the current flowing in a trace is conducted down the trace, and also via the kapton layer to the common ground trace, to be deposited in the flanges and cables connected to the feedthrough. To maximize the current carrying capability of the stripline, it is proposed the 200 μm wide signal trace be increased to 400 μm wide to match the common ground trace. It might also be desirable to increase the thickness of the copper to further increase current carrying capability.

Consider a warm calorimeter and assume the ends of the current supply striplines are held at 300 K. The maximum temperature rise in a stripline as a function of current is shown in Figure 52 for three different copper thickness arrangements. The stars indicate the required current supplies for each hadronic module. Consider the curve for 35 μm thick signal and ground trace, and assume the temperature rise must not exceed 60 K. The maximum current allowed on a single line would be $\sim$208 mA. The maximum required current of 624 mA would have to be supplied by three separate lines, others would require two lines, and those below 208 mA only one. In the latter scenario, the eight modules in a quadrant of the calorimeter would require $8 \times 48 = 384$ lines. The single feedthrough which must supply these lines has a maximum of $6 \times 64 = 384$ signal lines available for LT supply – precisely the number of lines required!

However, it might be deemed prudent to have at least a few "spare" lines available: in that case one of the other two options shown in Figure 52 might be adopted. In either of these cases a total of $8 \times 36 = 288$ lines would be required, leaving 96 "spare" lines per quadrant. The latter options would also reduce the maximum temperature rise in the stripline to 40-50 K but at the expense of making the stripline stiffer.

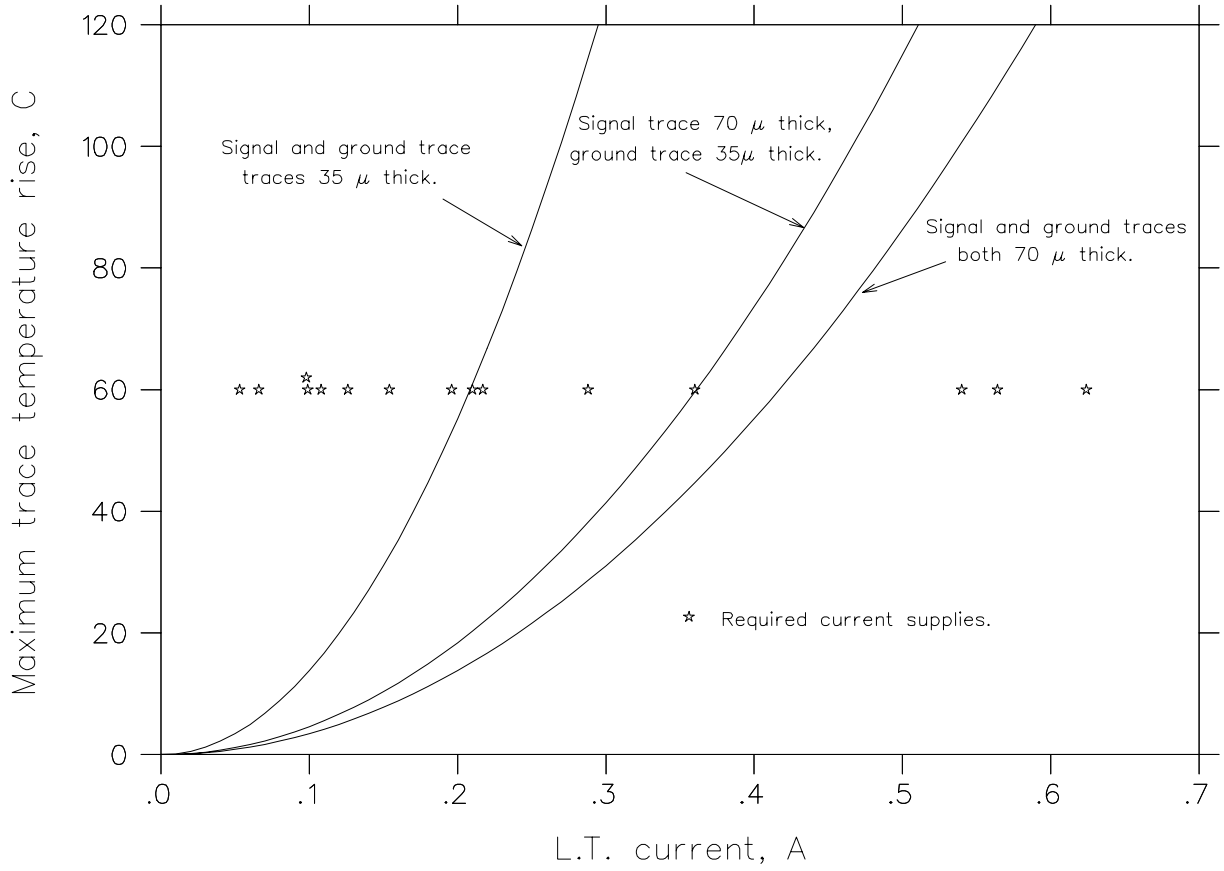

Figure 52: Maximum temperature rise of vacuum stripline as a function of the current for a warm calorimeter. Curves for various thicknesses of the signal trace and the ground trace are shown. The stars indicate the required current supplies for each hadronic module Both signal and ground traces are 400 μm wide.

12 Effect of Cooling Ambient Feedthrough Flange in LN vapour (Release of 97/09/03)

A number of tests are carried out on components and sub-assemblies of the ATLAS signal feedthrough as they are built. One such test on an ambient feedthrough flange caused leaks to develop in the pin carriers. The test involved cooling the flange by natural convection in the cold nitrogen gas above the liquid nitrogen in a container. To estimate the magnitude of the thermal stress induced by such cooling an FEA model of the ambient feedthrough flange was subjected to a cooling process which approximates those in the test. The assumptions made to apply convective cooling to the flange and pin carrier surfaces were as follows:

- Horizontal warm surfaces facing upward, heat transfer coefficient = 6.2 $Wm^{-2}K^{-1}$
- Horizontal warm surfaces facing downward, heat transfer coefficient = 2.8 $Wm^{-2}K^{-1}$
- Vertical surfaces, heat transfer coefficient = 6.2 $Wm^{-2}K^{-1}$

The bulk cold gas temperature was assumed to be 80 K and the initial flange temperature 300 K.

The ANSYS program was used to produce the time dependent temperature fields in the flange and pin carriers. Figure 53 shows the temperature contours for the flange after cooling for 15 minutes. Figure 54 shows the maximum and minimum temperature points on the flange as a function of time. The maximum temperature difference in the flange occurs after about 15 minutes of cooling. The temperatures in the flange after 15 minutes of cooling were applied in a static analysis to compute the thermal stresses. Figure 55 shows the Von Mises stresses in the pin carrier web (which contains the signal pins). The maximum stress in the vicinity of the pins is above 100 MPa, about 20 to 50 times the maximum stress seen in normal usage and uncomfortably large. There were also localized stresses in the areas where the pin carriers are welded to the flange of 400 MPa (cf yield stress of $\sim$230 MPa).

The same conditions applied to the cold flange would probably have a more severe effect (since the thermal mass of the cold flange is 55% greater than the ambient flange), increasing the temperature differences and thermal stresses during the cooling process.

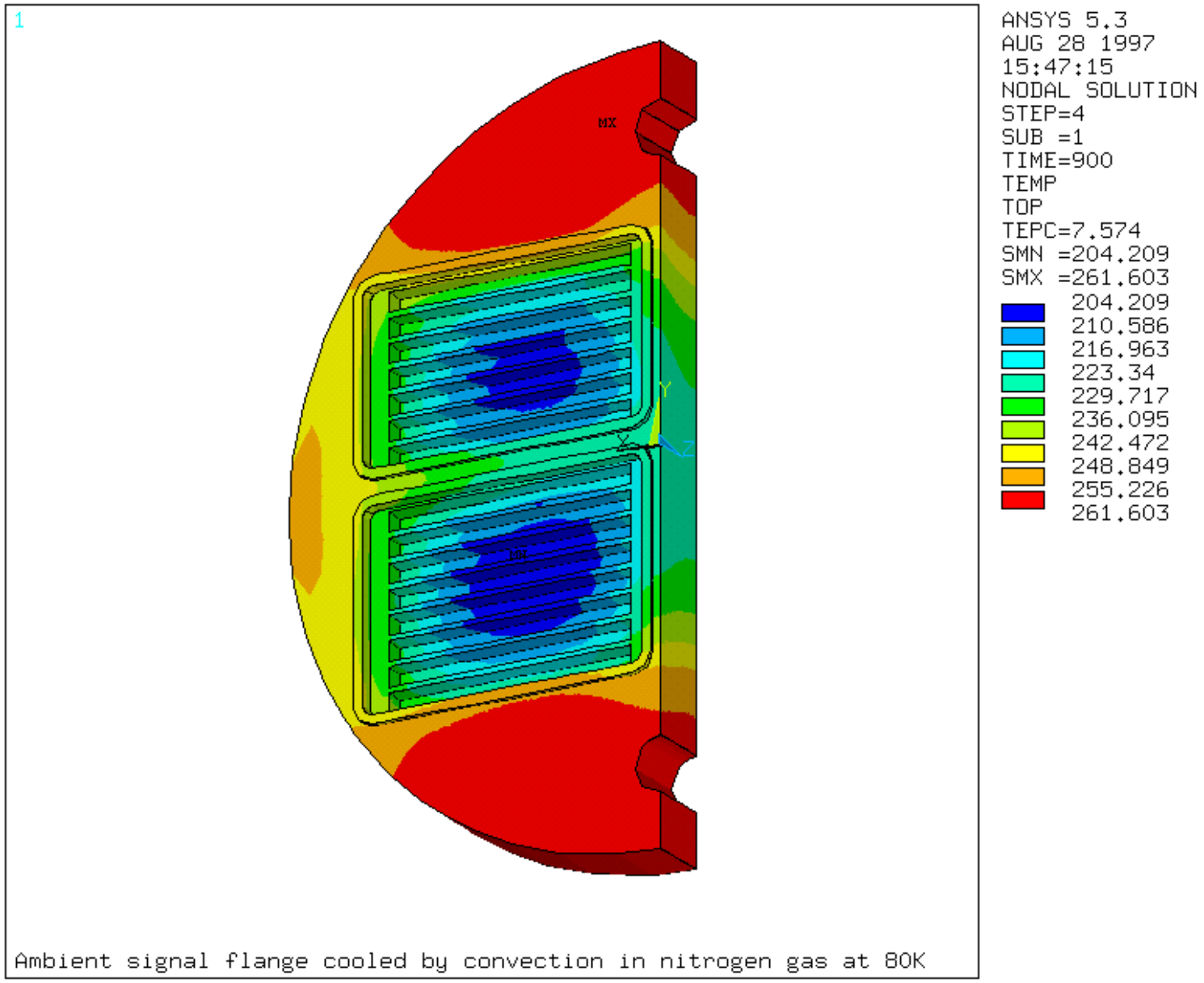

Figure 53: Ambient flange temperature in K after cooling 15 minutes in nitrogen gas at 80 K.

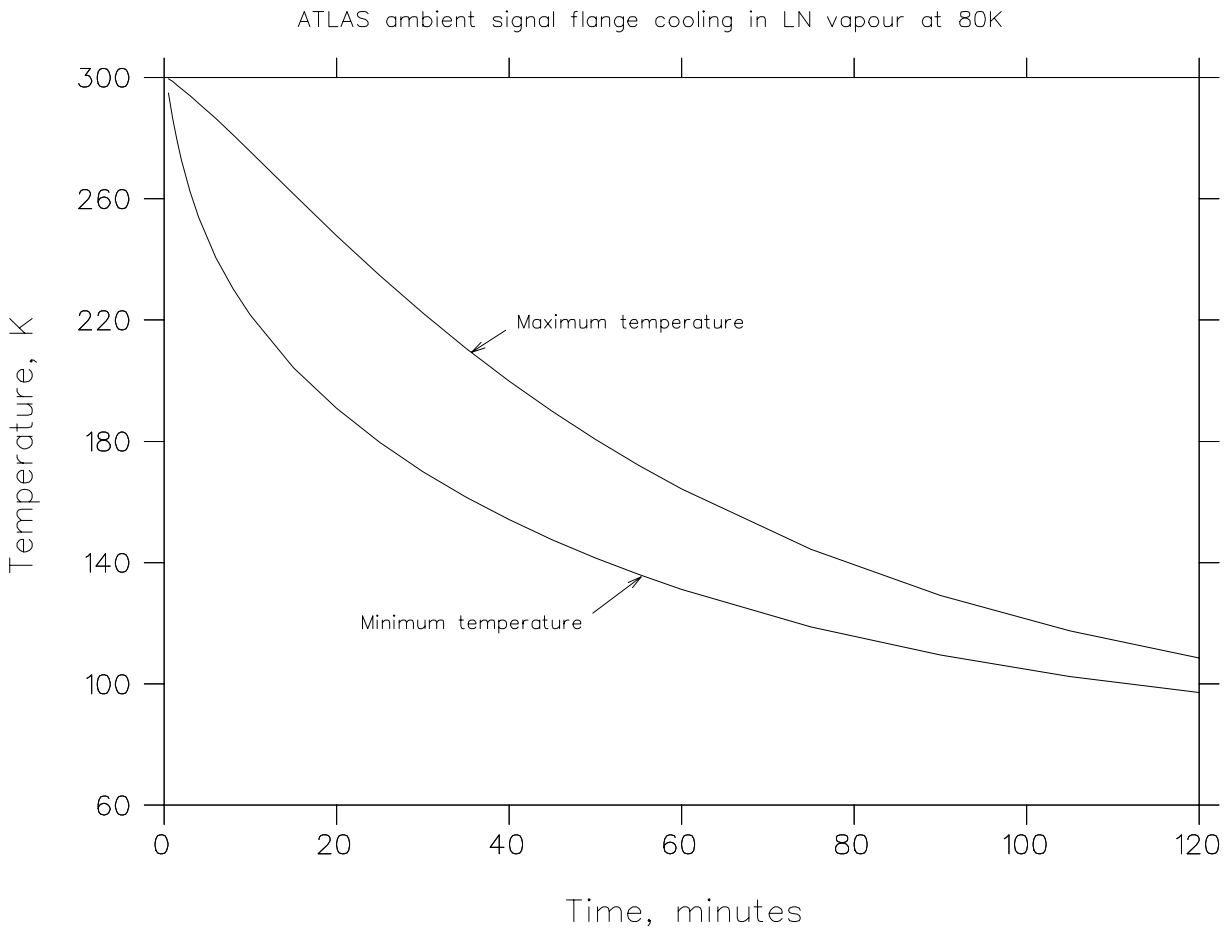

Figure 54: Ambient flange minimum and maximum temperature in K after cooling 15 minutes in nitrogen gas at 80 K.

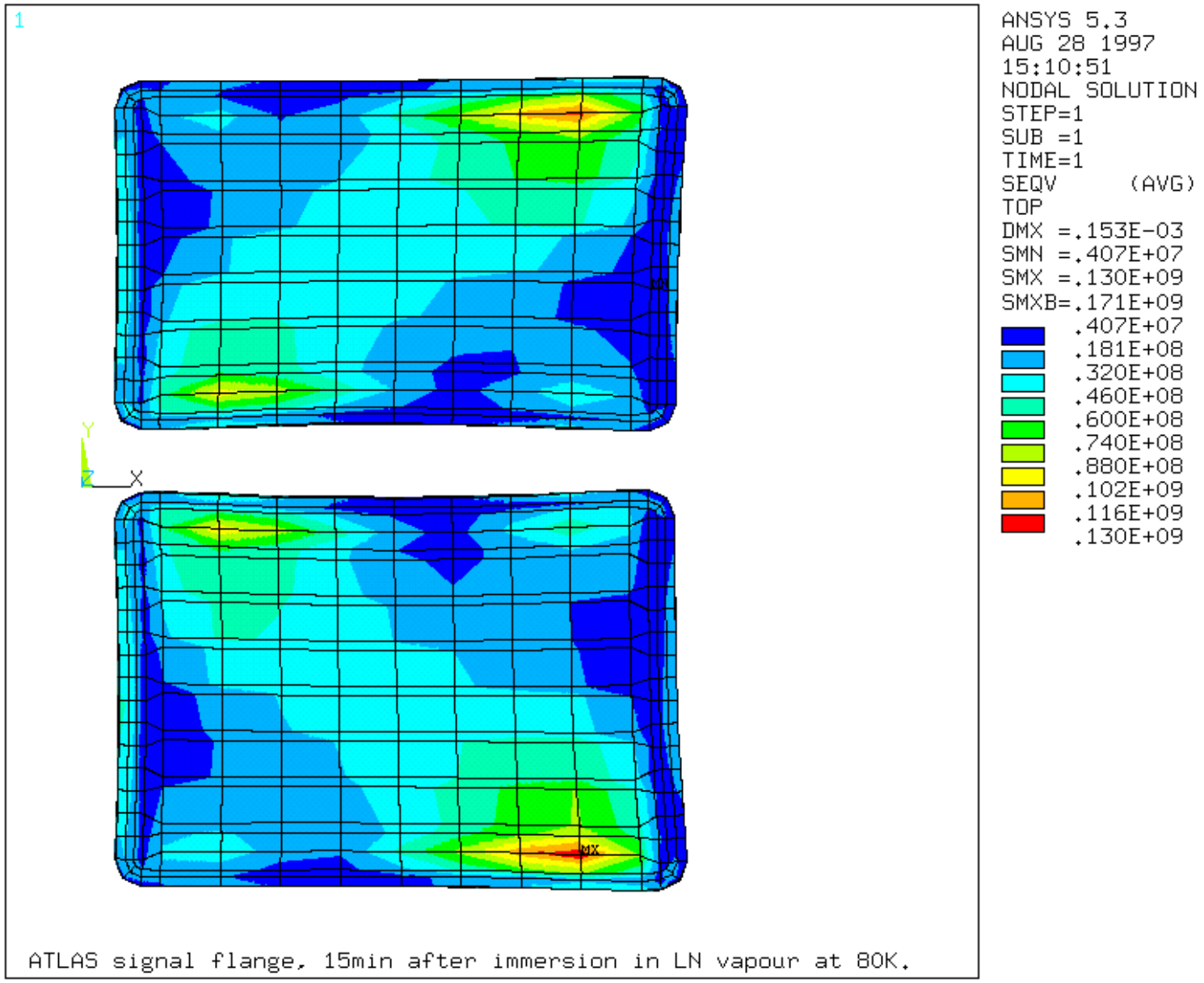

Figure 55: Von Mises stresses in Pa in the ambient flange pin carrier web after cooling 15 minutes in nitrogen gas at 80 K.

13 Updated Cold and Ambient Flanges Study (Release of 97/09/22)

The models of the ambient and cold signal feedthrough flanges have been modified as well as the pressure loading on them to comply with the requirements set out in the ATLAS Project Document ATL–CERN–A–CERN–0002 "Larg Cryostats – Load Cases for the Cryostats and Feedthroughs". I have used the barrel cryostat feedthrough data since the quoted pressures for calculations are generally slightly (0.1 bar) larger than those for the endcap.

For the cold flange, the maximum pressure for "Normal" situation (N5) is 2.8 bar with 0.1 bar added to allow for extra hydrostatic pressure on a feedthrough in the lower part of the cryostat. The maximum pressure of 3.5 bar experienced during the "Proof Test" situation (T5) is larger than all of the "Exceptional" situations. The results of the finite element analysis performed at the two pressures 2.9 bar and 3.5 bar are summarized in the first two rows of Table 3 and in Figures 56, 57, 58, 59 and 60.

The ambient flange under normal conditions has a maximum pressure load of 1 bar. Under the exception situation of a leak from the argon space into the bellows vacuum space of the feedthrough, a reverse pressure of 2.3 bar (3.3 bar less the atmospheric load) could be developed. The finite element analysis results for the flange under the latter load conditions is summarized in the last two rows of Table 3 and in Figures 61, 62, 63, 64 and 65.

flange type	pressure (bars)	deflection (μm)	maximum pin carrier stress (MPa)	maximum flange stress (MPa)	figures
cold	2.9	46.0	55.8	34.0	56, 57
cold	3.5	55.5	67.3	41.0	58, 59, 60
ambient	1.0	53.3	43.6	26.4	61, 62
ambient	-2.3	-117.	94.7	60.5	63, 64, 65

Table 3: Deflection and stress for cold and ambient flanges. Negative pressure and deflection are in opposite direction to normal atmospheric loading.

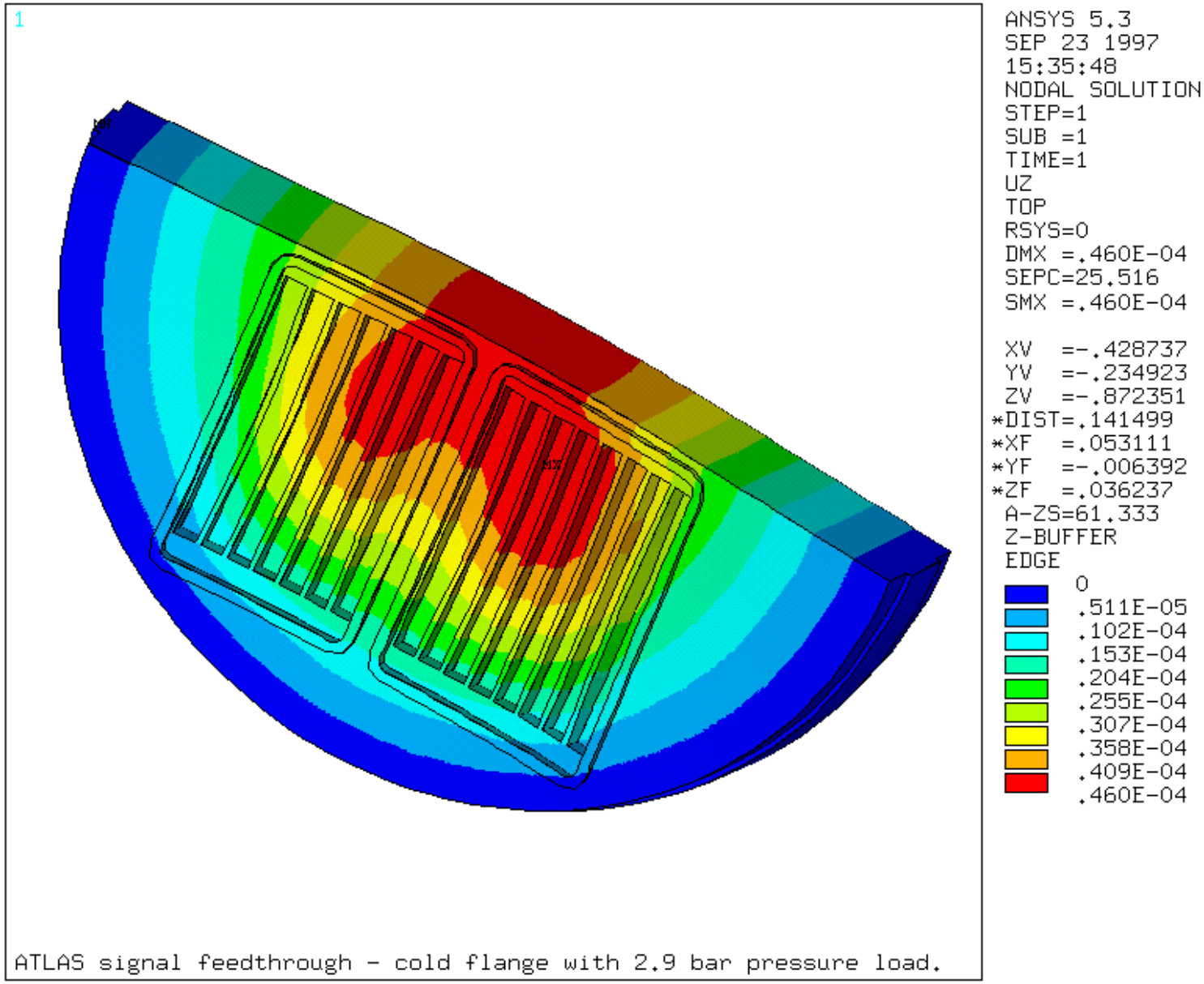

Figure 56: Finite element analysis of a cold flange with thickness 36.5 mm (1.4 inches) and web thickness 1.5 mm showing deflections in metres under an applied load of 2.9 bars.

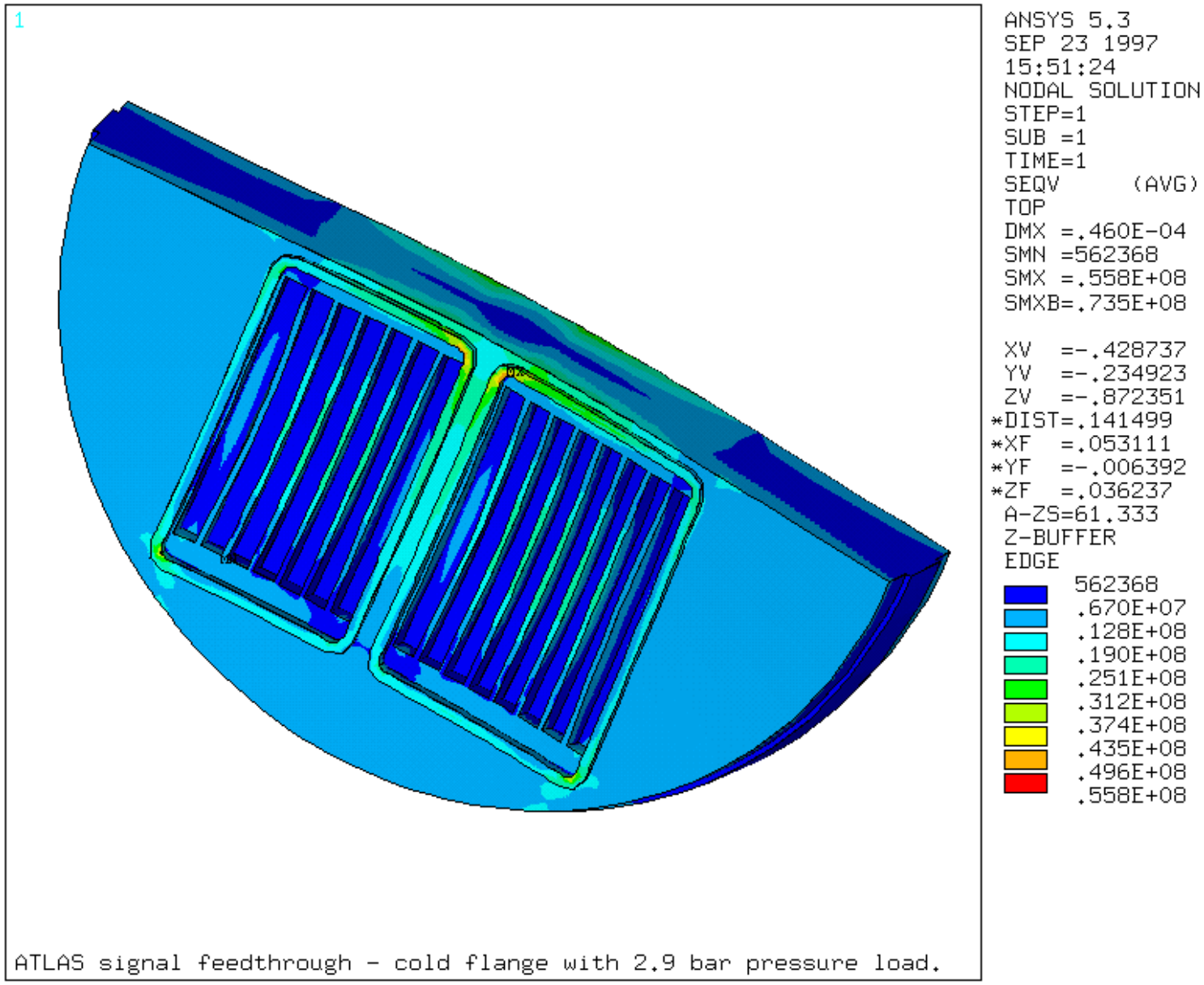

Figure 57: Finite element analysis of a cold flange with thickness 36.5 mm (1.4 inches) and web thickness 1.5 mm showing the (Von Mises) stress in Pascals under an applied load of 2.9 bars.

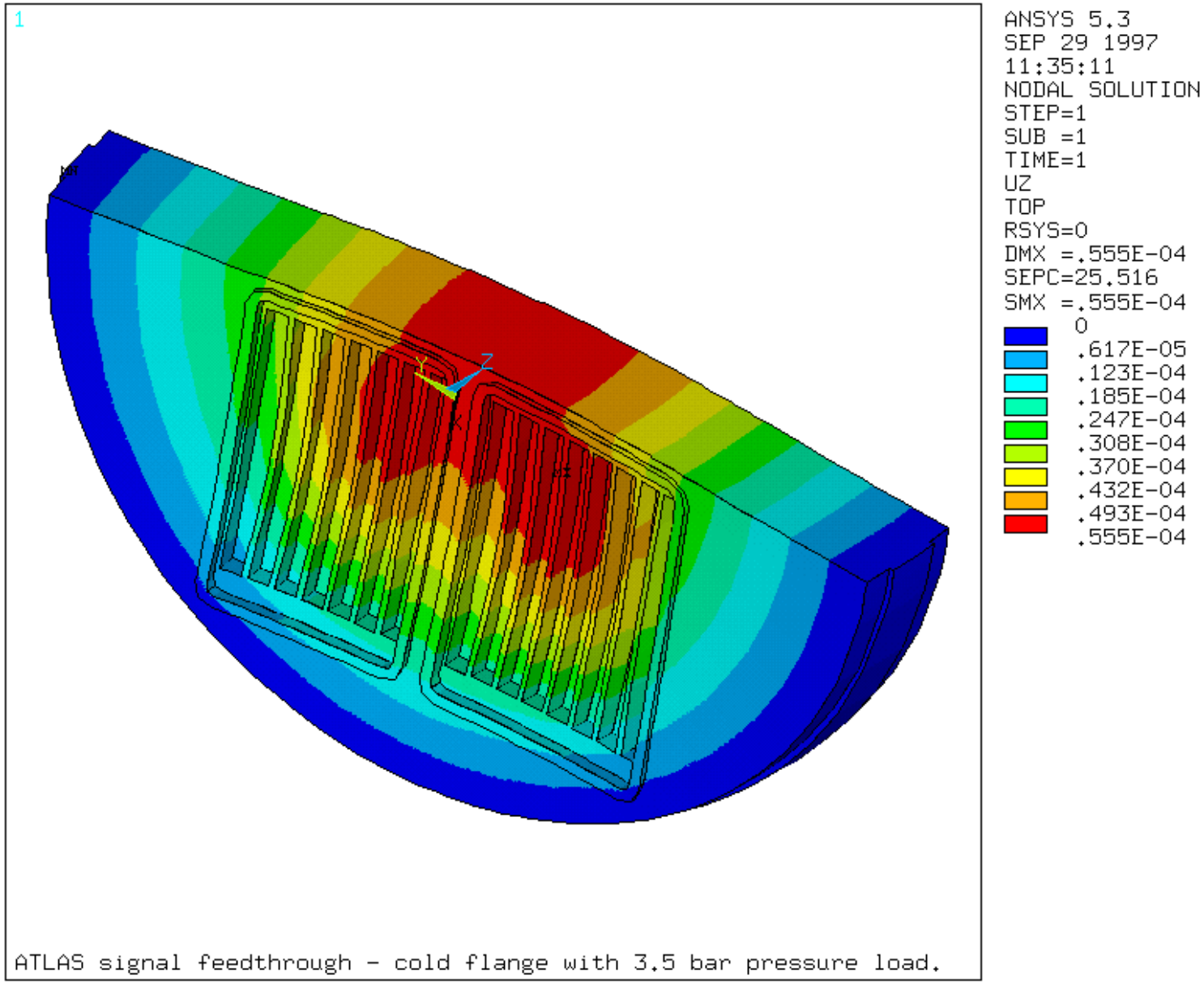

Figure 58: Finite element analysis of a cold flange with thickness 36.5 mm (1.4 inches) and web thickness 1.5 mm showing deflections in metres under an applied load of 3.5 bars.

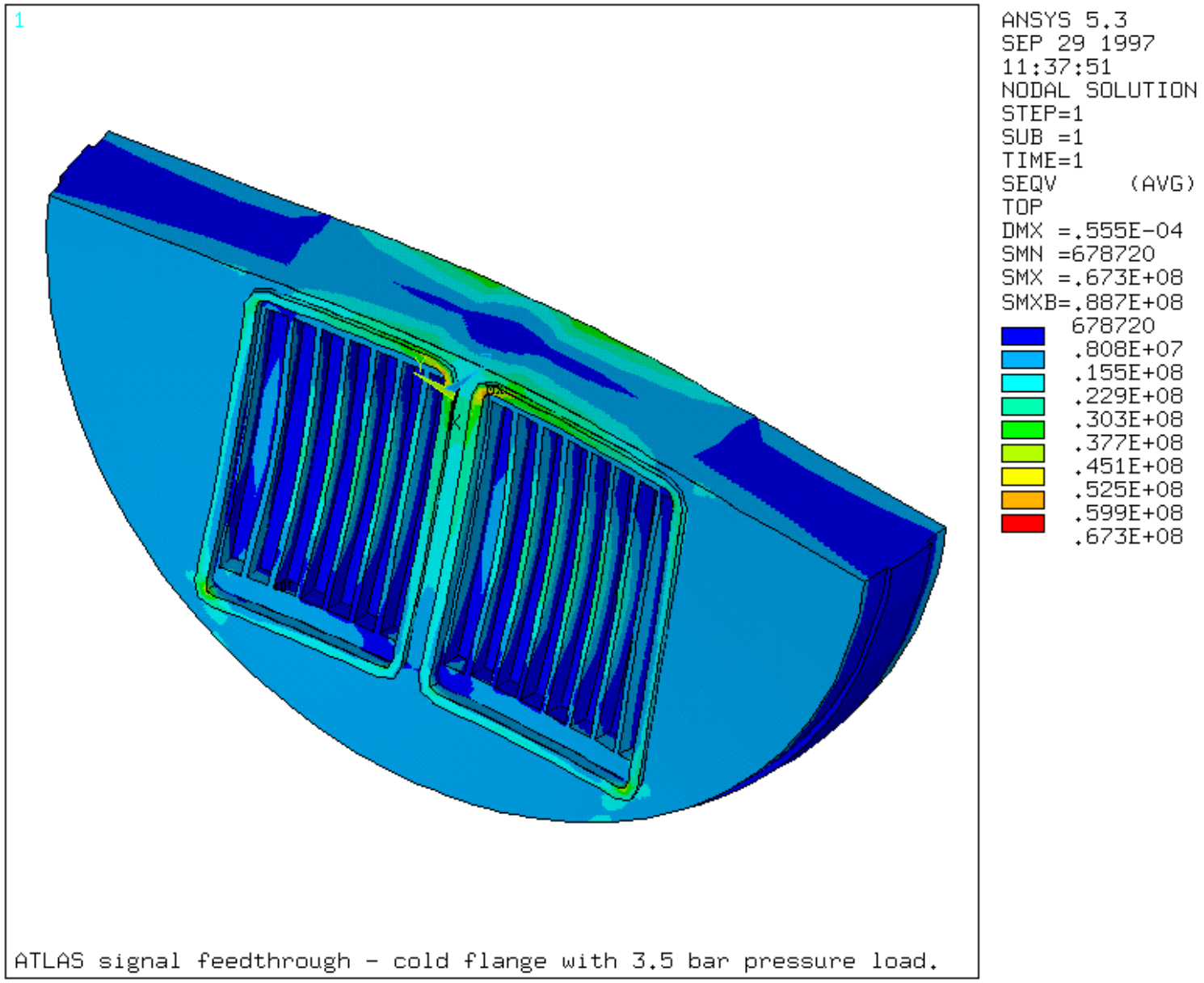

Figure 59: Finite element analysis of a cold flange with thickness 36.5 mm (1.4 inches) and web thickness 1.5 mm showing the (Von Mises) stress in Pascals under an applied load of 3.5 bars.

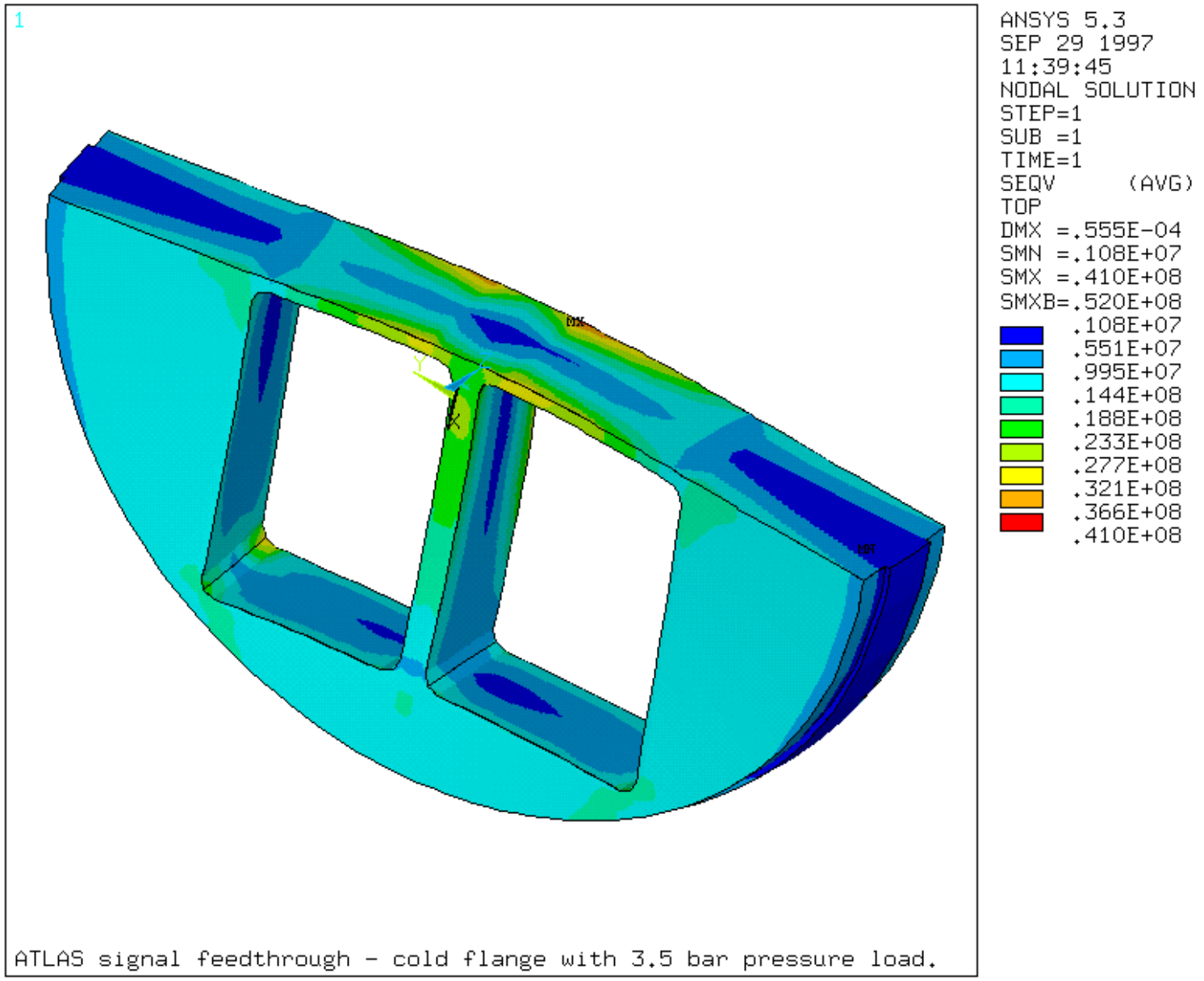

Figure 60: Finite element analysis of a cold flange with thickness 36.5 mm (1.4 inches) without the pin carriers showing the (Von Mises) stress in Pascals under an applied load of 3.5 bars.

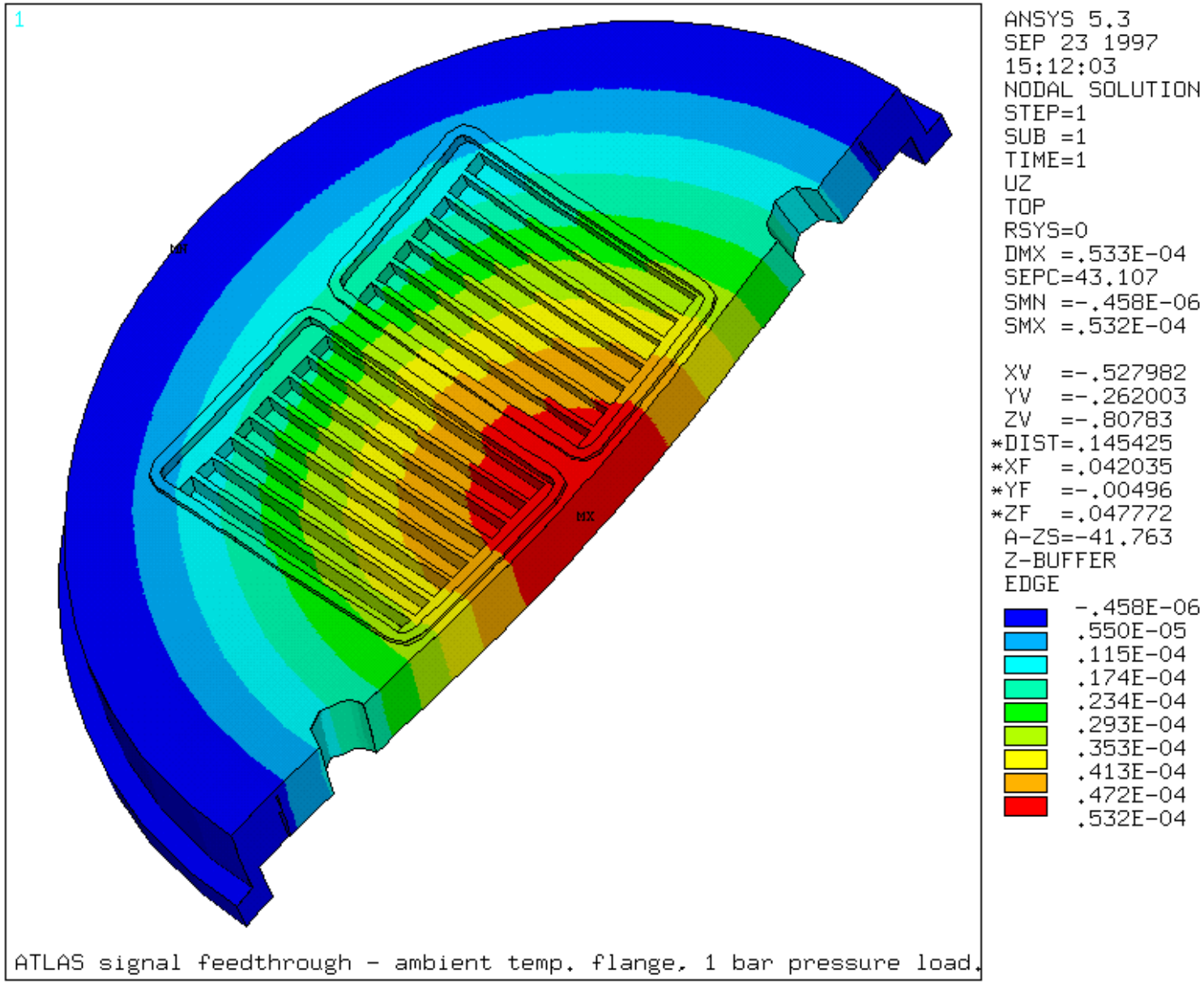

Figure 61: Finite element analysis of an ambient flange with thickness 22.9 mm (0.9 inch) and web thickness 1.5 mm showing deflections in metres under an applied load of 1 bar.

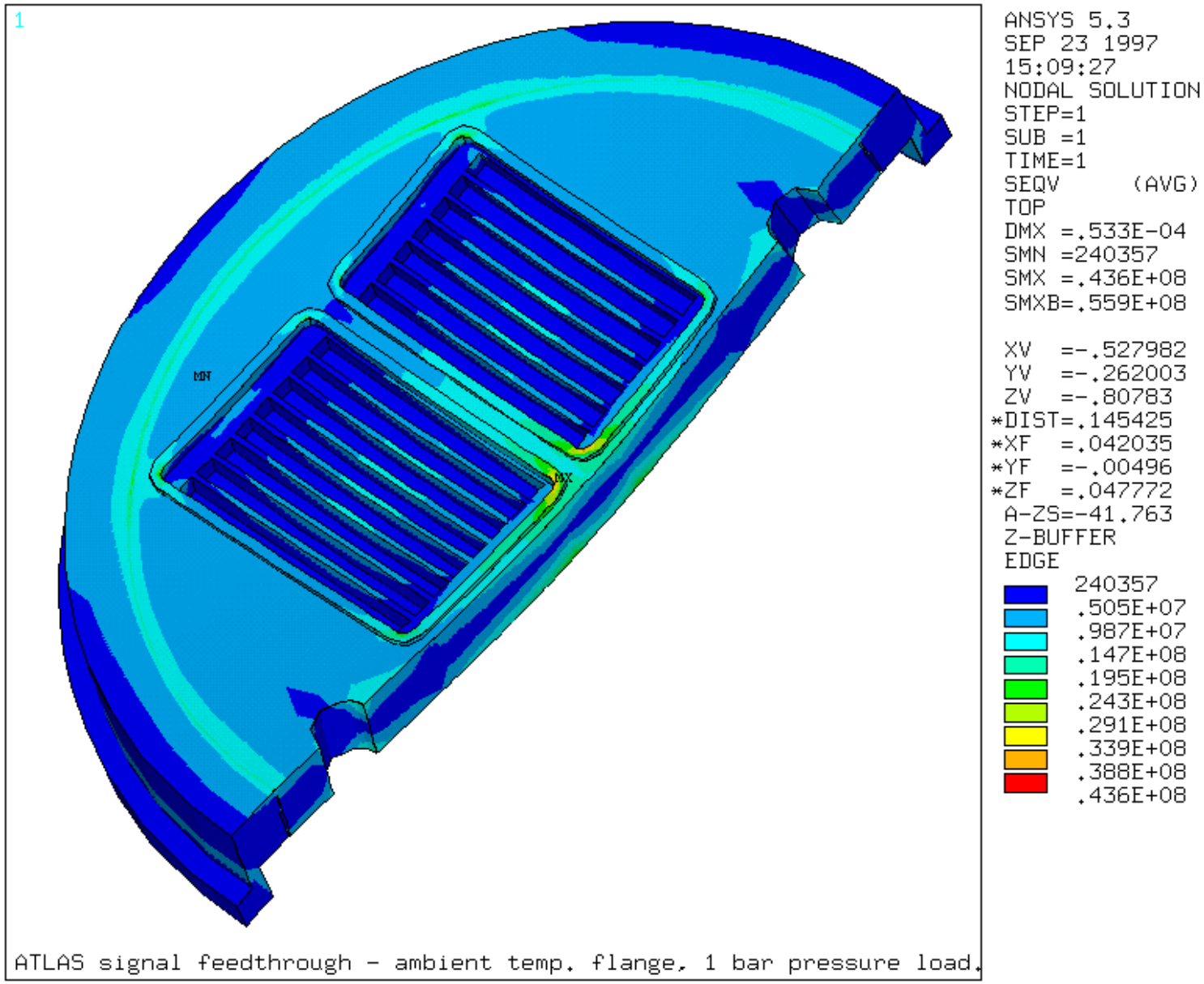

Figure 62: Finite element analysis of an ambient flange with thickness 22.9 mm (0.9 inch) and web thickness 1.5 mm showing the (Von Mises) stress in Pascals under an applied load of 1 bar.

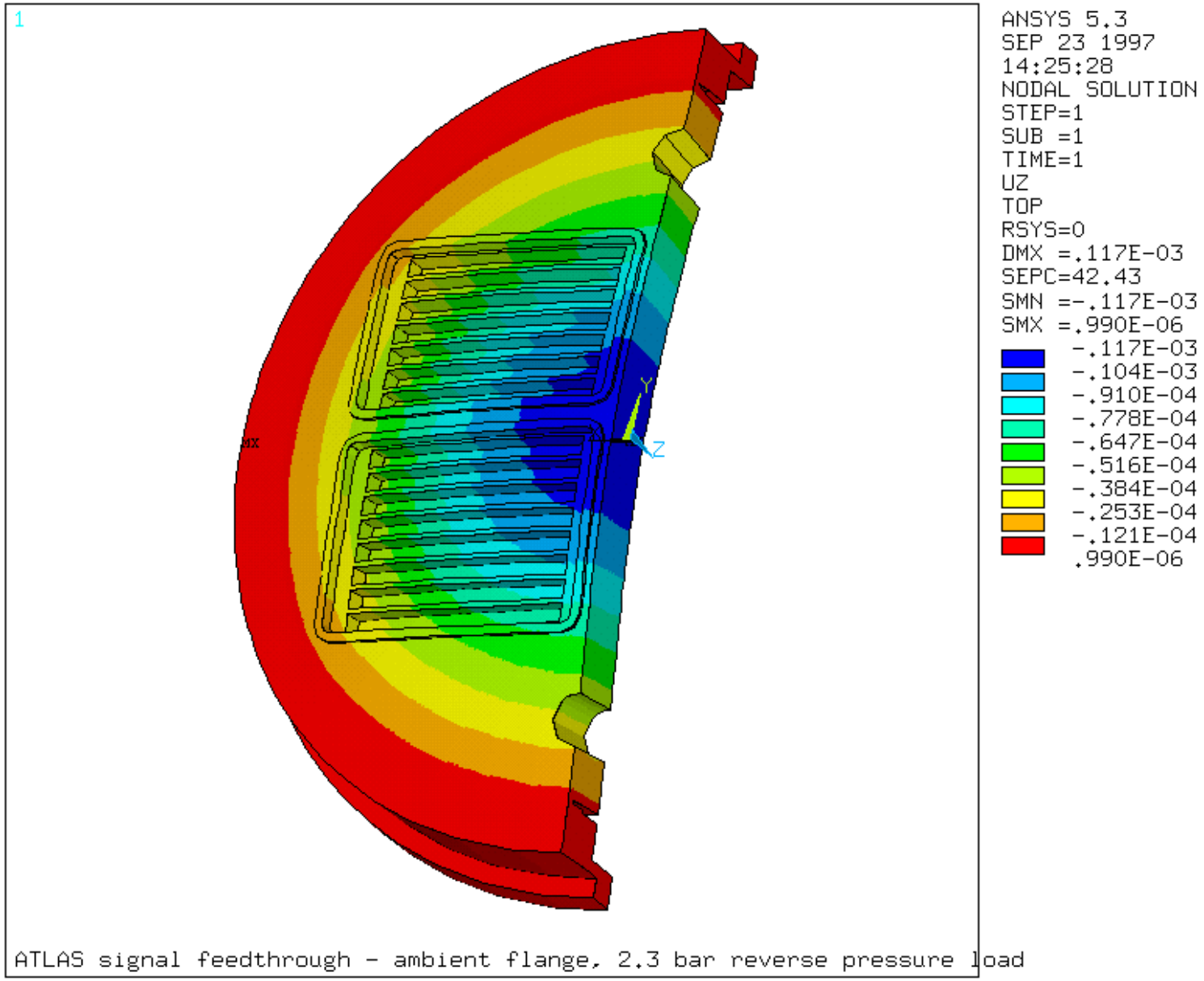

Figure 63: Finite element analysis of an ambient flange with thickness 22.9 mm (0.9 inch) and web thickness 1.5 mm showing deflections in metres under an applied load of 2.3 bars in opposite direction to normal atmospheric loading.

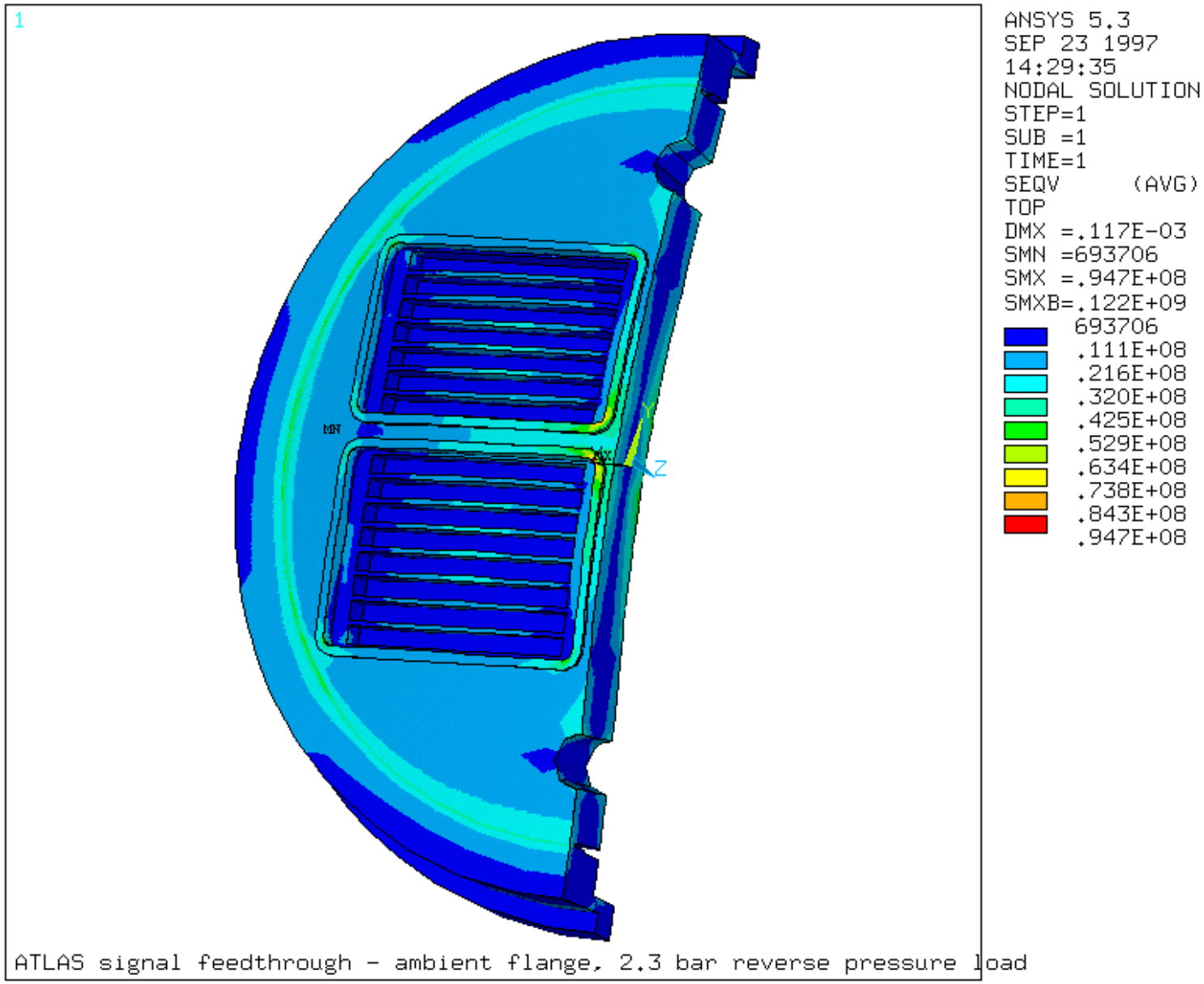

Figure 64: Finite element analysis of an ambient flange with thickness 22.9 mm (0.9 inch) and web thickness 1.5 mm showing the (Von Mises) stress in Pascals under an applied load of 2.3 bars in opposite direction to normal atmospheric loading.

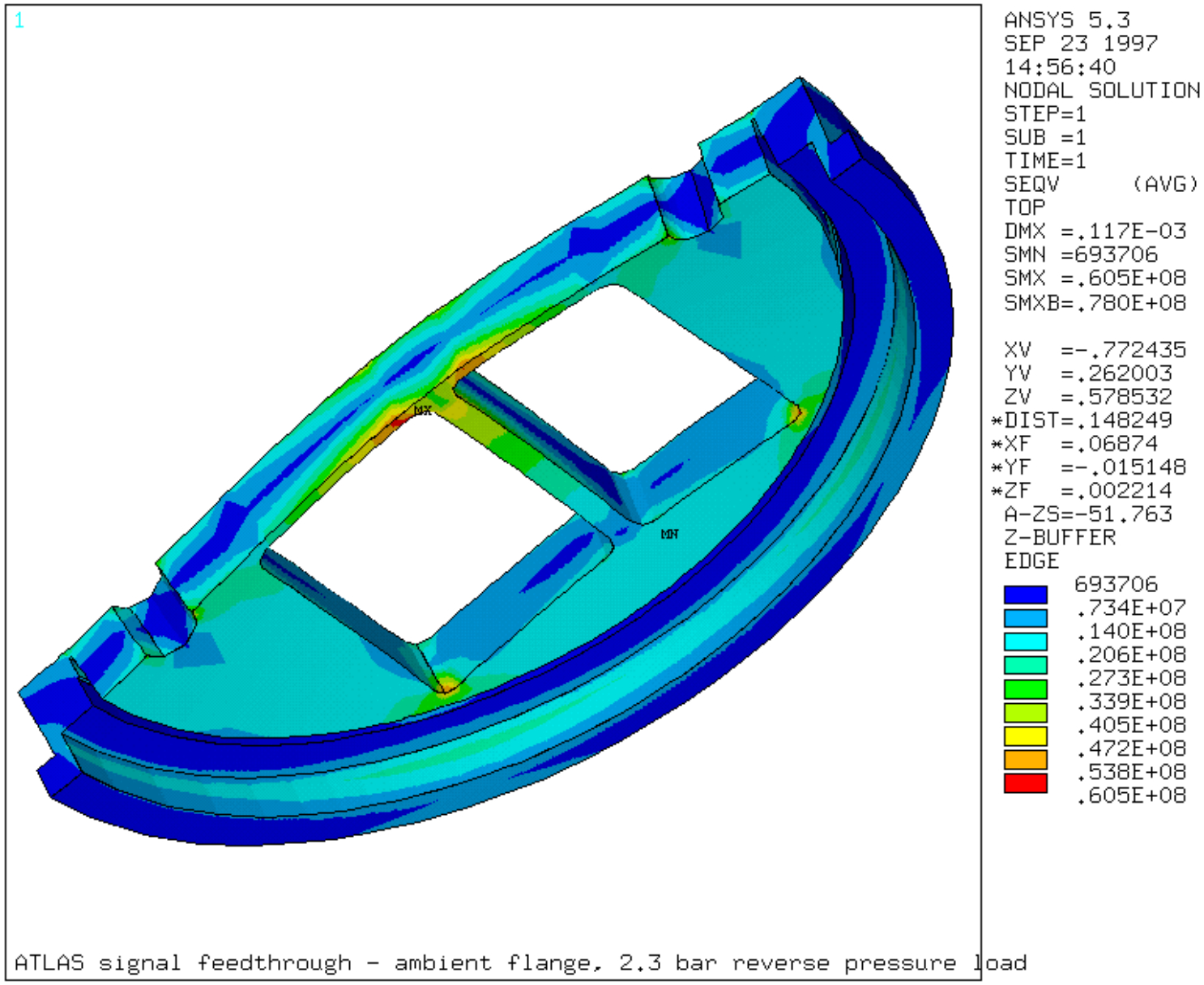

Figure 65: Finite element analysis of an ambient flange with thickness 22.9 mm (0.9 inch) without pin carriers showing the (Von Mises) stress in Pascals under an applied load of 2.3 bars in opposite direction to normal atmospheric loading.

14 Stresses Induced by Welding of Pin Carriers into Ambient Flange (Release of 97/11/28)

The finite element analysis model of the ambient temperature signal feedthrough flange of thickness 22.9 mm has been modified to include a weld preparation "rim" around the edges of the holes in the flange wherein the pin carriers are welded. Figure 66 shows a general view of (half) the ambient temperature flange and Figures 67 and 68 show a closer view of the flange weld preparation and a pin carrier respectively. The pin carrier "skirt" is the thin walled region between the the edge of the pin carrier that is welded to the "rim" of the flange, and the thick region of the pin carrier into which the signal cable plugs are inserted. The pin carrier "web" is the region of the pin carrier that contains the signal pins.

A series of calculations were made to determine the stresses developed in critical regions of the assembly, caused by deflection of the flange as a result of welding the pin carriers into the flange.

Vertical deflection (perpendicular to the flange face and typically 58 μm in magnitude) was produced by applying a pressure (1 bar) to the face of the flange around the pin carriers. Calculations were performed for different pin carrier skirt length and thickness and for three pin carrier web thicknesses, and are shown in Table 4.

Figures 73, 74 and 75 show the regions where the von Mises stresses are a maximum in the flange, the pin carrier, and the pin carrier web.

case no.	web thickness (mm)	skirt thickness (mm)	skirt length (mm)	maximum flange stress (MPa)	maximum pin carrier corner stress (MPa)	maximum pin carrier web stress (MPa)	figure
1	1.5	0.5	5	42.9	47.1	4.2	69
2	1.5	0.5	7	41.5	41.5	4.7	70
3	1.5	0.5	10	40.5	37.8	6.2	71
4	1.5	1.0	5	50.2	44.5	4.9	72
5	1.5	1.0	7	50.6	39.2	4.2	75
6	1.5	1.0	10	51.2	34.8	5.4	76
7	2.5	1.0	7	52.2	41.5	4.1	77
8	4.0	1.0	5	58.4	48.1	4.8	78
9	4.0	1.0	7	54.1	43.1	3.9	79
10	4.0	1.0	10	53.3	36.7	3.2	80

Table 4: Maximum (Von Mises) stress in critical regions of a 22.9 mm thick ambient flange for various pin carrier web thicknesses, skirt thicknesses and skirt lengths under an applied load of 1 bar.

To simulate (crudely) the effect on the pin carriers of in-plane distortion of the flange due to welding, the region where the pin carrier rim is welded to the flange weld

preparation was subjected to a 60 K temperature reduction, resulting in a shrinking of this region relative to all other regions. The temperature contours are shown in Figure 81. The magnitude of the temperature change was chosen to produce a maximum stress amplitude in the vicinity of the weld approximately equal to the material yield strength. The stresses produced in the pin carrier webs due to the compressive forces thus generated (plus the vertical deflection of 82 μm produced by the cooling) were investigated (see Table 5).

case no.	web thick-ness (mm)	skirt thick-ness (mm)	skirt length (mm)	maximum flange stress (MPa)	maximum pin carrier corner stress (MPa)	maximum pin carrier web stress (MPa)	fig-ure
11	4.0	1.0	9	256	196	11.2	82
12	4.0	1.0	7	248	196	11.9	83
13	1.5	1.0	9	256	197	13.8	84

Table 5: Maximum (Von Mises) stress in critical regions of a 22.9 mm thick ambient flange for various pin carrier web thicknesses and skirt lengths upon welding of the pin carrier into the ambient flange. See text.

For the vertical flange distortion, there appears to be a broad minimum in the pin carrier web stress versus skirt length, for a given skirt thickness. e.g. in cases 4, 5 and 6 above, the 7 mm skirt length is preferable over the 5 mm or 10 mm skirt length. As the pin carrier web thickness increases, the optimum skirt length increases.

For the in-plane flange distortion, a slow decrease in the maximum pin carrier web stress is seen with increasing skirt length and increasing web thickness.

For the likely range of web thicknesses (2 mm to 4 mm) a skirt length of 9 mm and thickness of 1.0 mm is a reasonable choice, with no foreseen problems in manufacturing.

For the typical 58 μm flange deflection, the flange and pin carrier corner stresses are modest and localized and would probably be acceptable with deflection several time larger. The pin carrier web stresses, however, should be kept to a minimum: flange deflection above 200 μm should be avoided.

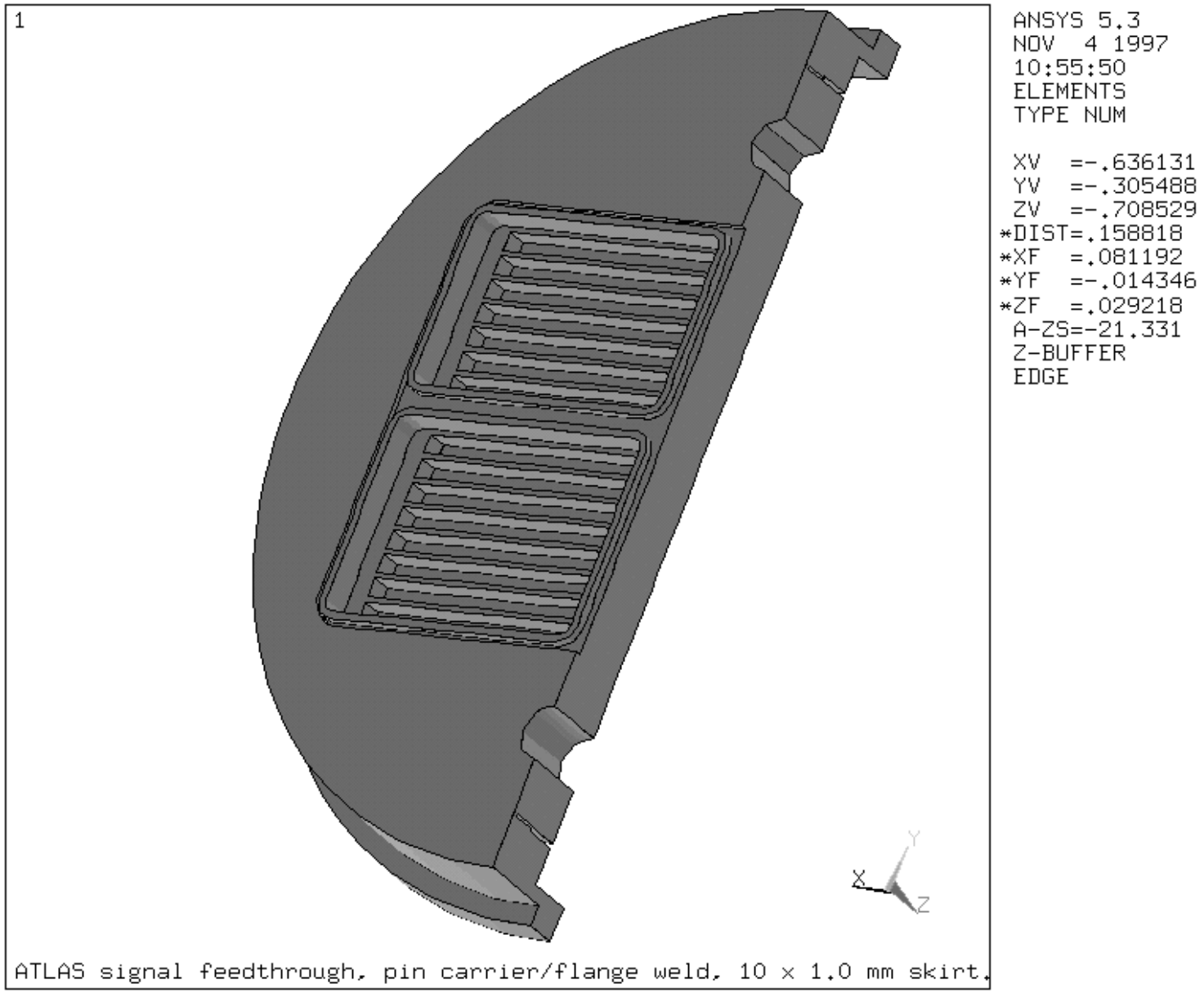

Figure 66: Finite element analysis model of (half) an ambient flange 22.9 mm thick.

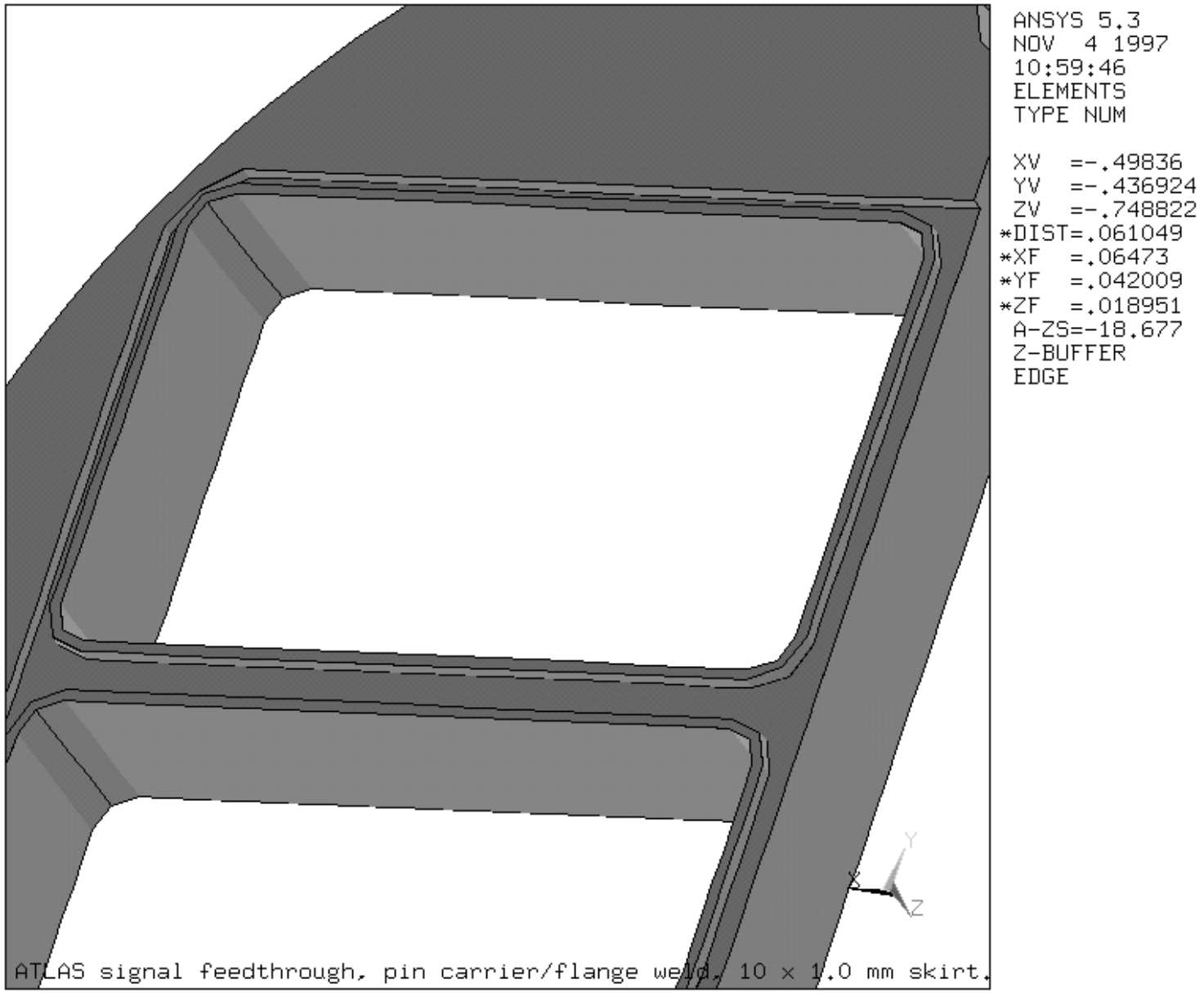

Figure 67: Finite element analysis model of ambient flange showing details of the weld preparation.

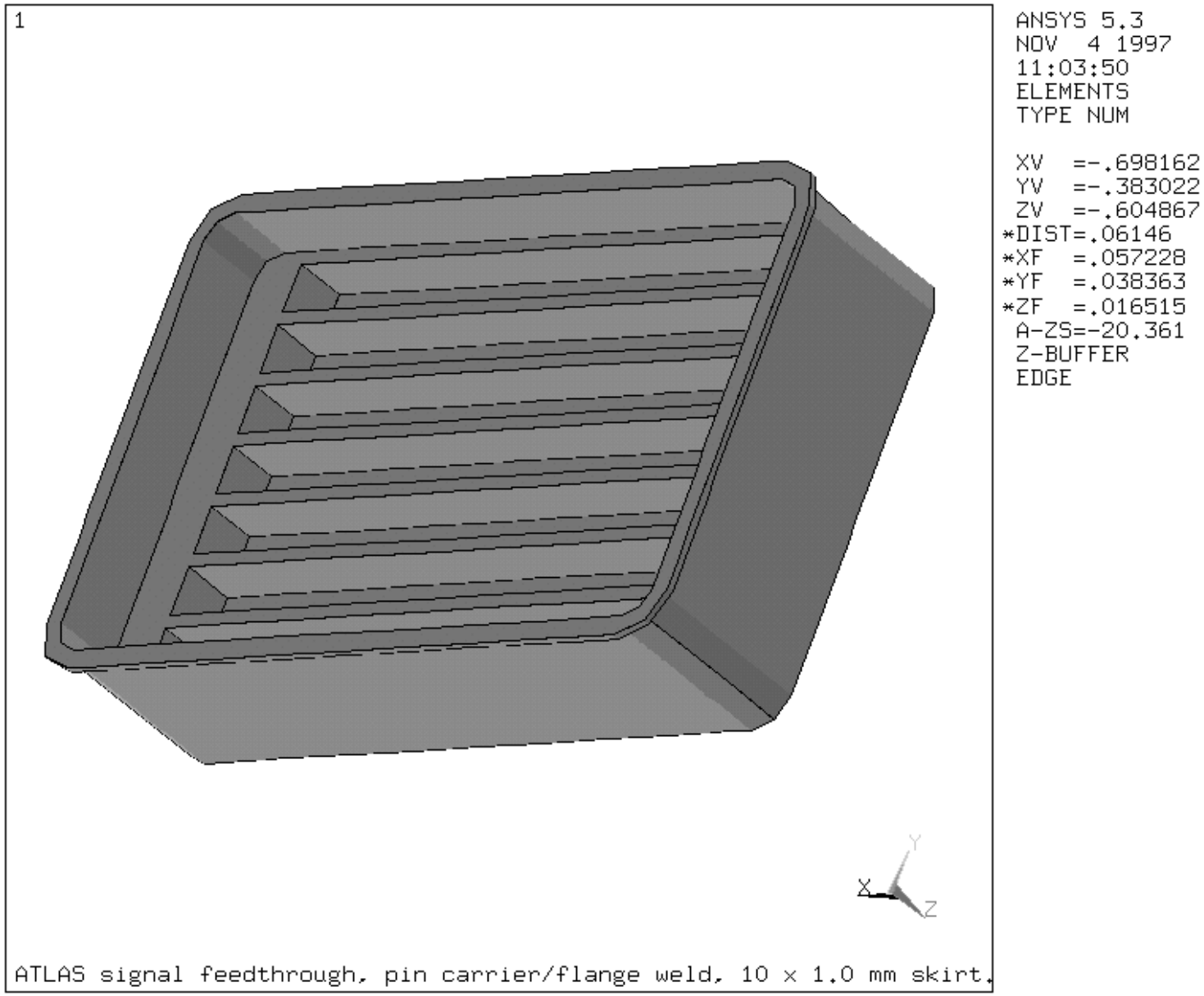

Figure 68: Finite element analysis model of a pin carrier with a 10 mm skirt length and a 1 mm skirt thickness.

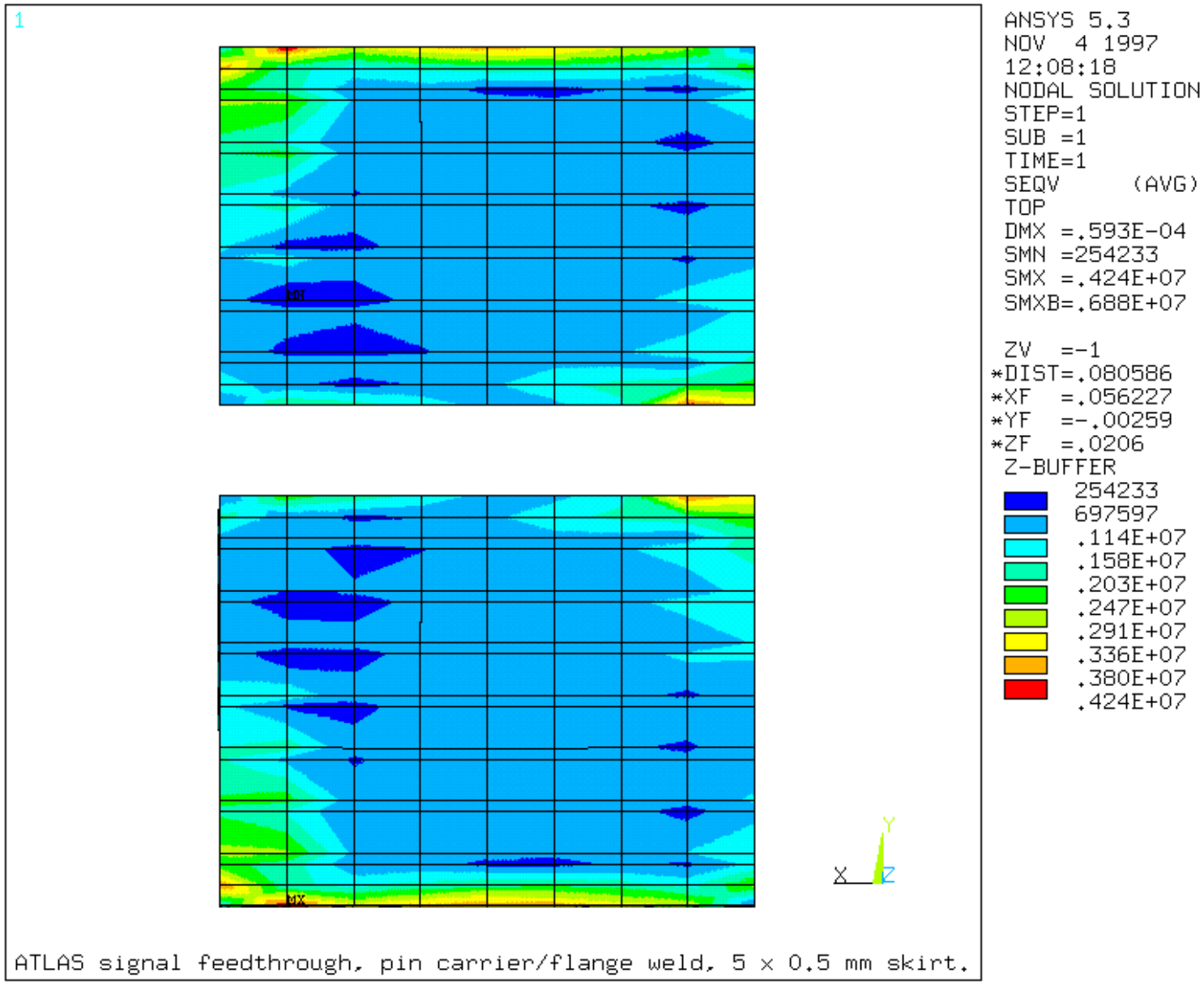

Figure 69: Finite element analysis of an ambient flange with thickness 22.9 mm (0.9 inches), web thickness 1.5 mm, skirt thickness 0.5 mm and length 5 mm showing (Von Mises) stress in Pascals under an applied load of 1 bar.

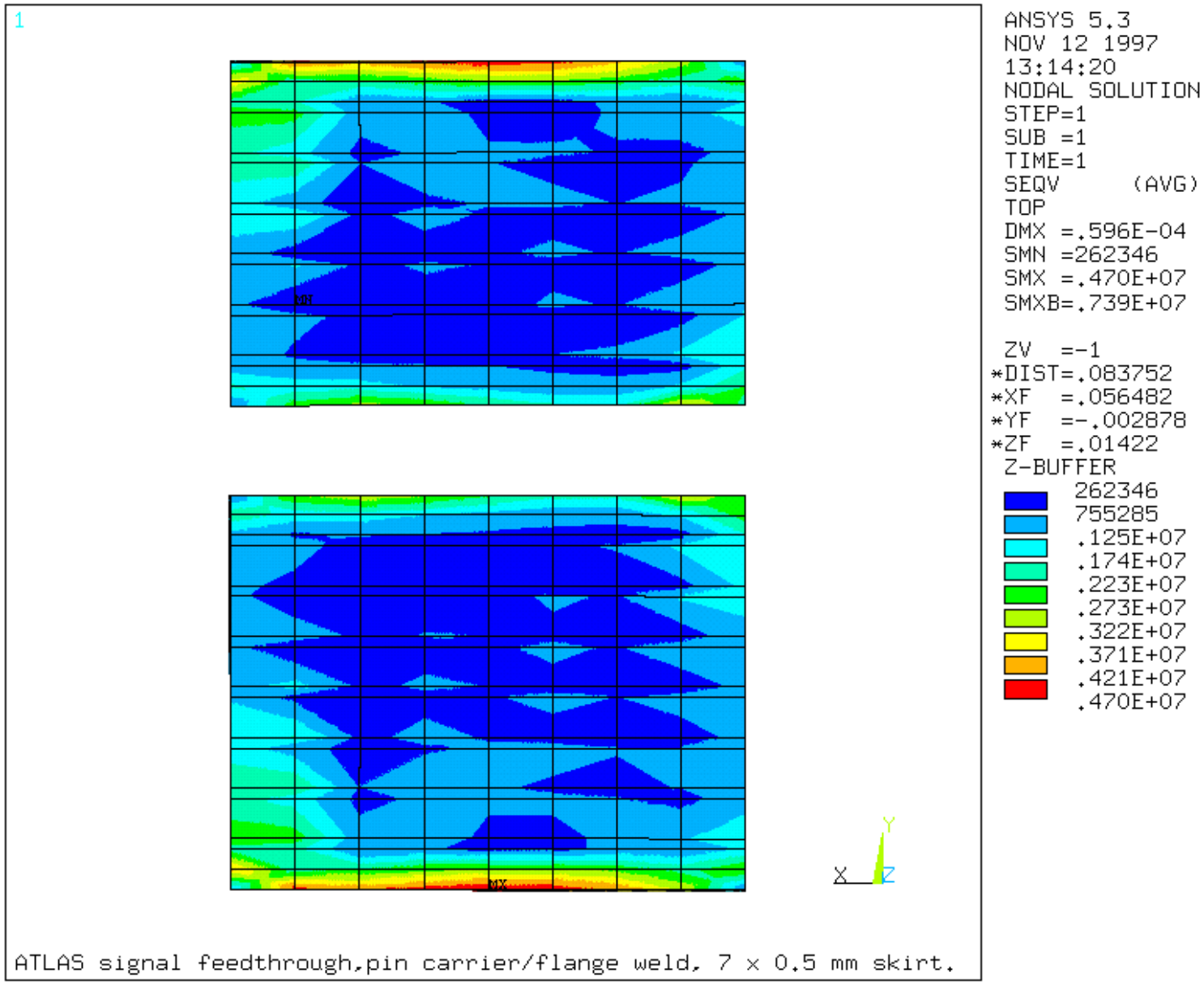

Figure 70: Finite element analysis of an ambient flange with thickness 22.9 mm (0.9 inches), web thickness 1.5 mm, skirt thickness 0.5 mm and length 7 mm showing (Von Mises) stress in Pascals under an applied load of 1 bar.

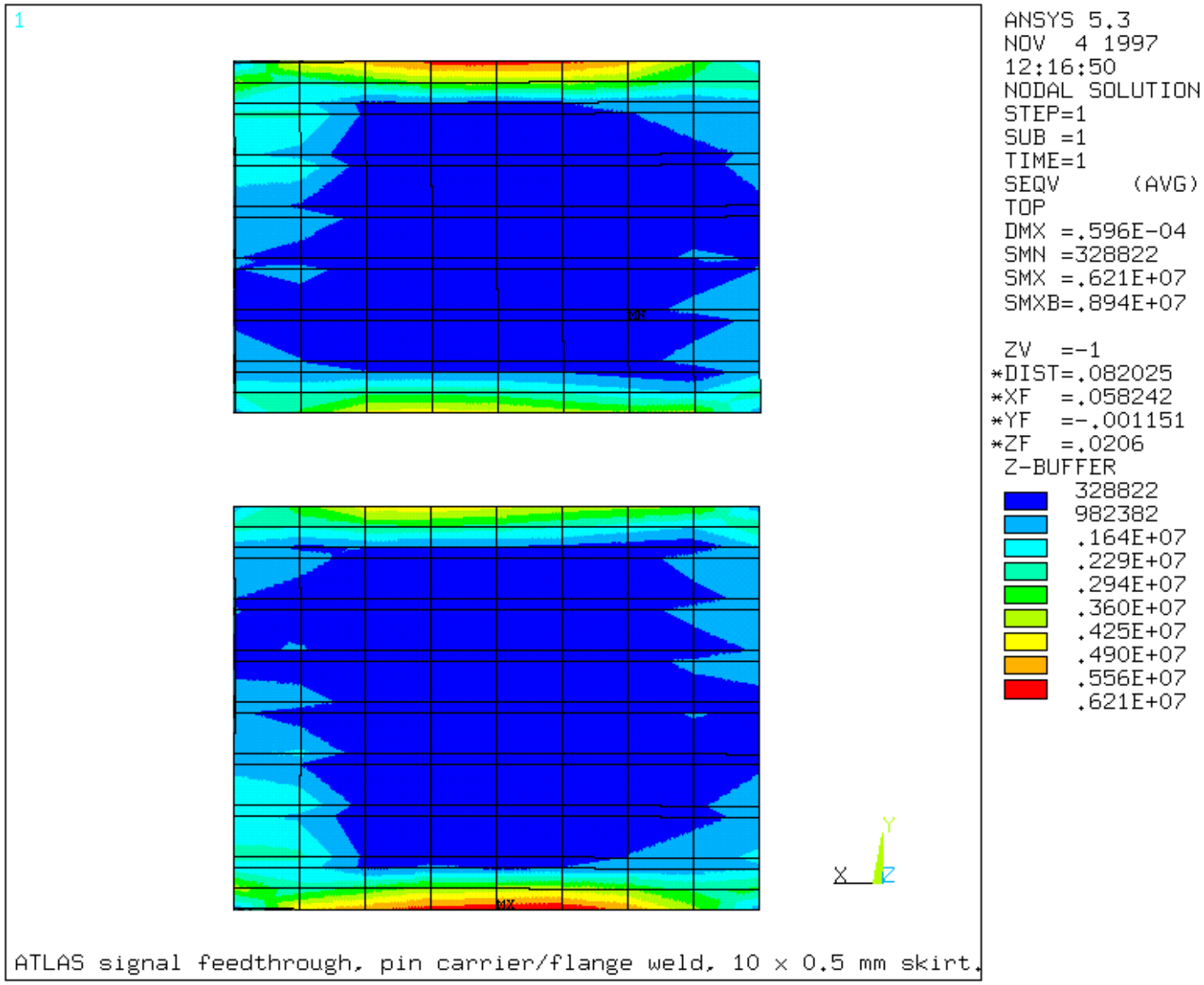

Figure 71: Finite element analysis of an ambient flange with thickness 22.9 mm (0.9 inches), web thickness 1.5 mm, skirt thickness 0.5 mm and length 10 mm showing (Von Mises) stress in Pascals under an applied load of 1 bar.

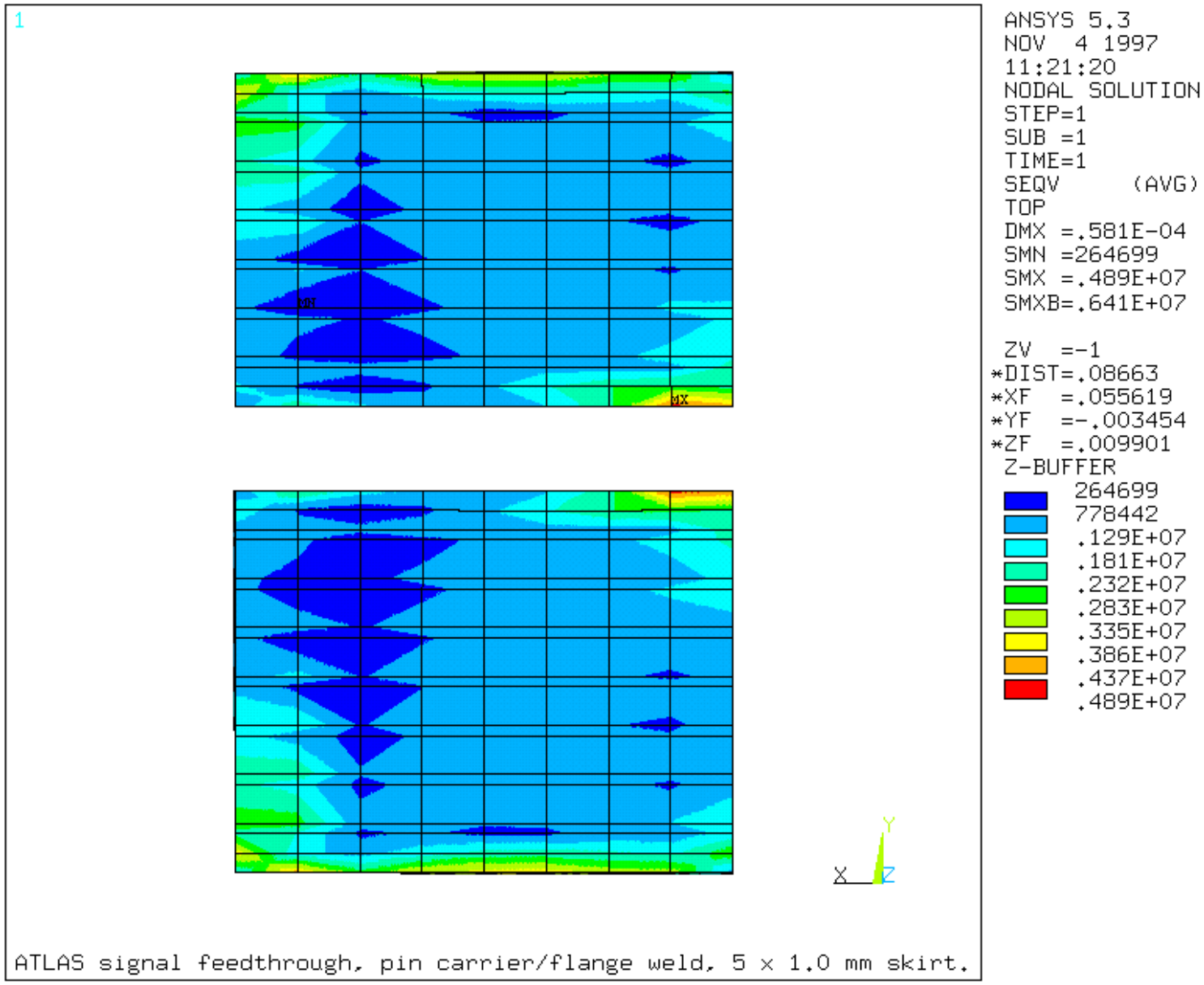

Figure 72: Finite element analysis of an ambient flange with thickness 22.9 mm (0.9 inches), web thickness 1.5 mm, skirt thickness 1 mm and length 5 mm showing (Von Mises) stress in Pascals under an applied load of 1 bar.

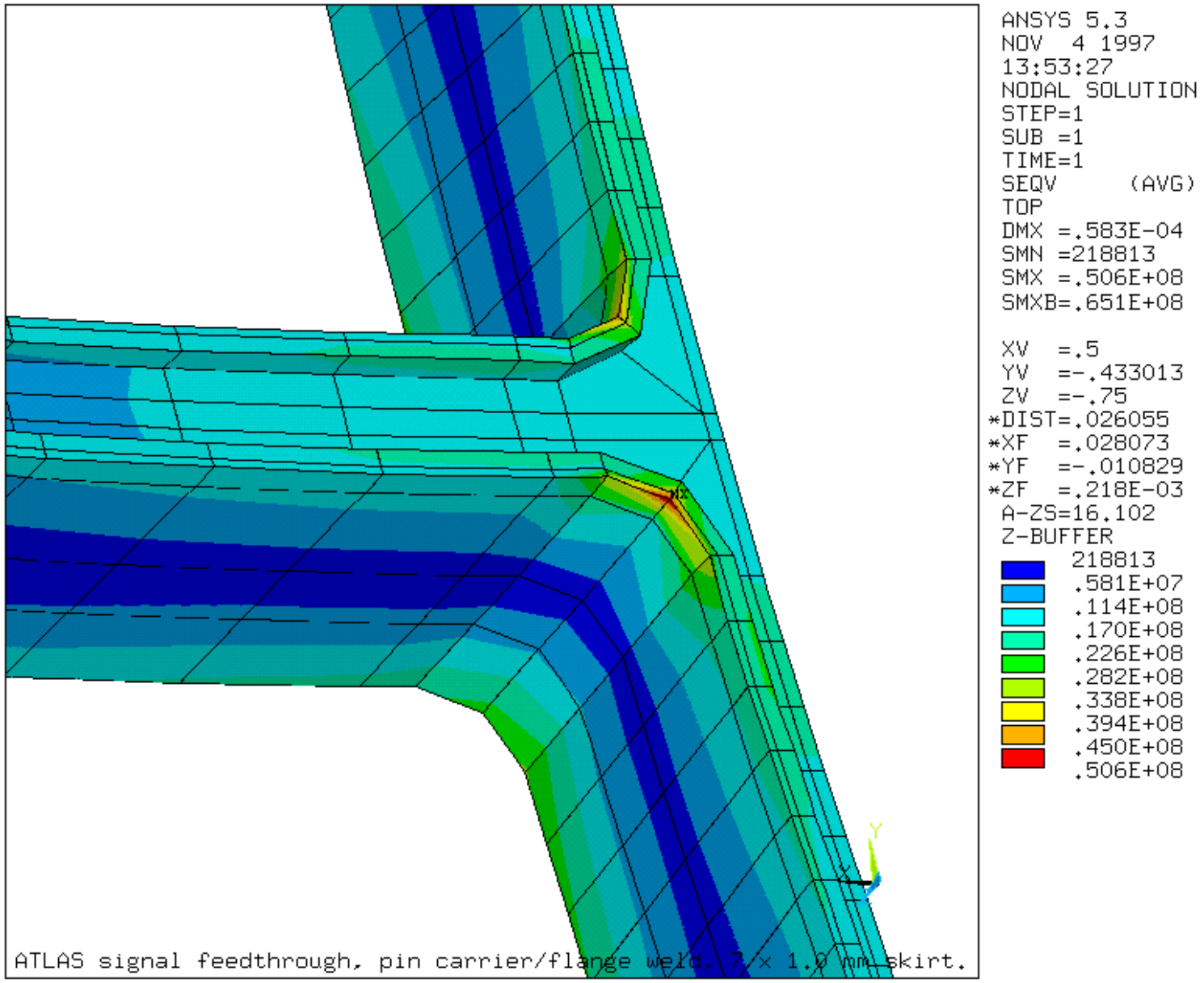

Figure 73: Finite element analysis of an ambient flange with thickness 22.9 mm (0.9 inches), web thickness 1.5 mm, skirt thickness 1 mm and length 7 mm showing the flange region with maximum (Von Mises) stress in Pascals under an applied load of 1 bar.

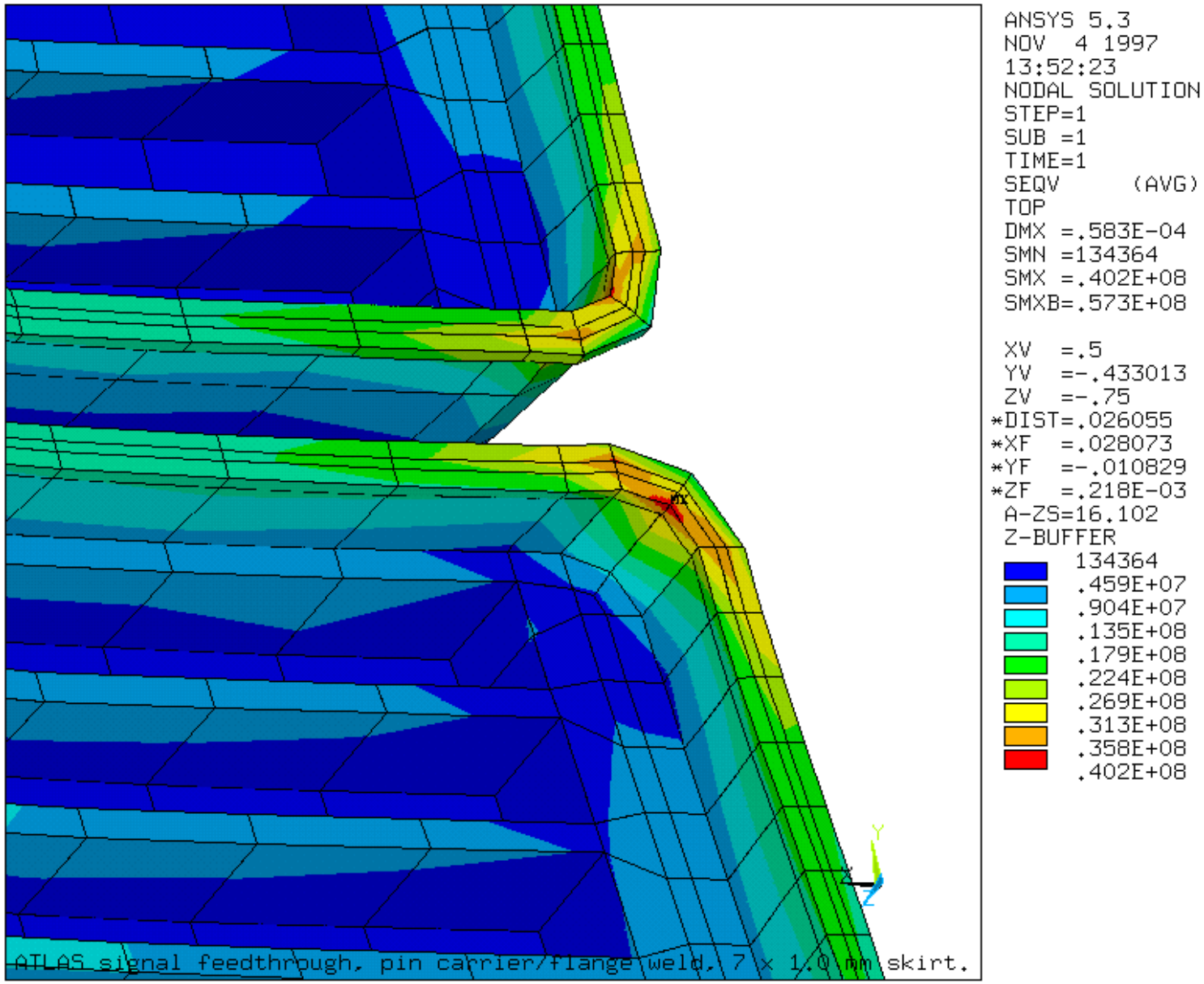

Figure 74: Finite element analysis of an ambient flange with thickness 22.9 mm (0.9 inches), web thickness 1.5 mm, skirt thickness 1 mm and length 7 mm showing the region of the pin carrier with maximum (Von Mises) stress in Pascals under an applied load of 1 bar.

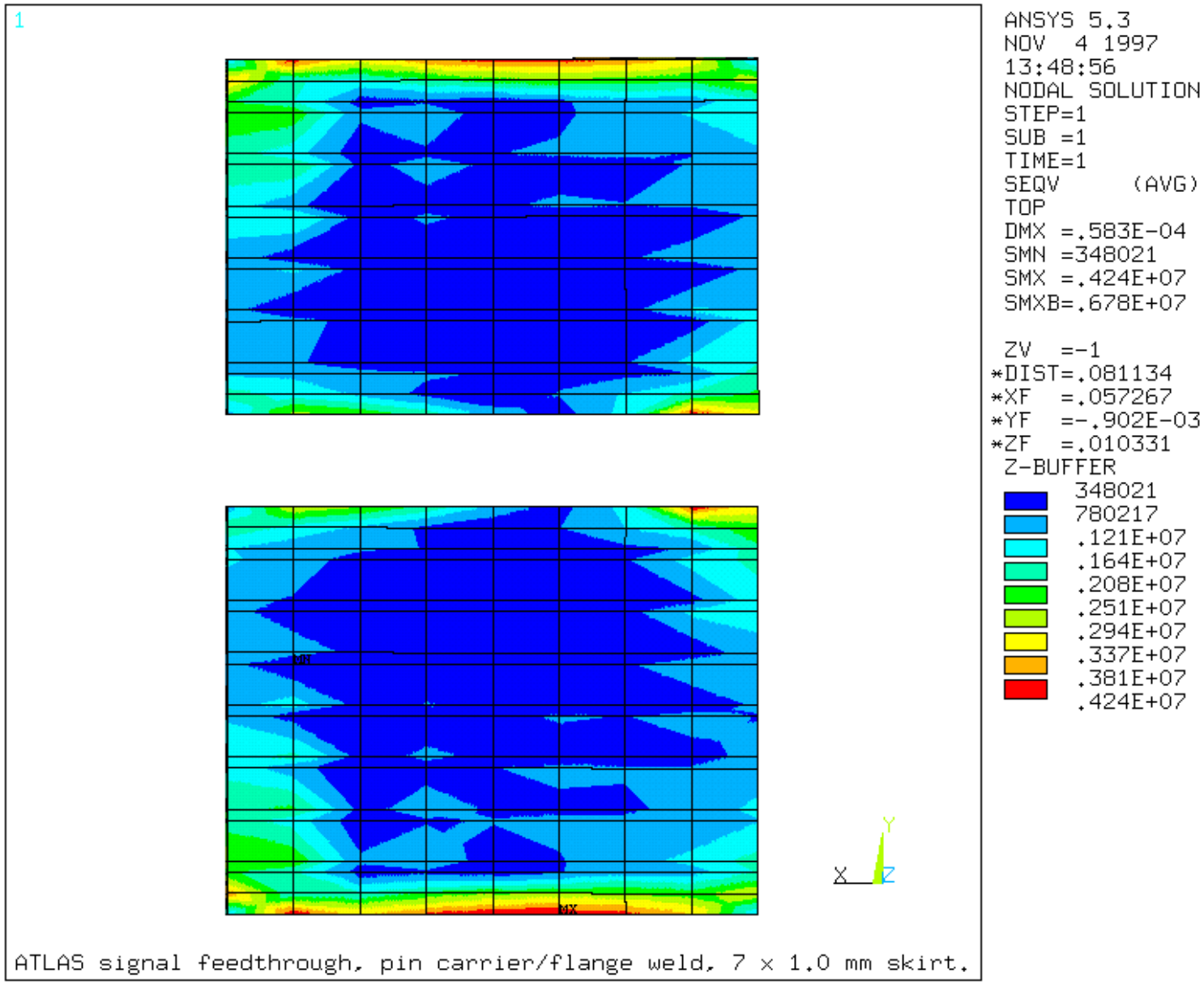

Figure 75: Finite element analysis of an ambient flange with thickness 22.9 mm (0.9 inches), web thickness 1.5 mm, skirt thickness 1 mm and length 7 mm showing (Von Mises) stress in Pascals under an applied load of 1 bar.

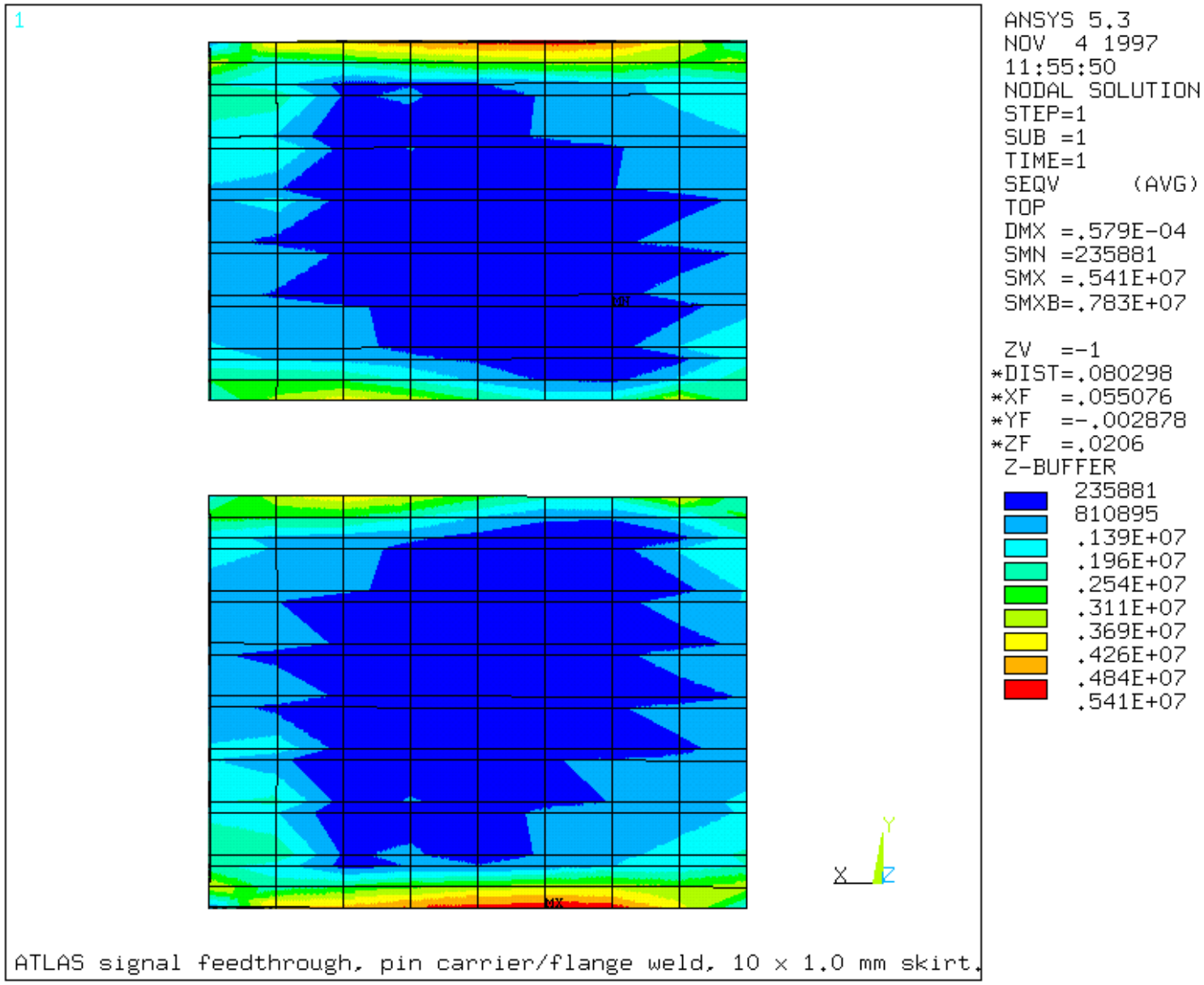

Figure 76: Finite element analysis of an ambient flange with thickness 22.9 mm (0.9 inches), web thickness 1.5 mm, skirt thickness 1 mm and length 10 mm showing (Von Mises) stress in Pascals under an applied load of 1 bar.

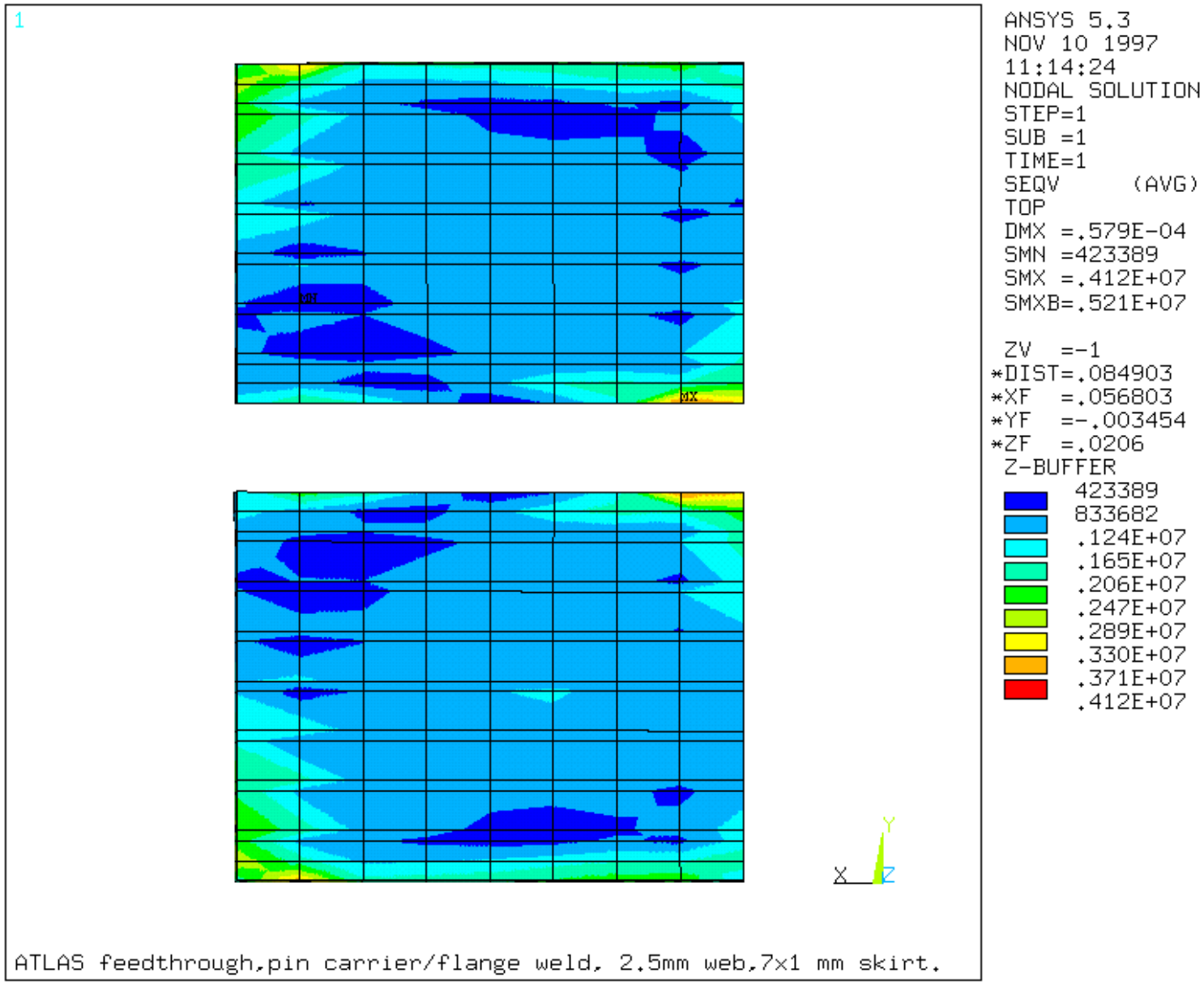

Figure 77: Finite element analysis of an ambient flange with thickness 22.9 mm (0.9 inches), web thickness 2.5 mm, skirt thickness 1 mm and length 7 mm showing (Von Mises) stress in Pascals under an applied load of 1 bar.

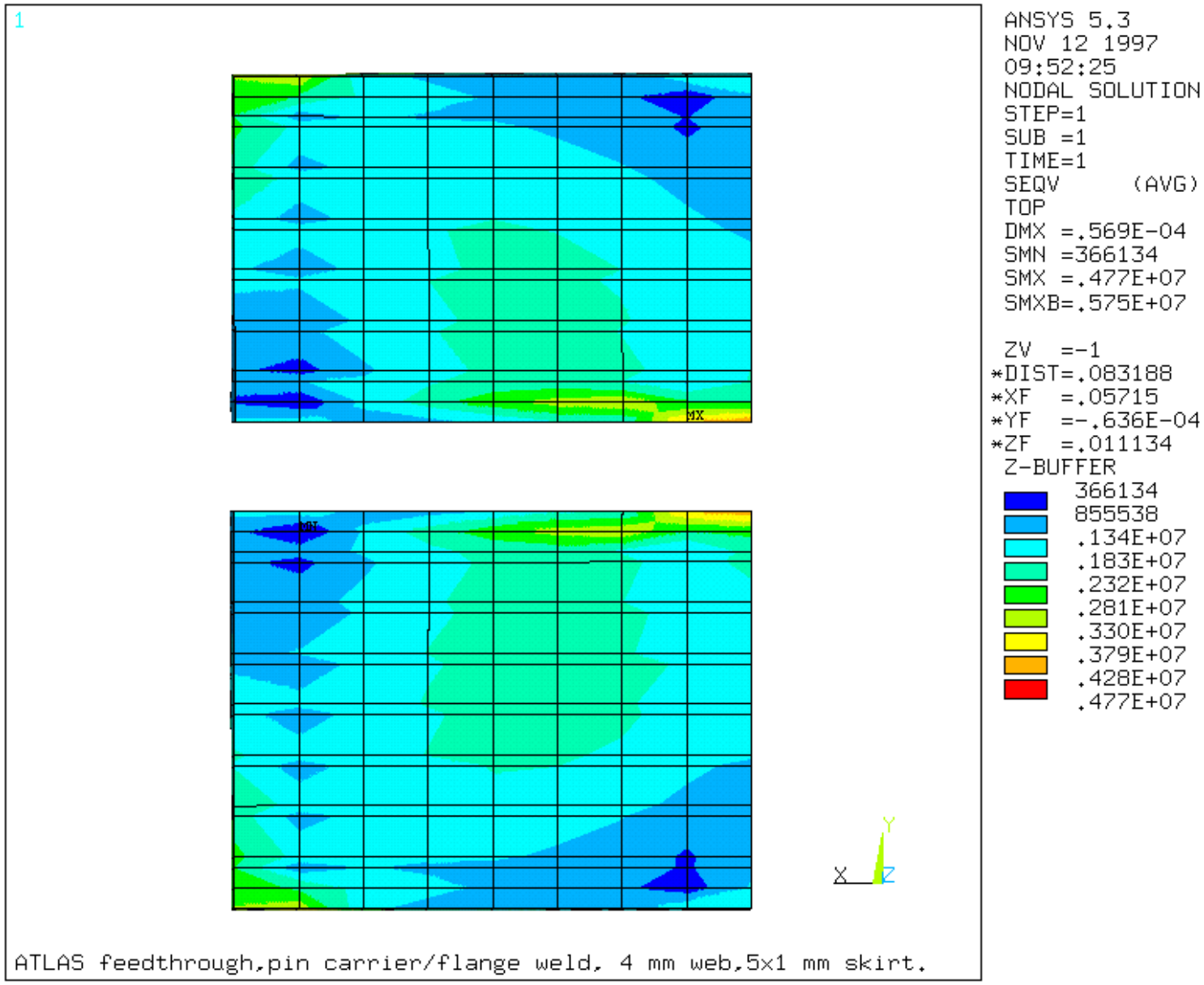

Figure 78: Finite element analysis of an ambient flange with thickness 22.9 mm (0.9 inches), web thickness 4.0 mm, skirt thickness 1 mm and length 5 mm showing (Von Mises) stress in Pascals under an applied load of 1 bar.

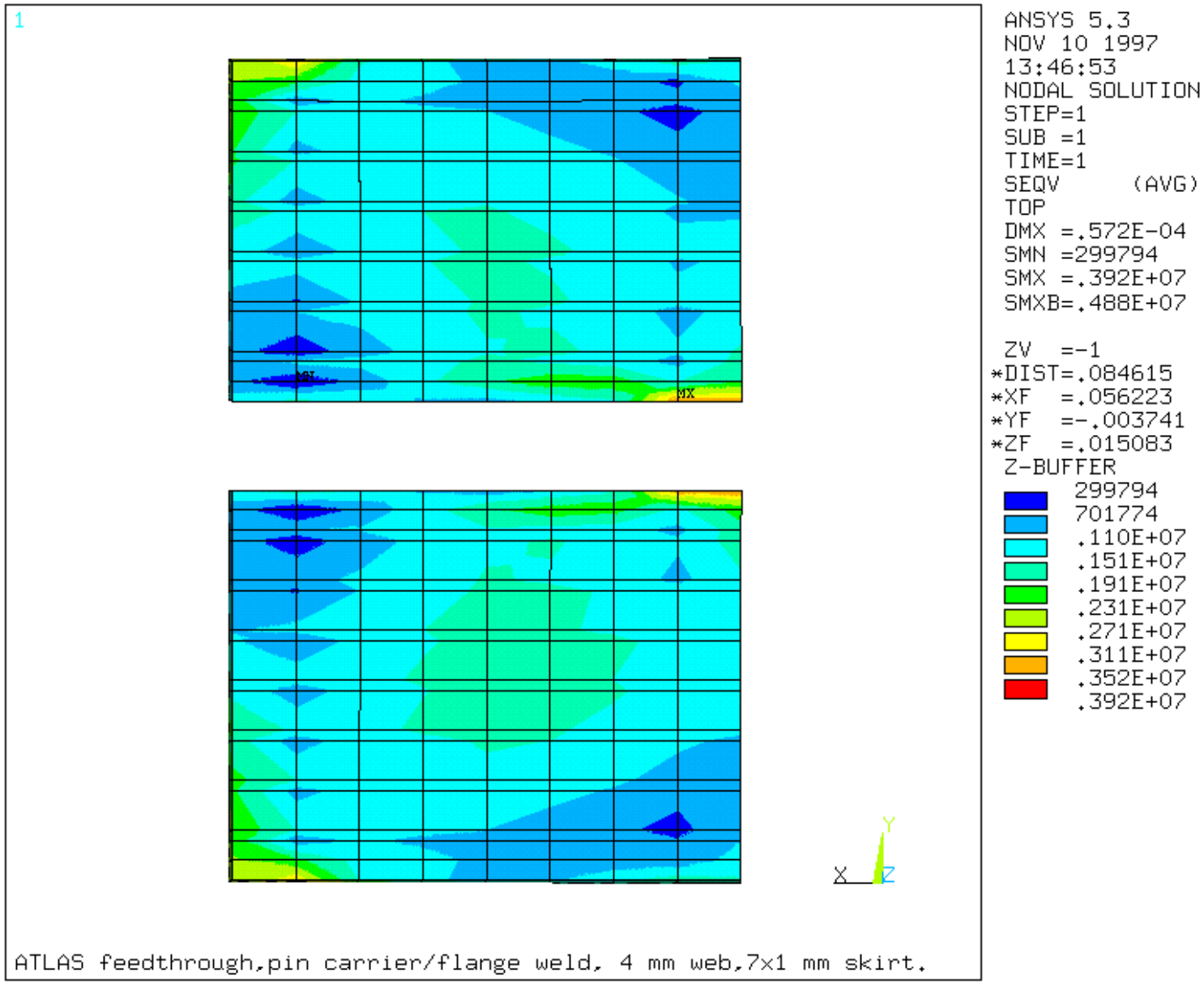

Figure 79: Finite element analysis of an ambient flange with thickness 22.9 mm (0.9 inches), web thickness 4.0 mm, skirt thickness 1 mm and length 7 mm showing (Von Mises) stress in Pascals under an applied load of 1 bar.

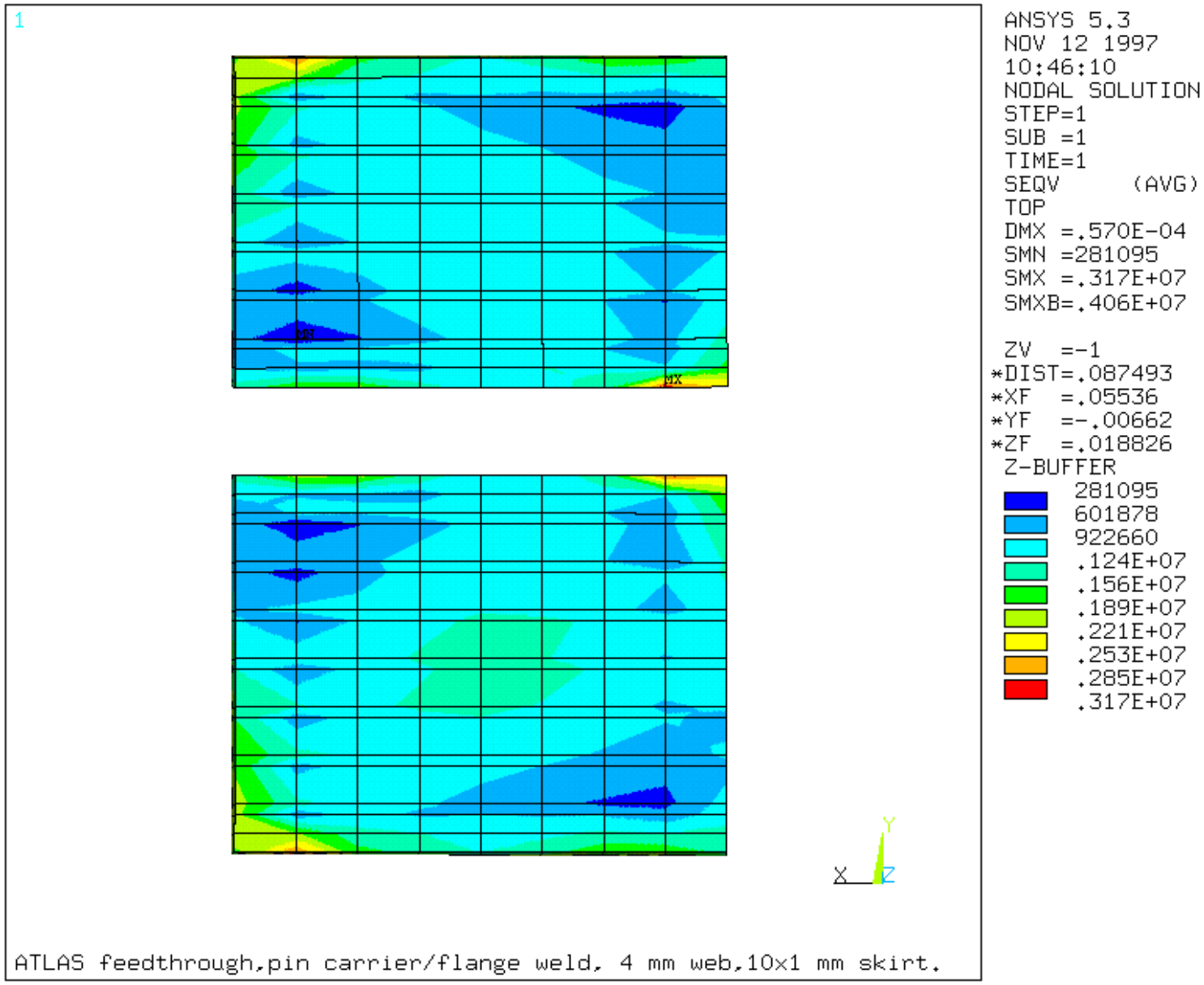

Figure 80: Finite element analysis of an ambient flange with thickness 22.9 mm (0.9 inches), web thickness 4.0 mm, skirt thickness 1 mm and length 10 mm showing (Von Mises) stress in Pascals under an applied load of 1 bar.

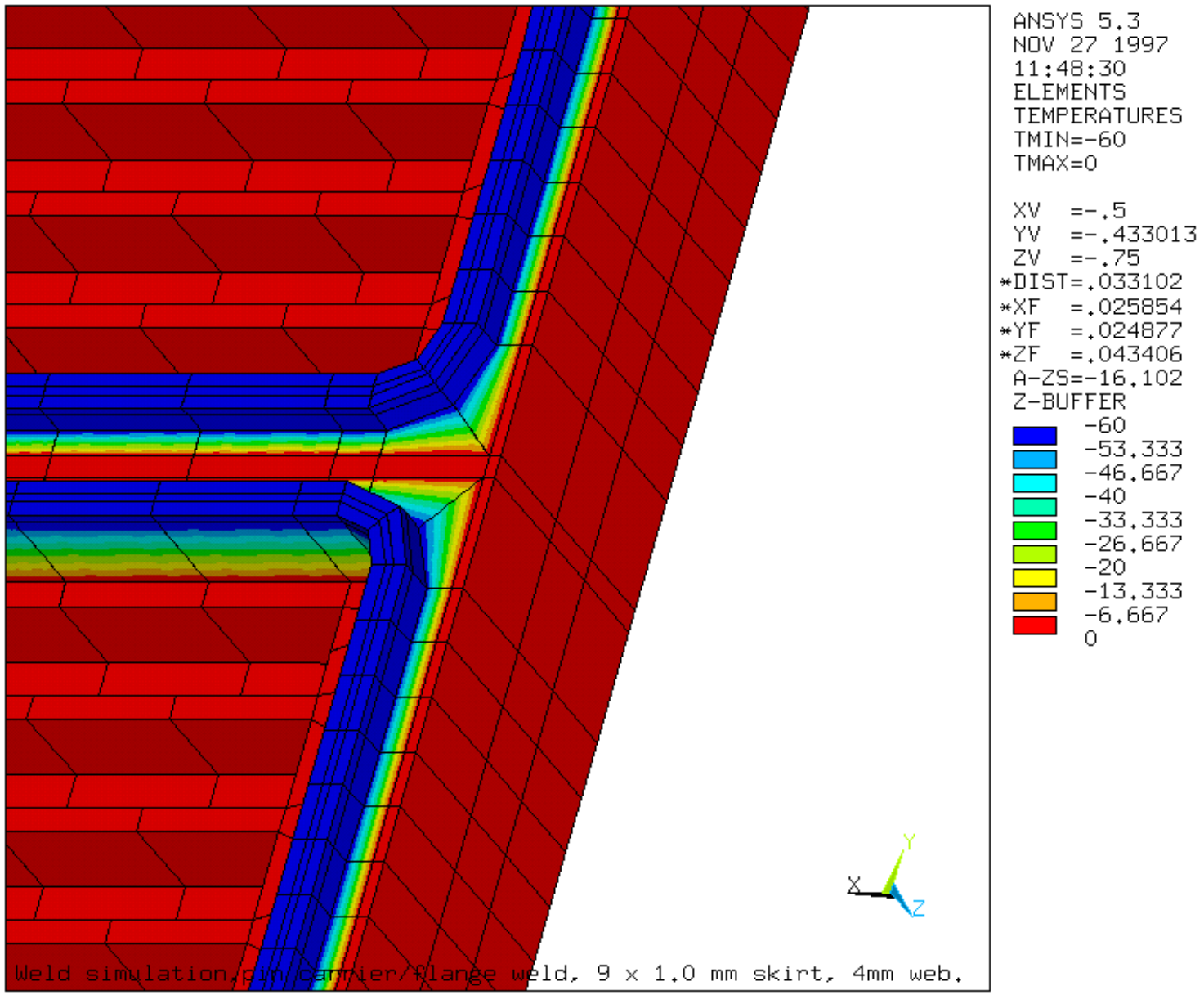

Figure 81: Finite element analysis of an ambient flange with thickness 22.9 mm (0.9 inches), web thickness 4.0 mm, skirt thickness 1 mm and length 9 mm showing the temperature preparation (in K with respect to the flange) simulating welding of the pin carrier into the ambient flange. See text.

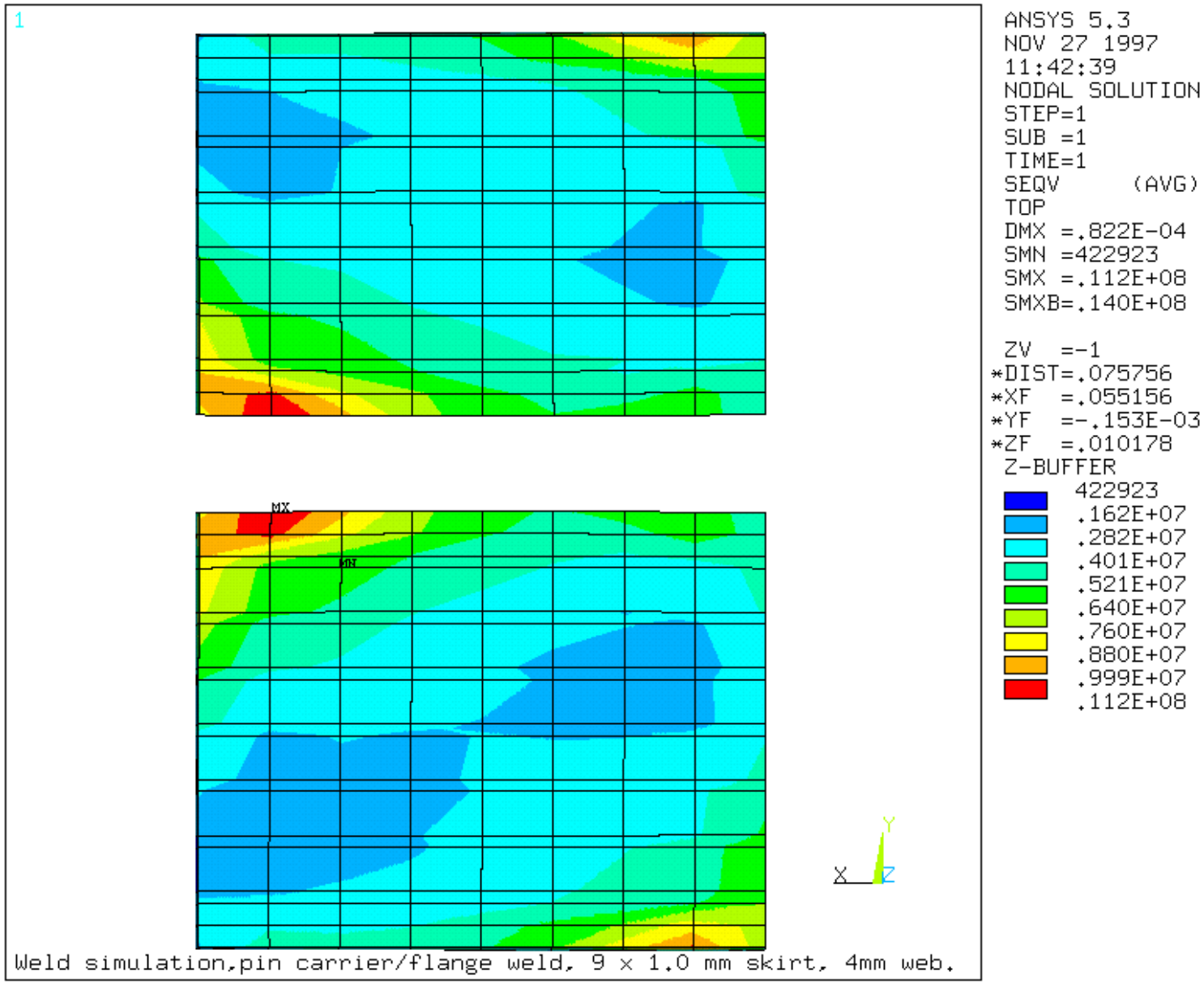

Figure 82: Finite element analysis of an ambient flange with thickness 22.9 mm (0.9 inches), web thickness 4.0 mm, skirt thickness 1 mm and length 9 mm showing (Von Mises) stress in Pascals upon welding of the pin carrier into the ambient flange. See text.

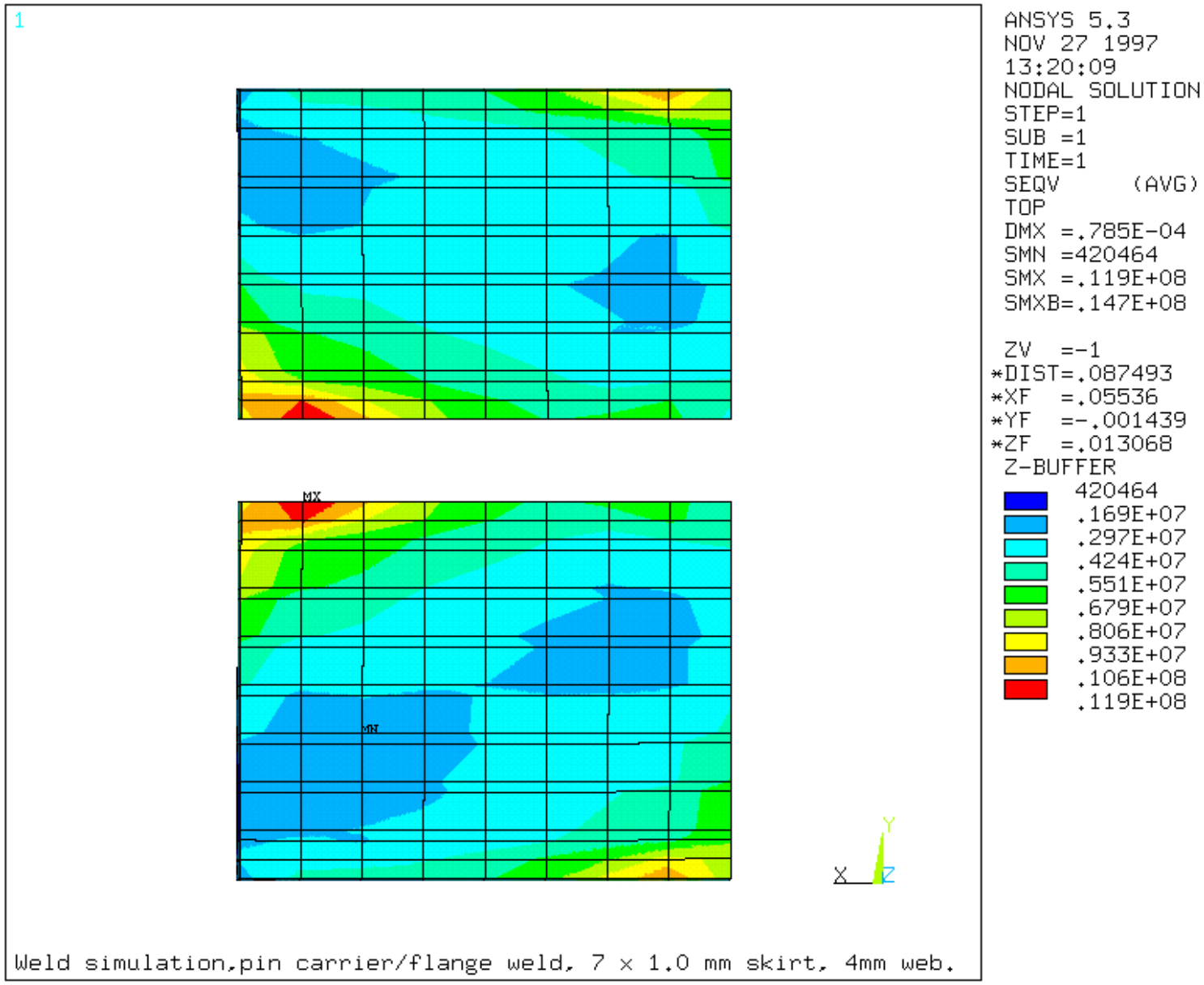

Figure 83: Finite element analysis of an ambient flange with thickness 22.9 mm (0.9 inches), web thickness 4.0 mm, skirt thickness 1 mm and length 7 mm showing (Von Mises) stress in Pascals upon welding of the pin carrier into the ambient flange. See text.

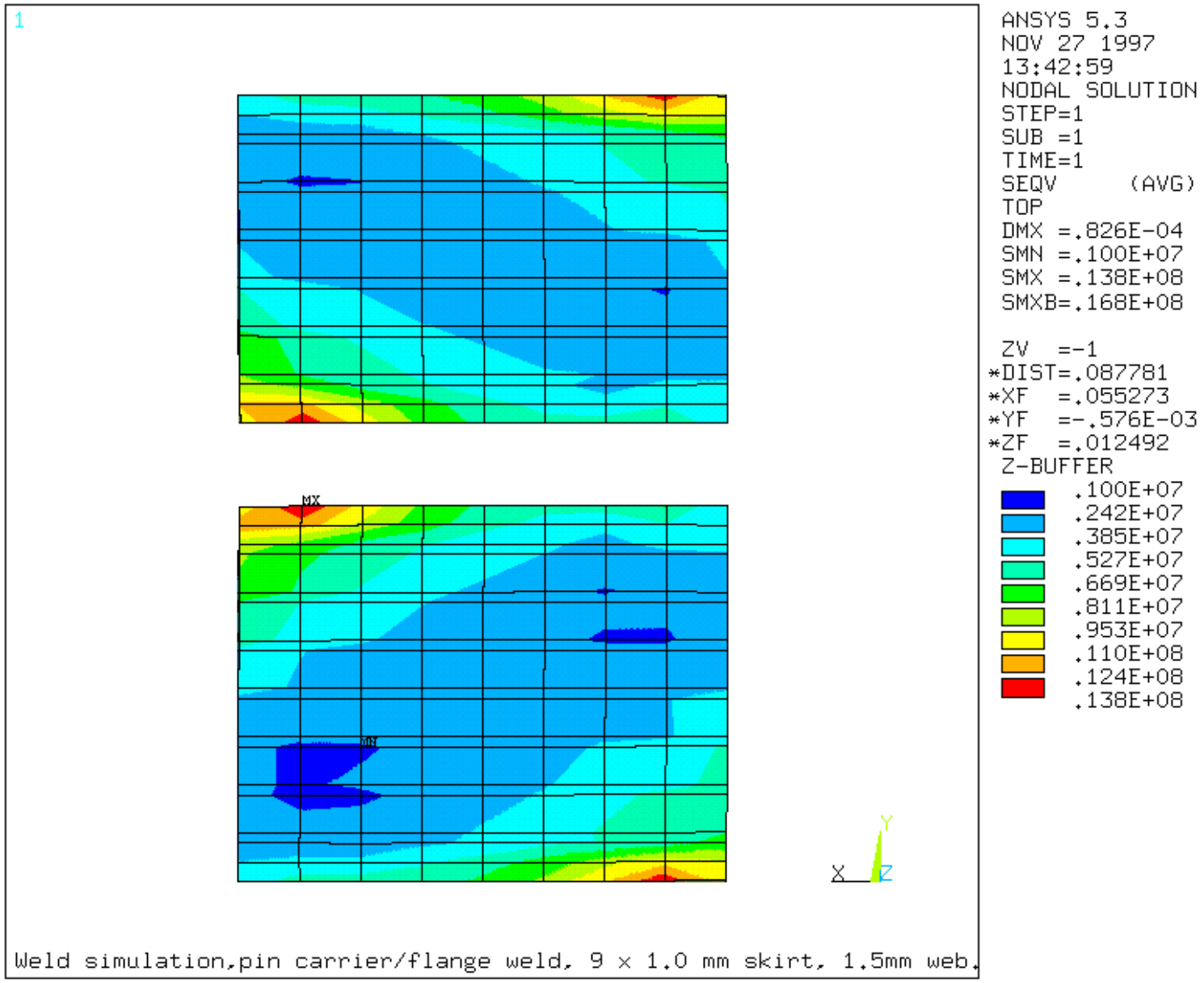

Figure 84: Finite element analysis of an ambient flange with thickness 22.9 mm (0.9 inches), web thickness 1.5 mm, skirt thickness 1 mm and length 9 mm showing (Von Mises) stress in Pascals upon welding of the pin carrier into the ambient flange. See text.

15 Current Supplies to HEC Circuit Boards via Signal Feedthroughs (Release of 98/01/21)

Fifteen different current supplies are required for the HEC circuit boards. The current is supplied via the signal feedthroughs on modified vacuum striplines which normally operate with one end in the liquid argon cryostat at 90 K and the other end on the outside of the cryostat vacuum vessel at ambient (300 K) temperature. During test procedures however, the striplines must operate with both ends at ambient temperature. In the latter scenario the current required rises by $\sim$70% and it is this mode of operation which fixes the maximum current supply requirements.

The calculations on the temperature rise in the feedthrough vacuum striplines due to ohmic heating have been updated. Two new Finite Element Analysis models have been used to produce the results.

The first model, shown in Figure 85, is of a single current supply trace plus ground trace separated by an electrically insulating kapton layer. Note that the current supply trace width is double the normal 200 μm wide signal trace, and that both current supply and ground traces are double the normal 35 μm copper thickness. Note also that the (common) ground trace is NOT used for the current return – a second trace is required for the return path. Figures 86 and 87 refer to the normal (ends at 300 K and 90 K) operating conditions. Figure 86 shows the temperature of a trace, as a function of distance from the ambient temperature end of the trace, for several current values. Figure 87 shows the potential difference across a trace as a function of current. Similar curves for the conditions where both ends of the trace are at 300 K are shown in Figures 88 and 89.

In the second model, shown in Figure 90, the two halves of a pair of adjacent traces are connected by the kapton substrate. The kapton, while electrically insulating the two traces, connects them quite strongly by thermal conduction. The temperature produced by ohmic heating of a trace is significantly modified by the temperature of adjacent traces: the effect is shown in Figures 91 and 92. The solid curves are the temperature profiles of single traces as a function of distance from the ambient temperature end of the traces, one carrying 300 mA the other 600 mA. The dashed curves between the solid curves, show the temperature of both traces (they are the same to within a degree or so) when they are adjacent to each other. Finally, Figure 93 shows the maximum temperature versus current for the most demanding situation, where the ends of the stripline are both at ambient temperature. The solid curve shows the maximum temperature as a function of current for an isolated trace. The dashed curve shows the maximum temperature the same trace would have if it were adjacent to a trace carrying one half of the current shown on the abscissa. The "stars" are placed at the fifteen required current supply values at the 330 K temperature level: the latter temperature is the maximum operating temperature felt acceptable. If the maximum current allowed in any trace were fixed at 300 mA, eleven of the current supplies could be delivered on single traces, one requiring 360 mA would require two parallel traces and the remaining three supplies would be delivered on three parallel traces. In the latter scenario the striplines would always operate below 330 K, even if one of the parallel traces for any of the heavier current supplies was broken. Of the 384 traces available for power supplies for each quadrant of the HEC, the above scheme

would use 352 traces per quadrant.

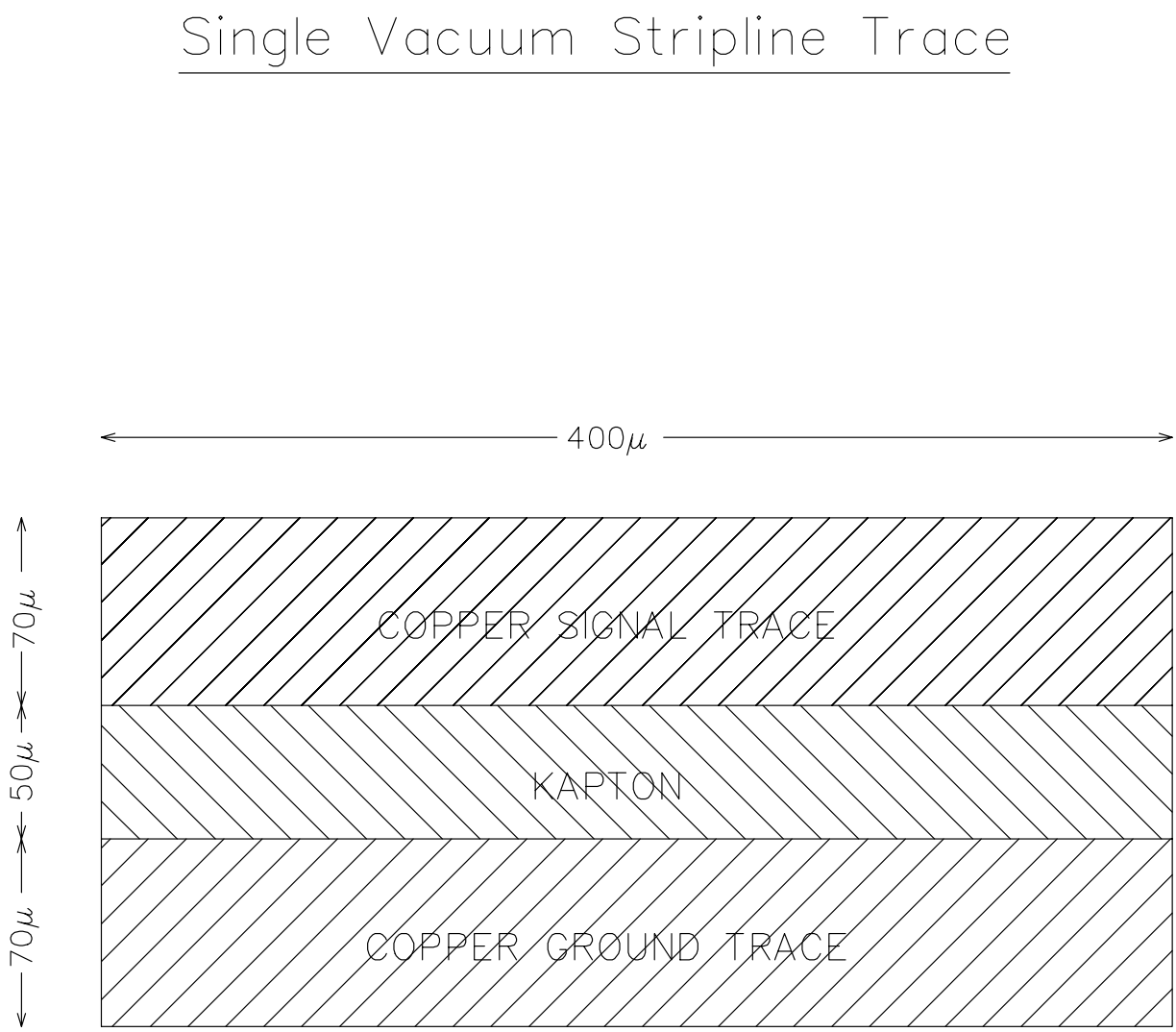

Figure 85: Finite element analysis model of a vacuum stripline to be used for low voltage distribution to the HEC, showing one signal trace and one ground trace separated by a kapton layer.

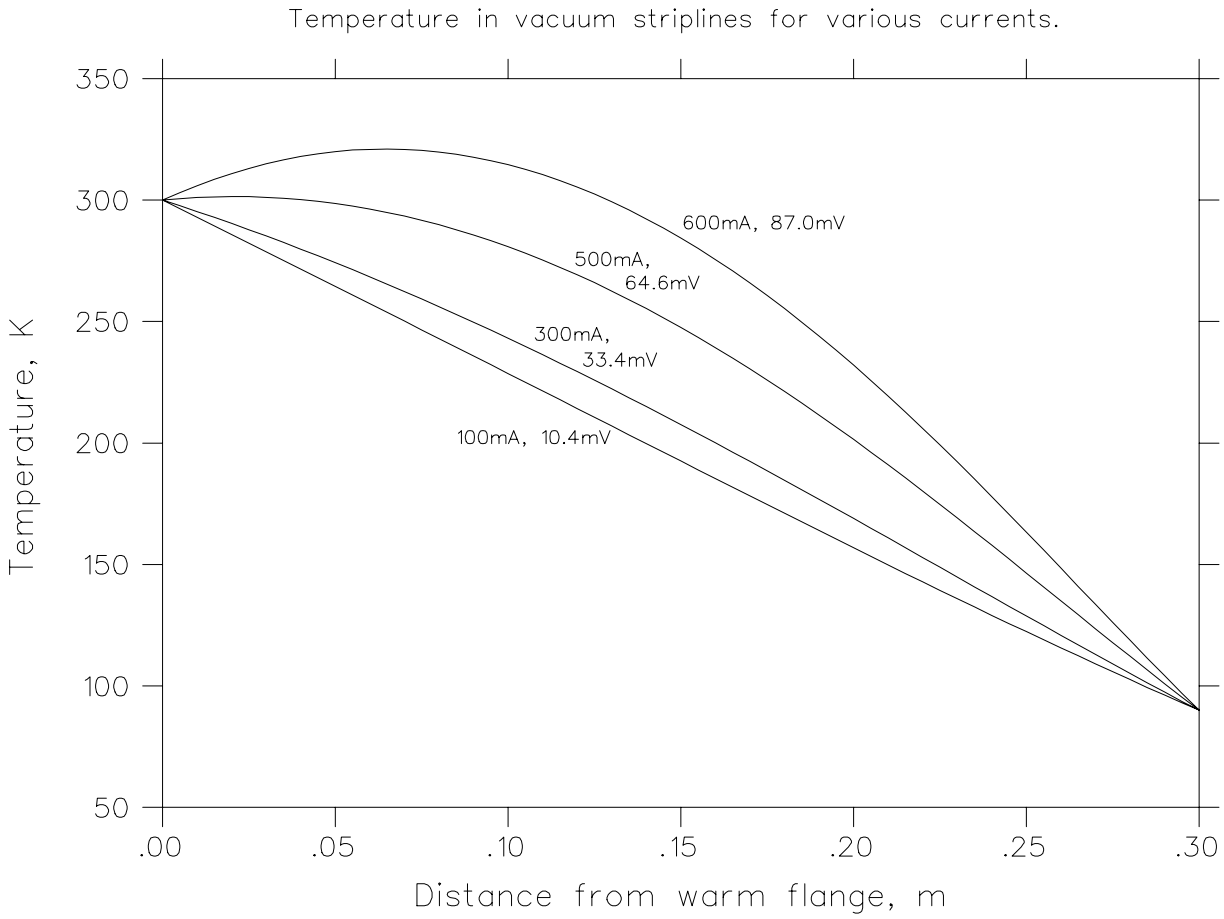

Figure 86: Temperature of a vacuum stripline trace (for operating conditions) as a function of distance from the ambient temperature end of the trace, for several current values. The potential drop across the trace is also shown.

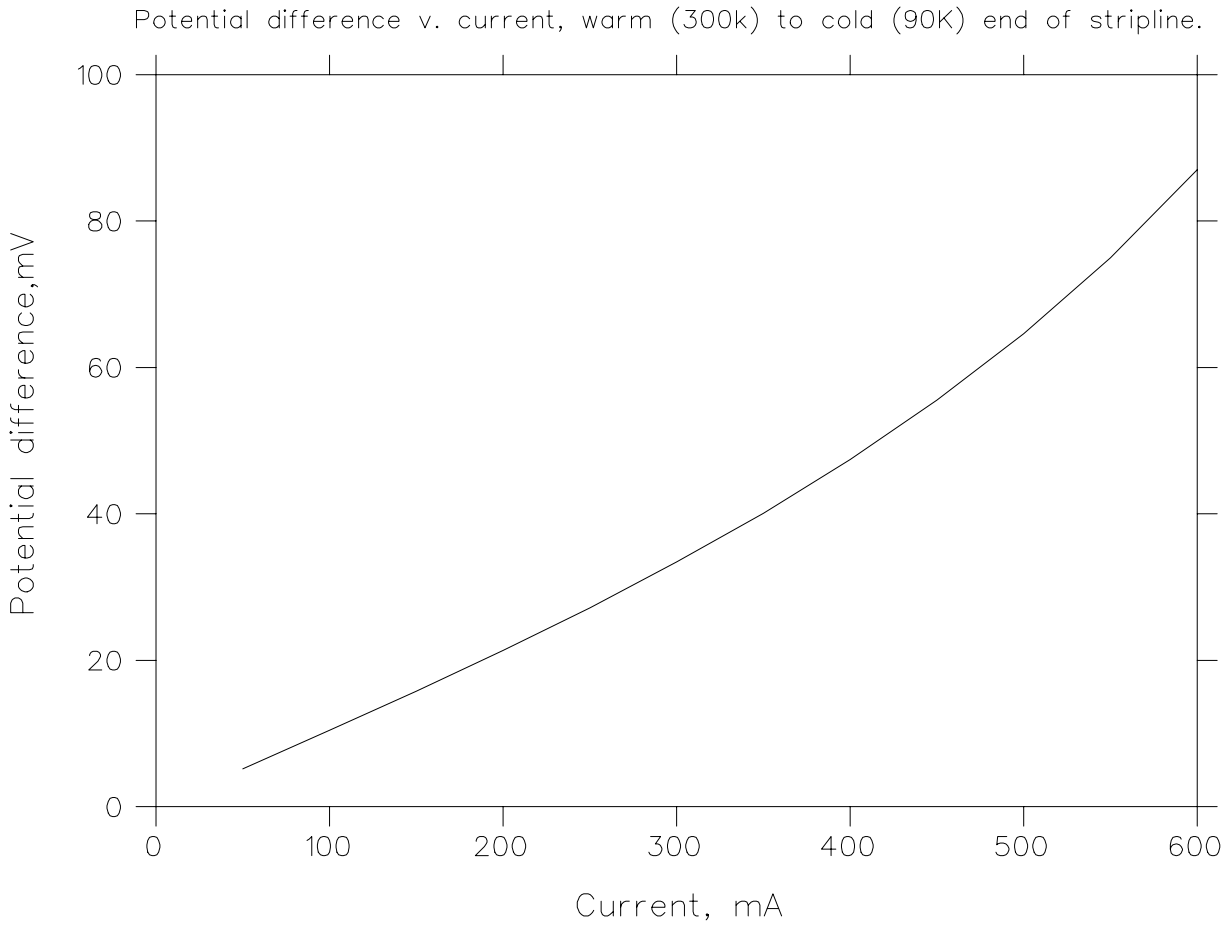

Figure 87: Potential difference across a vacuum stripline trace (for operating conditions) as a function of distance from the ambient temperature end of a trace, for several current values.

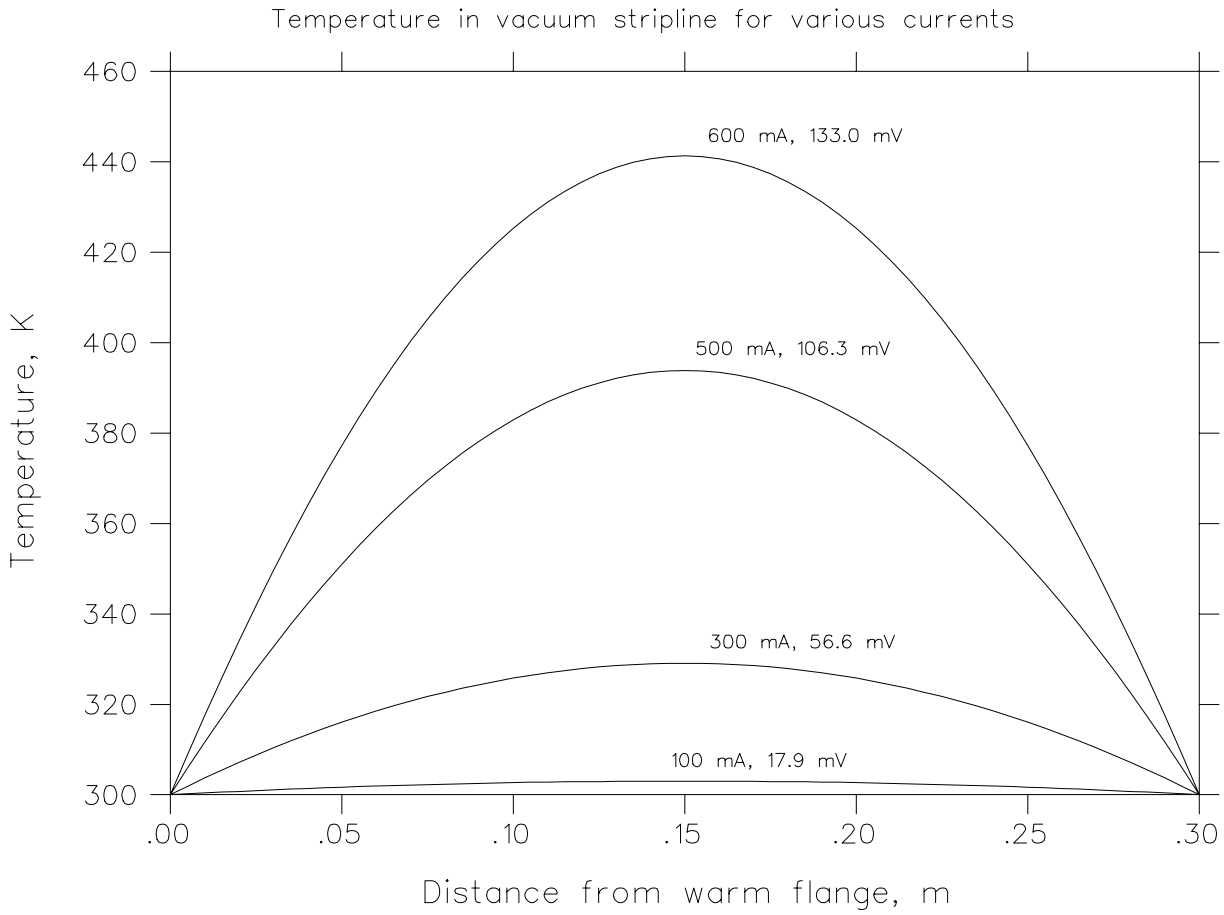

Figure 88: Temperature of a vacuum stripline trace (for warm conditions) as a function of distance from the ambient temperature end of the trace, for several current values. The potential drop across the trace is also shown.

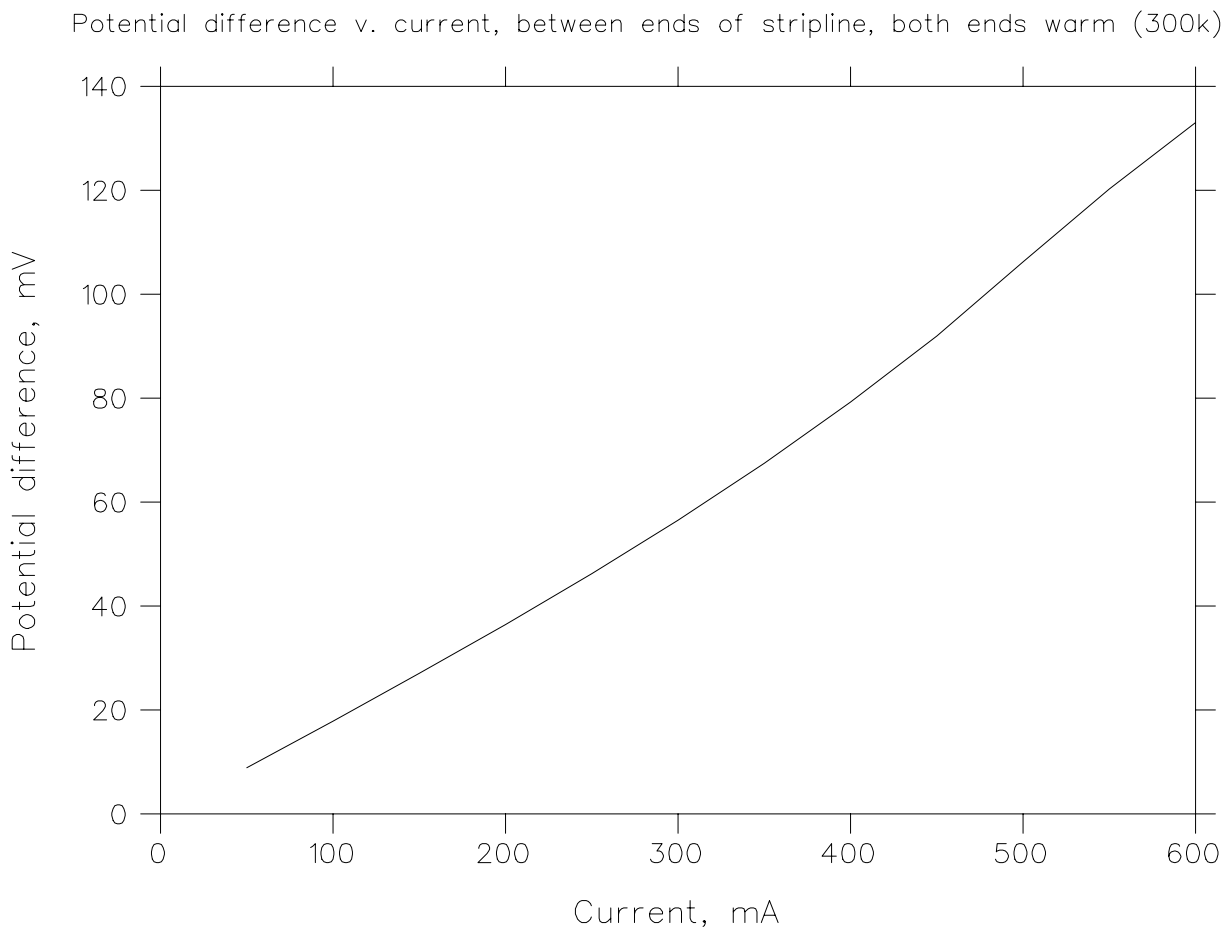

Figure 89: Potential difference across a vacuum stripline trace (for warm conditions) as a function of distance from the ambient temperature end of a trace, for several current values.

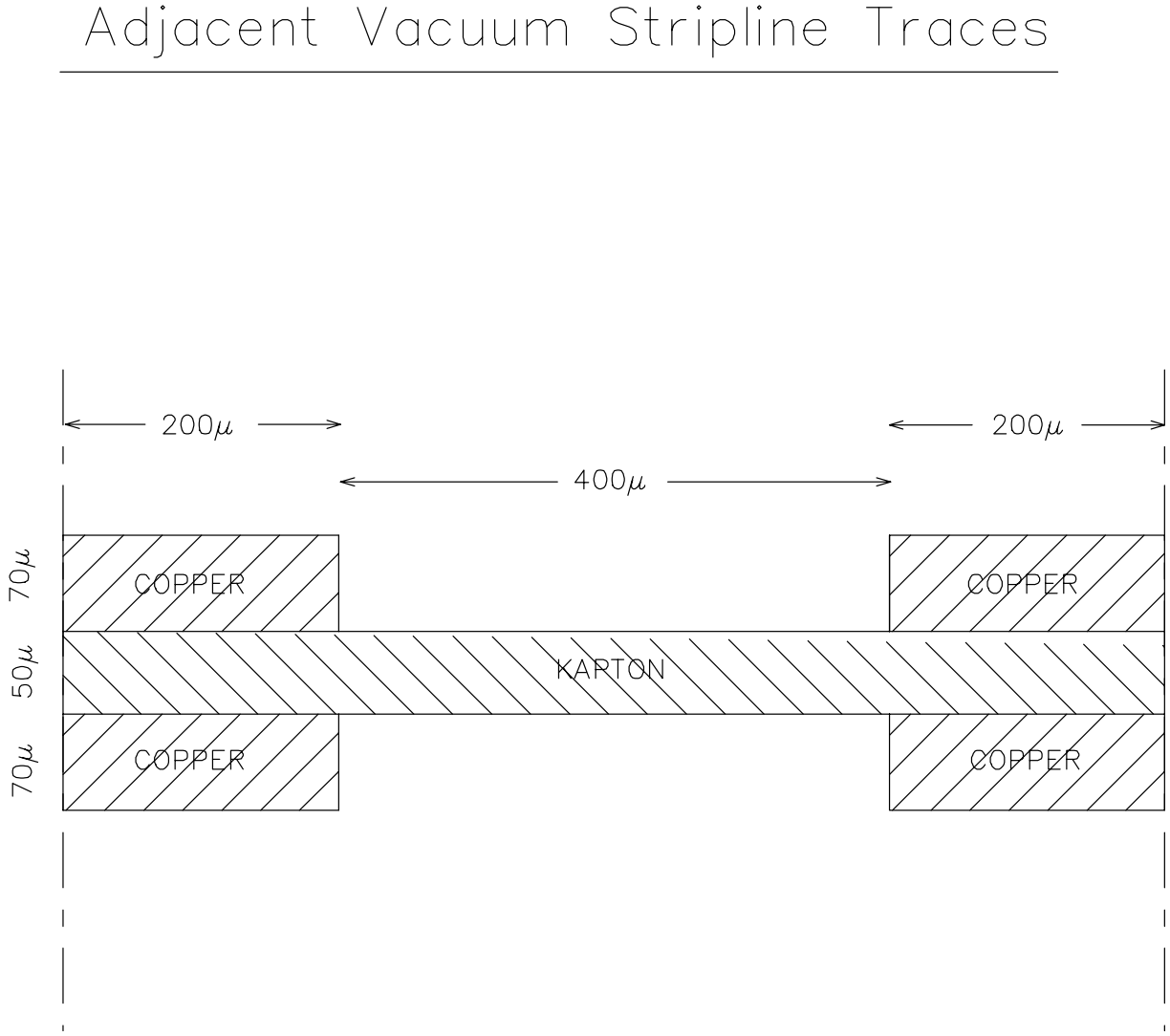

Figure 90: Finite element analysis model of a vacuum stripline to be used for low voltage distribution to the HEC, showing two halves of a pair of adjacent traces connected by the kapton substrate.

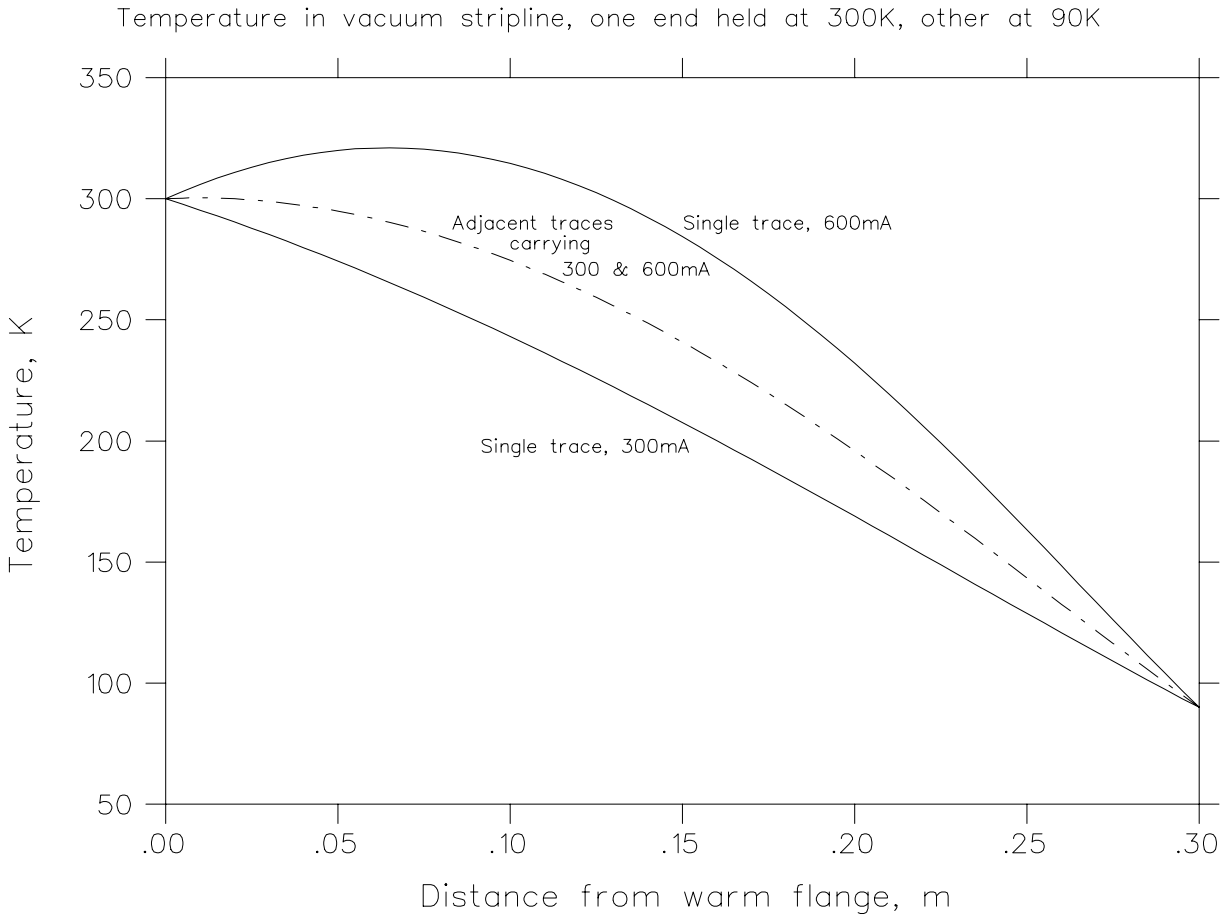

Figure 91: Temperature of a vacuum stripline trace (for operating conditions) as a function of distance from the ambient temperature end of the trace. The solid curves show the case of a 300 mA trace and of a 600 mA trace. The dashed curve shows the temperature of both traces if they are adjacent to each other.

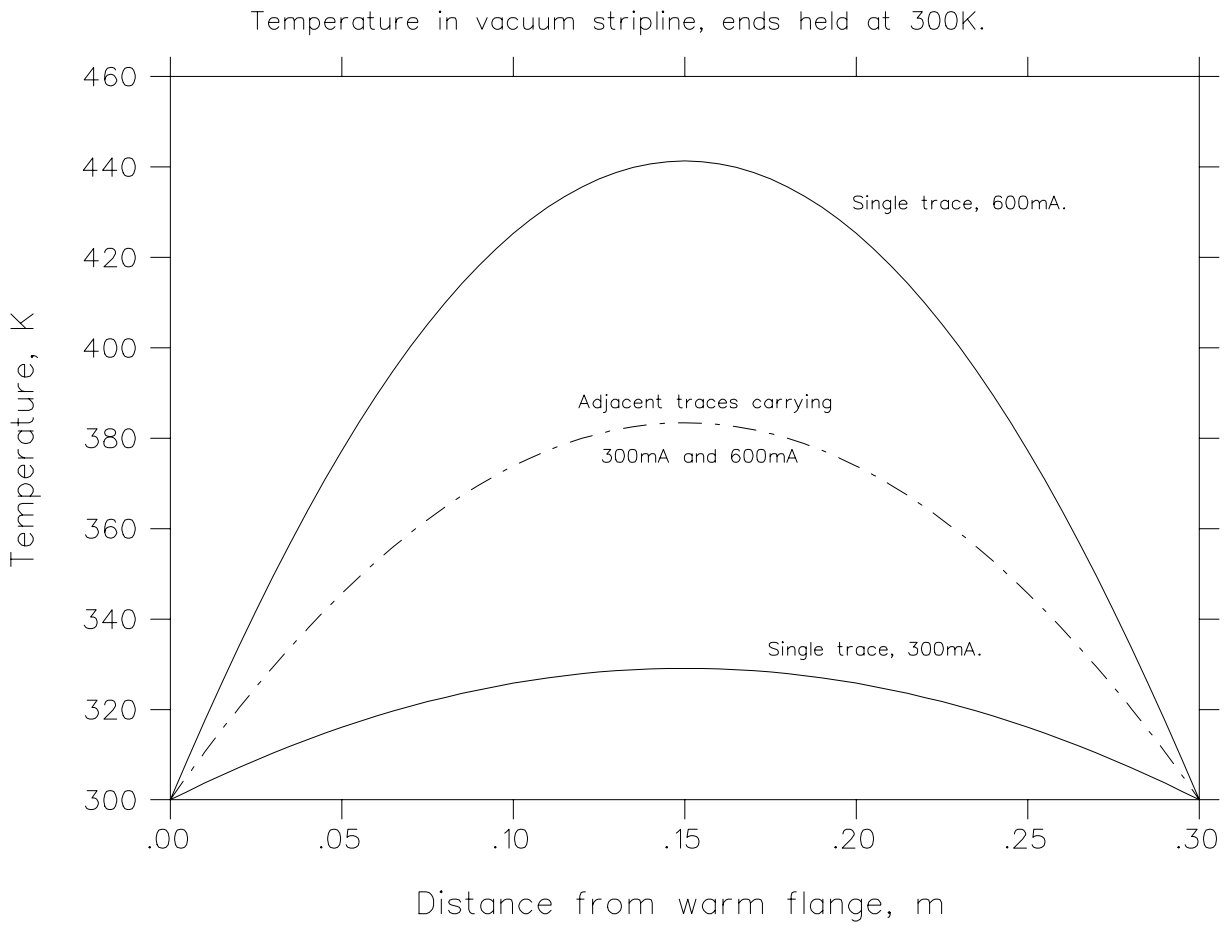

Figure 92: Temperature of a vacuum stripline trace (for warm conditions) as a function of distance from the ambient temperature end of the trace. The solid curves show the case of a 300 mA trace and of a 600 mA trace. The dashed curve shows the temperature of both traces if they are adjacent to each other.

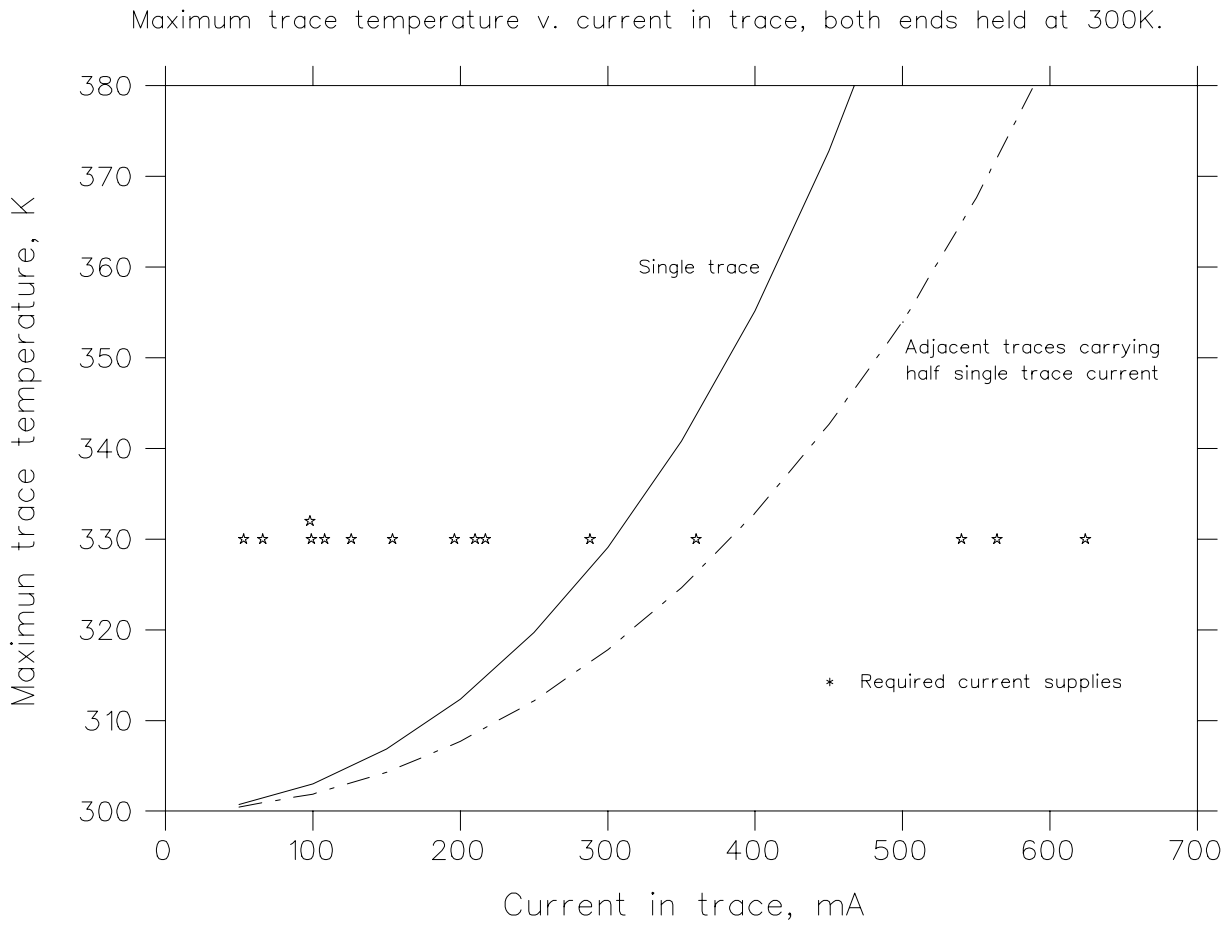

Figure 93: Maximum vacuum stripline trace temperature (for warm conditions) as a function of trace current. See text.

16 Preliminary Results of the FEA on the Ambient Flange (Release of 98/04/28)

We present here a "preview" of the results of the FEA on the ambient flange.

Figure 94 shows an element plot of the model of the ambient flange, 23 mm thick, with pin carrier weld prep groove as before plus 4 mm deep, 6 mm wide groove for the weld prep for joining the seal ring. The seal ring has a similar groove. The thickness of the material at the weld prep rim is 0.75 mm. Figure 95 shows the stress in the seal ring for atmospheric load only; Figure 96 shows the stress in the ambient flange for atmospheric load only; Figure 97 shows the stress at the junction of the flange and seal ring for atmospheric load plus 3.4 bar internal pressure.

The flange thickness and the weld prep thickness were varied to see how the results were affected. The stress plots were similar to the above figures with changes of stress magnitude only. The results for various cases are shown in Table 6.

case no.	flange thickness (mm)	weld prep thickness (mm)	internal pressure (over atm load) (bar)	flange deflection (μm)	maximum flange–seal ring stress (MPa)
1	23	0.75	0	64	81
2	23	0.75	3.4	156	201
3	29	0.75	3.4	94	174
4	29	1.00	3.4	92	140
5	29	1.25	3.4	91	115
6	29	1.50	3.4	89	98

Table 6: Ambient flange deflections and maximum (Von Mises) stress in the flange–seal ring region under atmospheric load and the shown internal pressure, for two flange thicknesses and 4 different seal ring weld prep ring thickness.

The 3.4 bar internal pressure is not the correct pressure to use. The test pressure for the endcap feedthroughs given in "The load cases for cryostat and feedthrough" ATLAS document was used instead. We believe we will be asked to use the one under "Exceptional situations (E1,E2)" of 3.2 bar plus a 0.1 bar allowance for the argon hydrostatic head, for a total of 3.3 bar. Note that this is different from a pressure of 2.8 bar (plus perhaps the 0.1 bar allowance for the argon hydrostatic head) which is the "Normal situation" described under N5 in the above document. This matter should be clarified with Pierre Pailler.

We favour the 1.25 mm thick weld prep which will probably leave a 2 mm high weld prep to make a new weld if the original weld has to be ground off. Making the flange thicker by 6 mm reduces deflection and stress; more important, it will reduce the deflection caused by welding in the pin carriers: on balance, we would prefer the thicker flange (the 1.25 inch plate required for manufacture is available).

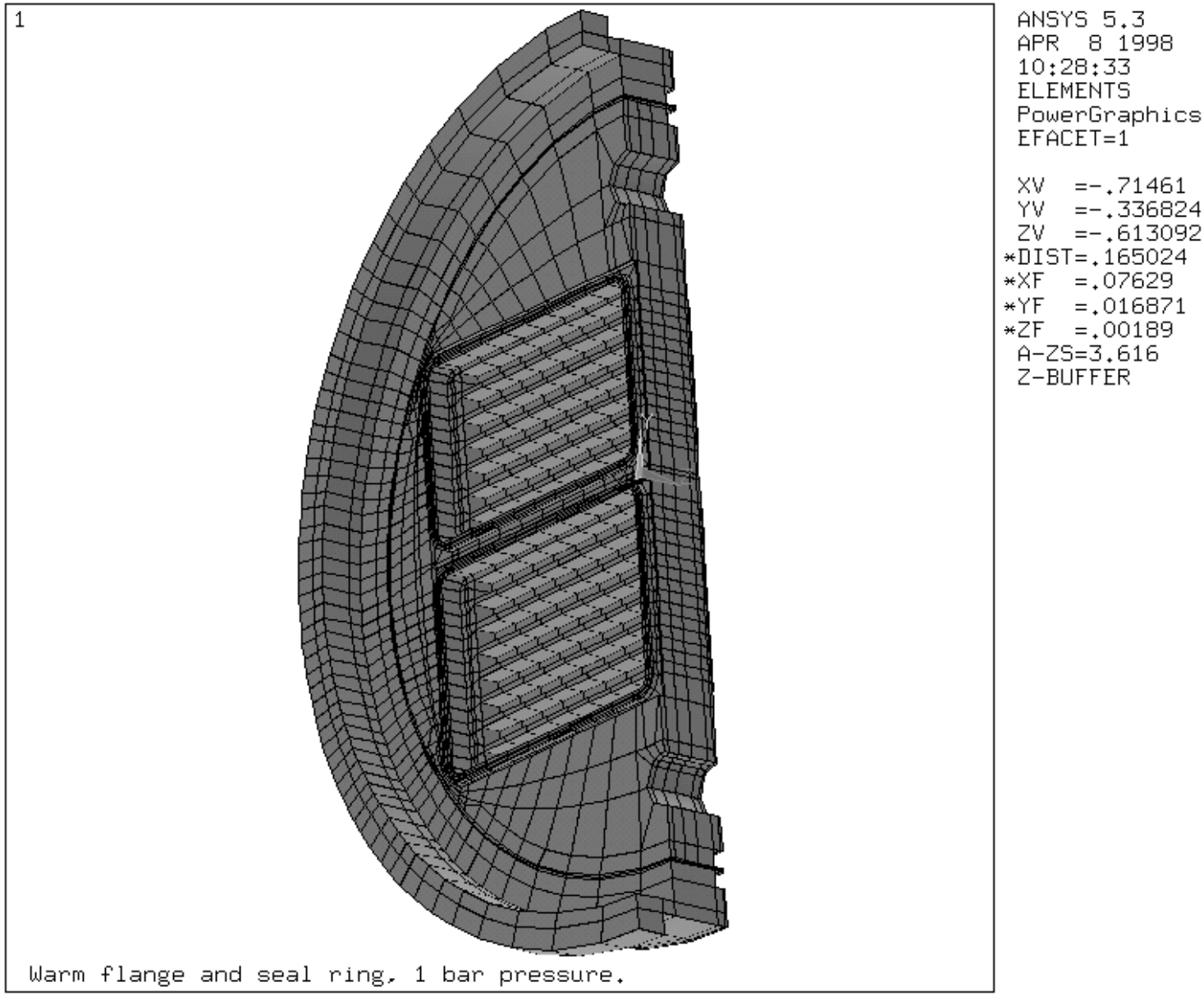

Figure 94: Finite element analysis model of (half) an ambient flange 23 mm thick, showing the weld prep for the pin carriers, as well as the seal ring and the related weld preps.

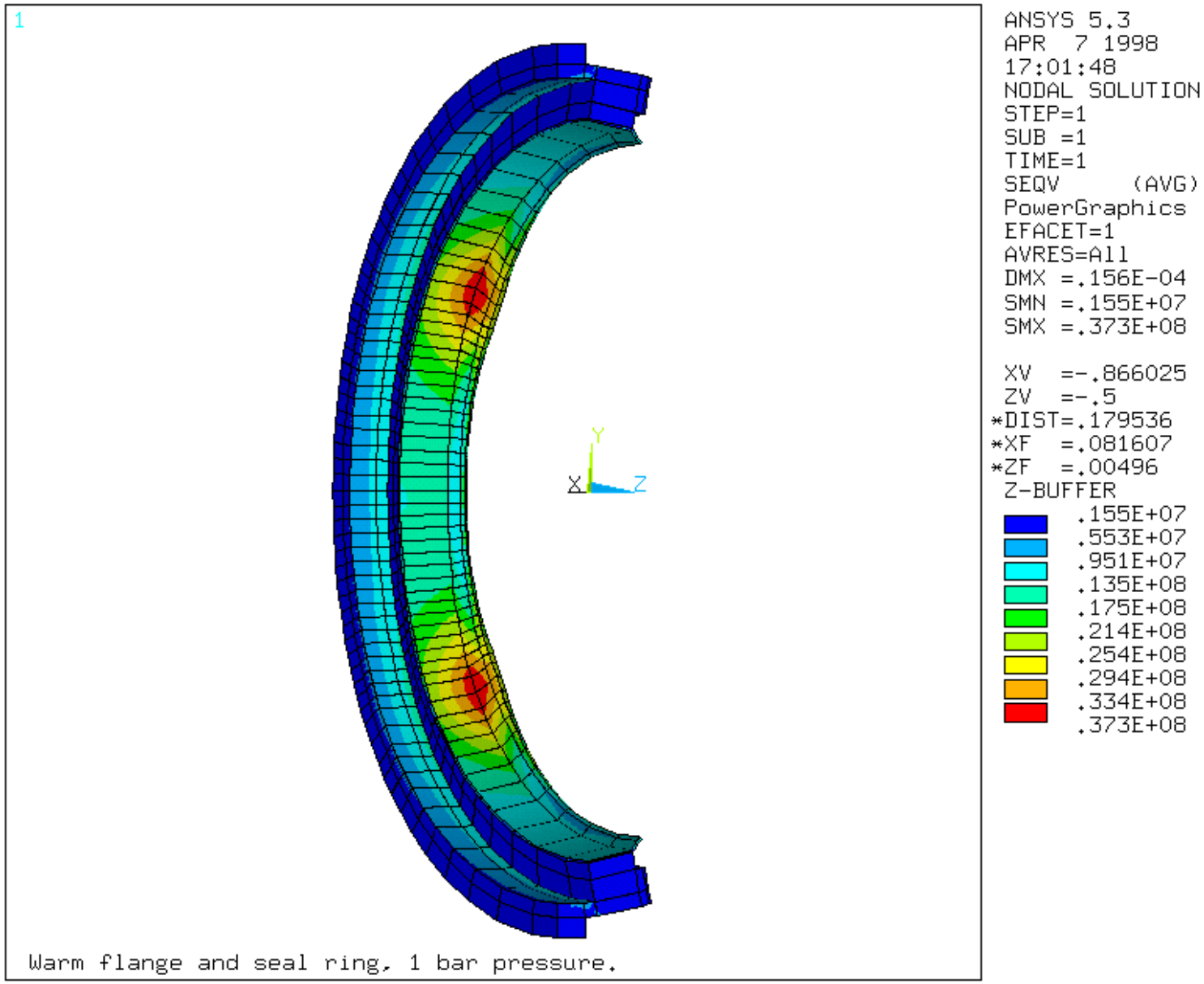

Figure 95: Finite element analysis of a seal ring showing (Von Mises) stress in Pascals under atmospheric load. The deflections (DMX) are in meters.

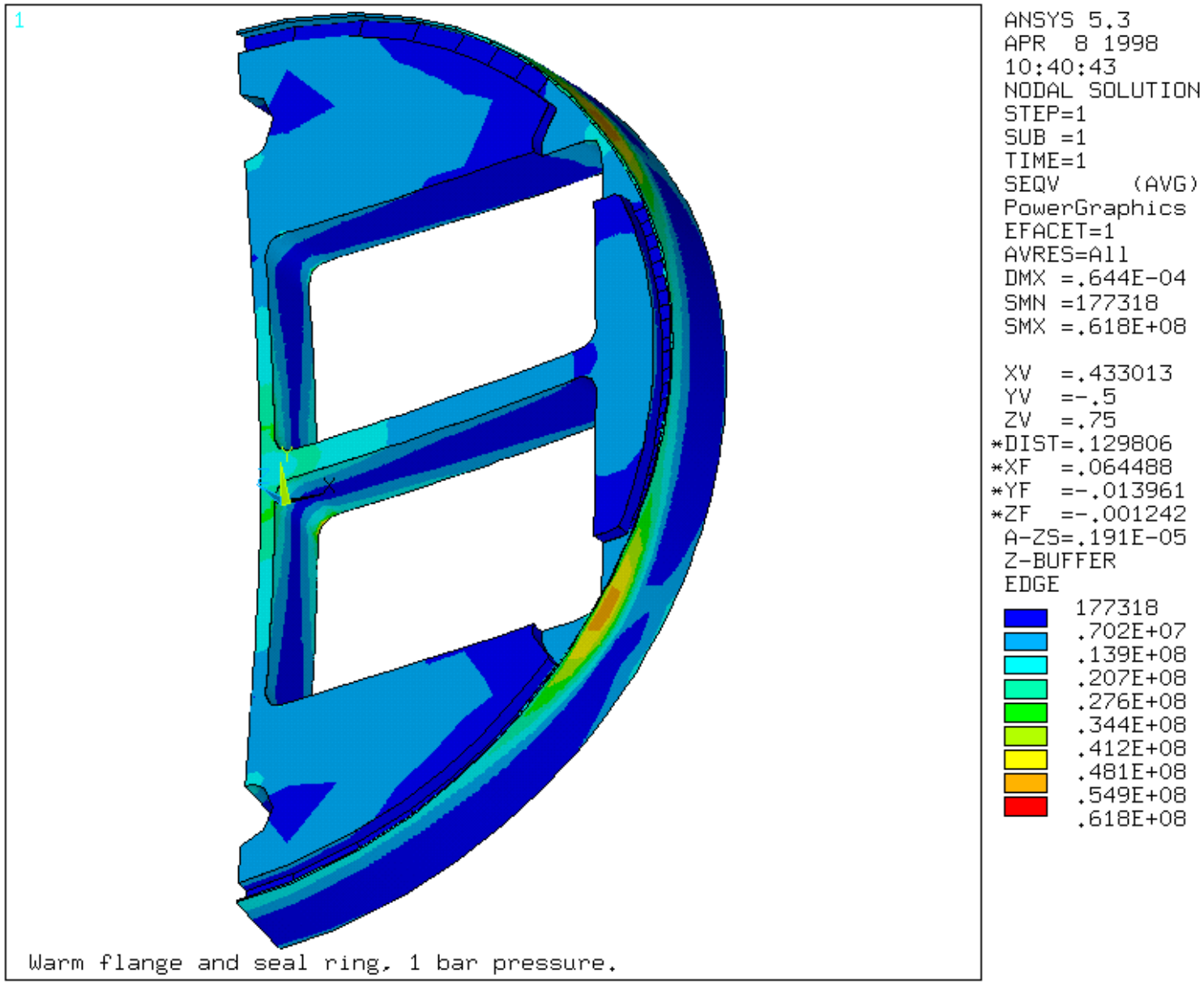

Figure 96: Finite element analysis of an ambient flange 23 mm thick showing (Von Mises) stress in Pascals under atmospheric load. The deflections (DMX) are in meters.

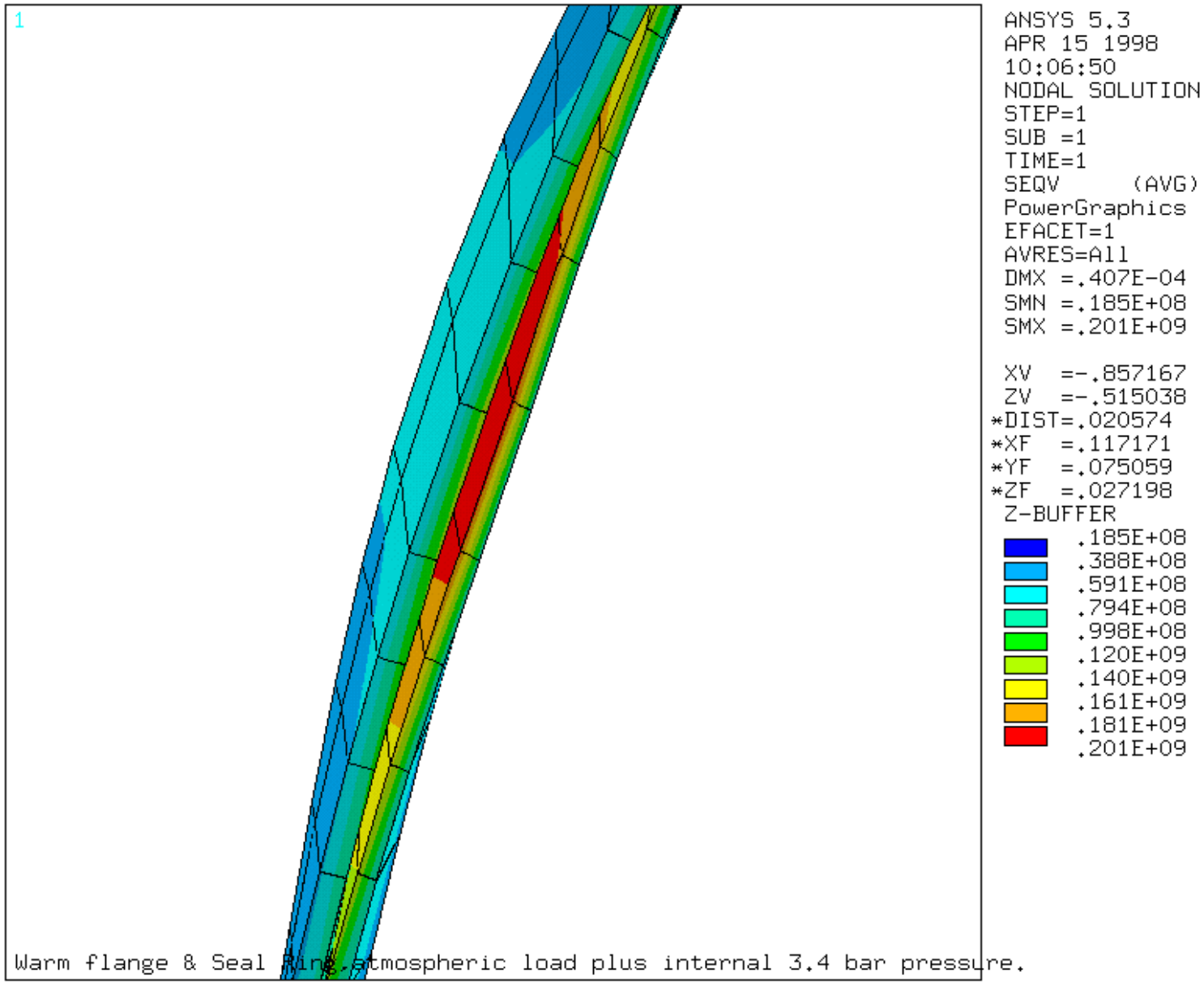

Figure 97: Finite element analysis of an ambient flange 23 mm thick and seal ring showing (Von Mises) stress in Pascals under atmospheric load plus 3.4 bar internal pressure. The deflections (DMX) are in meters.

17 Effect of Signal Currents in the Signal Feedthrough Stripline (Release of 98/06/29)

The standard signal vacuum cable, which connects each pair of 64-pin connectors in the ambient (300 K) and cold (80 K) flanges of the barrel and endcap signal feedthroughs, is a flexible circuit stripline. The flexible circuit is a sandwich of 38 micron thick kapton between two layers of 35 micron thick copper. Each pin in the feedthrough is connected to a copper trace 200 micron wide etched from one of the copper layers and is opposite a 400 micron wide ground trace etched from the other copper layer, see Figure 122. Such an arrangement provides the correct impedance for the signal lines.

The ANSYS finite element code has been used to investigate the temperature and power dissipation effects when signal currents are passed through the striplines. For the purpose of this investigation, the stripline length was taken to be 300 mm, the values for the electrical and thermal conductivities of the copper were made temperature dependant, but the thermal conductivity of the kapton was fixed at 3 Wm/K. The kapton is assumed to provide perfect electrical insulation but it is interesting to note that the signal and ground trace pairs are in very close thermal contact. The thermal contact between adjacent signal and ground traces is sufficient to markedly modify heat flow in the stripline.

For the first part of the investigation, it is assumed that adjacent lines carry similar currents so that a single signal/ground pair can be treated in isolation. Two operational regimes require investigation. The normal situation is with one end of the stripline at ambient (assumed 300 K) and the other end at or near liquid argon temperature (80 K). The other "test" situation is where the cryostat is not cold and both ends of the stripline are at 300 K. The temperature as a function of position along the stripline (measured from the ambient flange) is shown in Figures 123 and 124 for the "normal" and "test" situations respectively. The maximum temperature created in a stripline as a function of current flowing is shown in Figure 125. The potential difference produced between the ends of the signal trace as a function of signal current is shown in Figure 126. The heat flow to the cold and ambient flanges as a function of signal trace current is shown for the normal (300 K/80 K) situation in Figure 127. The ground return current is considered sufficiently widely distributed to cause negligible heating effects. As the signal current grows, the temperature profile along the signal trace is modified, the temperature gradient passes through zero at the 300 K end, causing a fraction of the resistive heating to begin flowing to the ambient flange. In the "test" situation half the resistive heat flows to each flange.

The second part of the investigation concerns the effect on the maximum temperature in a signal trace carrying a current, when it is among other traces carrying small or negligible currents. An analysis was made of a signal trace carrying a current of 150 mA with three neighbouring traces on either side of the signal trace carrying no current. The ends of all traces were held at 300 K. The half-model (using the plane of symmetry through the current carrying trace) is shown in Figure 128. Also shown in Figure 128 are the maximum temperatures in the traces and the percentage of the resistive heat from the current carrying trace, which is carried by each of the neighbouring traces. It is evident

that neighbouring traces are in good thermal contact and a single trace could carry 3 or 4 times the current one might specify for an isolated trace. A corollary to the latter is that a current overload in one trace could damage other traces on the same stripline.

18 Ambient Flange Study (Release of 98/07/16)

Modifications to the ambient flange model continued from the models of section 14 through the models of section 16 to the current model, with atmospheric and 3.3 bar reverse pressure loads.

This model now has the 4 mm deep flange weld prep for attaching the seal ring to the flange (although only 5.5 mm wide rather than the 6 mm shown on the latest drawings) and the 6 mm wide by 2.5 mm deep weld groove to facilitate welding of the pin carriers into the flange. The weld lips for the seal ring/flange weld are both 1.25 mm thick. The weld lips for the pin carrier/flange weld are both 1.0 mm thick (instead of the currently envisaged 0.75 mm thick). The width of hole for 7 row pin carrier is 65 mm (cf. latest drawing 64.97 mm). The width of hole for 8 row pin Carrier is 73.84 mm (cf. latest drawing 73.66 mm). The length of the hole for both pin carriers is 105.3 mm (cf. latest drawing 105.15 mm). The flange is 29.0 mm thick, and the holes for the pin carriers have been moved to leave 8.8 mm thick "cross webs" in the flange.

Subsequently, the weld lips for the pin carrier/flange weld were both corrected to the design thickness of 0.75 mm.

Figures 105 and 98 show and exploded view of the ambient flange, the pin carriers and the seal ring, while Figure 106 shows the corresponding element plot. A view of the pin carriers in the ambient flange is shown in Figure 99, while the whole assembly is shown in Figure 100. The (Von Mises) stresses under atmospheric load and 3.3 bar reverse pressure are shown in Figures 101 (view of the atmospheric side), 108 (view of the vacuum side), 102 (details of the pin carriers), 103 (details of the ambient flange), and 104 (details of the seal ring).

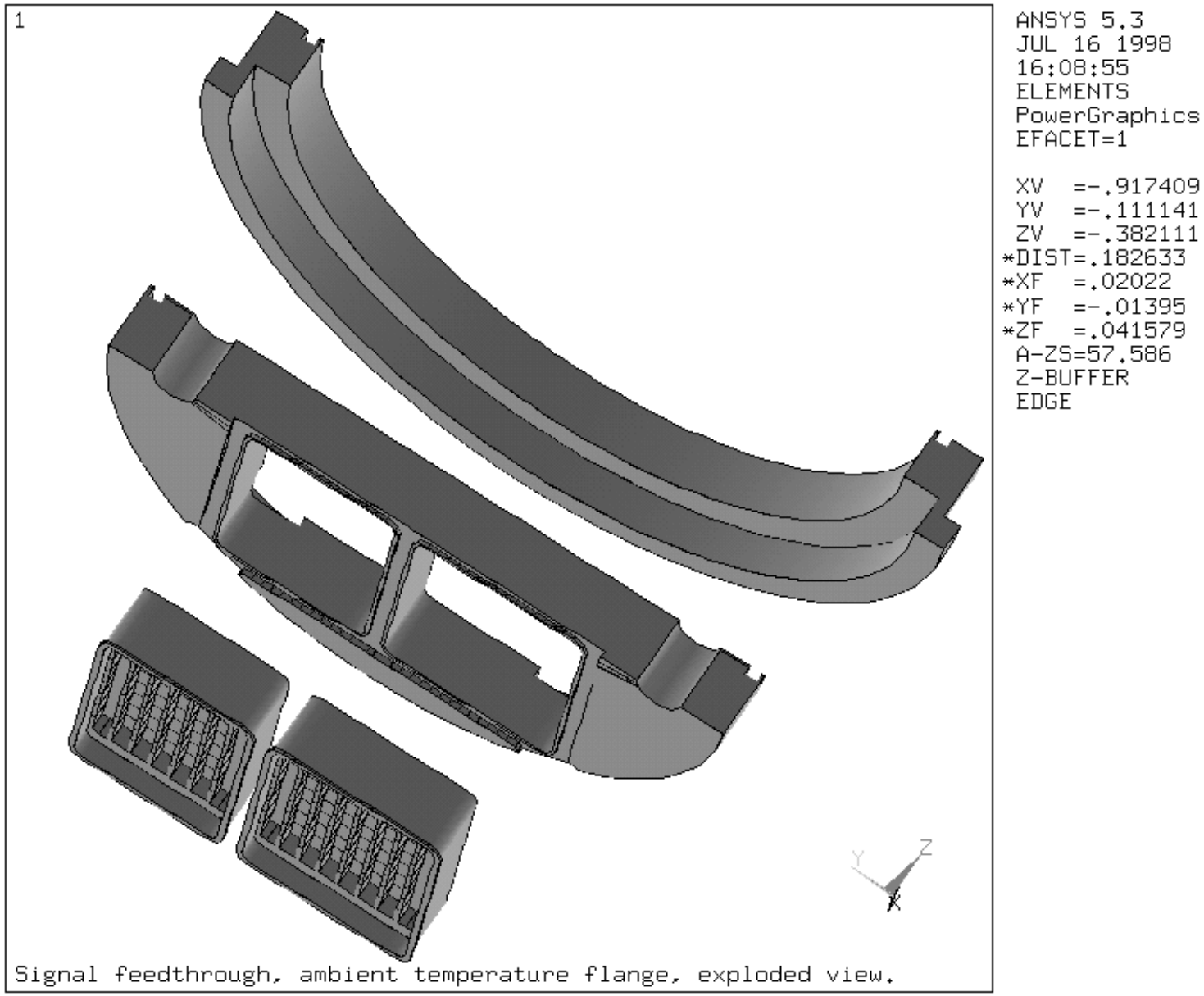

Figure 98: Exploded (half) view of the ambient flange, the pin carriers and the seal ring.

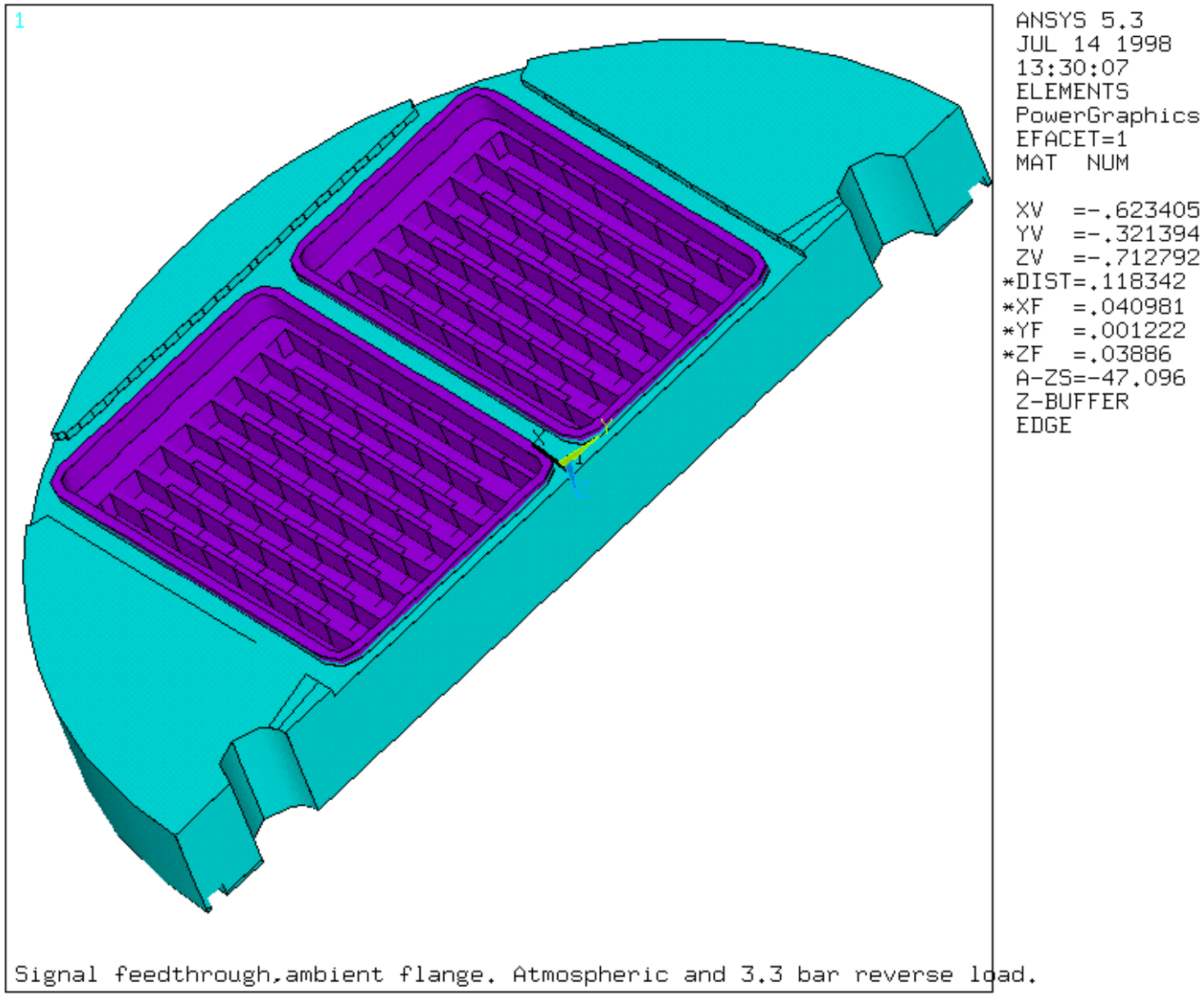

Figure 99: View of the pin carriers in the ambient flange.

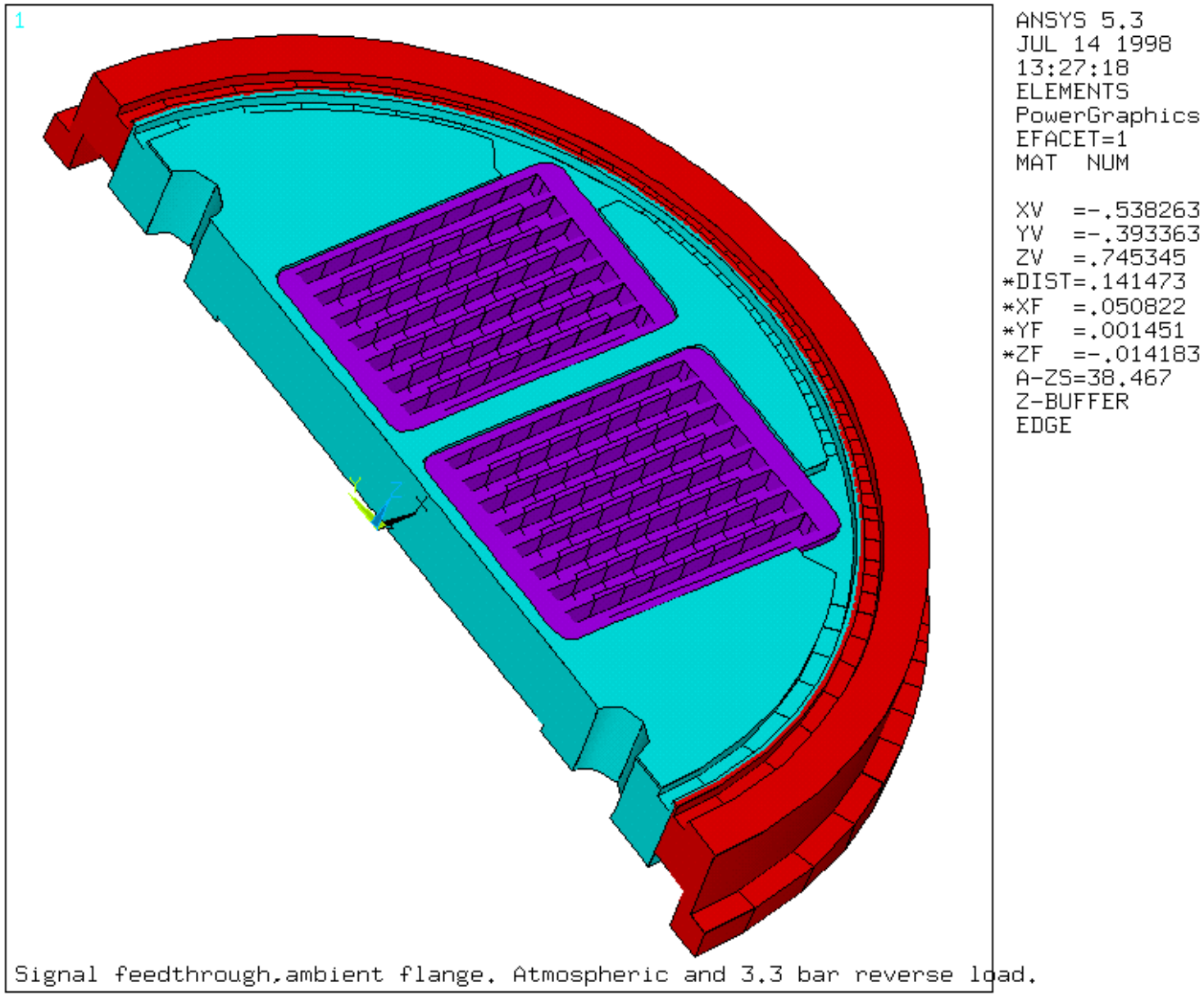

Figure 100: View of the pin carriers in the ambient flange, and the seal ring.

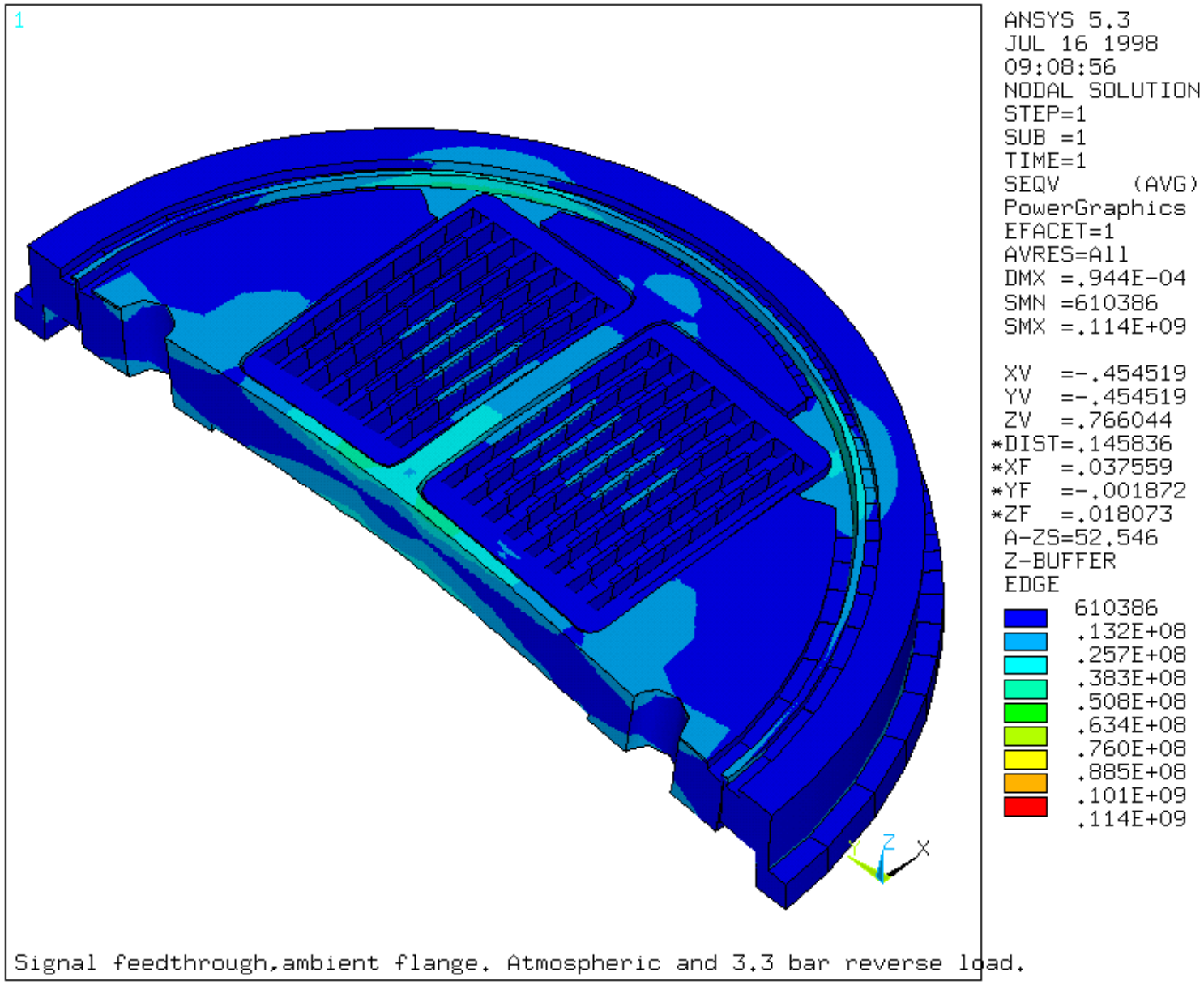

Figure 101: Finite element analysis of the ambient flange assembly under atmospheric and reverse 3.3 bar loads, showing (Von Mises) stress in Pascals. View of the atmospheric side.

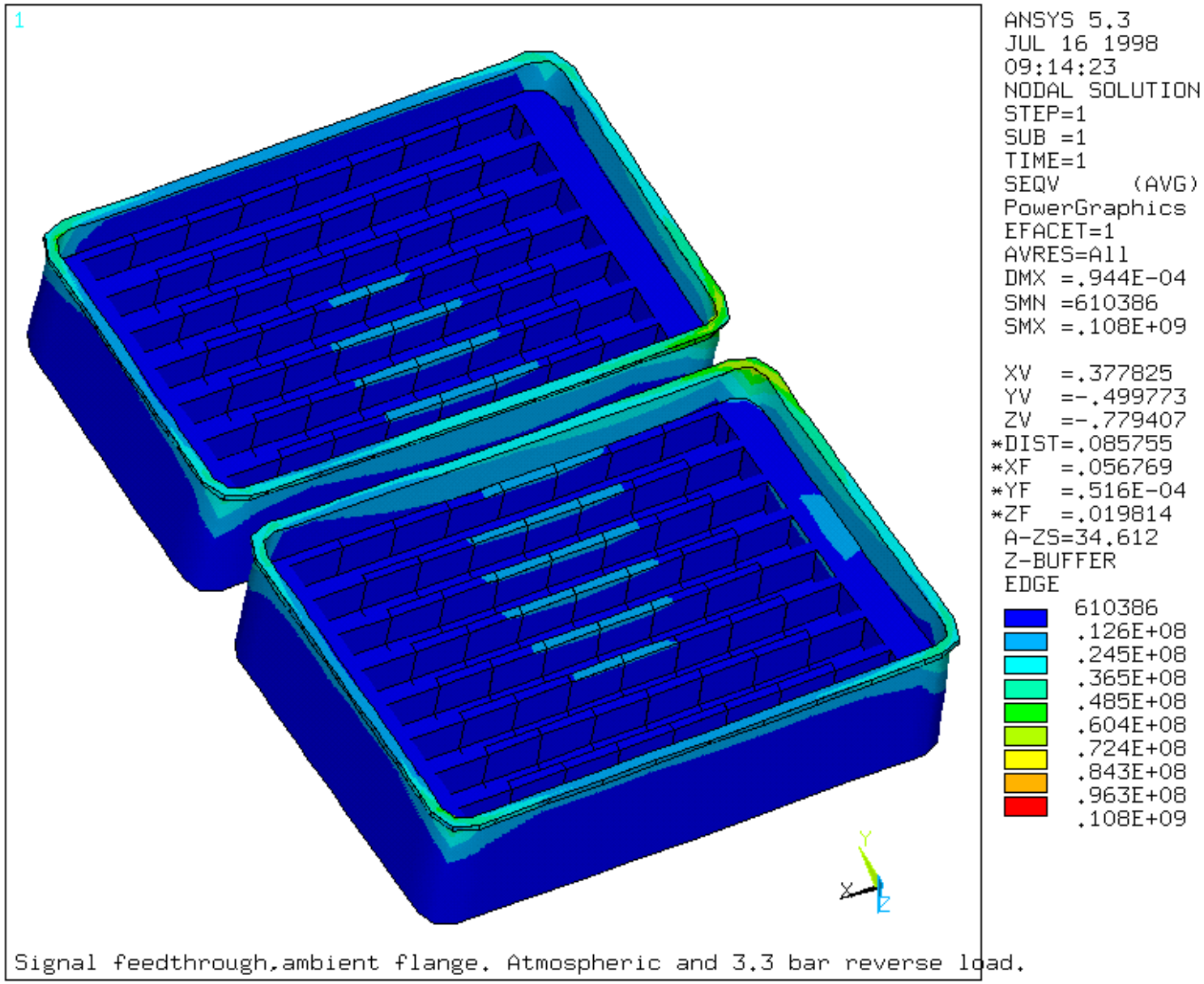

Figure 102: Finite element analysis of the ambient flange assembly under atmospheric and reverse 3.3 bar loads, showing (Von Mises) stress in Pascals. Details of the pin carriers.

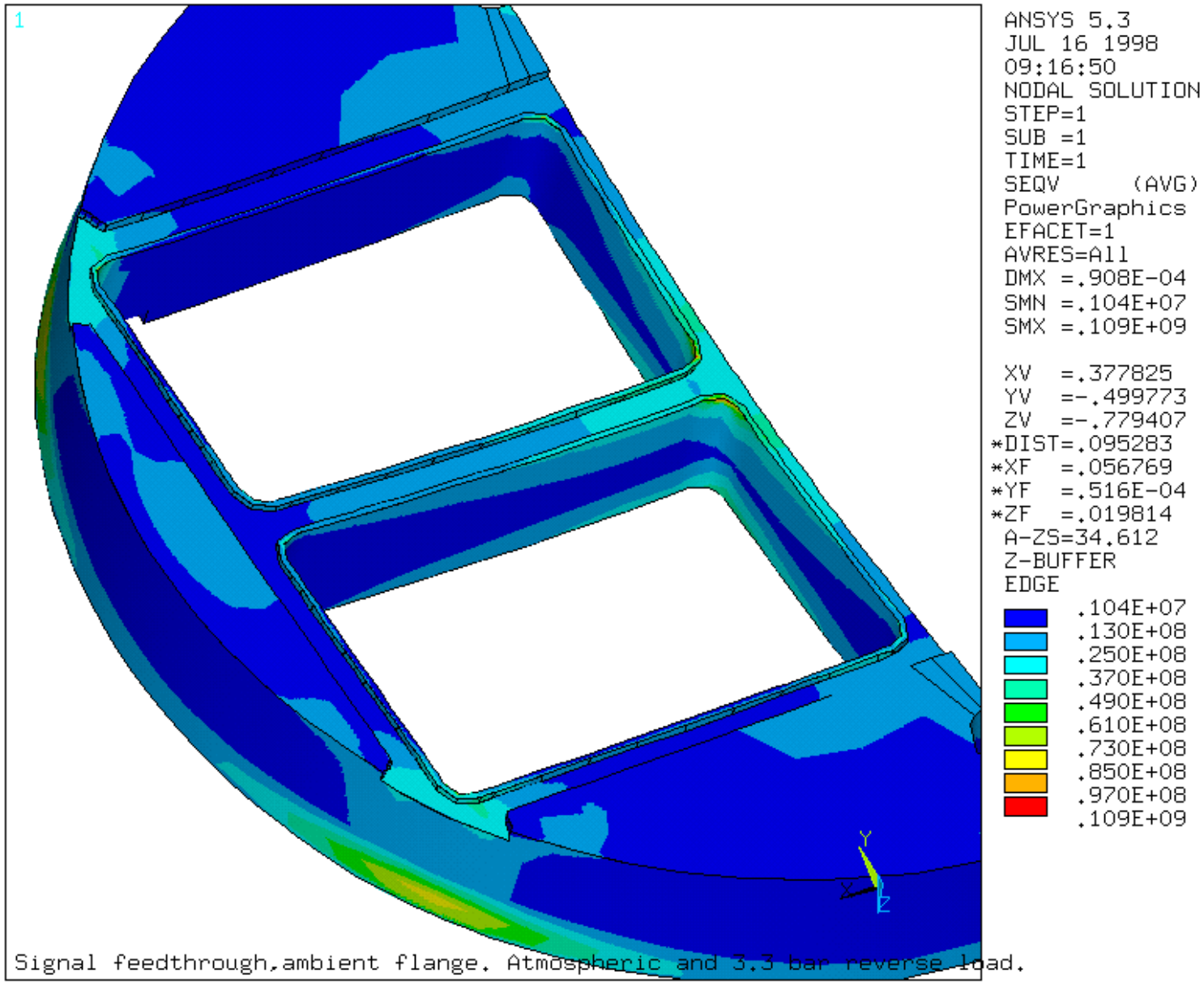

Figure 103: Finite element analysis of the ambient flange assembly under atmospheric and reverse 3.3 bar loads, showing (Von Mises) stress in Pascals. Details of the ambient flange.

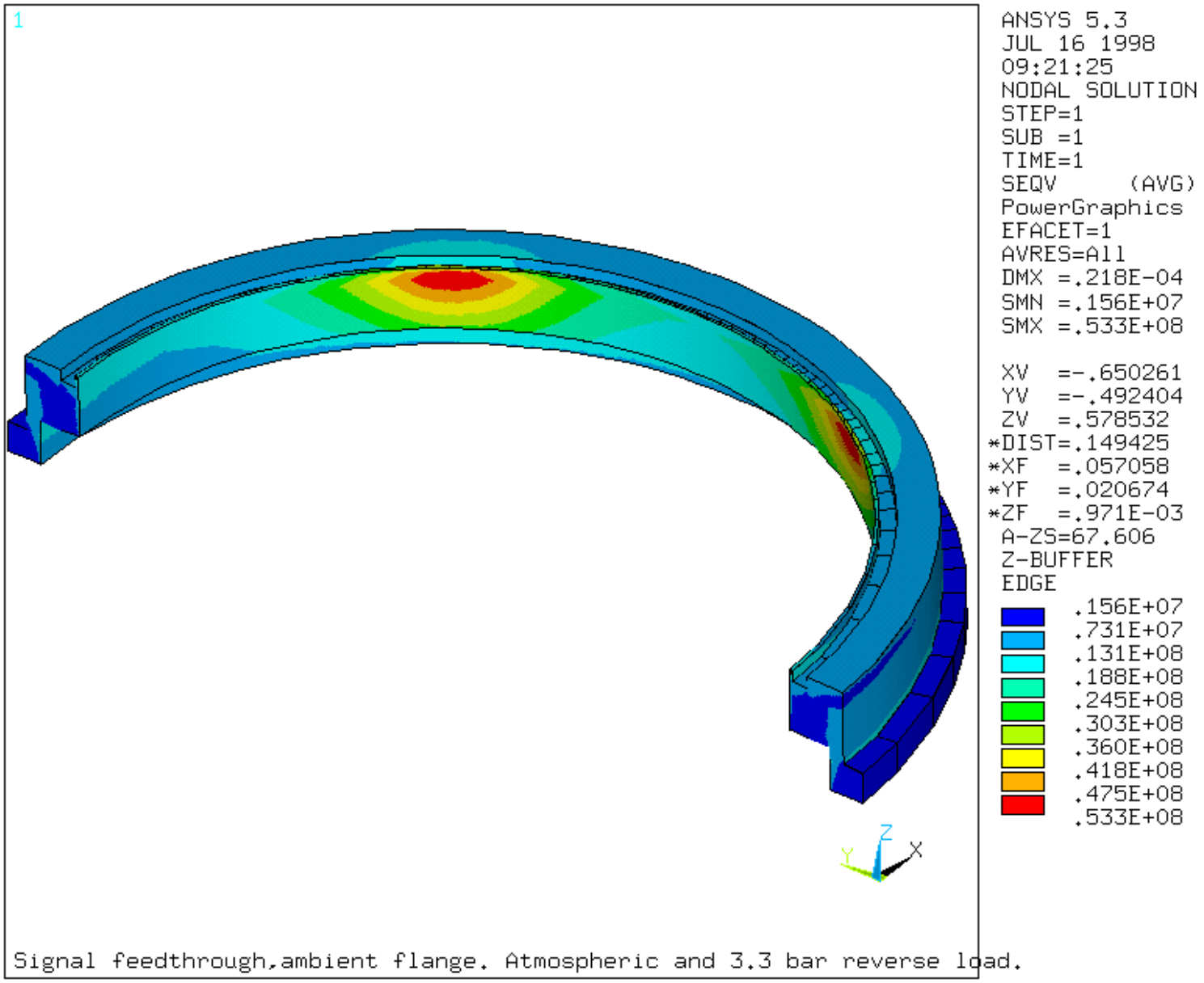

Figure 104: Finite element analysis of the ambient flange assembly under atmospheric and reverse 3.3 bar loads, showing (Von Mises) stress in Pascals. Details of the seal ring.

19 Signal Feedthrough PRR – Calculations and FEA – Mechanical Aspects (Release of 98/08/28)

19.1 General

Investigation of the various parts of the signal feedthrough assembly have been carried out using the Finite Element Analysis (FEA) code ANSYS [2]. The structures examined have a common plane of symmetry which enables the analyses to be carried out using one half of the structure. Symmetry constraints are applied on the plane of symmetry: motion parallel to the plane of symmetry is prevented by additional constraints applied as required.

In the following descriptions the term "stress" is the Von Mises stress, and SI units are used throughout. Deflections in models are exaggerated to enable them to be seen.

19.2 Ambient Flange

An exploded view of the ambient flange assembly is shown in Figure 105. The four pin carriers are welded into the flange on the vacuum side of the flange, and the flange is welded to the seal ring on the atmosphere side of the flange: not shown in the figure is the stainless steel bellows which will be already welded (on the vacuum side) to the seal ring by the bellows manufacturer.

During normal operation, atmospheric pressure will exist on one side of the flange and vacuum on the other. It is possible, in the event of a vacuum failure in the calorimeter, that the ambient flange could be exposed to a pressure rise in the vacuum space of 3.3 bar [3]. An FEA of the latter situation has been carried out using the model shown in Figure 106. Motion perpendicular to the plane of the flange is prevented by constraints on the seal ring surface where it contacts the cryostat and bolt ring; motion parallel to the symmetry plane is prevented by a single node constraint. Figure 107 is an overview of the deflection of the assembly under the above-mentioned pressure load, as seen from the normal vacuum side; the maximum of 94 microns occurring at the flange centre. An overview of the stress in the flange is shown in Figure 108. Generally the stress is low, with regions of higher stress occurring at the flange/seal ring weld, where the corners of the pin carriers approach the flange periphery, and also in the corner regions of the flange/pin carrier welds near the centre of the flange. These higher stress regions are very localized and are shown in close-up views in Figures 109 and 110. Simple hand calculations of the stress in the seal ring/flange weld yields an average stress of 16 MPa: this value lies between the minimum and maximum values of 11 MPa and 39 MPa from the FEA, which includes the discontinuity stresses from the flange distortion. The sensitive region of the feedthrough is in the pin carrier "web" which houses the glass or ceramic seals to the signal pins. The stress levels in the web are shown in Figure 111 to be less than 8 MPa.

No FEA was carried out on the bolt ring and bolts. A hand calculation of the load to bring the bolts to their yield stress was only 15% of the load produced by the exceptional 3.3 bar pressure loading.

[2] ANSYS v5.3 Swanson Analysis Systems Inc.,Houston,PA,USA

[3] LAr Cryostats, ATLAS Project Document No. ATL-CERN-A-CERN-0002

Heating resistors are attached to the ambient flange to prevent condensation occurring, particularly near the signal pins, due to the heat leak from the ambient flange to the cold flange via the signal striplines. An FEA of this situation was performed and the resulting temperature contours on the ambient flange are shown in Figure 112. The resistors are simulated by the fixed temperature regions of 310 K: the seal ring is held at 300 K where it touches the cryostat or bolt ring. A total of 7.4 W flows out of the resistors, 0.9 W to the seal ring and the remaining 6.5 W to the signal pins. Heat lost by convection to the air is not included, nor is the heat supplied to the signal pins by the warm cables: the latter effect might marginally reduce the signal pin temperature drop calculated here. The stress produced by the temperature fields above were maximum (167 MPa and 128 MPa) at the flange/pin carrier corners and flange/seal ring weld respectively. These stresses increased to 230 MPa and 115 MPa when the 3.3 bar pressure fault load was added.

19.3 Cold Flange

The FEA model of the Cold Flange is shown in Figure 113. Two weld preparation "lips" appear on the periphery of the flange; one to weld the flange to the bellows and the other to weld to the "funnel" - the latter connects the feedthrough to the cryostat via a bi-metal junction. Part of the Funnel is included in this FEA to investigate the cold flange/funnel weld. Motion perpendicular to the plane of the flange is prevented by constraints on the funnel edge remote from the flange.

Under normal operating conditions, the bellows side of the cold flange is under vacuum and the other side at a maximum pressure of 2.9 bar. The gas test pressure of 3.5 bar induces the most stressful condition however, and was the pressure used for the calculations. The maximum deflection of the flange due to the 3.5 bar pressure load is shown in Figure 114 to be 68 microns. An overview of the stress in the cold flange, seen from the liquid argon side, due to the test pressure load is shown in Figure 115. The maximum stress of 115 MPa is a localized stress in the corner of the weld region of the pin carrier. Stress in the flange alone is shown in Figure 116 to be generally low; with the higher stresses in the region where the corners of the pin carriers are welded to the flange. As in the ambient flange these high stress regions are very localized. The stress in the funnel/cold flange weld is maximum (61 MPa) where the corners of the pin carriers approach the flange periphery. These regions are visible in Figure 117, which shows the section of funnel abutting the cold flange.

The stresses in the sensitive web region of the pin carriers are shown in Figure 118 to be below 10 MPa.

Simple hand calculation of the stress in funnel/cold flange weld gives a value of 15 MPa. The FEA minimum and maximum stresses for this region are 2 MPa and 61 MPa and Figure 117 shows the very marked concentration of stress at the locations where the pin carrier corners are close to the flange periphery.

19.4 Funnel

The FEA model of the funnel and bi-metallic joint is shown in Figure 119. The part coloured red is aluminum, the rest is stainless steel. The open end of the aluminum section of the bi-metal joint, which connects the feedthrough assembly to the cryostat, was restrained from lateral and vertical motion. A force of 5387 Newtons was applied to the open end of of the funnel larger diameter cylinder, simulating the force on the funnel due to the internal pressure of 3.5 bar. A force of 695 Newtons was applied at the same location in a lateral direction, simulating the force required to displace the bellows laterally by 15 mm, this displacement occurring due to contraction of the barrel cryostat on cooling to liquid argon temperature. These forces are shown as red arrows in the latter figure. The maximum stress of 114 MPa occurs at the funnel plate/smaller cylinder junction, Figure 120. The maximum stress (50 MPa) in the transition joint region occurs near the weld at the lower edge of the smaller funnel cylinder, Figure 121. The stress in the bi-metal union is low, < 6 MPa.

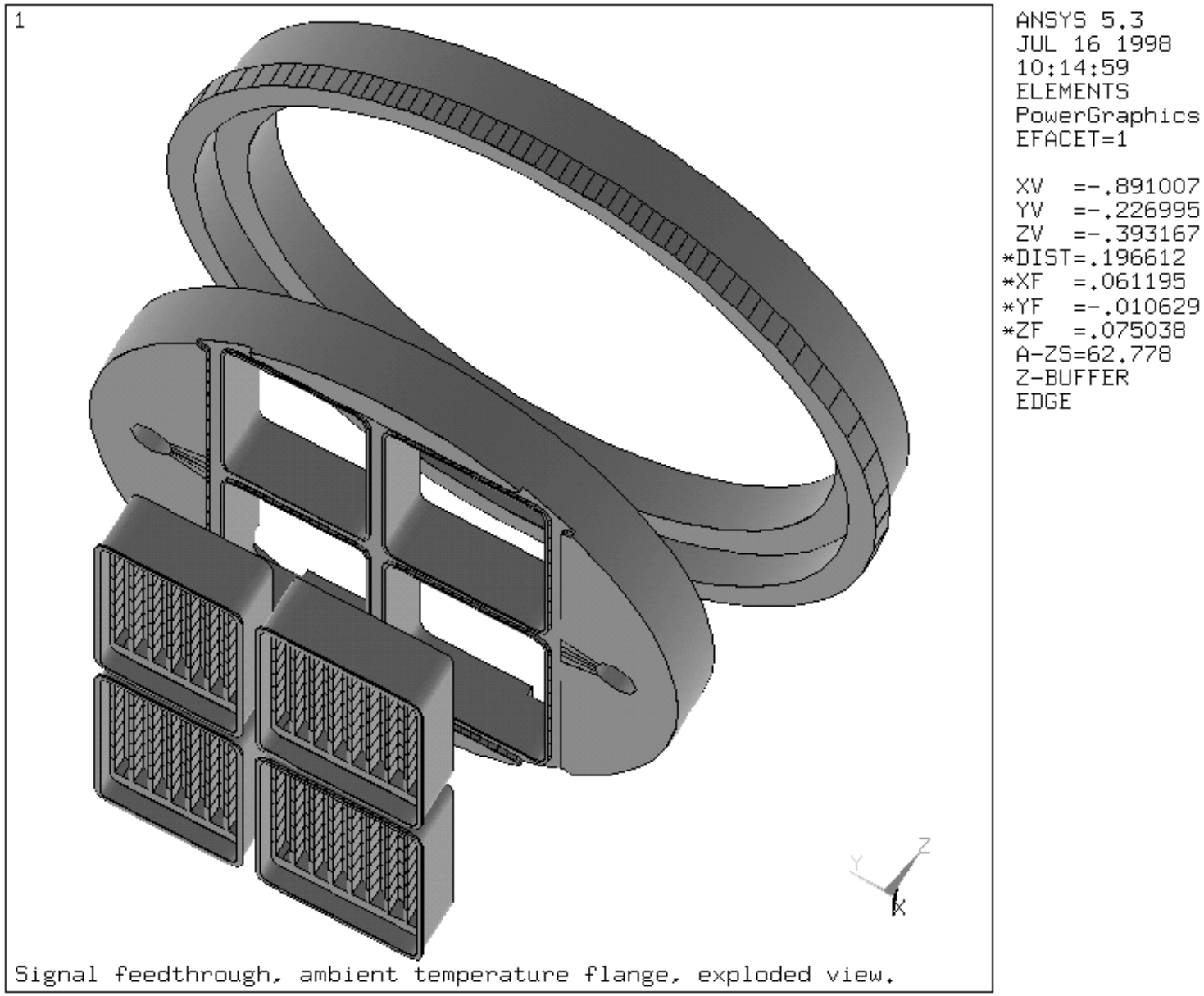

Figure 105: Exploded view of the ambient flange, the pin carriers and the seal ring.

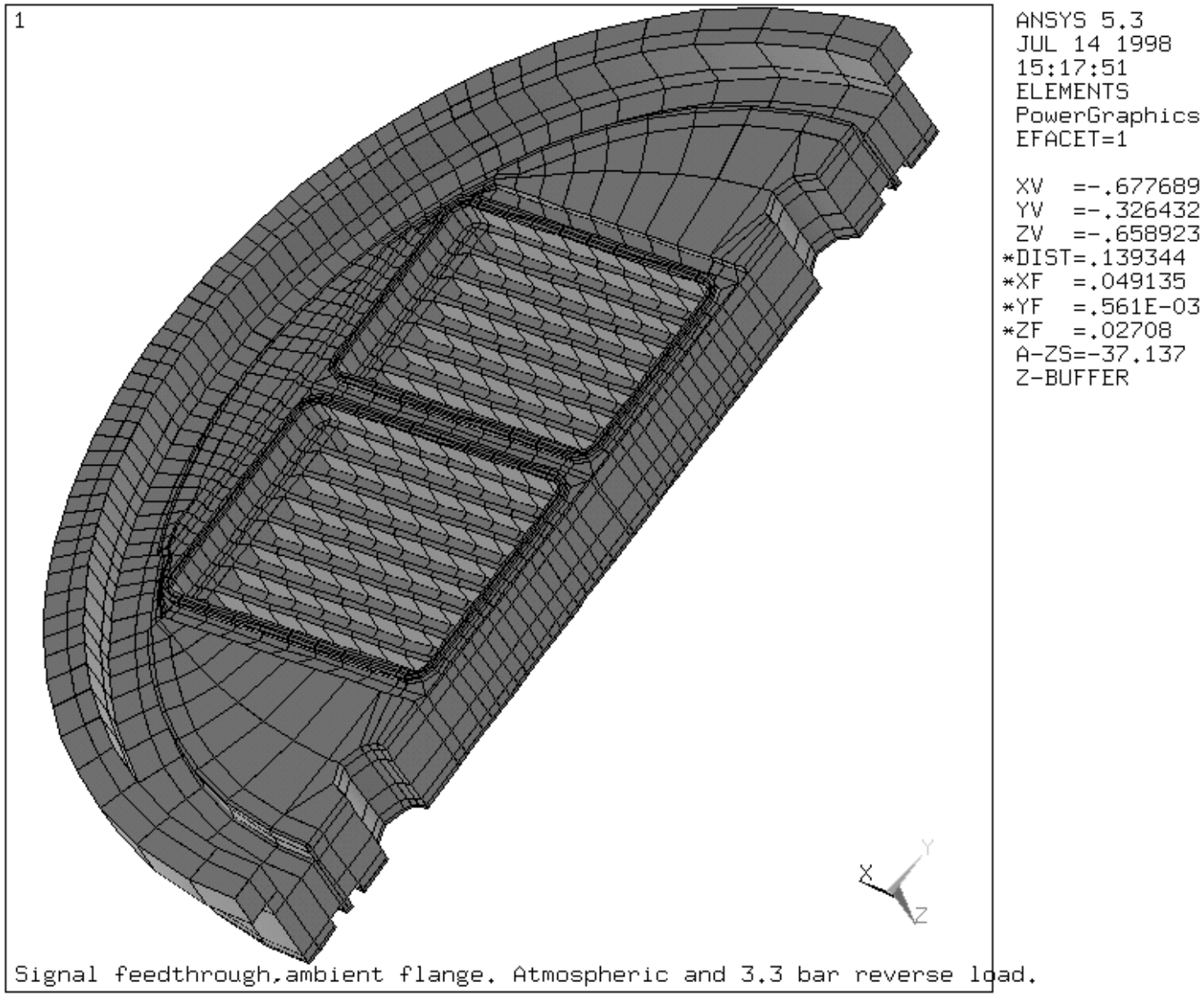

Figure 106: Finite element analysis model of the ambient flange with pin carriers and seal ring.

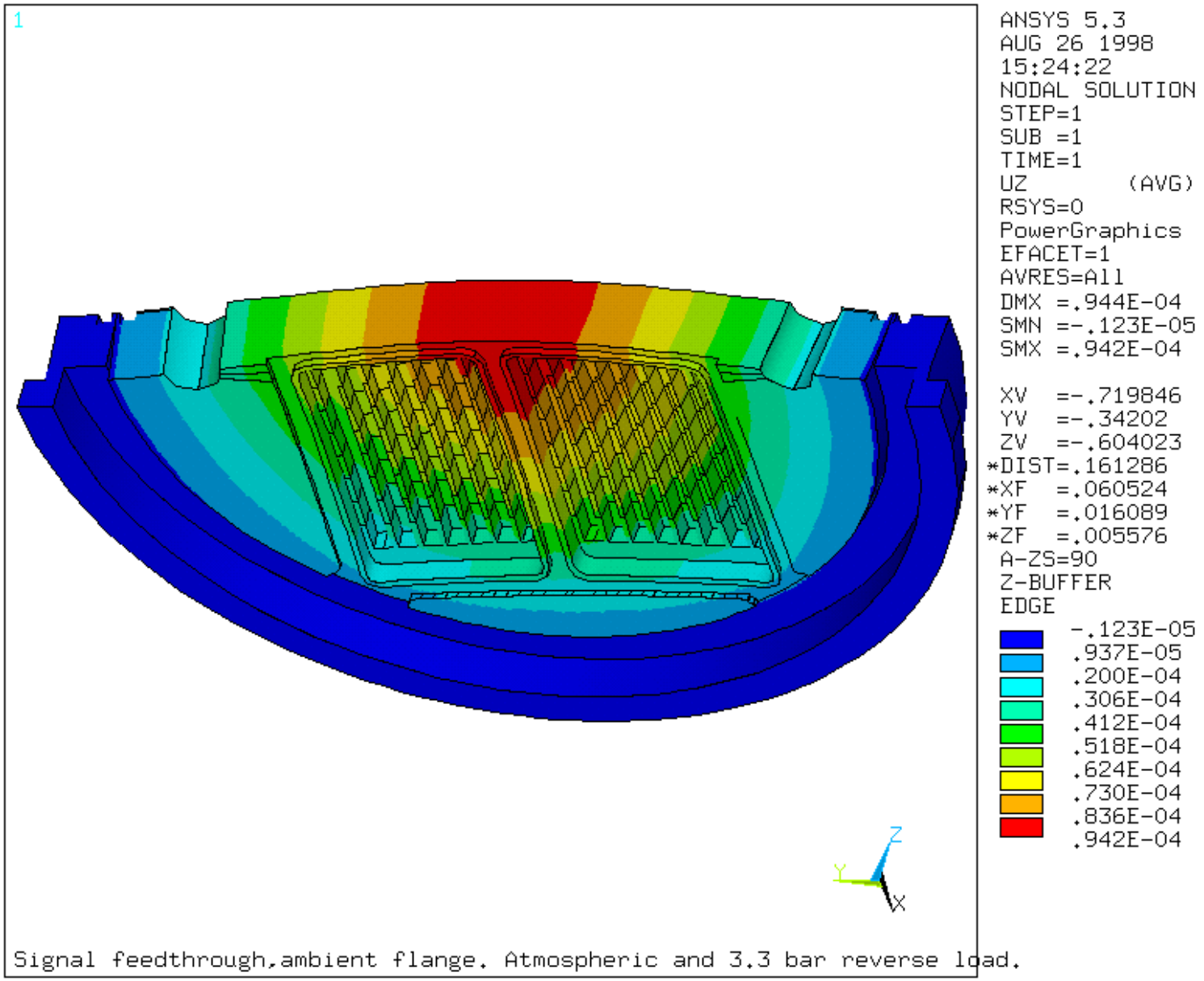

Figure 107: Finite element analysis of the ambient flange assembly under atmospheric and reverse 3.3 bar loads, showing the deflections in microns. View from the vacuum side.

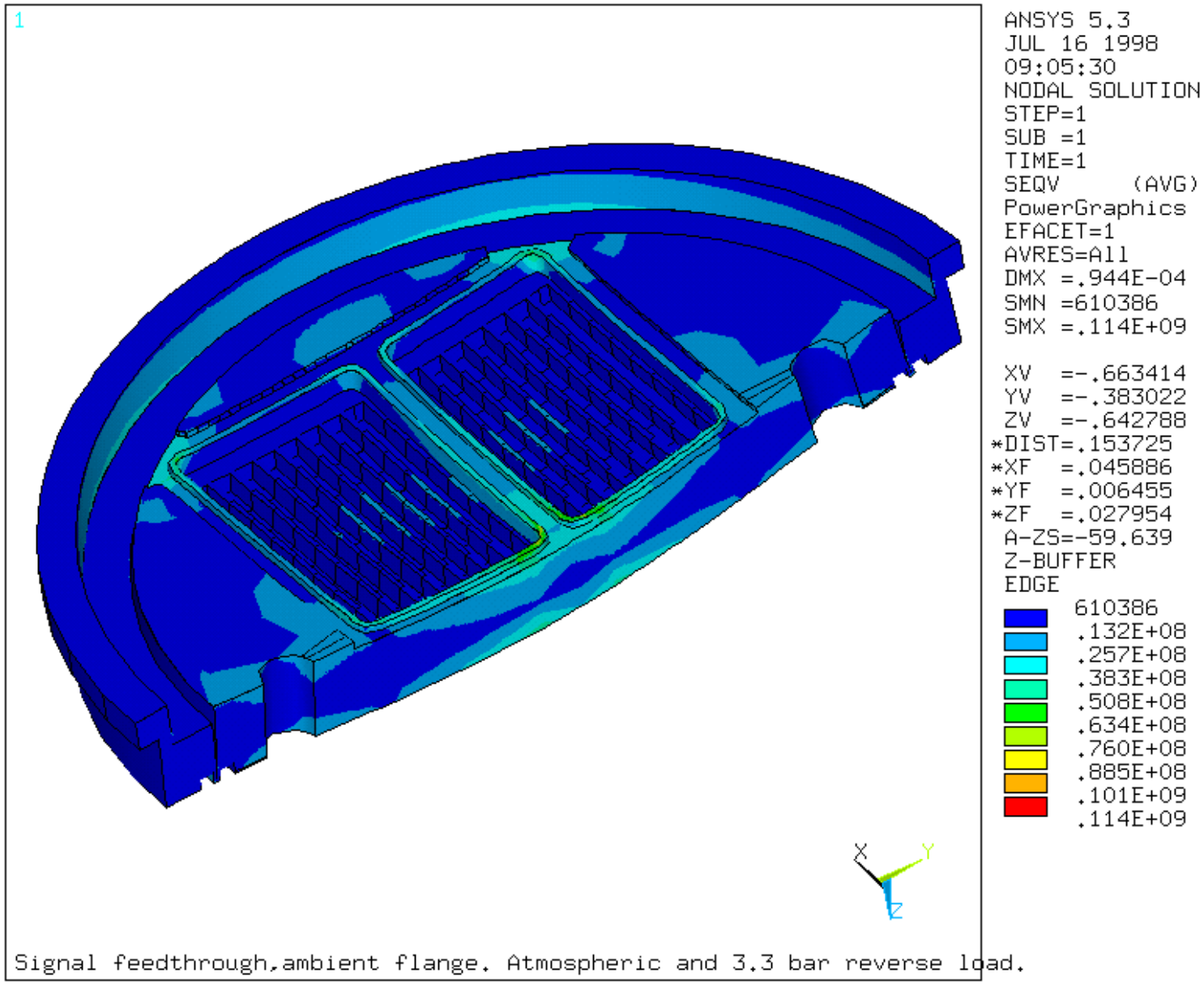

Figure 108: Finite element analysis of the ambient flange assembly under atmospheric and reverse 3.3 bar loads, showing (Von Mises) stress in Pascals. View of the vacuum side.

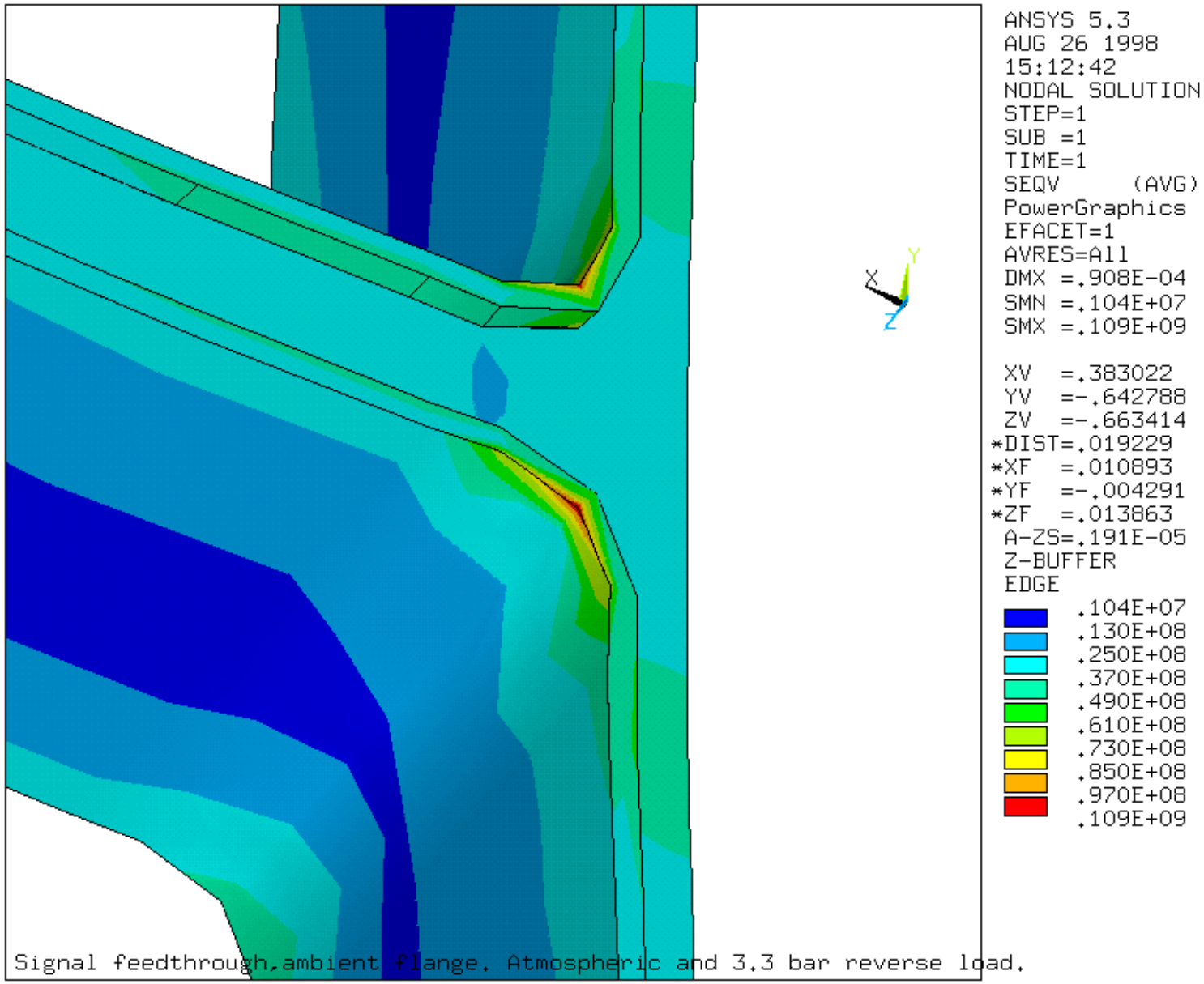

Figure 109: Finite element analysis of the ambient flange assembly under atmospheric and reverse 3.3 bar loads, showing (Von Mises) stress in Pascals. Detail View of the vacuum side of the pin carrier corners.

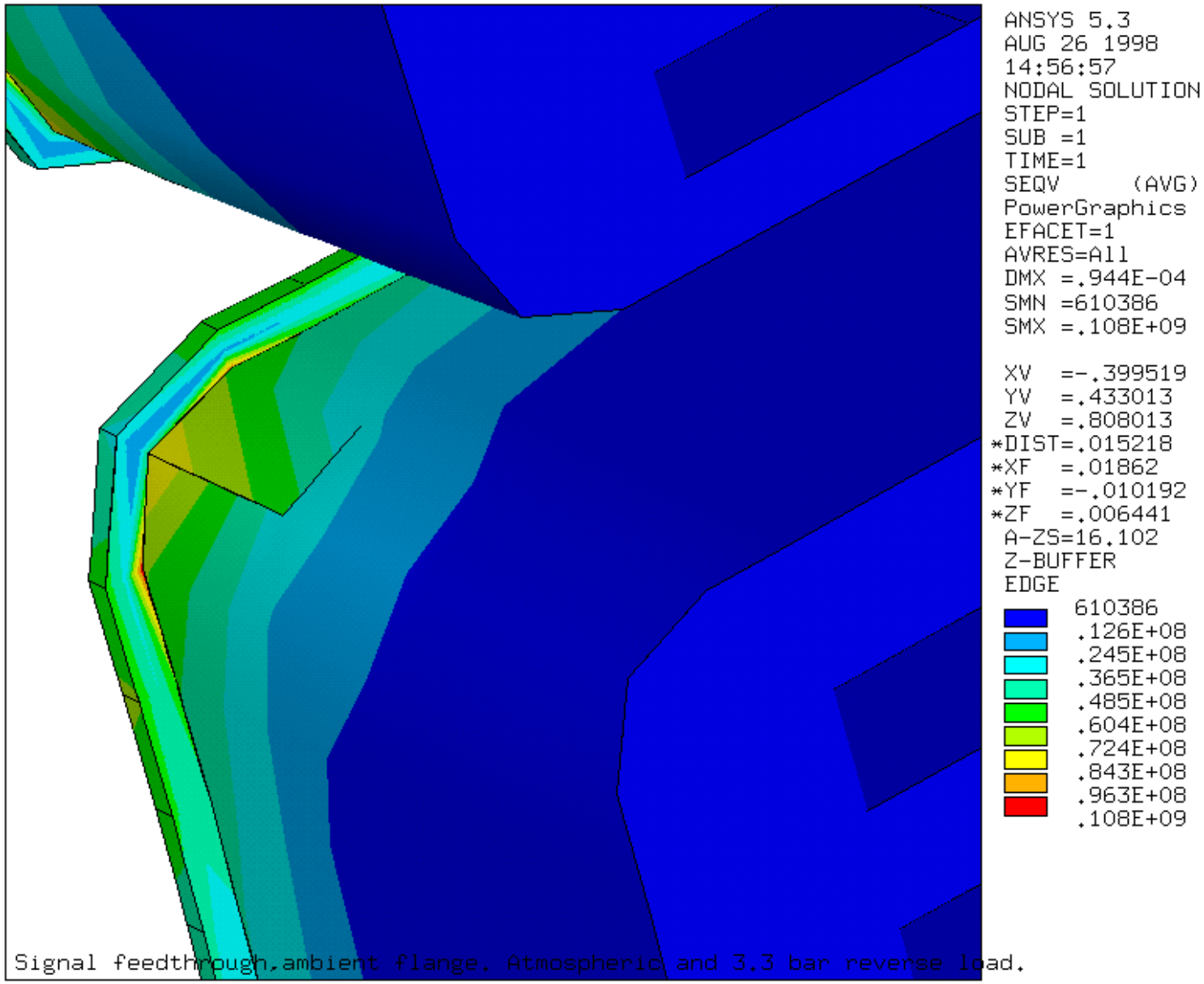

Figure 110: Finite element analysis of the ambient flange assembly under atmospheric and reverse 3.3 bar loads, showing (Von Mises) stress in Pascals. Detail View of the pin carrier corners as seen from the atmospheric side.

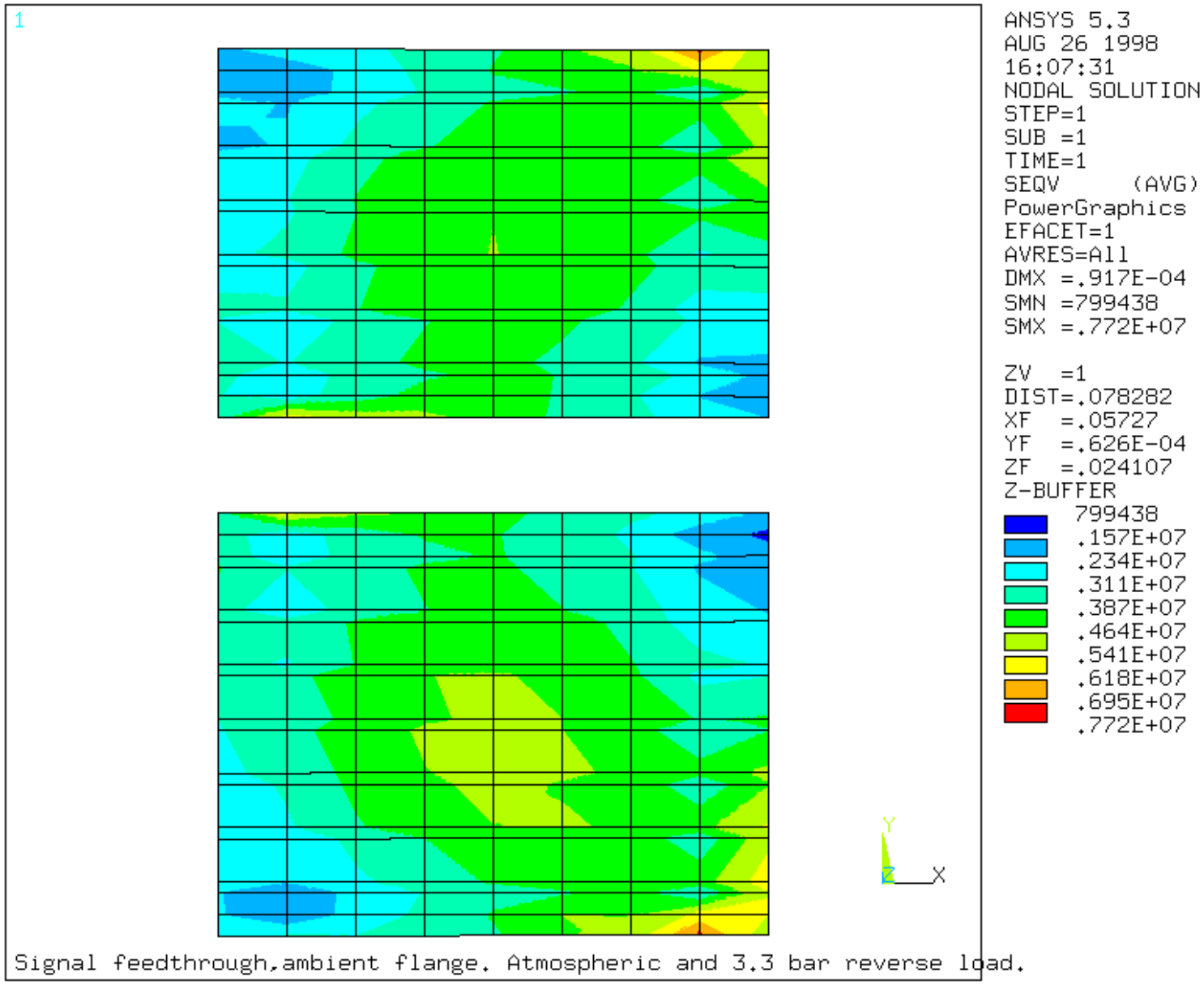

Figure 111: Finite element analysis of the ambient flange assembly under atmospheric and reverse 3.3 bar loads, showing (Von Mises) stress in Pascals. Detail View of the pin carrier web.

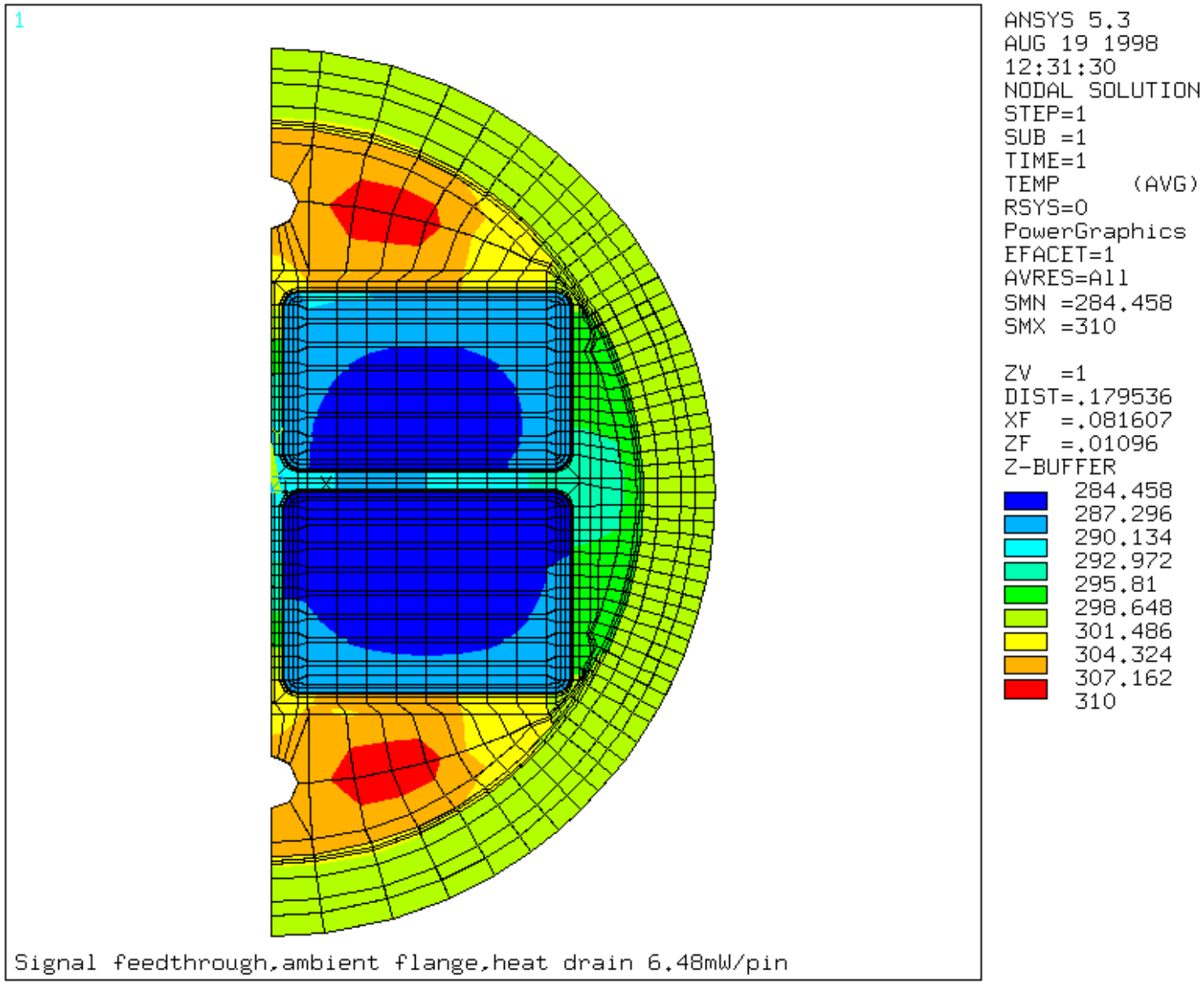

Figure 112: Finite element analysis of the ambient flange assembly under atmospheric and reverse 3.3 bar loads, showing the temperature in degrees Kelvin. See text.

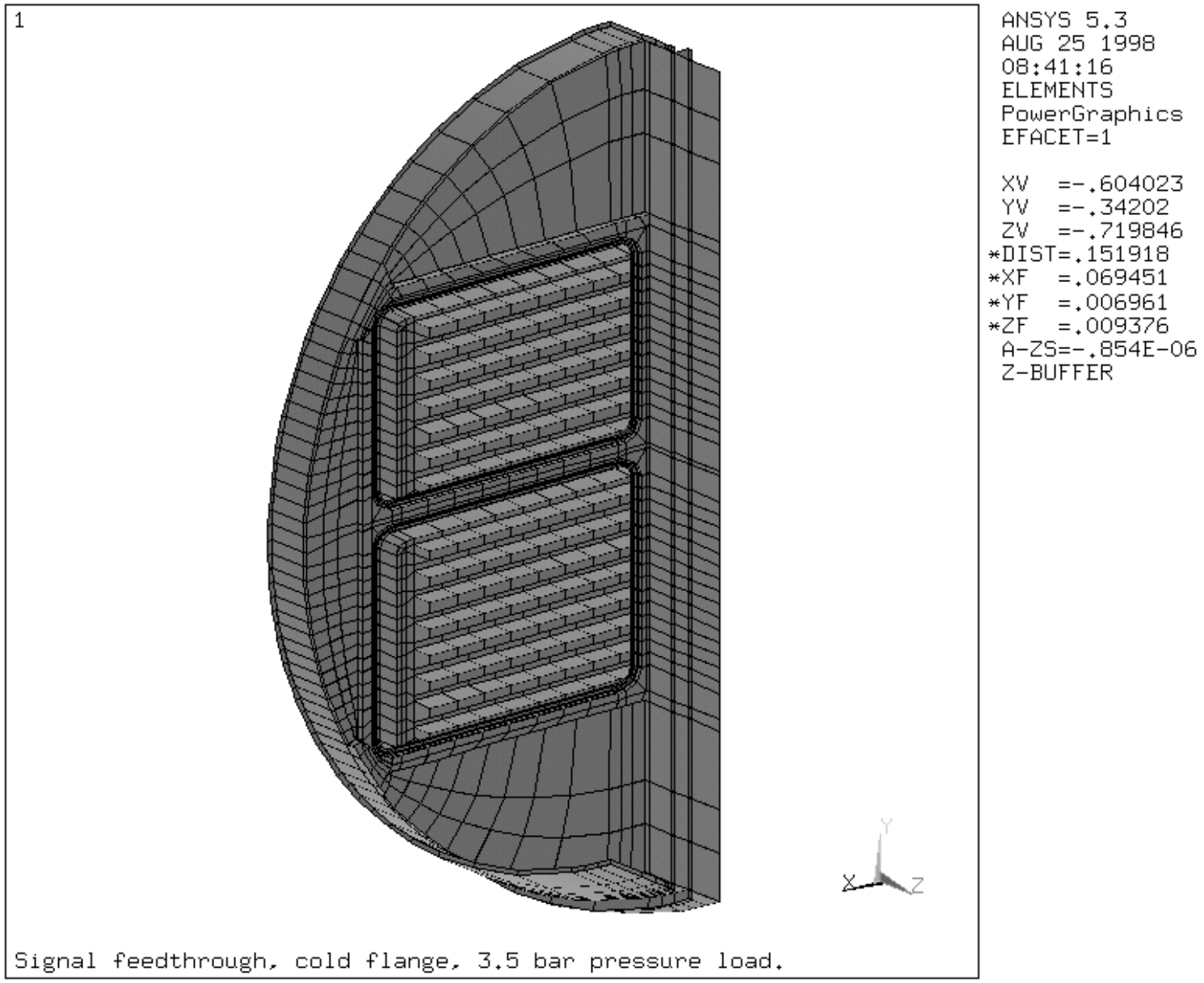

Figure 113: Finite element analysis model of the cold flange with pin carriers.

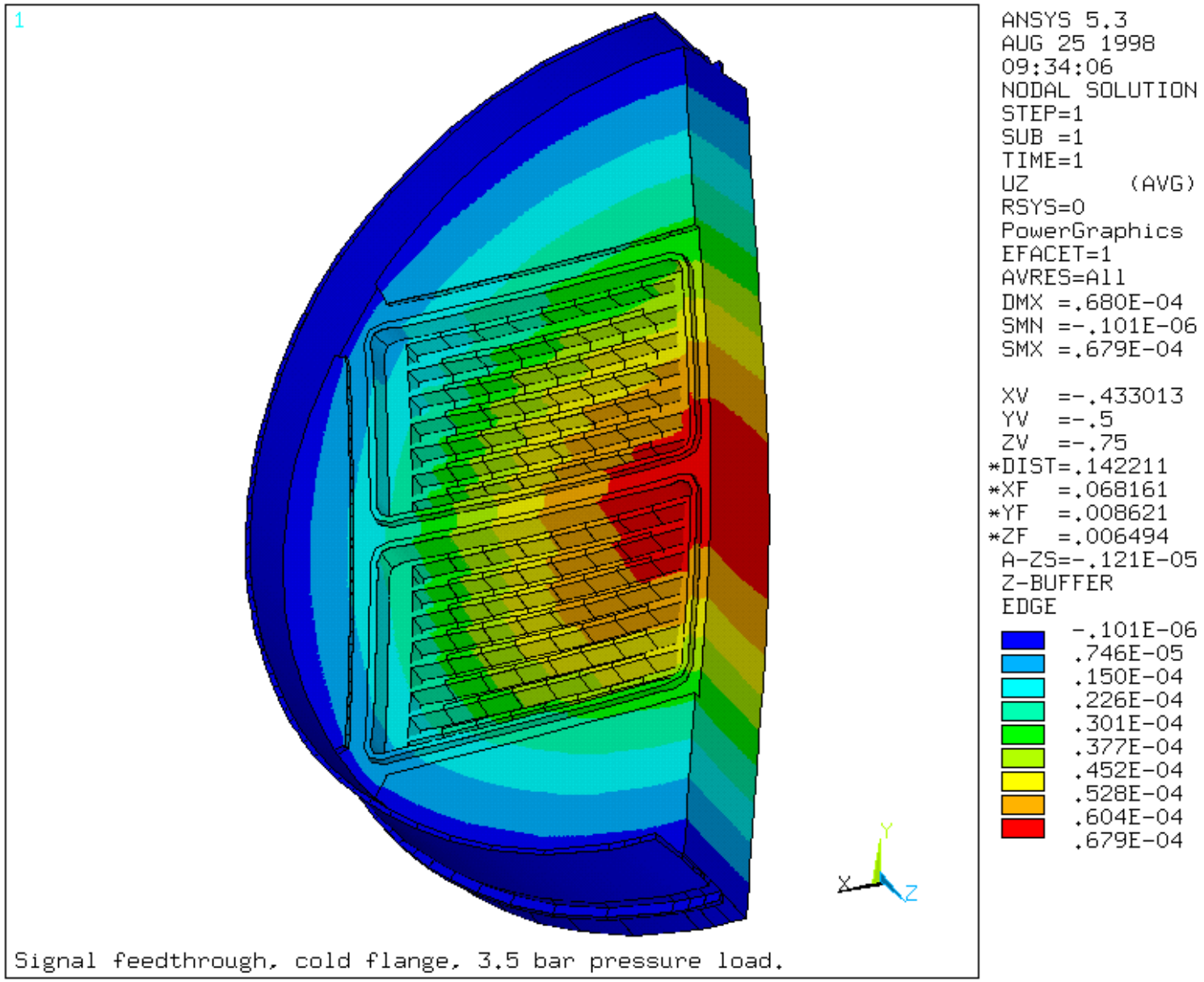

Figure 114: Finite element analysis of the cold flange assembly under 3.5 bar loads, showing the deflections in microns. View from the liquid argon side.

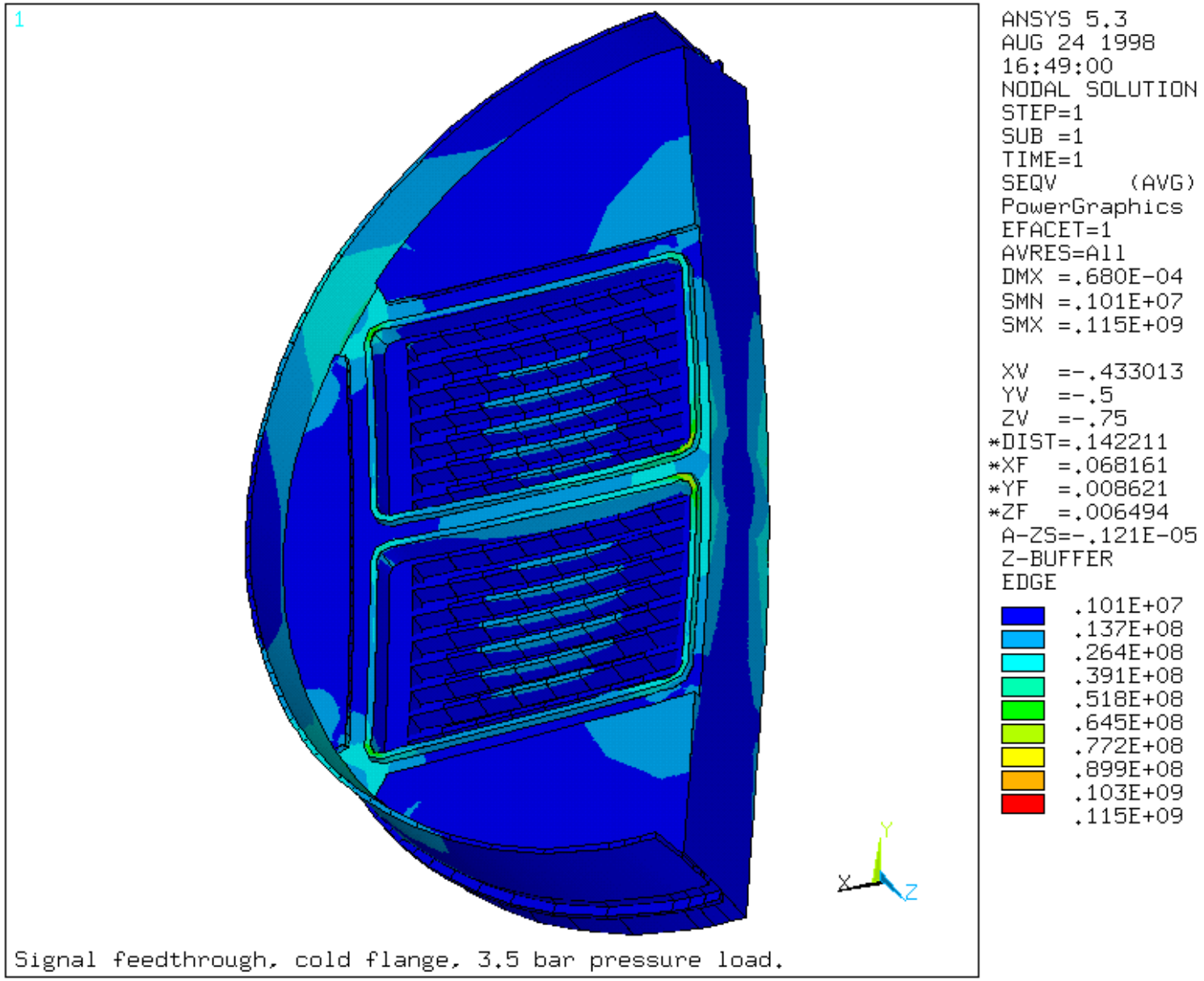

Figure 115: Finite element analysis of the cold flange assembly under 3.5 bar loads, showing (Von Mises) stress in Pascals. View from the liquid argon side.

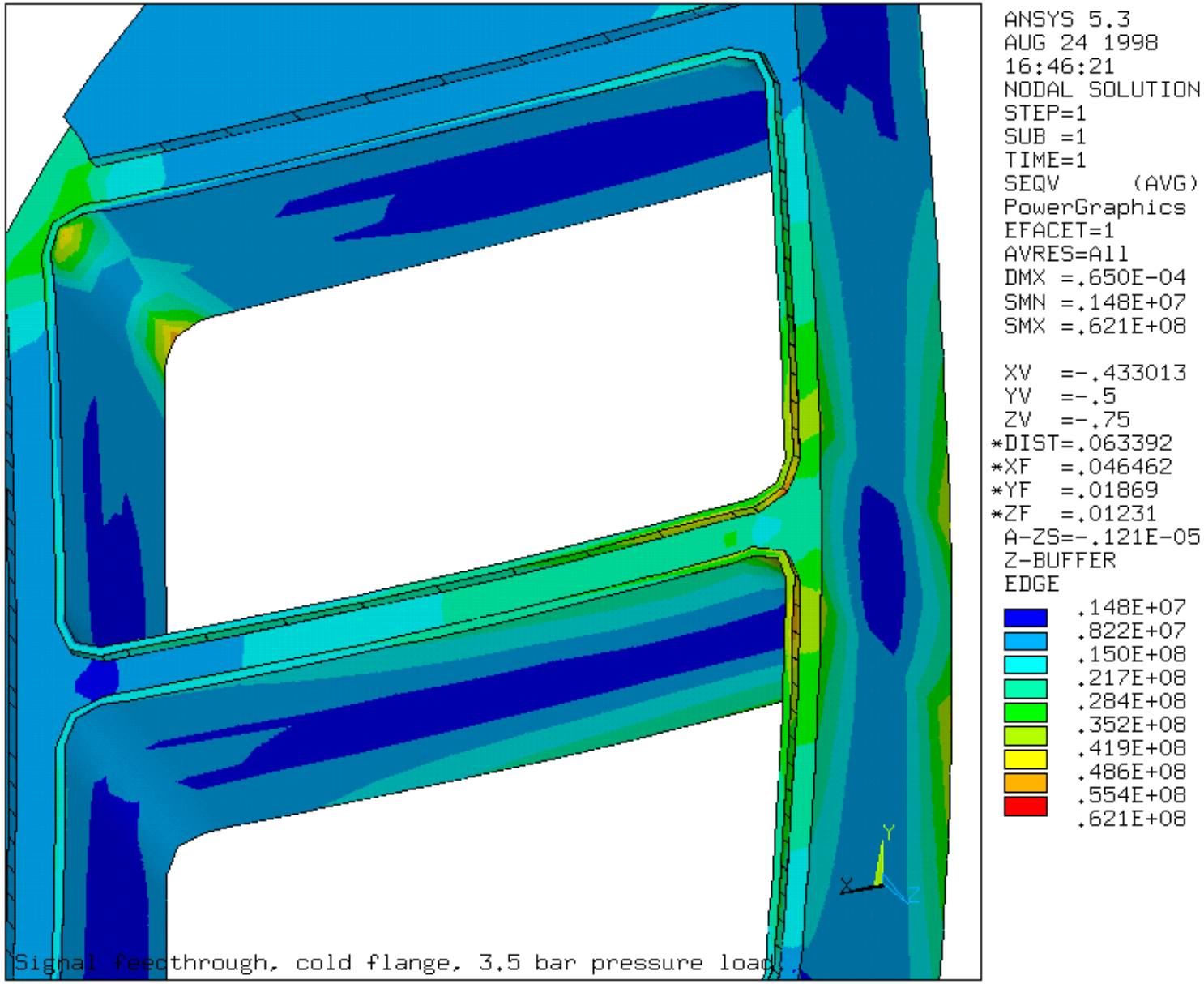

Figure 116: Finite element analysis of the cold flange assembly under 3.5 bar loads, showing (Von Mises) stress in Pascals in the flange alone. View from the liquid argon side.

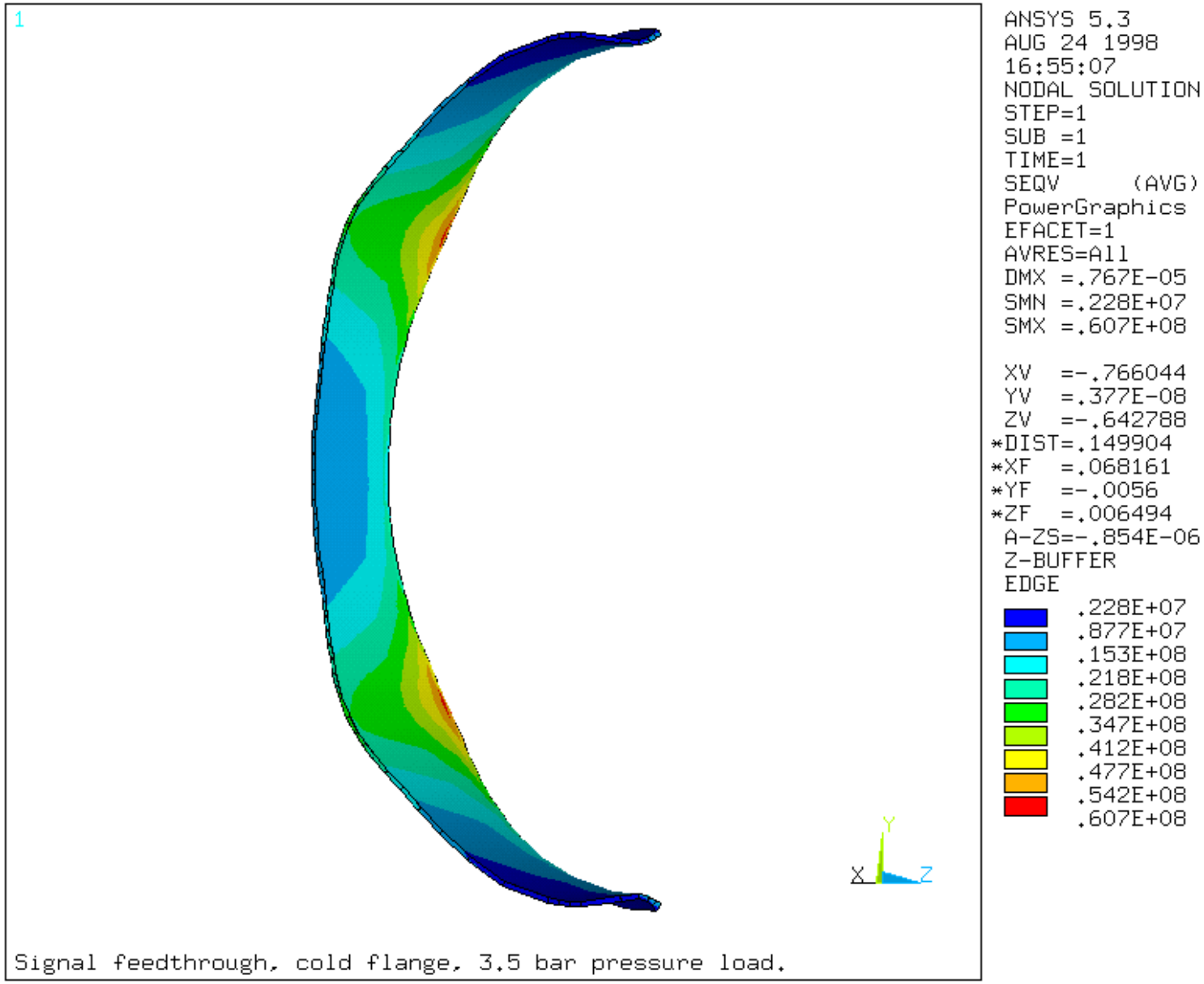

Figure 117: Finite element analysis of the cold flange assembly under 3.5 bar loads, showing (Von Mises) stress in Pascals in the funnel part abutting the cold flange.

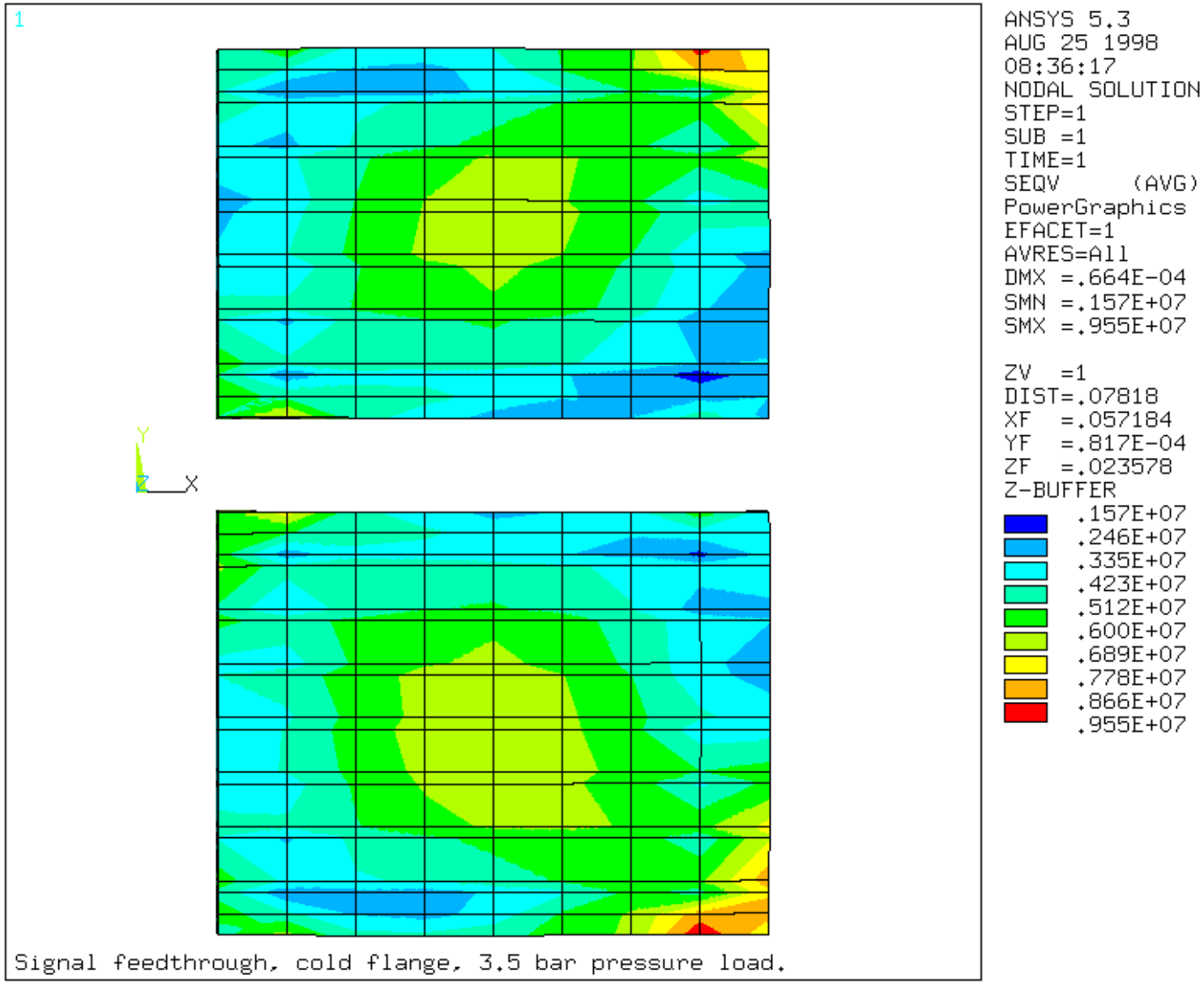

Figure 118: Finite element analysis of the cold flange assembly under 3.5 bar loads, showing (Von Mises) stress in Pascals in the pin carrier web.

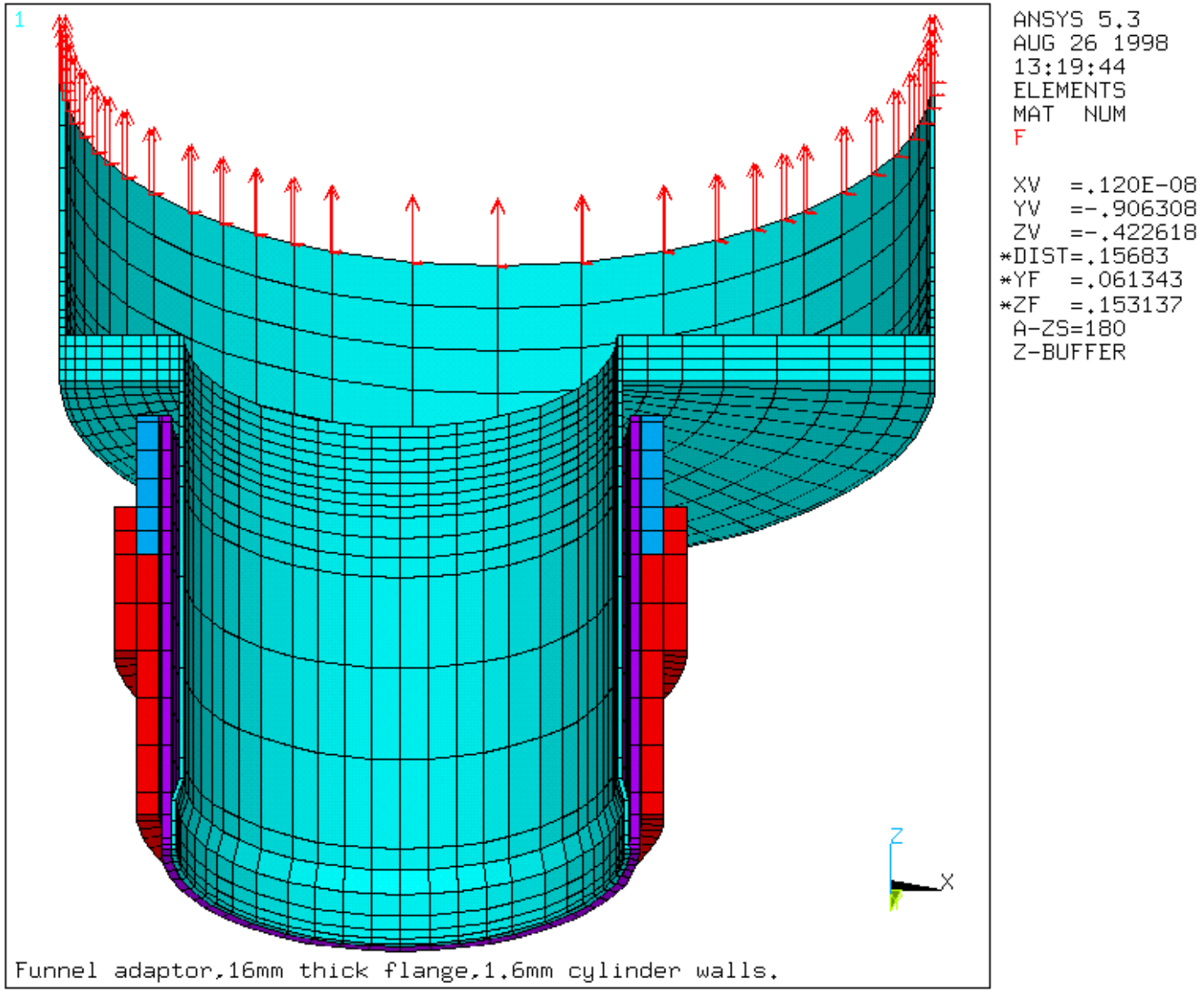

Figure 119: Finite element analysis model of the funnel showing the force applied to simulate the 3.5 bar pressure and the lateral displacement (for the barrel cryostat case). See text.

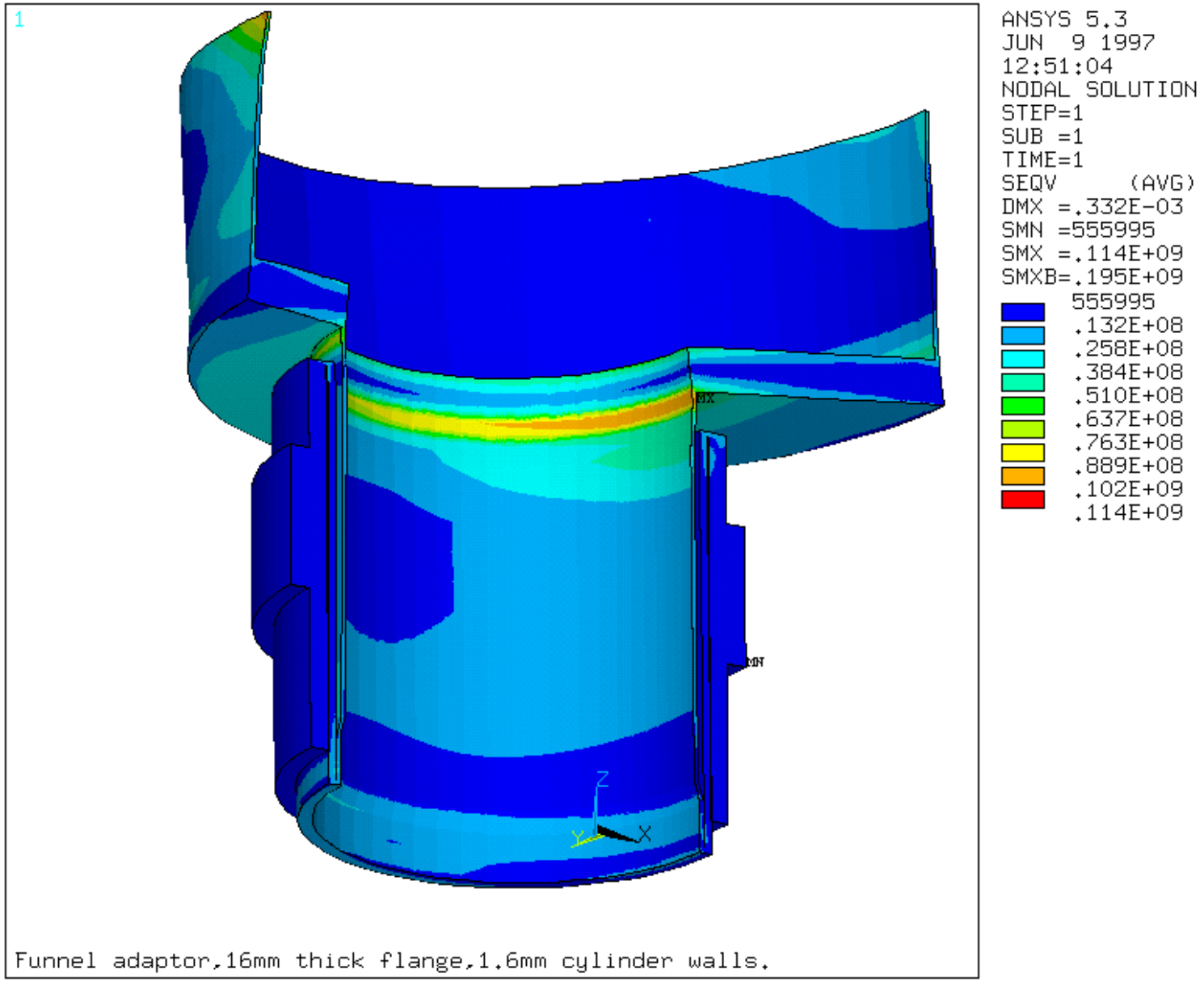

Figure 120: Finite element analysis of the funnel with a 16 mm thick flange and 1.6 mm thick cylinders, connected to a bi-metal joint, showing (Von Mises) stress in Pascals under an applied load of 3.5 bar, and a lateral load of 695 N (for a 15 mm barrel cryostat displacement).

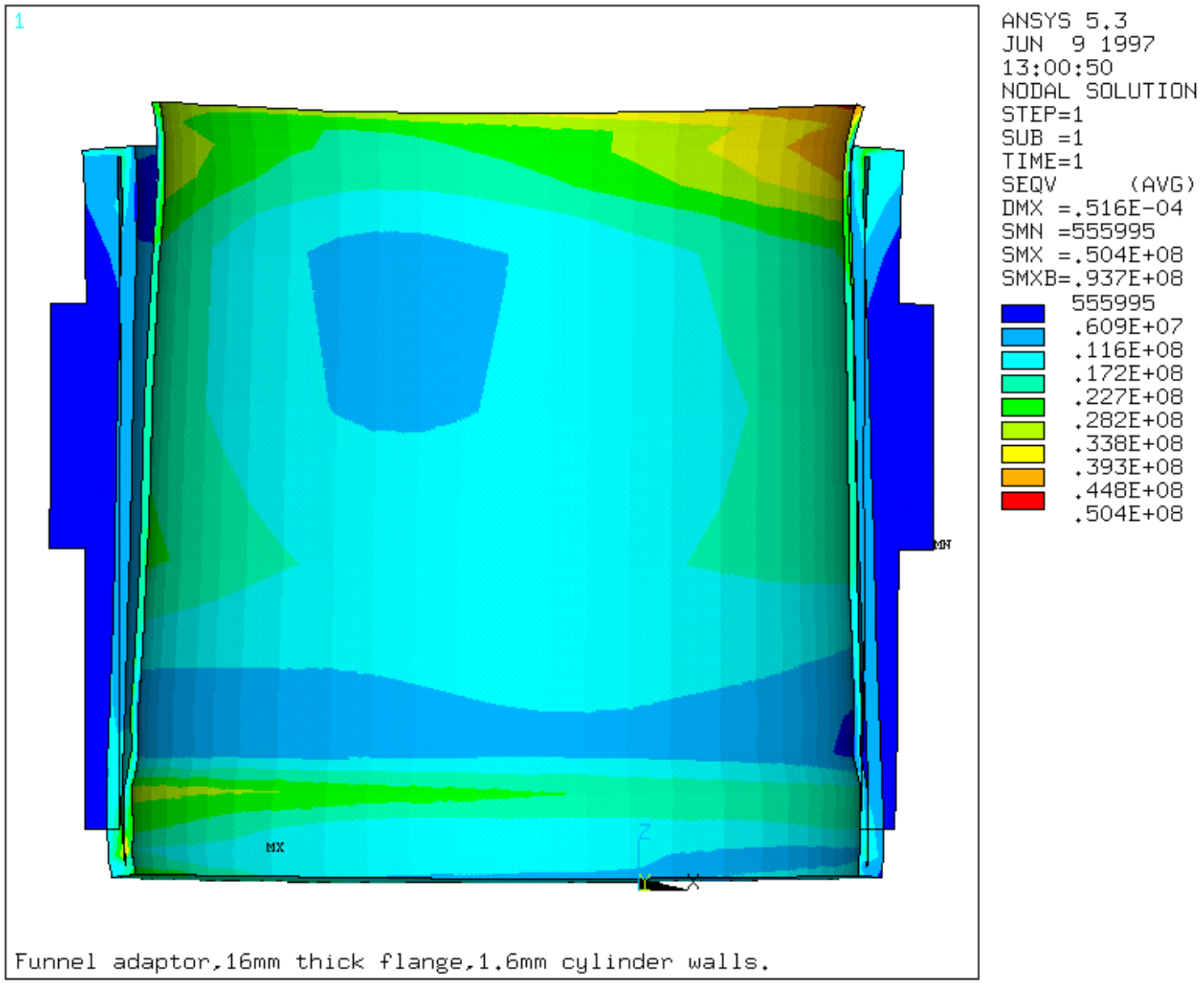

Figure 121: Finite element analysis of a funnel with a 16 mm thick flange and 1.6 mm thick cylinders, connected to a bi-metal joint, showing (Von Mises) stress in Pascals under an applied load of 3.5 bar, and a lateral load of 695 N (for a 15 mm barrel cryostat displacement). Zoom on previous figure.

20 Signal Feedthrough PRR – Calculations and FEA – Electrical Aspects (Release of 98/08/31)

20.1 Signal Feedthrough Vacuum Cable

The signal cable which connects each pair of 64-pin connectors in the ambient (300 K) and cold (80 K) flanges of the barrel and endcap signal feedthroughs is a flexible circuit stripline. The flexible circuit is a sandwich of 38 micron thick kapton between two layers of 35 micron thick copper. Each pin in the feedthrough is connected to a copper trace 200 micron wide etched from one of the copper layers and is opposite a 400 micron wide ground trace etched from the other copper layer, see Figure 122. Such an arrangement provides the correct impedance for the signal lines.

FEA has been used to investigate the temperature and power dissipation effects when signal currents are passed through the striplines. For the purpose of this investigation, the stripline length was taken to be 300 mm, the values for the electrical and thermal conductivities of the copper were made temperature dependant, but the thermal conductivity of the kapton was fixed at 3 Wm/K. The kapton is assumed to provide perfect electrical insulation, but note that the signal and ground trace pairs are in very close thermal contact. The thermal contact between adjacent signal and ground traces is sufficient to markedly modify heat flow in the stripline.

For the first part of the investigation, it is assumed that adjacent lines carry similar currents so that a single signal/ground pair can be treated in isolation. Two operational regimes were investigated. The "normal" situation is with one end of the stripline at ambient (assumed 300 K) and the other end at or near liquid argon temperature (80 K): the other "test" situation is where the cryostat is not cold and both ends of the stripline are at 300 K. The temperature as a function position along the stripline (measured from the ambient flange) is shown in Figures 123 and 124 for the "normal" and "test" situations respectively. The maximum temperature created in a stripline as a function of current flowing is shown in Figure 125. The potential difference produced between the ends of the signal trace as a function of signal current is shown in Figure 126. The heat flow to the cold and ambient flanges as a function of signal trace current is shown for the normal (300 K/80 K) situation in Figure 127. The ground return current is considered sufficiently widely distributed to cause negligible heating effects. As the signal current grows, the temperature profile along the signal trace is modified, the temperature gradient passes through zero at the 300 K end, causing a fraction of the resistive heating to begin flowing to the ambient flange. In the "test" situation half the resistive heat flows to each flange.

The second part of the investigation concerns the effect on the maximum temperature in a signal trace carrying a current, when it is among other traces carrying small or negligible currents. An analysis was made of a signal trace carrying a current of 150 mA with three neighbouring traces on either side of the signal trace carrying no current. The ends of all traces were held at 300 K. The half-model (using the plane of symmetry through the current carrying trace) is shown in Figure 128. Also shown in Figure 128 are the maximum temperatures in the traces and the percentage of the resistive heat from the current carrying trace, which is carried by each of the neighbouring traces. It is evident that neighbouring traces are in good thermal contact and a single trace could carry 3 or

4 times the current one might specify for an isolated trace. A corollary to the latter is that a current overload in one trace could damage other traces on the same stripline.

20.2 Signal Feedthrough Low Voltage Vacuum Cable

Work to be done later in the year.

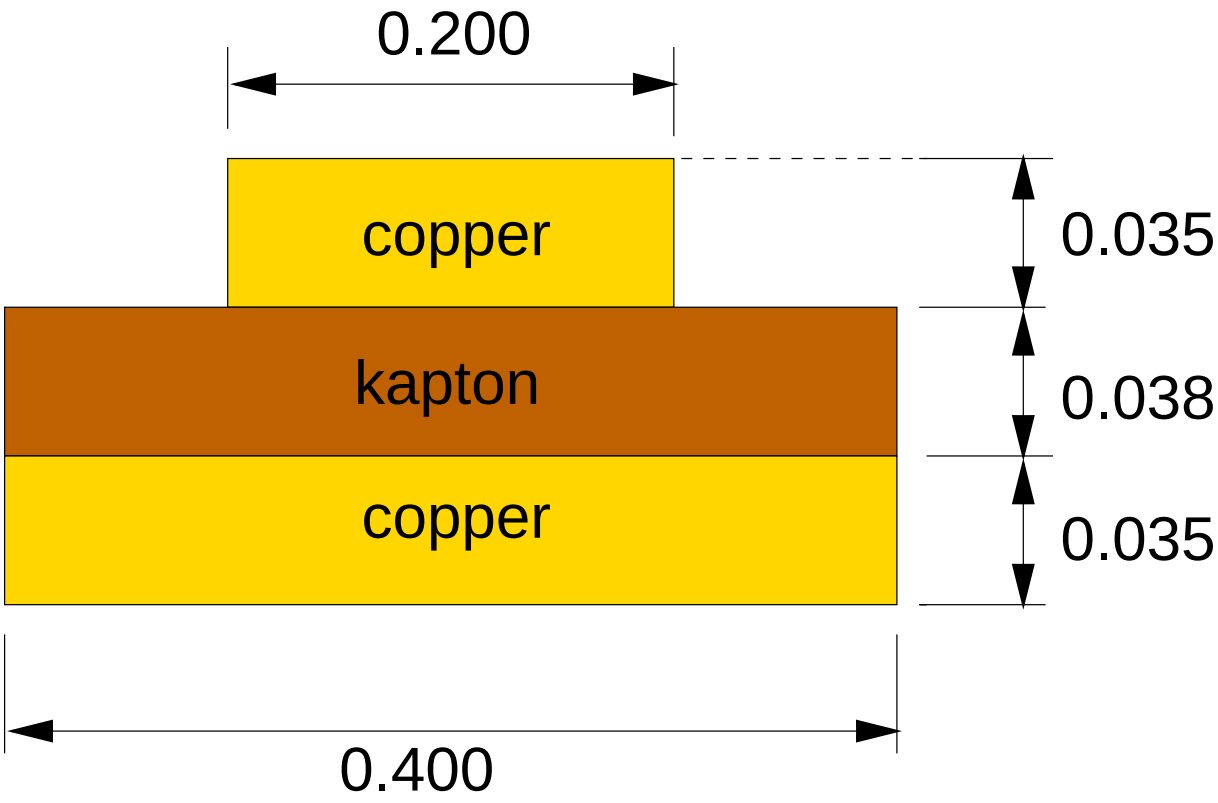

Figure 122: Finite element analysis model of one signal and return trace of the vacuum stripline. Dimensions in millimetres.

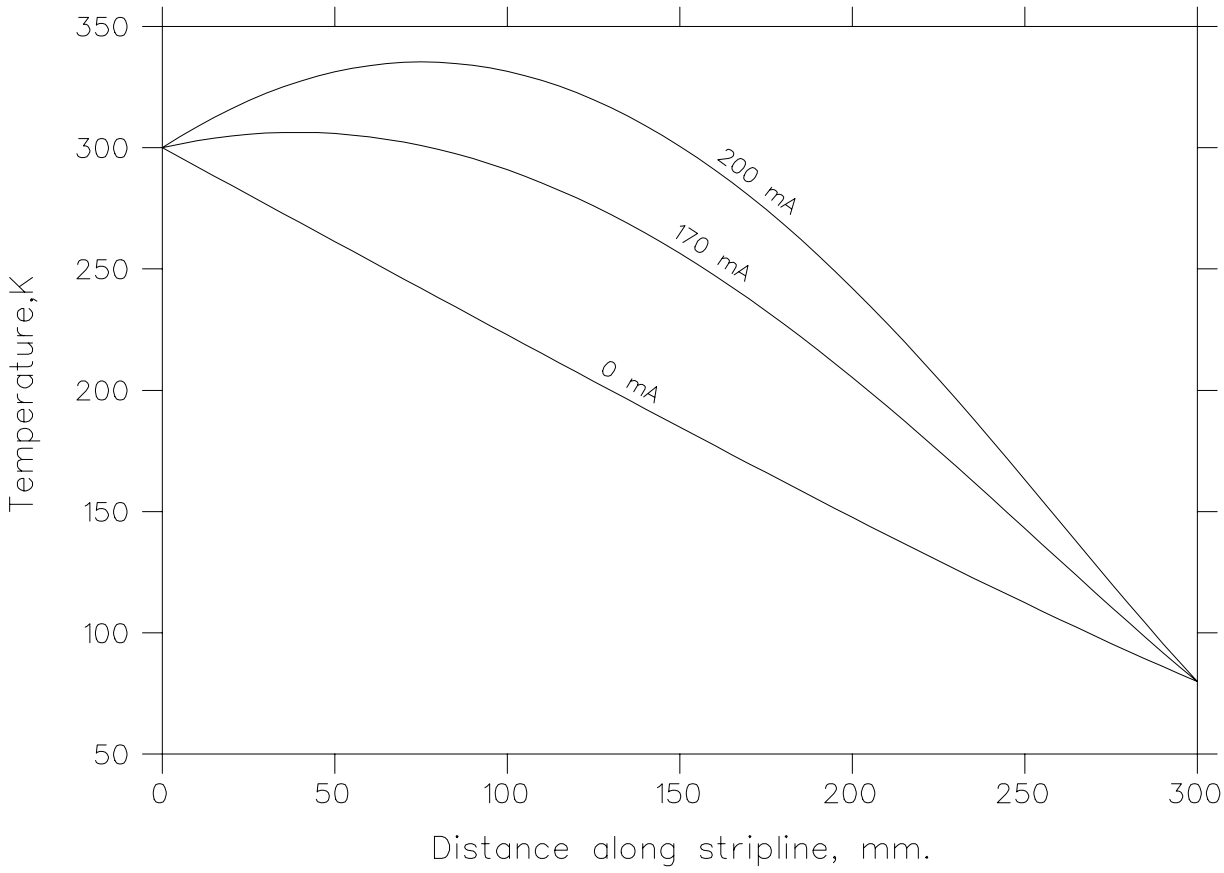

Figure 123: Temperature of vacuum stripline as a function of the distance from the ambient flange for several current values. Normal situation: the ambient flange is held at 300 K while the cold flange is held at 80 K.

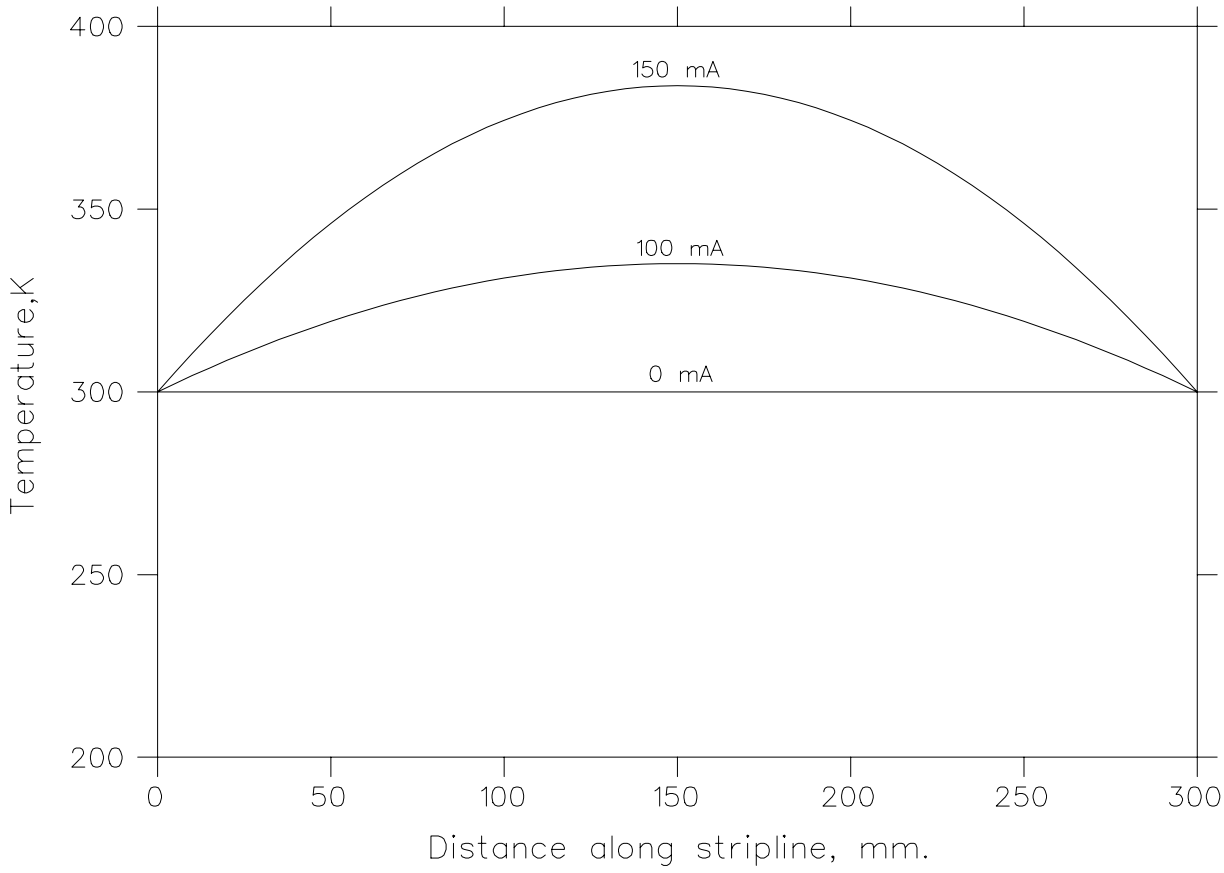

Figure 124: Temperature of vacuum stripline as a function of the distance from the ambient flange for several current values. Test situation: the ambient flange and the cold flange are held at 300 K.

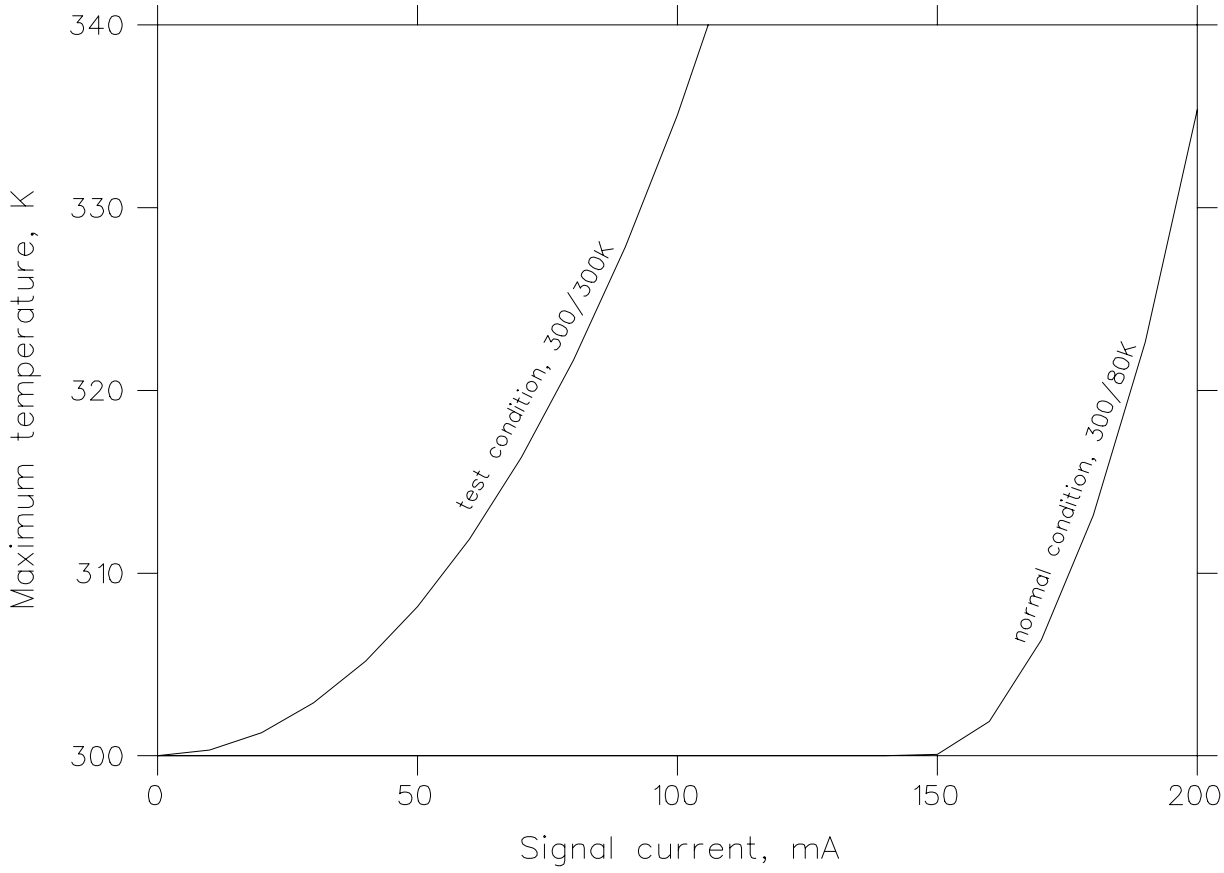

Figure 125: Maximum temperature of vacuum stripline as a function of the current for both the normal and test situations.

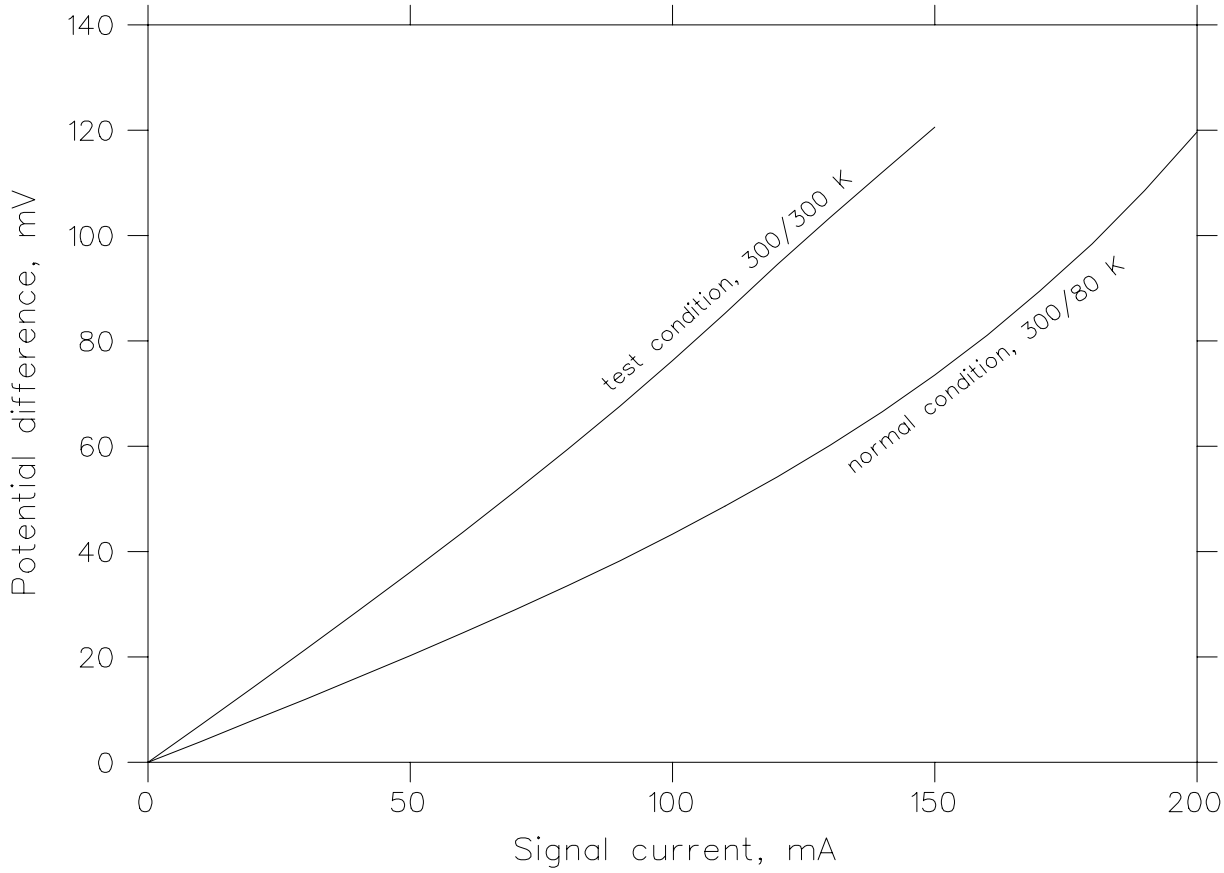

Figure 126: Potential difference between the ends of the vacuum stripline as a function of the current for both the normal and test situations.

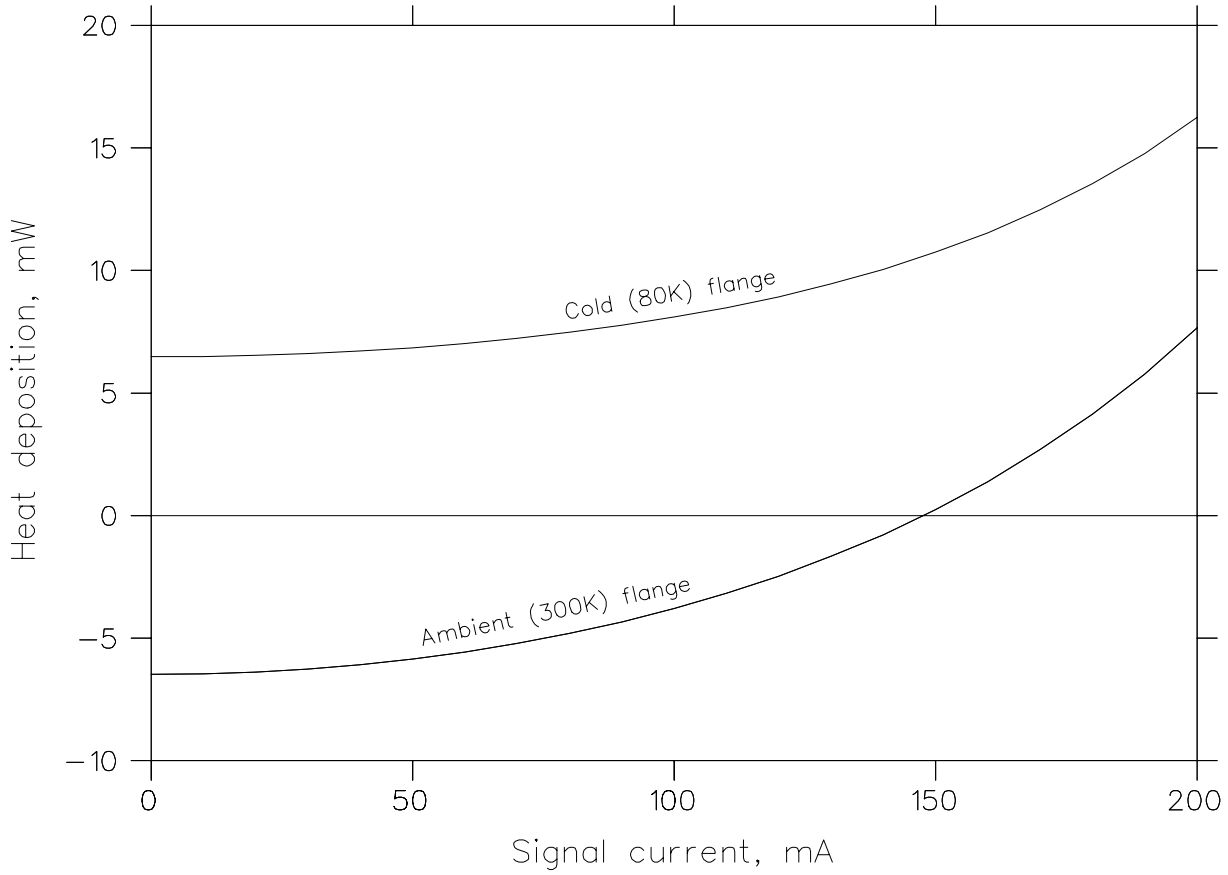

Figure 127: Heat flow to the cold and ambient flanges from the vacuum stripline as a function of the vacuum stripline signal trace current the normal (300 K/80 K) situation.

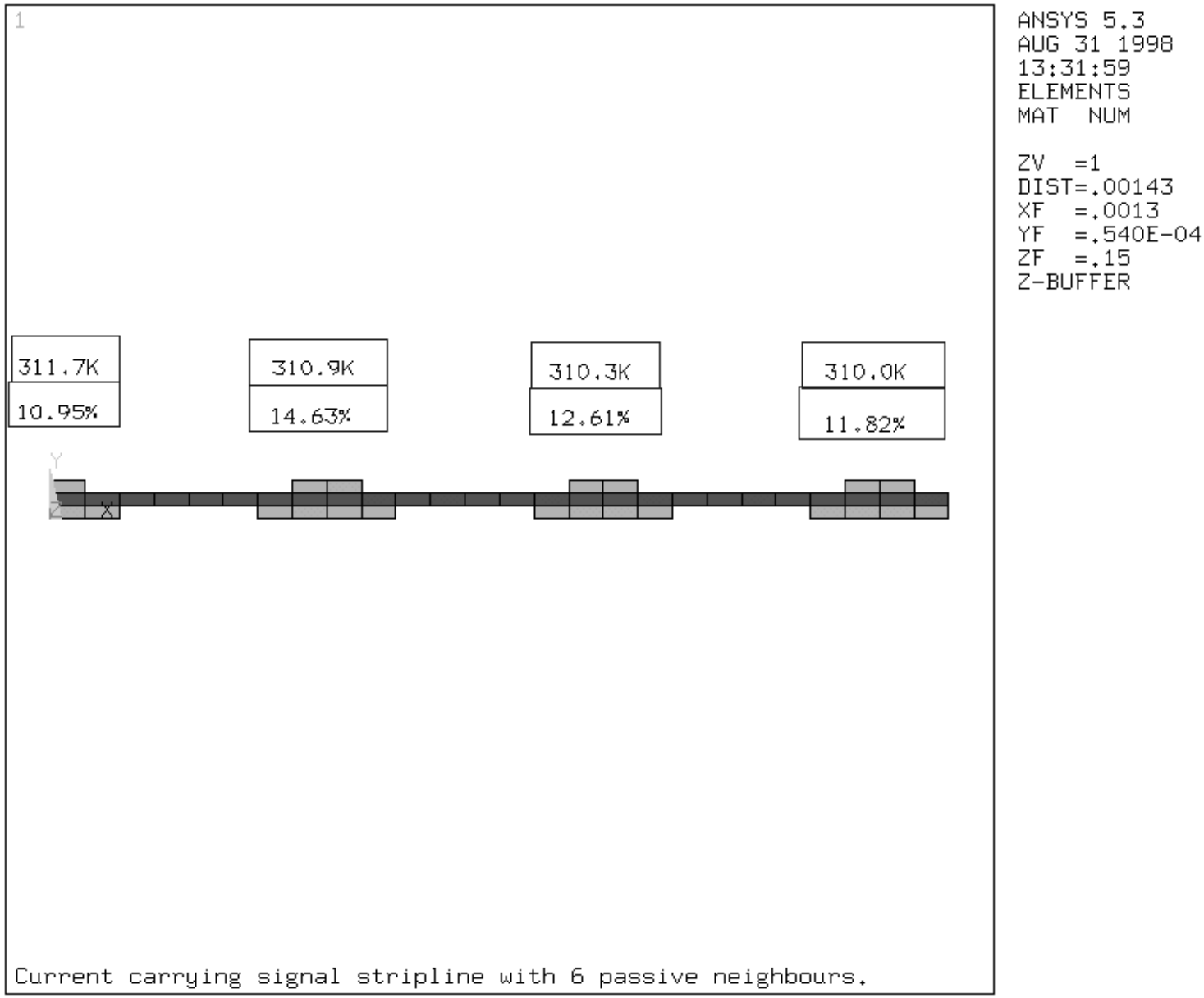

Figure 128: Finite element analysis model of half a vacuum stripline. The current carrying trace is located at the plane of symmetry (left). Also shown are the maximum temperatures in the traces and the percentage of the resistive heat from the current carrying trace which is carried by each of the neighbouring traces.

21 Signal Feedthrough PRR – Calculations and FEA – Mechanical Aspects Update on Coldbox (Funnel) (Release of 98/11/06)

21.1 Coldbox

The FEA model of the Coldbox and bi-metallic joint is shown in Figure 129. The part coloured red is aluminum, the rest is stainless steel. The open end of the aluminum section of the bi-metal joint, which connects the feedthrough assembly to the cryostat, was restrained from lateral and vertical motion. The larger diameter open end of the stainless steel section was constrained to remain circular, simulating the constraint applied by the joint to the cold flange at this location. A force of 5387 Newtons was applied at the latter location, simulating the force on the Coldbox due to the internal pressure of 3.5 bar. A force of 695 Newtons was applied at the same location in a lateral direction, simulating the force required to displace the bellows laterally by 15 mm, this displacement occurring due to contraction of the cryostat on cooling to liquid argon temperature. These forces are shown as red arrows in the latter figure. The maximum stress of 109 MPa occurs at the Coldbox plate/smaller cylinder junction, Figure 130. The maximum stress (63 MPa) in the transition joint region occurs near the weld at the lower edge of the smaller Coldbox cylinder, Figure 131. The stress in the bi-metal union is low, < 7 MPa. The tooling holes in the flange were simulated by removing elements in the flange, leaving rectangular holes of approximately twice the cross section and similar depth as the 8.5 mm diameter times 10 mm deep tooling holes; the introduction of the holes had very little effect, Figure 132.

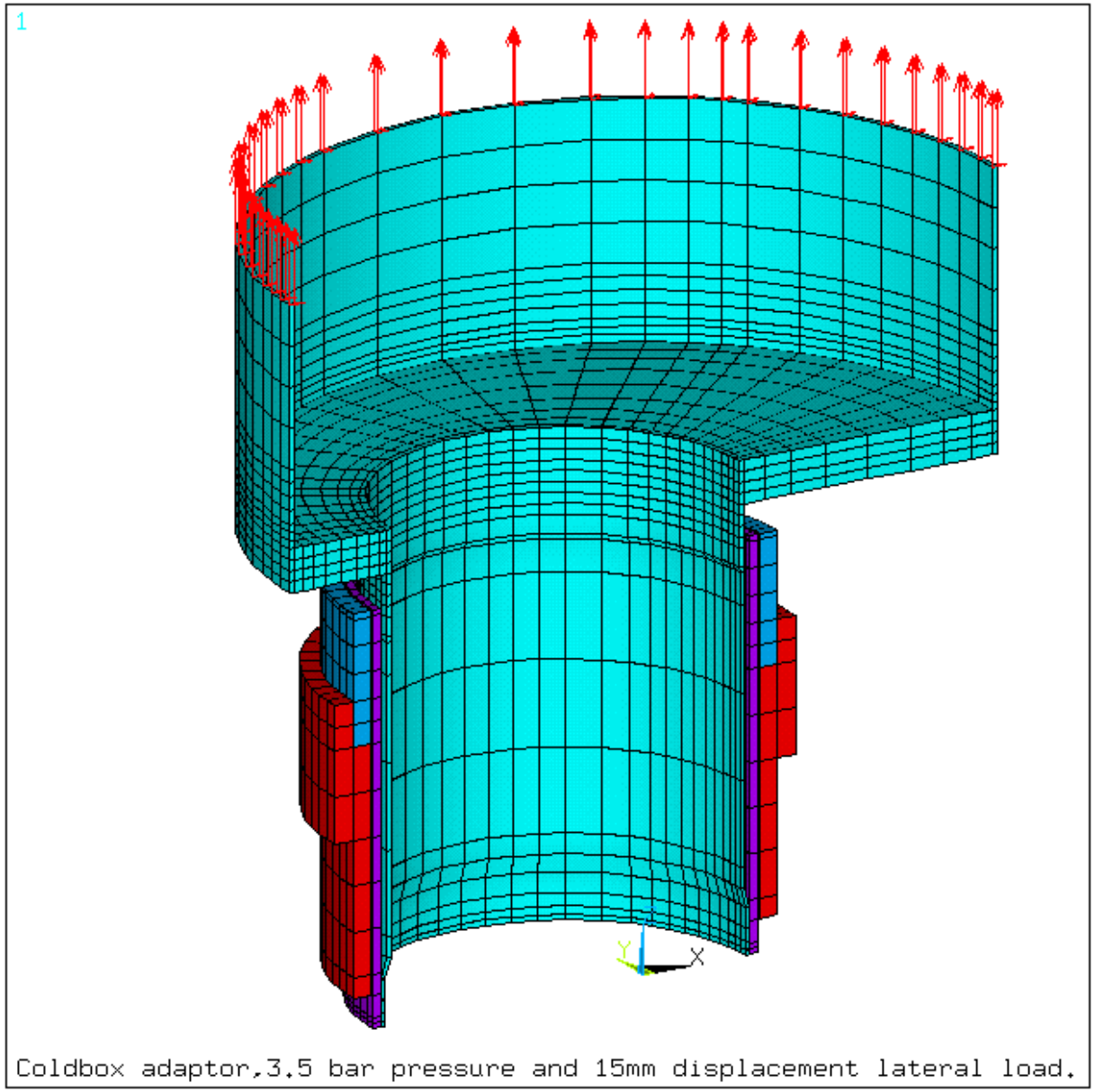

Figure 129: Finite element analysis model of the coldbox showing the force applied to simulate the 3.5 bar pressure and the lateral displacement (for the barrel cryostat case). See text.

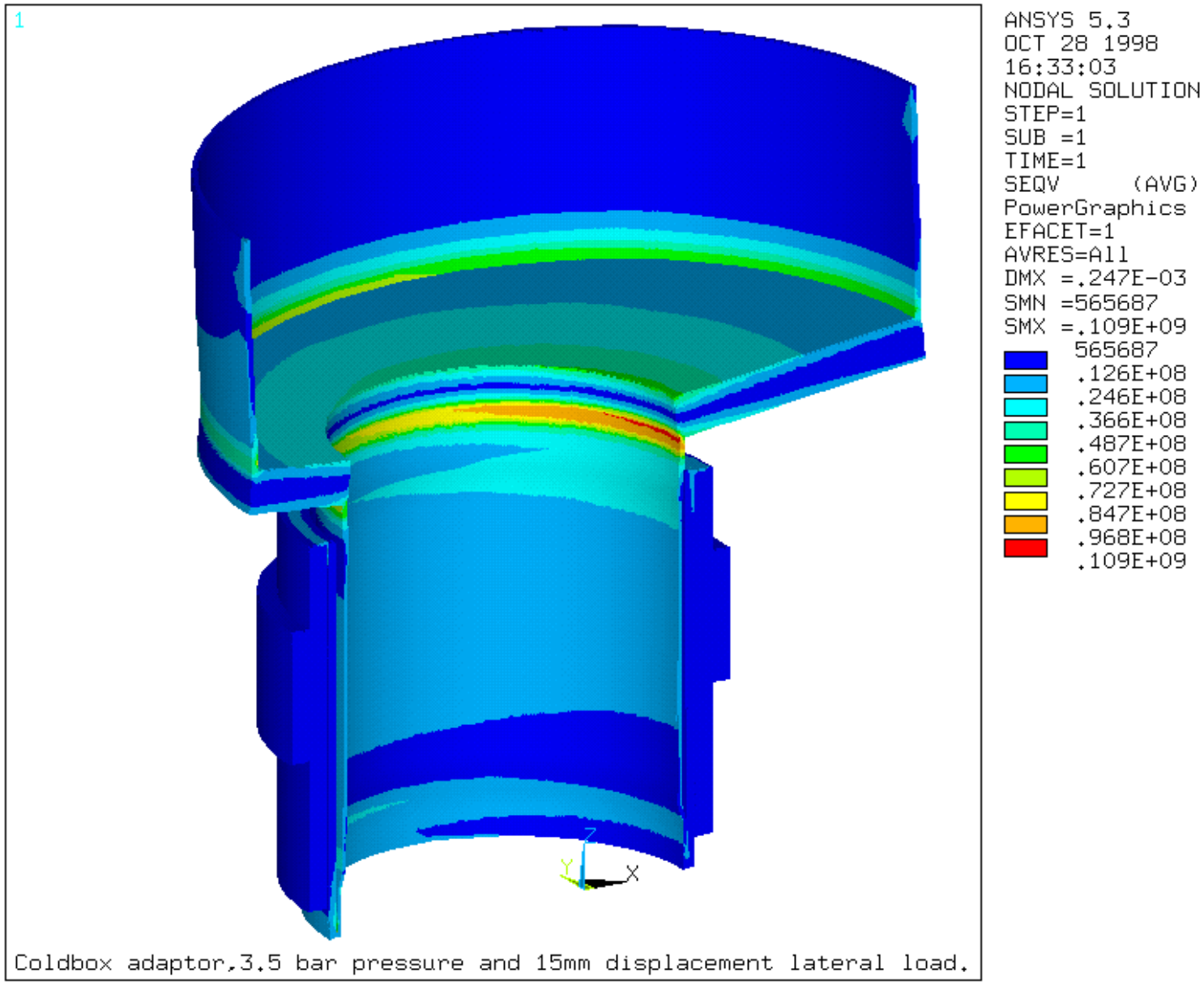

Figure 130: Finite element analysis of the coldbox with a 16 mm thick flange, connected to a bi-metal joint, showing (Von Mises) stress in Pascals under an applied load of 3.5 bar, and a lateral load of 695 N (for a 15 mm barrel cryostat displacement).

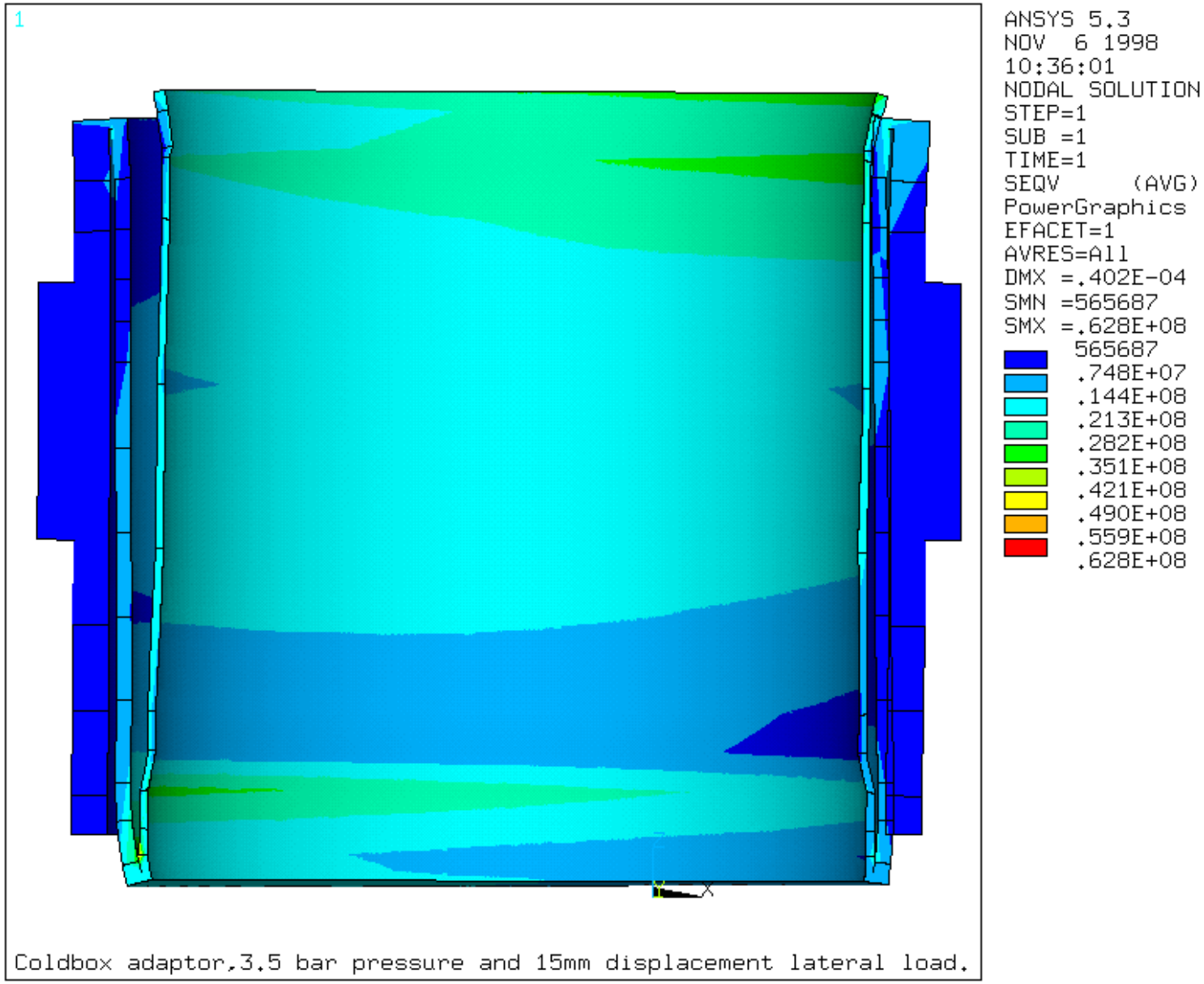

Figure 131: Finite element analysis of a coldbox with a 16 mm thick flange, connected to a bi-metal joint, showing (Von Mises) stress in Pascals under an applied load of 3.5 bar, and a lateral load of 695 N (for a 15 mm barrel cryostat displacement). Zoom on previous figure.

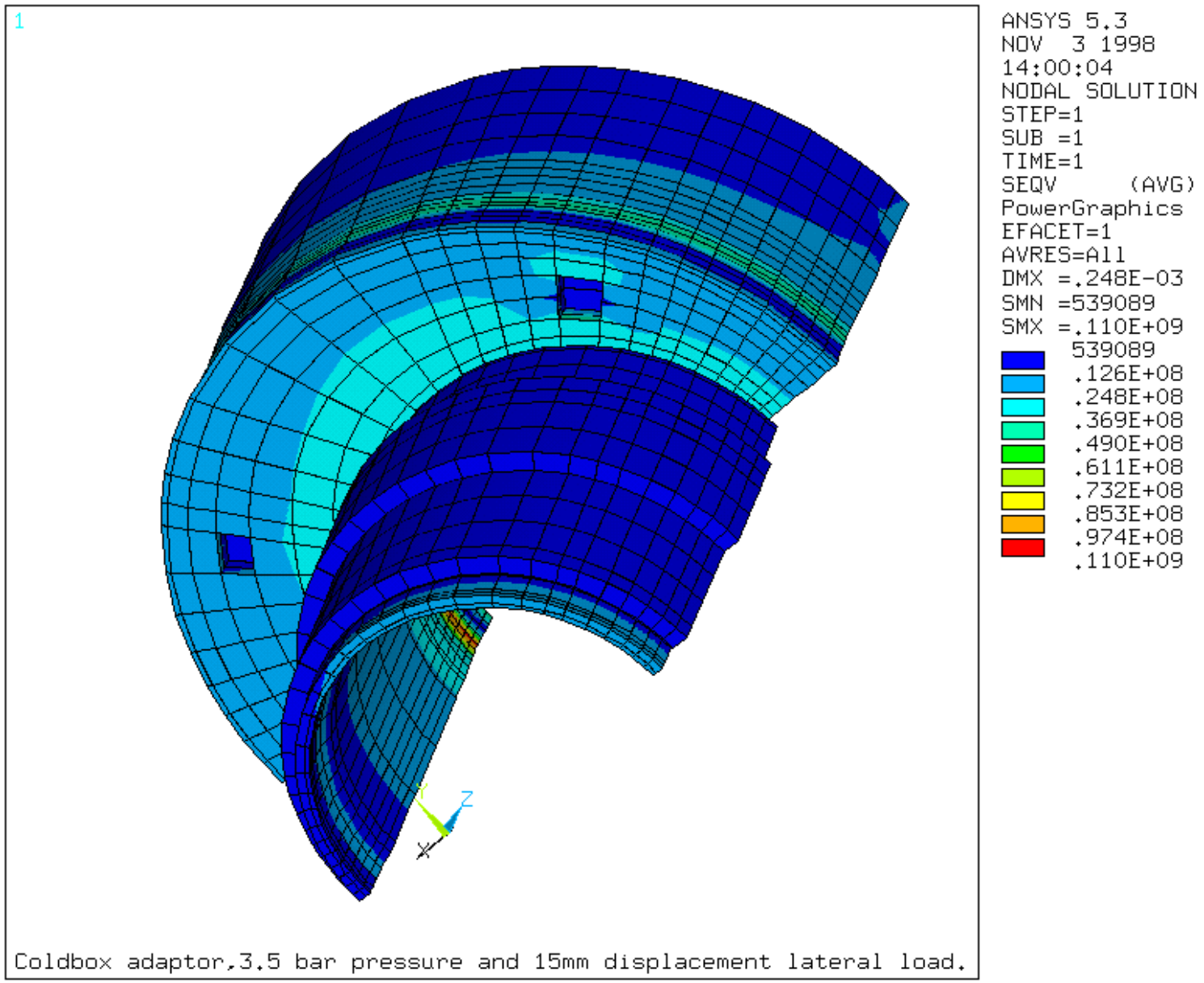

Figure 132: Finite element analysis of a coldbox with a 16 mm thick flange and tooling holes, connected to a bi-metal joint, showing (Von Mises) stress in Pascals under an applied load of 3.5 bar, and a lateral load of 695 N (for a 15 mm barrel cryostat displacement).

22 Signal Feedthrough PRR – Calculations and FEA – Electrical Aspects Update on Low Voltage Vacuum Cables (Release of 98/12/10)

Current supplies to the HEC cold electronics are carried on special vacuum cables located in four of the thirty cable positions in four of the signal feedthroughs per endcap. For the purpose of this study it is assumed they occupy the two outermost positions in each of the seven-row pin carriers. Heat flows through these cables from the ambient flange end to the cold flange end, which is assumed to be at liquid argon temperature. The heat flow for the proposed current supply cables has been calculated in HEC-note-068 and was used in an FEA calculation to estimate the temperature fields which would occur at the ambient flange. It is assumed that the heating resistors, which are provided to prevent condensation occurring, hold the temperature at the resistor locations at 310 K and that the seal ring is held at 300 K where it touches the cryostat or bolt ring. Figure 133 shows the resulting temperature field in the ambient flange with the region near the current supply cables well below the expected dew point. Some heat will be supplied by convection and conduction from the warm cables but the temperatures are unlikely to be changed by more than a few degrees. A solution being considered is to add electrical heaters (about 2 watts each) to the current supply cables, adjacent to the plugs connecting them to the ambient flange, thereby offsetting the heat drain close to the point of origin.

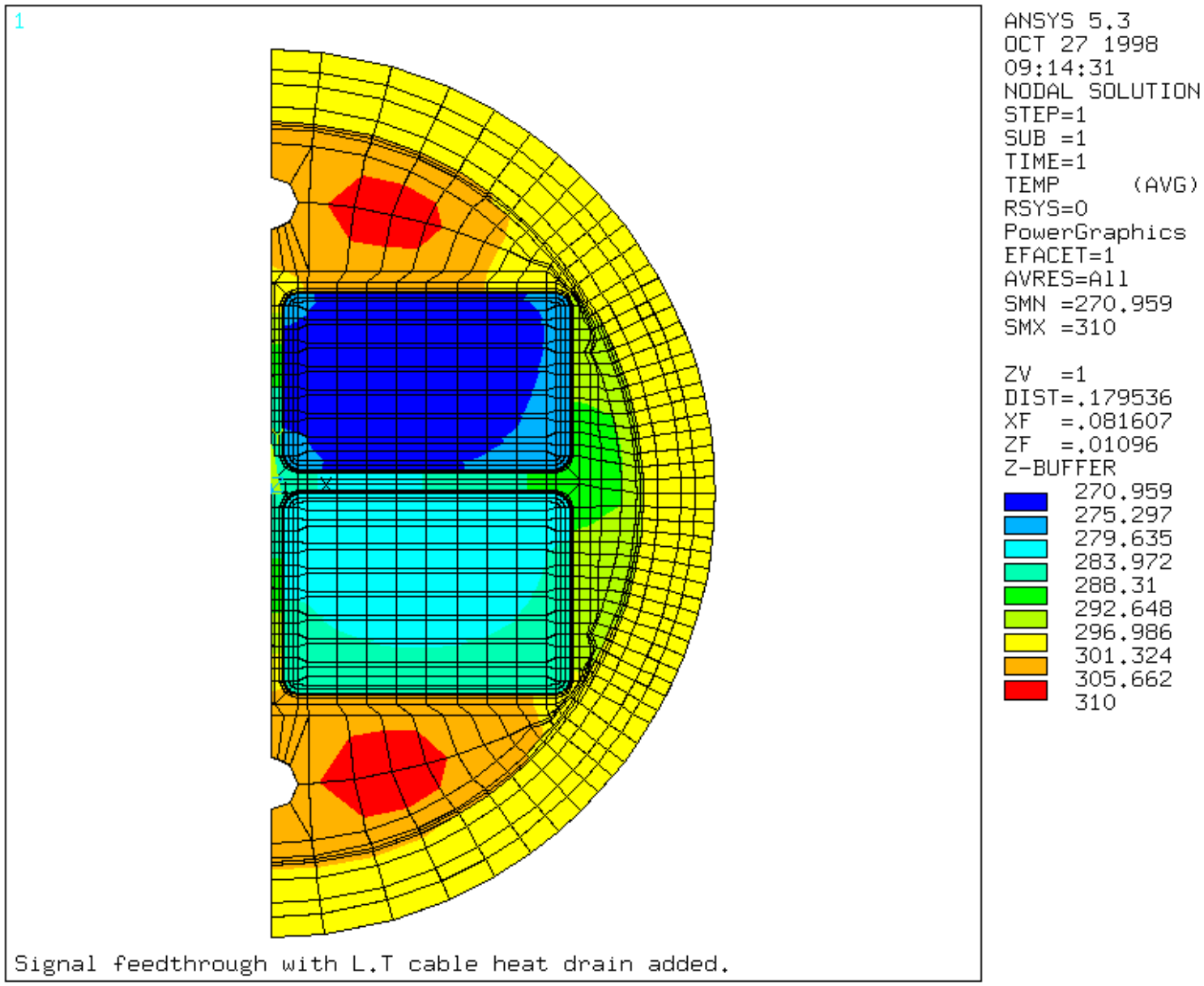

Figure 133: Finite element analysis of the ambient flange assembly for the HEC feedthrough, showing the temperature in Kelvin. The seven-row pin carrier connectors are connected to low voltage vacuum cables, which are assumed here not to carry any currents. See text